CONTENTS

EDITORIAL

The present volume of the journal is different from the others. It initiates recollections of Polish researchers using the synchrotron radiation in the difficult first years (mostly 1980's) of exploitation of the light emitted by the storage rings. The studies were difficult, but also exciting, because the users frequently had to design and build an equipment of new type, they had no computers at their disposal, and had to fight with various problems including the long unpredicted shutdowns. This issue starts with a paper by Leif Gerward on his collaboration with Professor Bronisław Buras, an eminent Polish scientist (at school, I learned physics from textbooks of his authorship shared with Jan Ehrenfeucht; by the way, Jan Ehrenfeucht and his wife were neighbours and friends of my grandmother despite she had nothing in common with physics). From the Gerward's paper we do not only learn about the collaboration and inventions: we also discover how important is, sometimes, a coffee break, permitting for scientific interactions that finally lead to great achievements. Welcome to read this and the other three interesting stories about the early days of studies at synchrotron beams, as well as the abstracts and extended abstracts of lectures and contributions of both meetings, where the coffee breaks may, again, have some influence on the paths the Science is going along.

SYNCHROTRON LIGHT NEWS

New type of intense light source reported*. February issue of *Nature Physics* provides an article by Schlenvoigt, *et al*.[a] reporting on the first successful combination of a laser-plasma wakefield accelerator, with an undulator to generate visible synchrotron radiation. With the pulsed light focused from a 5-TW optical laser into a 2-mm-wide gas jet, a beam of electrons accelerated to a peak energy of between 55–75 MeV has been obtained. The electron beam has been subsequently directed into a 1-m-long undulator producing light at the red end of the visible spectrum (with the wavelength of about 700-950 nm). This approach, that relies on the use of electron beams produced by a laser-driven particle accelerator, could substantially reduce, after some improvements, both the size and cost of synchrotron and FEL X-ray sources, the authors claim.

Free electron lasers based on the effect of self-amplified spontaneous emission (SASE-FELs) can deliver tunable, highly coherent monochromatic radiation in ultra-short pulses of only 10-50 fs and of peak power exceeding 1 GW in the wavelength range of XUV to X-rays[b]. SASE-FELs have been recognized as excellent sources capable to probe the dynamics of ultrafast processes, and to determine the structure of matter with unprecedented spatial and temporal resolution, inaccessible with other known types of radiation sources. After the theoretical predictions about a possibility of intense laser like emission at wavelengths shorter than UV have been successfully confirmed with XUV-FLASH in HASYLAB (Hamburg), the prototype of SASE-FEL facility, the construction of next three devices working in the range of hard X-rays started. SASE-FEL is a large-scale facility composed of a linear electron accelerator, a long undulator and bunch compressors (‘chicanes’) as its main parts. To initiate the SASE process in the undulator, the electron beam, in a form of a train of ultra-short bunches of possibly highest electron density, should be accelerated to energy up to a

[a] *H.-P. Schlenvoigt, K. Haupt, A. Debus, F. Budde, O. Jäckel, S. Pfotenhauer, H. Schwoerer, E. Rohwer, J.G. Gallacher, E. Brunetti, R.P. Shanks, S.M. Wiggins, D.A. Jaroszynski, "A compact synchrotron radiation source driven by a laser-plasma wakefield accelerator", Nature Physics 4 (2008) 130-133.*

[b] *R. Bonifacio, C. Pellegrini, L.M. Narduci, Opt. Commun. 50 (1984) 373–378.*

few GeV. This is achieved with a superconducting RF linear accelerator operating at an electric field that cannot exceed, at present, the intensity of about 40 MV/m. With this E-field, the accelerator should be as long as a few hundred meters to produce electron bunches of sufficient energy, making this way the whole FEL very large and expensive.

As it has been noted by Nakajima[c] in his interesting comment to the above-cited article by Schlenvoigt *et al*., the laser-plasma wakefield accelerator can be an alternative to the RF linacs applied currently at SASE-FELS. It uses the immense electric fields produced in the plasma at the focus of ultra-high intensity lasers to accelerate electrons over distances of just centimeters. That is thousands of times shorter than a conventional particle accelerator. In addition, the relative energy spread of accelerated electrons can be soon minimized to the order of 0.1% for a 1-GeV beam, with an emittance down to 0.1–1.0 π mm mrad. With these parameters an electron bunch of length as short as 10 fs, and an effective beam current of up to 100 kA could be produced without the need for a compression in chicanes. This would substantially reduce not only the accelerator, but also the required undulator length to just a few meters, instead of more than a hundred meters, that are necessary in X-FEL.

New infrared beamlines anounced.** New beamlines have been announced: (i) at FLASH, DESY, combining coherent IR pulses with the FEL radiation in the VUV spectral range[d], and (ii) at Ritsumeikan University for an infrared microspectroscopy.[e] A new beamline in this spectral range is also planned at the University of Wisconsin for medical applications[f] where multiple overlapping beams will be used to homogenously illuminate the sample area.

Upgrade for the European Synchrotron Radiation Facility.** After fourteen years of successful work of the facility, an upgrade is decided. The upgrade has an aim to maintain the ESRF at the status of one of leading third-generation light sources. In particular, up to 10 new beamlines are planned.[g]

Agreement on Collaboration*:** On April 8th, 2008, an Agreement on Collaboration between the Polish Synchrotron Radiation Society, PSRS (Polskie Towarzystwo Promieniowania Synchrotronowego – PTPS) and the Centre for Synchrotron Radiation Ltd. (Centrum Promieniowania Synchrotronowego Sp. z o.o. – CPS) has been signed. The PSRSS organisation has over 16 years experience in various forms of activity in the synchrotron users community. The CPS company has been created two years ago with the initiative of the Jagiellonian University in order to carry out the preparatory actions which eventually lead to the construction of a synchrotron light source in Poland and the creation of the National Centre for Synchrotron Radiation. The Agreement will notably contribute to the effectiveness of the mandatory actions of both institutions. In particular, the parties agree on co-ordination of their educational and scientific popularisation activities in the field of applications of the synchrotron light. The important elements of the common efforts consist in promotion of the synchrotron radiation as an exceptionally effective investigation tool in *e.g.* material engineering and medical sciences, and other fields where these methods are in Poland not widely enough used.

Meetings:**

Interaction of Free-Electron-Laser Radiation with Matter, Hamburg 2008. A workshop *Interaction of Free-Electron-Laser radiation with matter: Recent experimental achievements, challenges for theory*" is to be held on 8-10 October, 2008 at DESY, Hamburg. It is devoted to recent experimental and theoretical achievements based on studies on the interaction of intense VUV and soft X-ray FEL radiation with matter.[h]

8th National Symposium of Synchrotron Radiation Users, Cieszyn 2009. *The 8th National Symposium of Synchrotron Radiation Users* (8th KSUPS) will be organised by the Polish Synchrotron Radiation Society in co-operation with the University of Silesia in Cieszyn on 24th – 25th September 2009. Welcome!

Picked up for you by:
*J. Pełka (*), W. Paszkowicz (**,) and E.A. Görlich (***).*

[c] *K. Nakajima, "Compact X-Ray sources. Towards a table-top free-electron laser", Nature Physics 4 (2008) 92-93.*

[d] *M. Gensch, L. Bittner, A. Chesnov, H. Delsim-Hashemi, M. Drescher, B. Faatz, J. Feldhaus, U. Fruehling, G.A. Geloni, Ch. Gerth, O. Grimm, U. Hahn, M. Hesse, S. Kapitzki, V. Kocharyan, O. Kozlov, E. Matyushevsky, N. Morozov, D. Petrov, E. Ploenjes, M. Roehling, J. Rossbach, E.L. Saldin, B. Schmidt, P. Schmueser, E.A. Schneidmiller, E. Syresin, A. Willner, M.V. Yurkov, "New infrared undulator beamline at FLASH", Infrared Phys. Technol. 51 (2008) 423-425. (Proc. 4th International Workshop on Infrared Microscopy and Spectroscopy with Accelerator-Based Sources)*

[e] *T. Yaji, Y. Yamamoto, T. Ohta, S. Kimura, "A new beamline for infrared microscopy in the SR center of Ritsumeikan University", Infrared Phys. Technol. 51 (2008) 397-399. (Proc. 4th International Workshop on Infrared Microscopy and Spectroscopy with Accelerator-Based Sources)*

[f] *http://src.wisc.edu/meetings/UM2007/abstracts/ Hirschumgl_Abstract_SRC_UM2007.pdf.*

[g] *C. Detlefs, "Upgrade of An Upgrade for the European Synchrotron Radiation Facility", Synchrotron Radiation News 21 (1) (2008) 35-40.*

[h] *https://indico.desy.de/conferenceDisplay.py?confId=798.*

Synchrotrons in East–Central Europe

The latest directives of the European Council stress the need for '...improving the framework conditions for innovation and launching a new generation of world-class research facilities' not only in Pan-European dimensions but also in a regional scale.

The synchrotron radiation users community of East-Central Europe greatly contributed to recognition of the importance of the advanced medium size regional infrastructure investments '...enabling globally competitive basic and applied research'. A notable step in this direction was done at the conference "Synchrotron Facilities for the Development of Science and Technology in Central and Eastern Europe" held in November 2007 in Brno (Czech Republic). Both projects, Polish which had been pursued and developed for ten years and the Czech initiative which emerged a year ago, received then an understanding and a provisional agreement from the representatives of the European Commission institutions (DG Research and the European Strategy Forum on Research Infrastructures - ESFRI). This meant a significant change of a position which originally did not take into account the possibility even of a single synchrotron centre in this part of Europe. Another important result of this conference was working out the means of coordination of the two projects and defining the way a progress in construction of the light sources would be monitored by the above mentioned institutions.

In consequence the Memorandum of Understanding for Collaboration between Academy of Sciences of the Czech Republic and Jagiellonian University (referred further to as "MoU") has been signed on November 27, 2007 in order to achieve complementarity of designs and research possibilities of the new 3rd generation, medium sized synchrotrons in Brno and Kraków. The MoU parties expressed interest to cooperate in the technical and scientific activities involving the construction of synchrotron radiation sources and their beamlines in order to assure complementarity of both facilities. Among others the cooperation would include an exchange of technical specifications and design information, exchange of highly qualified scientists or engineers and assurance of mutual access to the beam-lines at the respective synchrotron facilities.

The construction of synchrotrons in Central and Eastern Europe was discussed in the frame of the ESFRI meeting in Brdo (Slovenia) on March 7, 2008. In order to ensure complementarity and promote an effective collaboration between the parties a committee has been appointed with the following members: Dr. Yves Petroff (France), Dr. Beatrix Vierkorn-Rudolph (Germany) and Prof. Andras Falus (Hungary).

The extended meeting of the Czech–Polish Common Board held on April 8, 2008 at Kraków

The creation of the Czech – Polish Common Board (CPCB) has been one of the prerequisites of collaboration on the synchrotron projects in our countries.

The representatives in CPCB are for the Czech Republic Ing. Vladimir Cháb (Institute of Physics, ASCR), Prof. Jiří Drahoš (ASCR), Prof. Stanislav Kozubek (Institute of Biophysics, ASCR), and for Poland Prof. Andrzej Burian (Institute of Physics, University of Silesia), Assoc. Prof. Edward A. Görlich (Institute of Physics, Jagiellonian University), Prof. Krzysztof Królas (Institute of Physics, Jagiellonian University).

On April 8, 2008 the first open meeting with six participants form the Czech Republic and eighteen participants from Poland took place in Kraków (see the photo below). The Conference was inaugurated by Prof. Karol Musioł, the Rector of Jagiellonian University. The presentations regarding the projects by the Czech and the Polish participants referred to actual organisational status, accelerator & storage ring proposals and beamlines planned at respective facilities.

In conclusion it was stated, among others, that the Czech synchrotron, which closely follows the ALBA (Barcelona, Spain) design can not be a subject of substantial changes. The Polish design will preferably use technical solutions of the Swiss Light Source (SLS) facility; while may be a subject of further studies/consultations if recommend by ESFRI experts. For the sake of complementarity this latter project will focus on a high current and time structure.

During the meeting a report with broad conclusions has been prepared and subsequently sent to Robert-Jan Smits (Director DG Research B) and Carlo Rizzuto (ESFRI Chairman). *(EAG)*

PROFESSOR BRONISLAW BURAS: THE ENERGY-DISPERSIVE METHOD AND SYNCHROTRON RADIATION

Leif Gerward*

Dept. of Physics, Technical University of Denmark,DK-2800 Lyngby, Denmark, email: gerward@fysik.dtu.dk

Abstract: In this note I am giving an account of my collaboration with Professor Bronislaw Buras during the early years of synchrotron radiation in the 1970's and 80's. In particular, I am focusing on the development of the energy-dispersive method for X-ray diffraction and its use in high-pressure structural studies. I also describe Buras' role in establishing the European Synchrotron Radiation Facility (ESRF).

Keywords: Bronislaw Buras, X-ray diffraction, energy-dispersive method, synchrotron radiation, personal recollections

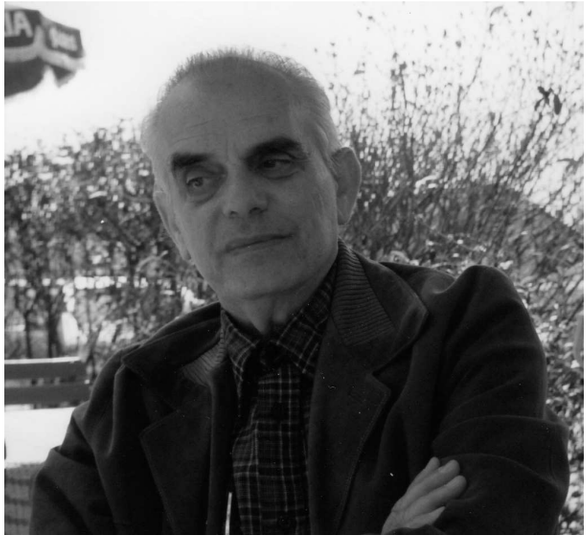

Figure 1. Professor Bronislaw Buras (1915–1994).

Photo: A. Buras.

1. Introduction

In 1971 Professor Bronislaw Buras (Fig. 1) – then a renowned physicist – immigrated with his family to Denmark. Buras was one of the inventors of the time-of-flight (TOF) method for neutron diffraction [1-3]. In the mid 1960's, he had initiated collaboration between the Institute of Nuclear Research in Świerk and the Danish Atomic Energy Commission Research Establishment Risoe (later Risoe National Laboratory) for building a TOF spectrometer at Risoe, similar to the one in Świerk and another one under construction in Dubna. The International Atomic Energy Agency had supported the project. In the beginning, the Risoe instrument was applied to powders, but the interest shifted to single-crystal methods [4]. Thanks to this earlier collaboration, it was possible to secure an academic position for Buras at the University of Copenhagen with opportunity to perform research work at Risoe.

As for myself – at that time a fresh post doc – I had got a job in November 1970 at the Technical University of Denmark (DTU) in Lyngby, where Professor Asger Lindegaard-Andersen was organizing a new Laboratory for the study of materials using X-ray diffraction methods. It was therefore very natural that we very soon took up discussions with Buras about possible common interests. This was the beginning of a lifelong and fruitful friendship and collaboration.

2. The energy-dispersive method

A few years before his arrival in Denmark, Buras *et al*. [5], and independently Bill Giessen and Glen Gordon [6], had invented the energy-dispersive method for X-ray diffraction. In this method the sample is irradiated with polychromatic radiation (the continuous spectrum) from an X-ray tube. The energy spectrum of X-rays scattered at a given angle is observed with a semiconductor detector coupled with a multichannel pulse-height analyser. The energy-dispersive method can be considered the X-ray counterpart of the neutron time-of-flight method.

Buras was of course eager to develop the energy-dispersive method further. We found it an exciting and unconventional way of looking at the Bragg equation. A joint project was set up with me from DTU, and Janus Staun Olsen from the H.C. Oersted Institute at the University of Copenhagen as the main participants. Several other colleagues were involved in the project during the course of time as seen in the list of references below.

To begin with, we repeated the original experiments [7]. We then set out doing a lot of methodological work. We reported the appearance of the silicon Kα escape peak [8], we derived simple relations between the integrated intensities of the various diffraction methods [9], and we studied the influence of polarization [10] and the optimum resolution [11]. Moreover, we extended the method to samples of single crystals [12].

3. Early experiments with synchrotron radiation

The potential use of synchrotron radiation for physical research was a much-discussed topic in the first half of the 1970's. We studied with great interest a pioneering paper by T. Tuomi *et al.* [13]. They had used synchrotron radiation in X-ray diffraction topography. It occurred to us that synchrotron radiation would be an ideal X-ray source for the energy-dispersive method in view of its high intensity, high degree of collimation, and the continuous spectrum, extending into the X-ray regime.

Dr. Christof Kunz of the German synchrotron facility DESY in Hamburg was an invited speaker at a Nordic solid-state physics meeting in Gothenburg, Sweden, in June 1975. He talked about the pioneering work with synchrotron radiation done by the DESY group. Staun Olsen and I approached him during a coffee break and mentioned that we had an experiment that seemed to be well suited for synchrotron radiation. It was agreed that we should make a test experiment at DESY. Buras, Staun Olsen and I went to Hamburg in October the same year to discuss the practical arrangements. Buras brought a two-page questionnaire, in his neat handwriting, about everything from beam characteristics to accommodation.

After a formal application, we could perform the test experiment in January 1976. The synchrotron radiation laboratory was situated in a small "bunker" close to the DESY synchrotron. The laboratory was crammed with experimental equipment. In order to get the beam on, one had to call the control room of the accelerator and ask for radiation: "*Strahlung an Bunker eins, bitte!*" In the beginning we were not even allowed to call ourselves, and a DESY technician was present all the time. The people in the control room must have been rather frustrated at our presence, since we needed to open and close the beam shutter very frequently during the test experiment.

Many people had told us in advance that our experiment was doomed to failure. The high level of background radiation at the synchrotron, so they said, would completely saturate the detector, making it impossible to record any meaningful spectrum. Therefore, we had brought a lot of lead plates to shield the detector and the diffractometer from the alleged background radiation. We started building a heavy wall of lead bricks. In one of the bricks, we had drilled a hole for a pinhole collimator. The powder sample was contained in a glass capillary placed on top of a goniometer. Burning a dark spot on a glass plate localized the incident X-ray beam (later, we used so-called green paper). A sketch of the experimental set-up is shown in Fig. 2.

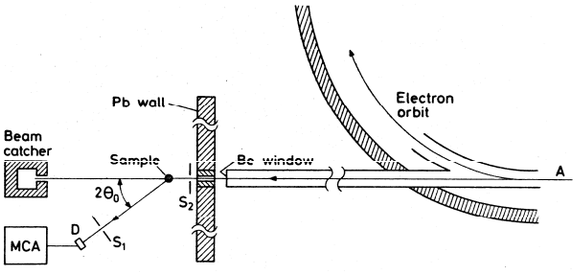

Figure 2. Experimental arrangement for the test experiment at the DESY synchrotron. $2\theta_0$ - fixed scattering angle, S_1 and S_2 - slits, A - focus point of radiation, D - semiconductor detector, MCA - multichannel pulse-height analyser.

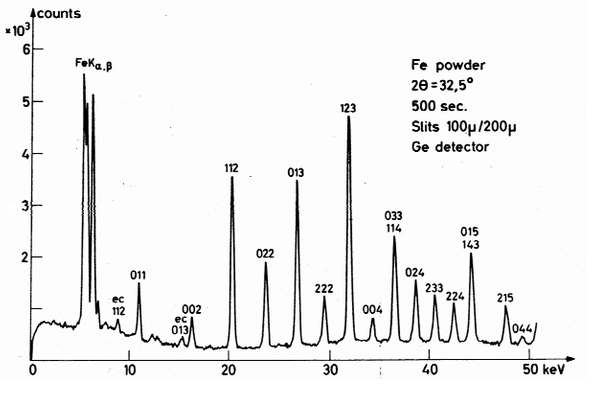

Figure 3. Diffraction spectrum of iron powder. Counting time 500 s. The Bragg angle is $\theta = 16.25°$, ec - escape peak.

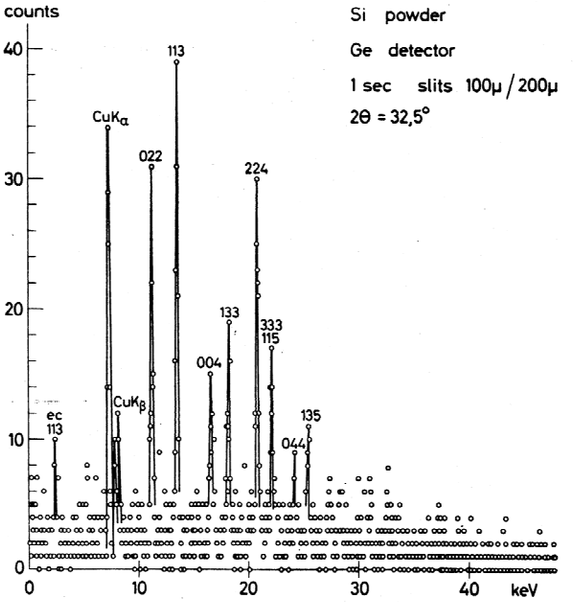

Figure 4. Diffraction spectrum of silicon powder. Counting time 1 s. The notation is as for Fig 3.

Much to our surprise, we got some rather nice diffraction spectra after a few trials with the alignment of the equipment. At the end of our beam time we boldly removed some of the lead shielding – and the spectra became even nicer! An example is shown in Fig. 3. As it turned out, we had created some background radiation ourselves with our excessive lead shielding. A one-second shot for a silicon powder (Fig. 4) demonstrated the sensitivity of the energy-dispersive method. The diffraction peaks are clearly visible, albeit with poor counting statistics, indicating that it should be possible to follow rapid phase transitions in the sample.

It was a happy group that returned home after this successful test experiment. A first note with preliminary results was quickly submitted to *Nuclear Instruments and Methods* and also published as a DESY preprint [14]. When preparing this note, we became aware of a preprint by J. Bordas *et al.* [15], who almost simultaneously had used the energy-dispersive method for small-angle scattering at the synchrotron NINA in Daresbury, UK.

Based on further work, we discussed the special features of the white-beam energy-dispersive method using synchrotron radiation in two subsequent, more detailed papers [16, 17]. We were now looking for some good physics that could be done with our method. Already in our preliminary paper [14], we had pointed out that the fixed geometry of the energy-dispersive method made it suitable for structural studies at extreme conditions, such as high pressure and high or low temperature. Accordingly, we built an oven for 50–850 ±0.25°C, and G. Will and E. Hinze of the University of Bonn introduced us to the diamond squeezer technique for high-pressure studies [18]. Later, we had our own diamond anvil cells of Syassen-Holzapfel type built at the workshop of the H.C. Oersted Institute.

Much better beam conditions could be obtained at the electron storage ring DORIS where a few beamlines were available. Together with Mike Glazer and M. Hidaka of the Clarendon Laboratory, Oxford, we demonstrated that structural refinement of the Rietveld type could be performed on energy-dispersive diffraction spectra recorded at the storage ring [19]. Figure 5 shows another one-second shot with much improved quality as compared with Fig. 4.

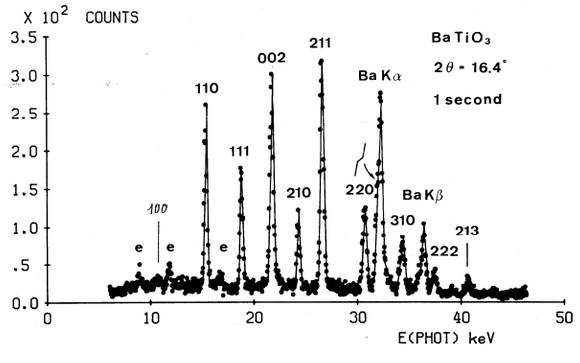

Figure 5. Diffraction spectrum of $BaTiO_3$ obtained at the DORIS storage ring. Counting time 1 s, $\theta = 8.2°$.

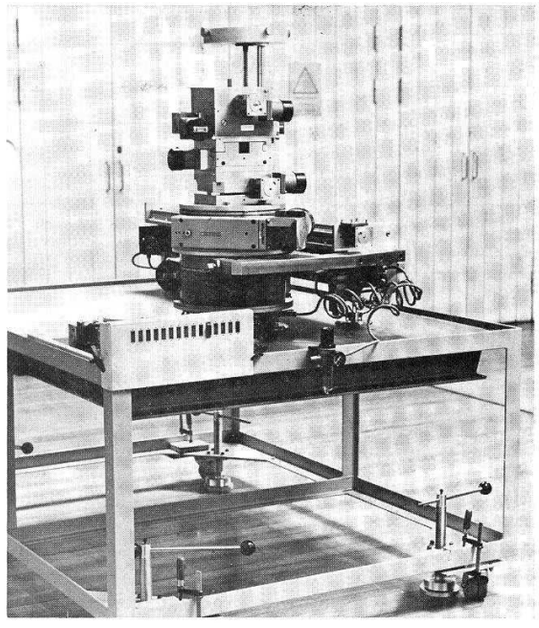

Figure 6. The energy-dispersive spectrometer (EDS).

Photo: F. Ferrall.

High-energy physicists ran DORIS, like the other accelerators of DESY, in the search for elementary particles. Synchrotron radiation was from their point of view a waste product, which was used in a "parasitic" way by us and other physicists. However, the demand for synchrotron radiation grew steadily, and it was decided to build a new laboratory hall at DORIS. Moreover, DORIS would run part time dedicated to synchrotron radiation (later it became a fully dedicated radiation source). The new laboratory, which was dubbed HASYLAB (Hamburg Synchrotron Radiation Laboratory), had 15 beamlines when it opened for the users in 1981. Later it was enlarged to 30 beamlines.

Our group became involved in constructing an energy-dispersive spectrometer for HASYLAB (Fig. 6). The main parts of the instrument were a robust Huber goniometer and a strong table with a smooth surface, on which the diffractometer and the detector arm could move on air cushions [20]. The instrument was built in the workshop of the H.C. Oersted Institute and transported to Hamburg on a truck. HASYLAB provided the electronics and a high-purity germanium detector. After some test experiments, the spectrometer was installed at beamline F3 of HASYLAB. It was going to be a workhorse for more than 25 years. In fact, the mechanical parts of the instrument are still in use, although the electronic system and the associated computer have been upgraded several times.

It should be mentioned here that scientists from Risoe National Laboratory also were heavily involved at HASYLAB. They constructed a flexible triple-axis spectrometer (Fig. 7), which was installed at beamline D4 [21, 22]. Later, Risoe implemented several other advanced instruments at the wiggler beamlines.

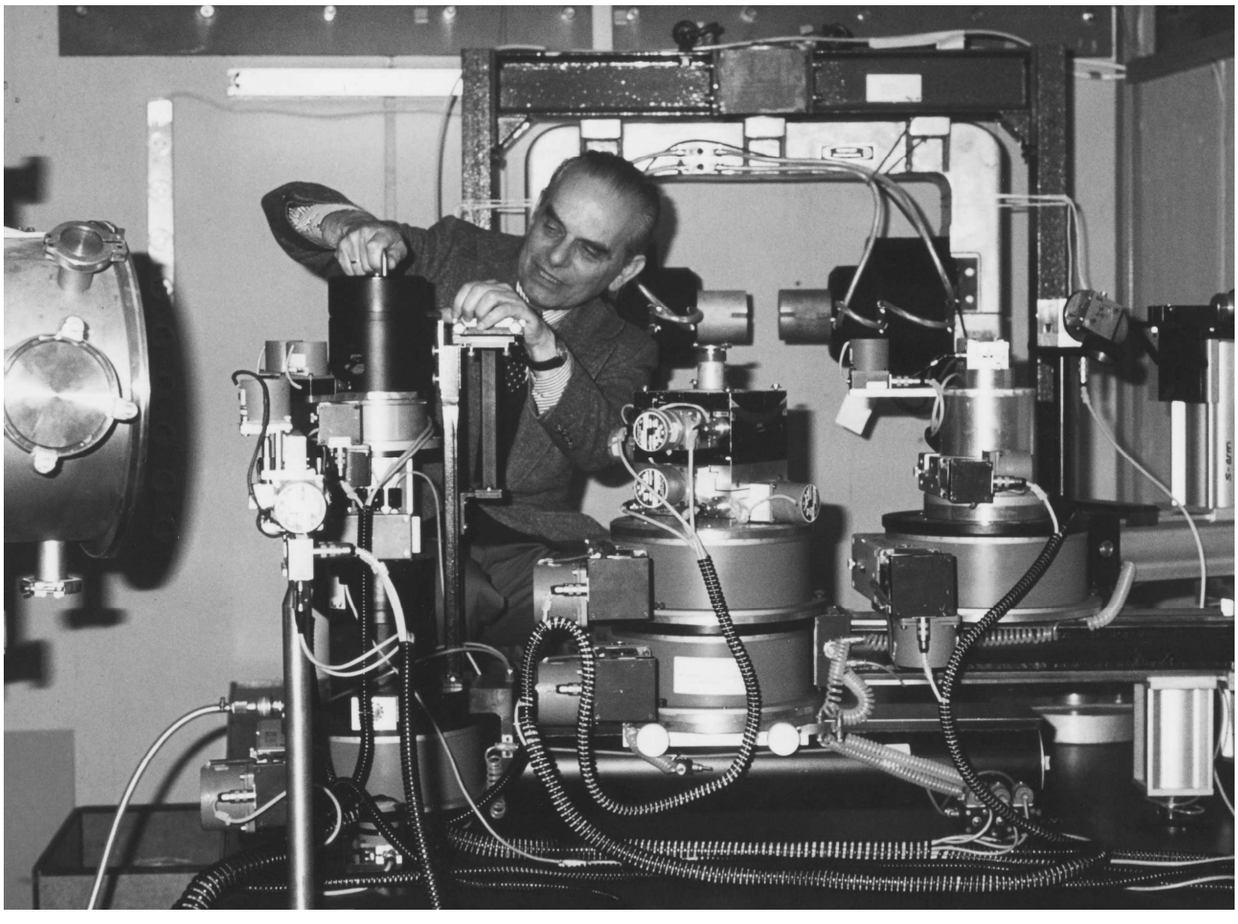

Figure 7. Buras at work, using the triple-axis spectrometer at HASYLAB (in energy-dispersive mode!).

Photo: B. Lebech.

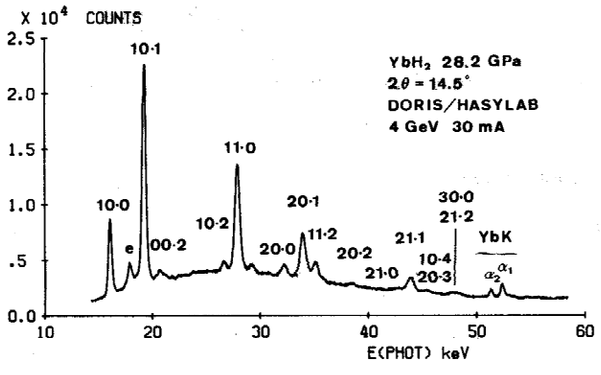

Figure 8. Diffraction spectrum of hexagonal YbH_2 at 28 GPa. Counting time 500 s, $\theta = 7.25°$.

Our first full-fledged high-pressure structural study was devoted to YbH_2. At ambient conditions, YbH_2 crystallizes in an orthorhombic structure with space group *Pnma*. By comparison with other rare-earth dihydrides it was expected that YbH_2 should transform into the fcc fluorite structure at high pressure, as the valence state of the Yb atom changes from $4f^n(5d6s)^2$ to $4f^{n-1}(5d6s)^3$.

Buras *et al*. [23] developed a high-pressure cell for neutron diffraction at Risoe, but no phase transformation in YbH_2 was observed up to 4 GPa. Using a diamond anvil cell and radiation from an X-ray tube we reached 11 GPa, but there was still no phase transformation. Using synchrotron radiation, however, it was possible to reach 28 GPa, and we clearly demonstrated a phase transformation at about 14 GPa [24].

It turned out that the high-pressure structure of YbH_2 was not fcc as expected but hexagonal (Fig. 8). Meanwhile, Bente Lebech *et al.* [25] had determined the crystal structure, including the positions of the hydrogen atoms, at ambient conditions using neutron diffraction. On the basis of their results, they suggested a high-pressure structure with space group $P6_3/mmc$ and with Yb atoms in (2*c*) and hydrogen atoms in (2*a*) and (2*d*) positions. A careful analysis showed that this suggestion was indeed consistent with our X-ray data [26].

The investigation of YbH_2 became the prototype for a long and ongoing series of high-pressure structural

studies by our group. Also internationally there was now a growing interest for the energy-dispersive method. Buras travelled to workshops and symposia in the United States to tell about the method and its application to high-pressure studies [27, 28]. Personally, I had the pleasure of representing Buras at the 1979 Spring Meeting of the American Crystallographic Association (ACA) in Boston [29]. It was my first visit to the United States, and Buras took great care in instructing me about the local conditions.

For two decades, the energy-dispersive method was *the* method for high-pressure structural studies in conjunction with the diamond anvil cell and synchrotron radiation. It is only recently that the energy-dispersive method gradually is being replaced by high-resolution angle-dispersive techniques. Still, it is an excellent method for getting a quick overview of the high-pressure behaviour of a given material.

4. European Synchrotron Radiation Facility (ESRF)

At this point I lost my almost daily contact with Buras, who was now moving on to new and greater challenges at the European level. We published a summary of our common work in a review paper [30], and in a contribution to the *International Tables for Crystallography* [31].

Particle-physics accelerators had become inadequate to meet the growing demand for synchrotron radiation. Third generation sources, which from the beginning were constructed and optimised for synchrotron radiation, were being planned in Europe and elsewhere. In the case of a European source, it was recognized that an international collaboration was needed in view of the complexity and cost of a machine for radiation in the hard X-ray regime.

H. Maier-Leibnitz presided over a working group set up in 1975 by the European Science Foundation (ESF) to study the feasibility of a synchrotron radiation source to span the entire X-ray region down to wavelengths of the order of 0.1 Å. In 1977 the ESF issued a report "Synchrotron Radiation. A Perspective for Europe", the so-called Black Book.

An ad-hoc committee was set up in 1978–79 and chaired by Y. Farge. Two subgroups were established, one dedicated to the machine and chaired by D.J. Thompson; and one dedicated to instrumentation and chaired by Buras. This work resulted in the publication of a four-volume document "European Synchrotron Radiation Facility. The Feasibility Study" (the Blue Book). An updated document "A Case for a European Synchrotron Radiation Facility" (the Yellow Book), edited by Jens Als-Nielsen, was worked out in 1980–82, incorporating new technological developments, in particular the so-called magnetic insertion devices, wigglers and undulators.

In 1983–84, a European Synchrotron Radiation Project group (ESRP) was created under the leadership of Bronislaw Buras and Sergio Tazzari and located at CERN. Its conclusions were given in "European Synchrotron Radiation Facility – Report of the ESRP" (the Green Book), describing the project goals, the source, experimental equipment, time scale, cost and construction requirements.

The location of ESRF was still undecided, and Risoe National Laboratory made a serious bid for hosting the facility [32]. However, in the end France and the Federal Republic of Germany proposed the implementation of ESRF in France and invited other countries to join. A provisional ESRF Council was formed in December 1985 to set up a construction team in Grenoble, led by Ruprecht Haensel, another synchrotron radiation pioneer from DESY. Electrons were injected into the storage ring for the first time on 17 February 1992, and the first user beamlines were installed during the autumn of 1992. The European dream of a third generation synchrotron radiation source had materialised.

5. Some personal recollections

Buras had an indomitable optimism, also in hard times, as his story of life clearly demonstrates. In the beginning of our collaboration, the experimental means were minute. We managed to raise the money for a Si(Li) detector, but the multichannel analyser was borrowed from another group, and the X-ray generator was an antiquated unit that had been delivered by the Germans shortly after World War II. Breakdowns were of course plentiful. At one occasion we removed the front panel and looked into the dusty interior. A post doc that happened to pass by exclaimed: "Look, it's brand new!" However, the experimental conditions improved as we began publishing papers on energy-dispersive diffraction.

Although he understood Danish conversation, Buras seldom used that language himself. He always communicated in English with his students and colleagues. Alan Macintosh, former head of Risoe, addressed this issue in a dinner speech at Buras' 70th birthday. In Denmark, so he said, Buras had got another native language – broken English!

Buras was an inspiring and well-liked teacher and adviser for students and colleagues. Even after having settled in Denmark, he continued to care for his former students in Poland. Buras felt most at ease at his home base, the Risoe National Laboratory. In the experimental hall, he liked to show any available neutron spectrometer to students and visitors. He always impressed by his ability to scan reciprocal space as effortlessly as other people are moving in their own sitting room.

Buras was a prolific writer and a travelling ambassador for science. He was always on the move, on his way to conferences and other meetings. In particular, he cared for the neutron time-of-flight method and its X-ray counterpart, the energy-dispersive method. These interests led him to take a great responsibility for the development of synchrotron radiation as an X-ray source in studies of materials.

In conclusion, I am deeply grateful for having had Bronislaw Buras as a mentor and colleague. During our years of collaboration I learnt a lot from his inspiring leadership and enthusiasm for scientific work, combined with a good sense of humour.

Acknowledgments: I wish to thank Wojciech Paszkowicz for suggesting this contribution to the *Bulletin of the Polish Synchrotron Radiation Society*. I am grateful to Andrzej Buras, Bente Lebech, Asger Lindegaard-Andersen and Jens Als-Nielsen for helpful discussions. Finally, I wish to thank Janus Staun Olsen for a nice collaboration over more than 30 years.

References

[1] B. Buras, J. Leciejewicz, "A time-of-flight method for neutron diffraction crystal structure investigations", *Nukleonika* **8** (1963) 75–77.

[2] B. Buras, J. Leciejewicz, "A new method for neutron diffraction crystal structure investigations", *phys. stat. sol.* **4** (1964) 349-355.

[3] B. Buras, J. Leciejewicz, V. Nitc, I. Sosnowska, J. Sosnowski, F. Shapiro, *Nukleonika* **9** (1964) 523–537.

[4] B. Buras, K. Mikke, B. Lebech, J. Leciejewicz, "Time-of-flight method for investigations of single-crystal structures", *phys. stat. sol*. **11** (1965) 567–573.

[5] B. Buras, J. Chwaszczewska, S. Szarras, Z. Szmid, *Report 894/II/PS*, Institute of Nuclear Research, Warsaw, 1968.

[6] B.C. Giessen, G.E. Gordon, "X-ray diffraction: A new high-speed technique based on X-ray spectrography", *Science* **159** (1968) 973–975.

[7] B. Buras, J. Staun Olsen, L. Gerward, B. Selsmark, A. Lindegaard-Andersen, *Energy dispersive spectroscopic methods applied to X-ray diffraction in crystals*, Monograph 73-12, Phys. Lab. II, H.C. Oersted Institute, University of Copenhagen, Copenhagen, 1973.

[8] B. Buras, J. Staun Olsen, A. Lindegaard-Andersen, L. Gerward, B. Selsmark, "Evidence of escape peaks caused by a Si(Li) detector in energy-dispersive diffraction spectra", *J. Appl. Crystallogr*. **7** (1974) 296–297.

[9] B. Buras, L. Gerward, "Relations between integrated intensities in crystal diffraction methods for X-rays and neutrons", *Acta Crystallogr. A* **31** (1975) 372–374.

[10] J. Staun Olsen, B. Buras, T. Jensen, O. Alstrup, L. Gerward, B. Selsmark, "Influence of polarization of the incident beam on integrated intensities in X-ray energy-dispersive diffractometry", *Acta Crystallogr. A* **34** (1978) 84–87.

[11] B. Buras, N. Niimura, J. Staun Olsen, "Optimum resolution in X-ray energy-dispersive diffractometry", *J. Appl. Crystallogr.* **11** (1978) 137–140.

[12] B. Buras, J. Staun Olsen, L. Gerward, B. Selsmark, A. Lindegaard-Andersen, "Energy dispersive spectroscopic methods applied to X-ray diffraction in single crystals", *Acta Crystallogr. A* **31** (1975) 327–333.

[13] T. Tuomi, K. Naukkarinen, P. Rabe, "Use of synchrotron radiation in X-ray diffraction topography", *phys. stat. sol. (a)* **25** (1974) 93–106.

[14] B. Buras, J. Staun Olsen, L. Gerward, "X-ray energy-dispersive powder diffraction using synchrotron radiation", *Nucl. Instrum. Meth.* **135** (1976) 193–195. Also *DESY SR*-76/10, April 1976.

[15] J. Bordas, A.M. Glazer, I.H. Munro, "Small-angle scattering experiments on biological materials using synchrotron radiation", *Nature* **262** (1976) 541-545.

[16] B. Buras, J. Staun Olsen, L. Gerward, "White-beam X-ray energy-dispersive diffractometry using synchrotron radiation", *Nucl. Instrum. Meth.* **152** (1978) 293–296.

[17] B. Buras, J. Staun Olsen, L. Gerward, "On the use of wide-angle energy-sensitive detectors in white-beam X-ray single-crystal diffraction", *Nucl. Instrum. Meth.* **178** (1980) 131–135.

[18] B. Buras, J. Staun Olsen, L. Gerward, G. Will, E. Hinze, "X-ray energy-dispersive diffractometry using synchrotron radiation", *J. Appl. Crystallogr.* **10** (1977) 431–438.

[19] B. Buras, L. Gerward, A.M. Glazer, M. Hidaka, J. Staun Olsen, "Quantitative structural studies by means of the energy-dispersive method with X-rays from a storage ring", *J. Appl. Crystallogr*. **12** (1979) 531–536.

[20] J. Staun Olsen, B. Buras, L. Gerward, S. Steenstrup, "A spectrometer for X-ray energy-dispersive diffraction using synchrotron radiation", *J. Phys. E: Sci. Instrum.* **14** (1981) 1154–1158.

[21] J. Als-Nielsen, *Synchrotron X-ray diffraction using triple-axis spectrometry*, Risoe-M-2268, (Risoe National Laboratory, Roskilde, 1980).

[22] J. Als-Nielsen, *An example of progress and future perspectives in X-ray synchrotron diffraction studies*. Risoe-M-2375 (Risoe National Laboratory, Roskilde, 1983).

[23] B. Buras, W. Kofoed, B. Lebech, G. Bäckström, *A high-pressure cell for neutron crystal spectrometry,* Risoe-R-357 (Risoe National Laboratory, Roskilde, 1977).

[24] J. Staun Olsen, B. Buras, L. Gerward, B. Johansson, B. Lebech, H.L. Skriver, S. Steenstrup. "High pressure diffraction studies of YbH_2 up to 28 GPa", in: *Physics of Solids under High Pressure,* J.S. Schilling, R.N. Shelton (eds.), Proc. International Symposium on Physics of Solids under High Pressure, Bad Honnef (North-Holland Publ. Co., Amsterdam 1981), pp. 305-309.

[25] B. Lebech, N.H. Andersen, S. Steenstrup, A.S. Pedersen, "Neutron diffraction studies of ytterbium dihydride: the crystal structure at 300 K", *Acta Crystallogr. C* **39** (1983) 1475–1480.

[26] J. Staun Olsen, B. Buras, L. Gerward, B. Johansson, B. Lebech, H.L. Skriver, S. Steenstrup, "A new high-pressure phase and the equation of state of YbH_2", *Phys. Scripta* **29** (1984) 503–507.

[27] B. Buras, *Some experiments with and future requirements for semiconductor detectors used for synchrotron radiation X-ray energy-dispersive diffractometry*. Workshop on X-ray Instrumentation for Synchrotron Radiation Research, Stanford Linear Accelerator Center (SLAC) (Stanford 1978).

[28] B. Buras, *Synchrotron radiation and energy-dispersive diffraction.* Symposium on Accuracy in Powder Diffraction, NBS Special Publication 567, Proceedings of a Symposium, Gaithersburg, 11-15 June 1979, S. Block, C.R. Hubbard (eds.), (National Bureau of Standards, Washington DC, 1980), 33-54.

[29] L. Gerward, B. Buras, *Special features of synchrotron radiation as applied to X-ray energy-dispersive diffraction. A review* [American Crystallographic Association (ACA), Boston, 1979].

[30] B. Buras, L. Gerward, "Application of X-ray energy-dispersive diffraction for characterization of materials under high pressure", *Prog. Cryst. Growth Charact.* **18** (1989) 93–138.

[31] B. Buras, L. Gerward, "X-ray energy-dispersive diffraction," in: C. Wilson (ed.), *International Tables for Crystallography*, Vol. C (Kluwer, Dordrecht, 1992), pp. 84–87.

[32] J. Als-Nielsen, B. Buras, *ESRF at Risoe – Denmark.* Study prepared for the Danish Science Research Council, (Risoe National Laboratory, Roskilde, 1981).

MY FIRST EXPERIENCES WITH SYNCHROTRON RADIATION

Andrzej Kisiel

Instytut Fizyki im. Mariana Smoluchowskiego, Uniwersytet Jagielloński
30 059 Kraków, ul. W. Reymonta 4, Poland

1. FIRST CONTACT WITH SYNCHROTRON RADIATION

My experience with the use of synchrotron radiation begun 33 years ago when, in January of 1975, I started my half-year fellowship sponsored by the Italian National Research Committee (CNR) in the Laboratori Nazionali di Frascati (LNF). Frascati the town famous for a nice view and excellent local vine is situated about 20 km south-east from Rome. LNF is hidden in the surrounding Frascati hills covered by the olive grows and vineyards in a very beautiful landscape typical for the Albanese mountains. My first main task in the Laboratory, carried out jointly with Emilio Burattini, was a preparation of the hydrogenated palladium thin films for the spectroscopic studies with the use of the synchrotron light radiation from the 1.1 GeV electron synchrotron as a source. The electron synchrotron (Electronsicrotrone) in Frascati constructed by the Italian National Committee of the Nuclear Energy (CNEN) started in 1958. At that time this synchrotron was the biggest electron synchrotron of the first generation in the world, applied only to the nuclear physics research. In 1967 this synchrotron has been adapted to the synchrotron radiation extraction and to the solid state physics purposes. For me, it brought also a real possibility to apply the synchrotron radiation to the optical spectroscopy analysis of palladium. A problem of absorption of huge quantities of hydrogen in Pd was known already in XIX century. However, a mechanism of this absorption and a form of hydrogen bonding in Pd has not been satisfactory explained up to the 70 years of XX century. In contradiction to the previous models of the hydrogen atoms or protons free diffusion through Pd sample, in 1971 Estman at al [1] suggested the existence of PdH compounds in the Pd/H system. Their statement was based on the photoelectron emission spectra analysis of the hydrogenated Pd samples. For the final confirmation of this revolutionary suggestion the use of other independent experimental method was necessary. The corroboration of this suggestion could be evidently supported by the spectroscopic analysis of the electronic transitions from $4p_{1/2}$ and $4p_{3/2}$ Pd core levels to the conduction band density of states for pure and hydrogenated Pd. We proposed the idea of this experiment and carried out it with the use of the unique vacuum spectrometer and electron synchrotron operating in the 30 –60 eV energy range. A several-year experience of my Italian colleagues with the use of synchrotron radiation gave a guaranty for the success of our project. Unfortunately, in course of our measurements in 1976 the electron synchrotron has been heavily damaged, then closed and in several months rapidly dismantled. This incident stopped our interest in the Pd problem and we did not return to it in our later research. From our preliminary studies of pure and hydrogenated Pd thin films remained only a publication concerning the electrical properties of the PdH thin films with which we tested a quality of samples applied to the optical measurements [2].

2. AN EXPERIENCE WITH THE ADONE STORAGE RING

Due to the damage of the electron synchrotron me and my Italian colleagues lost the unique possibility of application of the synchrotron radiation for the solid state physics. In result of his situation in Autumn of 1976 the Italian solid state physicists from the LNF and the Institute of Physics of Rome University “La Sapienza” begun very rapidly, under the auspices of professor Franco Bassani, the construction of the synchrotron radiation beam lines. At the same time, the ADONE storage ring situated in another place of the LNF has been adapted to the solid state physics purposes. ADONE storage ring which started to work in LNF in 1969 was at that time the first in the world 1.5 GeV storage ring dedicated only to the nuclear physics applications. In 1978, after two-year ADONE reconstruction and building the synchrotron radiation beam lines the PULS (Progetto Utilizzo Luce di Sincrotrone) laboratory started to work. It was used to perform experiments in the fields of atomic and molecular spectroscopy with the use of high vacuum optical spectroscopy line in 2-30 eV energy range (Mario Piacentini), material structure with the use of X-ray absorption spectroscopy (XAS) line in 2 – 6 keV energy range (Settimio Mobilio) and photo-emission line (Paolo Perfetti). In 1980 started Wiggler XAS line in the laboratory PWA (Progetto Wiggler Adone) directed by Emilio Burattini and Adolfo Savoya. Wiggler line operated in hard X-ray energy range from about 3 keV to about 30 keV with use Ge or Si monocrystals in the double crystalline monochromator. In course of the construction and commission of the experimental facilities I was present during my short visits in Frascati in several informal discussions of the Italian constructors and was also invited to the further collaboration. During one of the meetings Giorgio Margaritondo shown us his project of the trade mark of the PULS laboratory which has been accepted and later commonly used by the PULS laboratory. The first years of the work in the PULS and PWA laboratories were not easy. The synchrotron radiation beam time dedicated by nuclear physicists for

the solid state applications was for us not sufficient. The users from Italy and abroad obtained very short periods of the synchrotron radiation dedicated beam time. ADONE worked mainly for the nuclear physicists purposes, and was often applied by them in nuclear physics experiments far from the stable work conditions of the facility. It caused that ADONE was often destroyed, or at least the modifications affected instability of the electron current for a longer time. Sometimes we waited for a long time, even several days, for the successful and stable electron injections. For the above reasons the solid state experiments with the use of the synchrotron radiation proceeded slowly.

2.1. EXAFS analysis for $Cd_{1-x}Mn_xTe$

As I remember, I obtained the first dedicated beam time from ADONE in 1979 to realize a project concerning EXAFS studies of the local disorder in $Cd_{1-x}Mn_xTe$ ternary compounds. As it is well known, at that time the unique and the best high quality $Cd_{1-x}Mn_xTe$ monocrystals in the world were produced by Professor Witold Giriat at the Institute of Physics of the Polish Accademy of Sciences in Warsaw. $Cd_{1-x}Mn_xTe$ ternary compounds were intensively studied for their very interesting electrical, magnetic and optical properties. Also me and my group from the General Physics Department of the Jagellonian University started the studies of the electronic structure of $Cd_{1-x}Mn_xTe$ with the use of the fundamental reflectivity of light. The smearing of the distinct fundamental reflectivity structure with increase of the Mn content suggested some form of the local disorder inside the monocrystalline structure [3]. It was very strange because the diffraction analysis for this monocrystals showed an excellent crystalline order. We expected the EXAFS analysis to be able to give us a correct answer. Anyone who remembers the political situation in Poland at the end of 70th will understand well that organization of the periodic visits abroad from the communistic country was not simple. My close contact with the Italian colleagues and their understanding of our political situation resulted in the direct collaboration agreement between the Institutes of Physics of the Jagellonian University and the Rome University La Sapienza. This agreement allowed me and my Polish collaborators to start and to continue the suggested by us program in the PULS laboratory. Our collaborating group consisted from the Polish side of Marek Czyżyk, Marek Podgórny, Marta Zimnal-Starnawska and me and from the Italian side of Francesco Antonangeli, Adalberto Balzarotti, Nunzio Motta and Mario Piacentini. Our relatively rare visits in Frascati and very limited runs of the synchrotron radiation dedicated beam time caused a slow progress of our measurements. Often breaks of the ADONE created a nervous atmosphere when we waited for the start of storage ring. We were also not free from the events of misfortune. I remember well one our spring visits in Frascati (probably in June 1981) when Adalberto and me waited without result for several days for the synchrotron radiation beam. Finally, on Sunday which was the last day of our dedicated time, ADONE started fortunately to work in the morning. Unfortunately, our happiness was very short, at noon a spring storm arrived and a lightning blew into the LNF power station. A very short jump of the voltage in the net was sufficient to switch off the electron beam in ADONE storage for the next 24 hours. In this moment it occurred clearly for us that we had just lost our last chance of the measurements for at least next half a year. The complete experimental EXAFS results for Cd and Te L and Mn K edges were finally ready in 1982 and were presented during the International Conference on EXAFS and Near Edge Structures held in Frascati [4]. We considered our results and the research supposition as unique, but also found out during this Conference that J.C. Mikkelson and J.B. Boyce presented a very similar communication with their excellent EXAFS experimental results for ternary $Ga_{1-x}In_xSb$. This news had some dramatic aftertaste because we understood that we should very quickly publish our results with a full theoretical explanation. Mikkelson and Boyce published their EXAFS experimental results for $Ga_{1-x}In_xSb$ earlier than us, however with not correct theoretical explanation [5]. As I remember, our correct statistical model for $Cd_{1-x}Mn_xTe$ describing EXAFS experimental results arose during very hard discussions with Adalberto Balzarotti during his visit in Cracow. Our approach [6,7] cited later in the literature as a “rigid cation model” explained correctly also the Mikkelson and Boyce experimental results for $Ga_{1-x}In_xSb$ and measured later by us EXAFS results for CdZnTe and ZnMnS. Very intensive EXAFS studies in the period of 1980 - 86 for several semiconducting ternary compounds crystallizing in the zinc blende structure were very fruitful. We published more than 15 articles and conference communications cited often by other authors. This group of our publications were granted the Awards of the Minister of the Polish Ministry of the High Education and of the Secretary of the Polish Academy of Sciences.

2.2. Fundamental Reflectivity and XANES studies

As the time passed, the interest of the nuclear physicists in ADONE was smaller, thus the optical and x-ray absorption spectroscopy measurements in PULS and the acess to PWA laboratories becme easier and they worked without greater surprises. Our main interest in the band structure analysis directed us to the studies of the fundamental reflectivity of many semiconducting compounds in the vacuum ultraviolet energy range. To this investigations we used the vacuum ultraviolet optical line with the Hilger & Watts monochromator, presented in Fig.1. The first article on the fundamental reflectivity in the vacuum ultraviolet up to 30 eV for ZnTe, CdTe and HgTe commonly with Mario Piacentini , Nicola Zema and Francesco Antonangeli was published in 1986 [8]. Parallel to the optical investigations of the valence and conduction bands structure we studied the conduction band structure with the use of XANES analysis also for binary and ternary semiconducting compounds from II–VI group. We presented the first results of this activity together with Emilio Burattini and Giusppe Dalba during the International Conference on

the Physics of Semiconductors in Warsaw in 1988 and next year during the 2nd European Conference on the Progress in X-ray Synchrotron Radiation Research in Rome [9]. Since then Emilio Burattini and Mario Piacentini have very closely and effectively collaborated with us. At the Rome Conference in 1989 a group of several European physicists erected the European Synchrotron Radiation Society (ESRS). I was also in this group and, as the founder member of the ESRS, I stood the first representative of Poland in this Society. One a half year later, in February 1991 the late Professor Julian Auleytner and me organized in Cracow the First Symposium of the Synchrotron Radiation Users. During this Symposium the Polish Synchrotron Radiation Society was erected, officially registered in May 1991. I am not certain but I believe that PSRS was the earliest registered national synchrotron radiation society in Europe.

3. **Final Remarks**

My experience with synchrotron radiation is still alive and maintains up today and, what is not strange, is mainly connected with Italy. Me and my colleagues worked in Italy up to the time of closing of ADONE in 1993 and later when we started to use the ELETTRA storage ring in Trieste. We returned again to Frascati when there started the infrared and X-ray absorption of the synchrotron radiation lines installed in the DAFNE storage ring. My long and close contact with Italy has two sides: a scientific and personal. In Italy I found a very convenient technical conditions to my scientific activity and very inspiring Italian collaborators, and what is for me even more important, I found there some true friends. These friends allowed me and my family to fell in love in the beautiful Italy and to feel well in Italy as in our second patrimony. I am very grateful to them for that.

References

[1] D.E. Eastman, J.K. Cashion, A.C. Switendick, *Phys. Rev. Lett.* **27** (1971) 35

[2] F. Antonangeli, A. Balzarotti, A. Bianconi, E. Burattini, P. Perfetti, A. Kisiel, *phys. stat sol. (a)* **42**, (1977) K44.

[3] M. Zimnal-Starnawska, M. Podgórny, A. Kisiel, W. Giriat, W. Demianiuk, J. Żmija, *J. Phys. C* **17** (1984) 615.

[4] F. Antonangeli, A. Balzarotti, N. Motta, M. Piacentini, A. Kisiel, M. Zimnal-Starnawska, W. Giriat, in: *Proc. Internat. Conf. omEXAFS and Near Edge Structures*, ed. by A. Bianconi, L. Incoccia, S. Sticich (Springer Verlag, Berlin 1983).

[5] C. Mikkelsen, J.B. Boyce, *Phys. Rev. Lett*. **49** (1982) 1412; *Phys. Rev. B* **28** (1983) 7130.

[6] A. Balzarotti, M. Czyżyk, A. Kisiel, N. Motta, M. Podgórny, M. Zimnal-Starnawska, *Phys. Rev. B* **30** (1984) 2295.

[7] A. Balzarotti, N. Motta, A. Kisiel, M. Zimnal-Starnawska, M.T. Czyżyk, M. Podgórny, *Phys. Rev. B* **31** (1985) 7526.

[8] A. Kisiel, M. Zimnal-Starnawska, F. Antonangeli, M. Piacentini, N. Zema", *Il Nuovo Cimento* **8D** (1986) 436.

[9] A. Kisiel, G. Dalba, P. Fornasini, M. Podgórny, J. Oleszkiewicz, F. Rocca, E. Burattini, *Proc. 19th Internat. Conf. on the Physics of Semiconductors*, Warsaw, Ed. W. Zawadzki, 1988, pp. 921–924s;. *Phys. Rev. B* **39** (1989) 7895–7904.

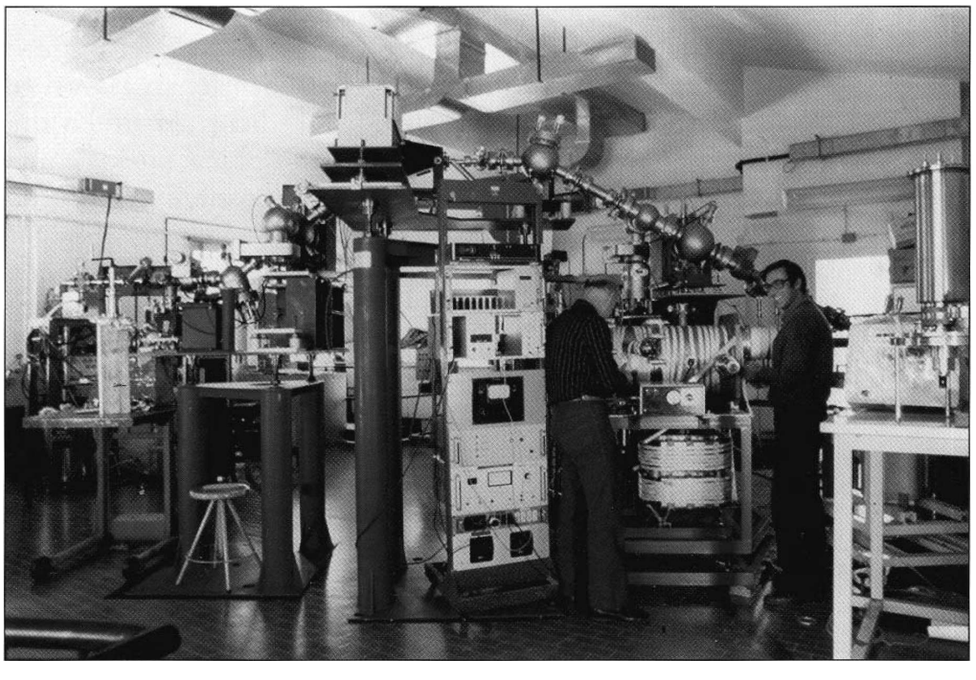

Figure 1. Adolfo Savoya and the author of this article (turned back) at the PULS optical line in the year 1980.

INVESTIGATION OF DIAMONDS AT SRS IN DARESBURY AND AT ROYAL HOLLOWAY COLLEGE

W.K. Wierzchowski

Institute of Electronic Materials Technology, 01-919 Warsaw, ul. Wólczyńska 133

As one of the early Polish synchrotron users, the author describes his synchrotron topographic experiments with diamonds at Daresbury during his employment as postdoctoral research assistant at London University from 1988 till 1991.

Keywords: Daresbury, synchrotron, diamond, topography

My synchrotron activities started in October 1988, when I was employed as a postdoctoral research assistant at the Royal Holloway College, one of the colleges of London University. More exactly, in that period the name of the college was "Royal Holloway and Bedford New College" as it had been recently joined with Bedford College but later the college came back to the historic name.

Royal Holloway College is located close to the Great Windsor Garden in a nice campus between two small suburbs of London, Egham and Englefield Green. It was established on the base a former school for women founded by Thomas Holloway. He was a famous Victorian drug maker, a great philanthropist and an admirer of science and philosophy. The main building of the college, the so called Founders Building was designed by Sir William Crossland borrowing some concepts from the Chambord castle. It is, however, much smaller and furnished in red Victorian brick. The interesting thing was, that a part of the campus was considered as the possible location for the first British synchrotron.

I was the third Polish scientist participating in topographic investigations at Daresbury Laboratory after Marian Surowiec and Grzegorz Kowalski. At that time, synchrotron topography was very popular among Polish scientists and two other persons were making topographic experiments at HASYLAB in Hamburg.

My position was partly supported by De Beers diamond concern and the main subject of the investigations were synthetic and natural diamonds. The synchrotron investigation were an integral part of my activity, together with the conventional X-ray diffraction topographic experiments at the college. During my two years and nine month stay at RHBNC I took part in almost twenty five-days synchrotron experimental tours. The conventional X-ray investigations were very similar to my former activities at my Institute.

The important and very interesting novelty was the material – particularly large synthetic diamonds already attaining high crystallographic perfection. The large diamonds were obtained using the reconstitution method, which involves replacing the commonly used graphite carbon source with powder from small synthetic diamonds, preventing the change of carbon solution in longer processes of growing large diamonds.

Figure 1. A fragment of the Founders Building at the Royal Holloway College designed by Sir William Crossland.

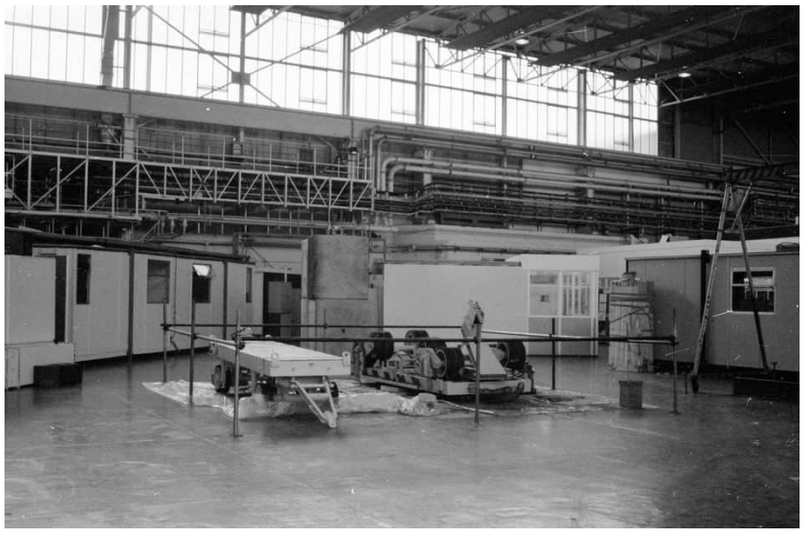

Figure 2. The view of the 7.6 "topographic" station in the SRS experimental hall at Daresbury Laboratory.

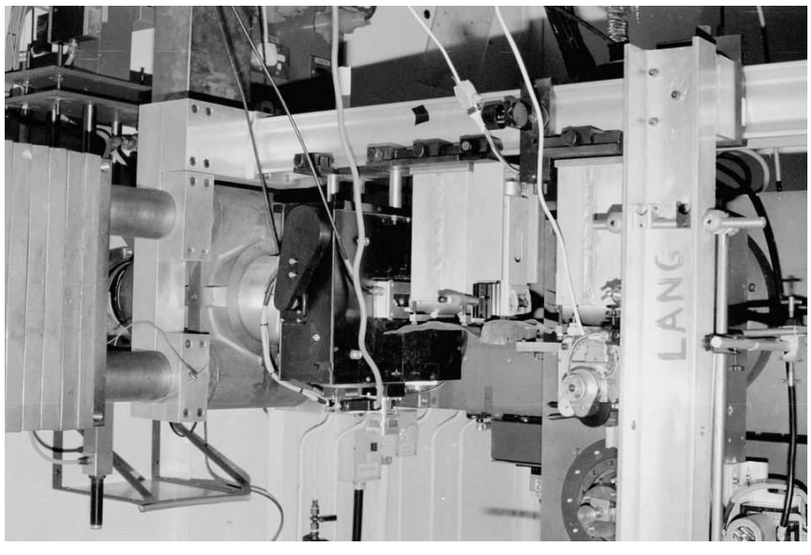

Figure 3. Our typical experimental setup constructed using a lot of additional mechanical items.

At that moment, almost twenty years ago, diamonds with the diameters greater than 1 cm were already grown, but the growth processes were long and expensive. These, being the subject of our studies (grown by De Beers and Sumitomo) were up to 5 mm in diameter. From the point of view of topographic experiments, a very pleasant feature of the diamond is its composition of very light atoms resulting in low attenuation of the second wave-field. Consequently, a large amount of various interference fringes is often present in the topographs.

My supervisor, Professor Moreton Moore was not only a brilliant scientist but also an activist to the local community. In the last few years he was elected as the Mayor of historical Runnymede county. Our team usually included also one or two PhD students, but a very important thing was a close cooperation with Professor Andrew Lang FRS from Bristol University, who was formally retired but is still scientifically active until today. Andrew Lang is acknowledged as the inventor of X-ray topography, as he first proposed a really matured and good working topographic method. He took part in more than a half of our Daresbury synchrotron experiments. It was for me a great pleasure to observe Andrew Lang at experimental work and learn his way of doing very good scientific work using relatively simple but very clever ideas.

The main topic of our investigation were the exact measurements of lattice parameters differences, between different growth sectors in large crystals of synthetic diamond, connected with different concentration of nitrogen. At that time the important problem in the synthetic diamond was the common presence of nitrogen impurity and its strong segregation in various growth sectors causing a considerable stress on growth sector boundaries.

The principle of our measurements of lattice parameter differences was not very complicated but the evaluations had to be performed very systematically. They were based on a huge number of topographs exposed in series passing a diffraction peak for different azimuths. The growth sectors were carefully identified not only on the base of crystallographic planes but also by observation of the cathodoluminescence features, providing very impressive colour patterns [1].

In the course of studying many synthetic and natural diamond we looked for various interference effects. My

personal interest was mostly connected with the formed sample plate prepared from a cuboctahedral synthetic diamond grown by Sumitomo, by cutting off the areas of cubic vertex (one close to the seed) and other plates cut out from De Beers [2]. The interesting observation was some very intensive interference fringes in synchrotron transmission double crystal measurements, shown in Fig. 4,which finally we succeed to attribute to some growth sector boundaries. According to Andrew Lang's suggestion, to solve the problem we performed an experiment adopting the "Haruta pairs" technique to the case of transmission double crystal topographs – completing the pairs from a numerous series of double crystal topographs [3, 4] .

Figure 4. The interference fringes observed in the synchrotron transmission double-crystal crystal topograph of the Sumitomo synthetic diamond, taken in a $2\bar{2}0$ reflection of the 0.1 nm radiation. The fringes appear on dislocations, stacking faults and some growth sector boundaries [4].

Figure 5. The back reflection (Bragg-case) synchrotron double-crystal topograph of (001) oriented diamond plate in 113 reflection of 0.154 nm radiation revealing interference fringes in images of the two stacking faults [7].

At some moment I was also able to propose some experiments of my own. In particular, I proposed an experiment involving observation of the transmitted beam images of also in Bragg case, which was fully published very recently [5]. The other experiment involved revealing the interference fringes in Bragg-Case double crystal topographic images of stacking faults, shown in Fig. 5, which were also explained theoretically on the basis of classical dynamical theory [6, 7]. Some interference effects were also observed using the section topography (spherical wave diffraction) in Bragg case both for dislocations [8] and stacking faults [9].

In case of natural diamonds the most important investigation concerned some new diffuse scattering effects observed with synchrotron double crystal arrangement on Ia type natural diamonds containing the so called "platelets", also caused by incorporation of nitrogen [10].

After finishing my period of employment in 1991 I had a three years break and I came back to synchrotron topographic experiments in 1994 at HASYLAB. But that is another story.

References

[1] A.R. Lang, M. Moore, A.P.W. Makepeace, W. Wierzchowski, C.M. Welbourn, "On the dilatation of synthetic type Ib diamond by substitutional nitrogen", *Philos. Trans. R. Soc. Lond. A* **337** (1991) 497.

[2] W. Wierzchowski, M. Moore, A.P.W. Makepeace, A. Yacoot, "X-ray topographic studies and measurement of lattice parameter within synthetic diamond grown by the reconstitution technique", *J. Cryst. Growth* **114** (1991) 209.

[3] M. Moore, A.R. Lang, W. Wierzchowski: "The stereoscopic observation of synthetic diamond with Haruta-pairs of synchrotron double-crystal topographs", *Acta Phys. Polon. A* **85** (1994) 53.

[4] M. Moore, W. Wierzchowski, "The transmission double-crystal synchrotron studies of synthetic diamond with Haruta stereo-pairs technique", *Philos. Trans. R. Soc. Lond. A* **357** (1999) 2671.

[5] W. Wierzchowski, M. Moore, "Bragg-case K_g and K_0 beam double-crystal synchrotron studies of growth sectors and dislocations in synthetic diamonds", *J. Appl. Phys.* **101** (2007) 053518.

[6] W. Wierzchowski, M. Moore, "Observation of interference fringes in Bragg-case synchrotron double-crystal images of stacking faults in diamond", *Acta Phys. Polon. A* **82** (1992) 185.

[7] W. Wierzchowski, M. Moore, "Bragg-case images of stacking faults", *Acta Crystallogr. A* **51** (1995) 831.

[8] W. Wierzchowski, M. Moore, "The images of dislocations in synchrotron Bragg-case section topography of diamond", *Acta Phys. Polon. A* **82** (1992) 193.

[9] M. Moore, W.K. Wierzchowski, "Bragg-case section topographic images of stacking faults in diamond", XVIIIth IUCr Congress & General Assembly 4th-13th August 1999 Glasgow, Scotland, Abstracts P 05.1. 018, *Acta Crystallogr. A* **55** (1999) 543.

[10] M. Moore, R. Waggett, W. Wierzchowski, "Synchrotron spike topography of natural type Ia diamond", *Diamond Relat. Mater.* **2** (1993) 115.

DARESBURY LABORATORY IN THE 1980s – BRISTOL UNIVERSITY X-RAY GROUP

G. Kowalski

Institute of Experimental Physics, University of Warsaw, Hoża 69, 00-681 Warsa,w Poland

e-mail: kowal@fuw.edu.pl

Keywords :Synchrotron radiation, X-ray diffuse scattering, X-ray double refraction, topography

Abstract: In 1980's, the SRS Daresbury laboratory was the site of the first dedicated synchrotron source. Bristol University H.H.Wills Physics laboratory X-ray group with A.R.Lang as a leader was the place where splendid experimental ideas for the use of synchrotron source were born. From many there obtained experimental results only two were selected for this paper since they represent non-standard experimental approach which could be of interest even in the days when personal computing and new electronic equipment can allow us now for superb experimental advances. Diffuse scattering form static lattice disorder rand X-ray double refraction experiment are real highlights of the all experiments performed at Daresbury source in 1985.

SRS Daresbury Laboratory, mid-way between Liverpool and Manchester, is the site of the first (in 1980 the only one world wide) dedicated UK's synchrotron radiation source. Established mainly for the academic research, it also serves the needs of other scientific institutions as well as industry. Today, UK and foreign scientific community have to their disposal a second laboratory, the DIAMOND synchrotron source newly build and opened for the users in 2007 at Harwell campus...

Going back to year 1984, I was given a unique opportunity to work in UK with the Bristol University X-ray group. The group was headed by Prof. Andrew Lang, the collaboration with whom was a great experience for me. The "Lang topographic camera" is a world wide well known piece of equipment every X-ray lab was equipped with in those days. He was designer inventor of the method and our guru in the subject. We have met at Crystallography Congress in Hamburg in August 1984 and after quick discussion between Andrew, Yves Epelboin and myself I was given unique chance to join the Bristol group. Considering that I was following the footsteps of Norio Kato, Satio Takagi, André Authier and many other "names" in the X-ray world who have visited Andrew Lang's Lab, not forgetting the Lang's PhD students like Mike Hart one may imagine how I was delighted.

Shortly after my arrival at Bristol University in January 1985 I had to quickly learn about diffuse X-ray scattering in depth since our first visit to Daresbury SRS laboratory was planned for beginning of February 1985 and that was the subject of my first synchrotron experiment with A.R. Lang and collaborators. Diffuse X-ray reflections are commonly studied by monochromatic incident beam of X-rays and can either deal with "normal" thermal vibrations, or as in our, case permit to study static disorder of the crystal lattice. Our specimen was a natural diamond of spectroscopic type 1a [1] which contained so called "voidites" – submicroscopic defects we can envisage as voidlike (empty) volumes bound by {111} crystallographic planes, the presence of which give rise to specific star-like scattering pattern (Fig. 1). That was quickly published in *Philosophical Magazine* and in *Daresbury Newsletter* [2, 3].

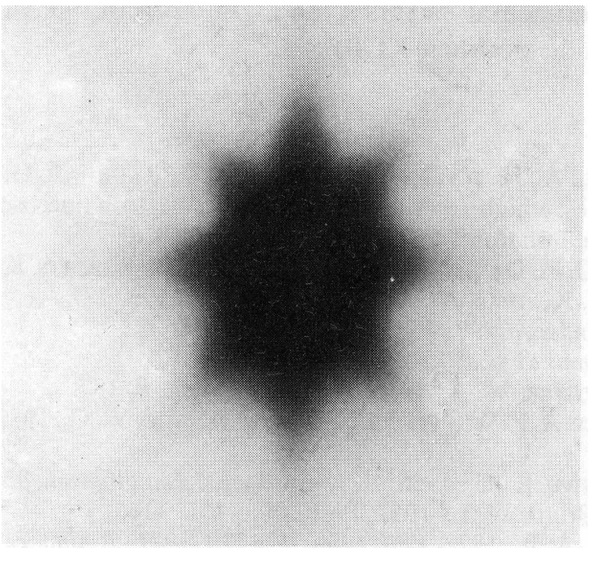

Figure 1. Diffuse scattering pattern observed from (111) growth sector of diamond. 400 reflection in symmetrical transmission.

That particular work as well as almost all other during my first three years long visit to Bristol University was done at station 7.6 at the end of so called topography line which in those days was probably the longest one (80 m) at any available synchrotron source (Fig. 2).

Figure 2. Topography line with 7.6 station hutch at the end (yellow box further away). The one in the foreground was station 7.2.

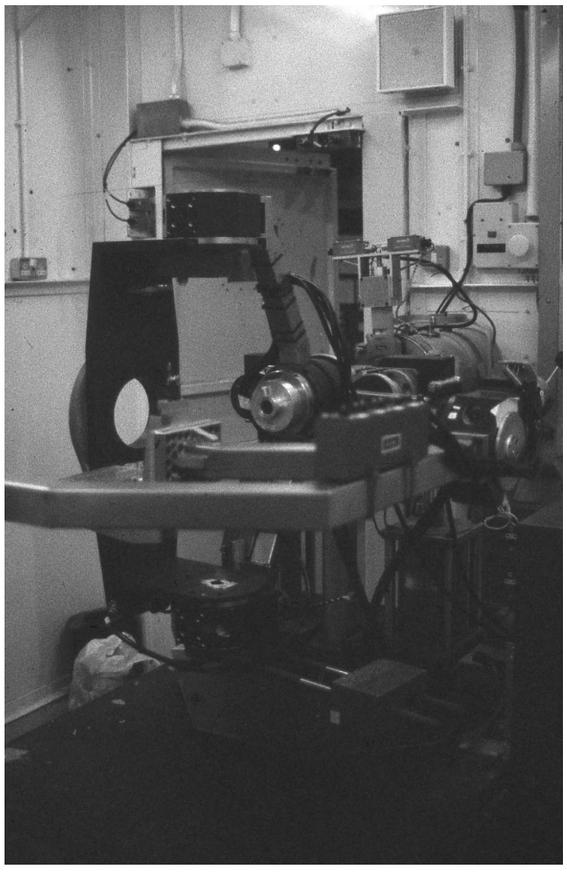

Figure 3. White beam topography camera, no longer in SRS. It was replaced by double crystal camera later and extensively used by our group.

The 7.6 hutch housed in those days a topographic camera (Fig. 3) which was later replaced by a dedicated double crystal camera.

Today, the station 7.6, reconstructed already for several times serves as x-ray optics test bench although it still houses the DC camera. Another highlight of my stay in Bristol and in Daresbury, where we spent, at the local laboratory hostel, many beam-hours as well as beam-days, was another excellent idea by Andrew Lang, namely the observation of double refraction of X-rays. Andrew was always full of splendid ideas for experiments as well as for constructing his own apparatuses to recompense the lack of specific equipment at Daresbury. Our locker close to 7.6 station was already full of Andrew inventions and we have constructed more equipment later as well. Special type of cameras, film holders, arms of every kind together with first motorised and computer driven film plate mover for taking multiple topographs on one plate. We should remember that those were very early days of PC computing and we did have, from Tony Makepeace, the so-called BBC type computer with BASIC language system only, not even IBM like PC. The topography camera in 7.6 hutch was driven by simple software from Texas Instruments programmable calculator. That was really great fun since I was given the function of main computer operator (including the Texas Instruments). It was simply because I was preparing for our X-ray group in Bristol all simulations packages for x-ray experiments like stacking fault contrast study, Borrman–Lehmann fringes, rocking curves calculations and whatever of smaller calibre was necessary [4,5].

The refractive index, n, of X-rays can be simply written as $n=1-\delta$ where δ is in the range of 10^{-5} to 10^{-6} and depends on electron density of the material,

wavelength and $r_0=e^2/mc^2$ – the classical electron radius. That is when we are far from any Bragg reflection. But when we have the crystal Bragg diffracting, the matter is different since one of the branches of dispersion surface can lead to the situation when refractive index can be greater then unity (Fig. 4). That was very elegantly shown by Andrew Lang designed experiment, with the help of synchrotron source since large intensity was a must [6].

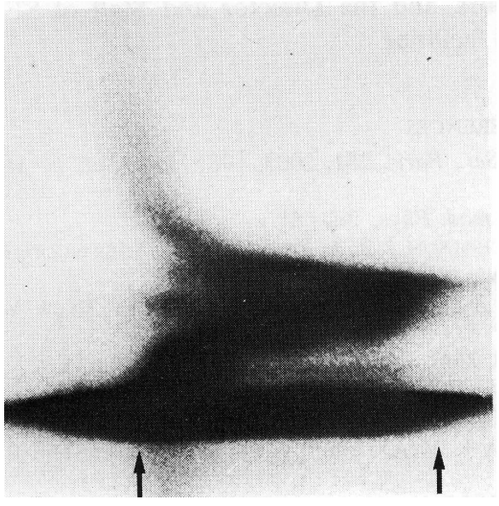

Figure 4. Refraction pattern of X-rays. We have used 111 Bragg reflection to produce a beam of Bragg diffracted X-rays directed towards the upper crystal surface to be later refracted and recorded on the photographic plate. Faint shadow close to the left hand arrow is the x-ray beam refracted with *n* value greater than unity. That phenomenon was reported for the very first time by our group.

Many other beam-hours and days we spend at SRS Daresbury ring but that first year 1985 was really a milestone. I would like to thank all colleagues and friends from Bristol Physics Department and Royal Holloway College University of London for their help and advice which was invaluable, thanks to Andrew Lang, Tony Makepeace and Moreton Moore (Fig. 5).

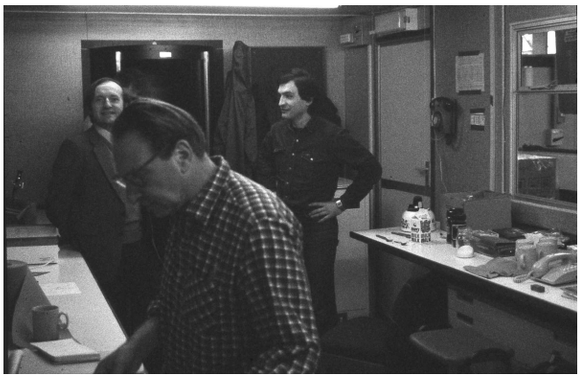

Figure 5. Inside the sample preparation and dark room area for 7.6 station. A.R. Lang in the front, and M. Moore and the author in the background.

SRS Daresbury laboratory will close for users and will be shutdown in September of this year (2008) maybe it was time to write about those early days.

References

[1] J.E. Field, *Diamond: Properties and definitions*, Booklet (Cavendish Laboratory, Cambridge, UK, 1983).

[2] A.R. Lang, G. Kowalski, A.P.W. Makepeace, M. Moore, "Recording diffuse X-ray reflections with continuous synchrotron radiation. An application to type la diamond", *Philos. Mag. A* **52** (1985) L1-L6.

[3] A.R. Lang, G. Kowalski, A.P.W. Makepeace, M. Moore, "Absorption edge eclipsing: an aid to diffuse reflection studies with white X-radiation", *SRS Bull.* **6** (1985) 9-15.

[4] G. Kowalski, A.R. Lang, "Developments in computer simulation of X-ray diffraction contrast images of stacking faults", *J. Appl. Crystallogr.* **19** (1986) 224-228.

[5] G. Kowalski, A.R. Lang, "Borrmann-Lehmann interference patterns - experiments and simulations", 14-th Congress of the International Union of Crystallography, Perth, Australia, 1987, Collected Abstracts, *Acta Crystallogr. A* **43** (1987) C-220.

[6] A.R. Lang, G. Kowalski, A.P.W. Makepeace, M. Moore, "Direct observation of double refraction of X-rays undergoing diffraction by a perfect crystal", *Philos. Mag. B* **53** (1986) L53-L58.

KRZEM JAKO WZORZEC W BADANIACH WSPÓŁCZESNYCH MATERIAŁÓW

J. Kucytowski [1*] i K. Wokulska [1]

[1] Instytut Nauki o Materiałach, Zakład Krystalografii, Uniwersytet Śląski, 40 – 007 Katowice, ul. Bankowa 12

Słowa kluczowe: kryształy krzemu, parametr sieciowy, metoda Bonda.

**) kucyto0@konto.pl*

Streszczenie: W pracy przedstawiono możliwości zastosowania krzemu jako materiału wzorcowego do wyznaczania parametrów sieciowych. Przeanalizowano wartości parametrów sieciowych zarówno polikrystalicznego jak i monokrystalicznego krzemu. Uzyskane w Instytucie Nauki o Materiałach wartości parametrów sieciowych monokryształu krzemu przy pomocy metody Bonda porównano z danymi literaturowymi.

Abstract: In this work, possibilities of application of silicon as a standard reference material to the lattice parameter determination are shown. The values of the lattice parameters of polycrystalline silicon and silicon single crystals are analyzed. The values of lattice parameters of silicon single crystals obtained in the Institute of Materials Science, Silesian University, by the Bond method are compared with the literature data.

1. Wstęp

W badaniach materiałowych oczekuje się obecnie nie tylko dużej precyzji pomiarów, ale i ich udokładnienia. Szczególnie wyraźnie widać to w badaniach strukturalnych, gdzie wykorzystuje się coraz doskonalsze techniki pomiarowe, komputerową rejestrację wyników i numeryczną analizę danych. Dzięki temu stało się możliwe uzyskanie wartości parametrów sieciowych z wysoką dokładnością. W pomiarach parametrów sieciowych precyzja wyznaczenia odległości międzypłaszczyznowych ograniczona jest precyzją profilu linii dyfrakcyjnej i jej intensywnością, a także kątem ugięcia θ. Profil linii dyfrakcyjnej i jej intensywność w dużym stopniu zależy od geometrii wiązki kolimatora, rozbieżności wiązki rentgenowskiej jak również funkcji odbicia kryształu. Ważnym również czynnikiem jest sama aparatura badawcza (tj. kolimacja wiązki rentgenowskiej).

Ponieważ zgodnie z równaniem Bragga wyznaczenie odległości międzypłaszczyznowej, która posłuży do wyznaczenia parametrów komórki elementarnej kryształu jest powiązana nie tylko z długością fali promieniowania rentgenowskiego, ale również z określeniem kąta θ metody stosowane w pomiarach parametrów sieciowych monokryształów różnią się znacząco dokładnością ich wyznaczenia. W tradycyjnych metodach pomiaru parametrów sieciowych w których wykorzystuje się kliszę fotograficzną (np. metoda obracanego monokryształu) dokładność wyznaczenia odległości międzypłaszczyznowej jest w granicach $\Delta d/d = 1\cdot10^{-3}–1\cdot10^{-4}$. Przy wykorzystaniu specjalnych metod badania monokryształów, między innymi stosując np. goniometr trójkołowy dokładność ta wzrasta do $\Delta d/d = 1\cdot10^{-4}–1\cdot10^{-5}$.

W celu zwiększenia dokładności i precyzji wyznaczenia odległości międzypłaszczyznowych stosowane są metody, w których wykorzystuje się dyfraktometrię wielokrystaliczną. Metody te polegają głównie na wyeliminowaniu wpływu asymetrii linii rentgenowskiej. Do metod tych zalicza się między innymi metody dyfraktometrii dwukrystalicznej, wielowiązkowej dyfraktometrii i topografii dwukrystalicznej. Metody te pozwalają uzyskać wysoką precyzję pomiaru w granicach $\Delta d/d = 10^{-7}$, a maksymalnie $\Delta d/d = 10^{-9}$ w metodach opartych o interferometrię rentgenowską. Podobnie dużą precyzją pomiarów charakteryzują się metody porównawcze stosujące komparatory wielowiązkowe, które są układami wielokrystalicznymi. Ich zasada pomiaru opiera się na wykorzystaniu dwóch oddzielnych wiązek rentgenowskich, które wychodzą z dwóch lub jednego źródła. Układ dwukrystaliczny pozwala na pomiar bezdyspersyjny, a dyfrakcja promieni rentgenowskich zachodzi w transmisji (przypadek Lauego). Metody oparte na komparatorach wielowiązkowych wykorzystuje się głównie do określania wzorców odległości międzypłaszczyznowych, jak również kontroli stechiometrii monokryształów półprzewodników o wysokim stopniu czystości i doskonałości strukturalnej. Szczegółowe omówienie wyżej wymienionych metod zostało przedstawione w [1].

Drugą grupę metod wyznaczania odległości międzypłaszczyznowych stanowią tzw. metody bezwzględne. W metodach tych znane są długości linii emisyjnej promieniowania rentgenowskiego, natomiast brana pod uwagę dokładność musi być co najmniej taka jak samego pomiaru. Ma to szczególne znaczenie dla zaawansowanych technologii z wykorzystaniem materiałów półprzewodnikowych. Zarówno precyzyjne

jak i dokładne wyznaczanie parametrów sieciowych pozwala na określenie jednorodności materiałów, naprężeń powstających w trakcie wzrostu, wpływu domieszek [2] i zmian pod wpływem napromieniowania.

2. Wzorce parametrów sieciowych polikrystalicznego krzemu

Zastosowanie polikrystalicznych dyfraktometrów do wyznaczania struktury krystalicznej wymaga znajomości parametrów komórki elementarnej z jak najwyższą precyzją a kryształ wzorcowy konieczny jest do kalibracji dyfraktometru. Doskonały wzorzec ważny jest dla porównań danych pomiarowych w laboratorium. Zastosowanie wzorców wewnętrznych dla dyfraktometrii polikrystalicznej, choć znane od lat, pozwala na uzyskanie zgodnych danych dla różnych próbek i w różnych laboratoriach tylko wówczas, gdy użyty zostanie ten sam wzorzec. Zatem pomiary względne można prowadzić z dużo większą precyzją niż absolutne. W tym celu w NIST (National Institute of Standards and Technology), dawniej NBS (National Bureau of Standards) od wielu lat przygotowuje się certyfikaty wzorcowe parametrów sieciowych m.in. krzemu. Są to tzw. SRMy – Standard Reference Materials ®. Dla SRM 640, SRM 640a i 640b przeprowadzono procedury pomiarowe w latach 1975 – 1987 [1-3]. Zestawienie wyników przedstawiono w Tabeli 1.

Tabela 1. Parametry sieciowe wzorców polikrystalicznego krzemu; długość promieniowania λ $CuK\alpha_1$ = 0.15405981 nm [6].

Materiał	Parametr sieciowy [nm]	Wzorzec wewnętrzny	Literatura
SRM 640	0,543 088 0 ±35·10^{-8}	Wolfram	[3]
SRM 640a	0,543 082 5±36·10^{-8}	Wolfram, srebro	[4]
SRM 640b	0,543 094 0±35·10^{-8}	Wolfram, srebro	[5]
SRM 640c	0,543 1194 6±92·10^{-9}	-	[7]

Wyniki pomiarów parametrów sieciowych otrzymano w oparciu o wzorce wewnętrzne srebra i wolframu przy użyciu promieniowania $CuK\alpha_1$, ale także $CoK\alpha_1$ i $NiK\alpha_1$. Jednak już same wzorce były mało dokładne, bowiem zostały scharakteryzowane klasycznymi metodami fotograficznymi, a długość promieniowania rentgenowskiego nie była podana w jednostkach metrycznych. Wyniki pomiarów parametrów sieciowych były później skalowane [8] do dokładniejszej wartości długości promieniowania wyznaczonej przez Deslattes'a i Henins'a λ = 1,5405981(15) Å [6], wyłącznie dla $CuK\alpha_1$. Stąd wynika duża rozbieżność danych literaturowych dotyczących wartości parametrów sieciowych krzemu.

W ostatnich latach pojawiły się nowe techniki badawcze umożliwiające wyznaczenie parametrów sieciowych materiałów polikrystalicznych ze znacznie większą dokładnością oraz lepszą techniką otrzymania wzorcowych próbek. W 2000 r. J.P. Cline i in. [7] sporządzili wzorzec do kalibrowania pozycji linii dyfrakcyjnej i jej kształtu. Nowy wzorzec polikrystalicznego krzemu SRM 640c stosowany jest do dnia dzisiejszego. Jednostkowy wzorzec zawiera ~7.5 g proszku krzemu zamkniętego w ampule wypełnionej argonem. Proszek spreparowany był z bryłki monokrystalicznego, ultra czystego, samoistnego krzemu przez zmielenie go do rozmiaru ziarna 4.5 μm. Otrzymany proszek był wygrzewany w atmosferze argonu, w 1000^{0}C przez 2 godziny a następnie hermetycznie zamknięty w ampule z argonem. Szczegółowe omówienie przeprowadzonych pomiarów przedstawiono w pracy [7]. Wartość parametru sieciowego tego wzorca wynosi a = 0,54311946 ± 9,2·10^{-7} nm. Ponieważ pomiary prowadzone były w zmiennej temperaturze wartość parametru sieciowego została skorygowana do temperatury 22.5ºC z zastosowaniem do korekty temperatury współczynnika rozszerzalności termicznej α = 2,581·10^{-6} K^{-1} [9]. Wykorzystano też nową wartość długości promieniowania rentgenowskiego Cu $K\alpha_1$, λ = 0,15405929±5·10^{-7} nm, wyznaczoną przez Hölzera i in. [10].

3. Wzorcowe parametry sieciowe monokryształów krzemu

Długość stosowanego promieniowania stała się wartością krytyczną dla otrzymania odpowiednich wzorców parametrów sieciowych krzemu. W Tabeli 2 zestawiono chronologicznie stosowane wartości długości λ dla promieniowania $CuK\alpha_1$. Obecnie znane są absolutne długości promieniowania $K\alpha_{1,2}$ oraz Kβ dla: Cu, Cr, Co, Mn, Fe, i Ni w skali metrycznej z dokładnością 10^{-7}- 10^{-9} nm, ta ostatnia wartość dla promieniowania Cu [10].

Otrzymane wyniki są rezultatem pomiarów parametrów sieciowych niemal idealnych, bezdefektowych monokryształów krzemu w wyniku kompleksowej rentgenowskiej i optycznej (laserowej) interferometrii, które prowadzone były w systemie metrycznym [6]. Pomiary przeprowadzono na monokrysztale WASO 9. Monokryształ ten otrzymano metodą wielokrotnego topienia strefowego w Wacker Chemitronic w Burghausen i stanowił on część dużej partii materiału monokrystalicznego.

Tabela 2. Chronologiczne zestawienie długości stosowanego promieniowania $CuK\alpha_1$.

Autor	λ, $CuK\alpha_1$	Literatura
Tablice Krystalograficzne	0,154 05	[11]
J.A. Bearden – 1967 rok	0,154 056 2	[12]
R. Deslattes i in. – 1973 rok	0,154 059 81	[6]
J. Härtwig i in. – 1991 rok	0,154 059 292	[13]
G. Hölzer i in. – 1997 rok	0,154 059 29(5)	[10]

Monokryształ ten o niskiej zawartości tlenu i węgla (N_C = 9·10^{15} cm^{-3}, N_O=2·10^{15} cm^{-3}), kalibrowany był względem wcześniej badanego wzorca [14] za pomocą dwukrystalicznego, transmisyjnego komparatora, a jego

jednorodność była sprawdzana przy pomocy dwukrystalicznej topografii rentgenowskiej ($\Delta d/d$=2·10^{-8}, gdzie d – oznacza odległość międzypłaszczyznową) [15]. Parametr sieciowy monokryształu WASO 9 został określony w jednostkach metrycznych i wynosił w próżni, w temperaturze 22,5ºC, a = 0,543101988±3,4·10^{8} nm [15], a w odniesieniu do normalnego ciśnienia atmosferycznego i temperatury 20ºC, a = 0,543098367 ± 3,4·10^{-8} nm. Po uwzględnieniu śladowych ilości zanieczyszczeń, które są nie do uniknięcia w trakcie monokrystalizacji, wyznaczone zostały parametry sieciowe "idealnie czystego" monokryształu krzemu Si^{P} jako wartość wzorcowa a = 0,543098396 ±3,4·10^{-8} nm [16]. Inną metodą stosowaną do pomiaru parametrów sieciowych niemal doskonałych kryształów jest metoda Bonda [17-18]. Wyniki otrzymane tą metodą z udziałem wzorcowej długości fali w układzie metrycznym mogą być uważane za bezwzględne [13]. Pomiar metodą Bonda opiera się na wyeliminowaniu błędów niecentryczności i ustawienia zera goniometru poprzez wykorzystanie nieruchomego w czasie pomiaru licznika, będącego jedynie monitorem położenia kryształu. Rejestracja krokowa profilu dyfrakcyjnego dla wybranego układu płaszczyzn (*hkl*) odbywa się dwukrotnie poprzez obrót kryształu wokół osi ω w dwóch symetrycznych położeniach R_1 i R_2 (Rys. 1). Oba położenia kryształu różnią się o kąt $\alpha = (180^{o} - 2\theta)$. Wartość kąta θ_B wynosi:

$$\theta = 90^{\circ} - \frac{(R_1 - R_2)}{2}$$

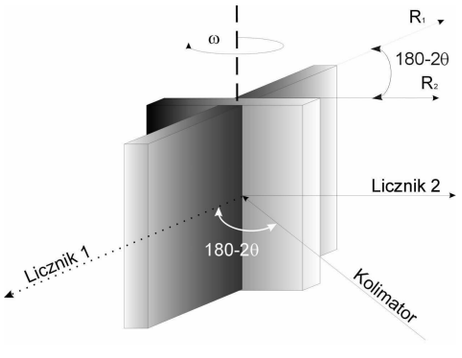

Rysunek 1. Geometria pomiaru kąta Bragga w metodzie Bonda.

Metoda Bonda zasadniczo pozwala na wyznaczenie odległości międzypłaszczyznowej w jednym punkcie kryształu i w trakcie jednego cyklu pomiarowego. Skanuje się wyłącznie maksimum profilu. Ponieważ wiązka promieniowania padająca na kryształ nie jest ściśle monochromatyczna ani zupełnie równoległa, prowadzi to do przemieszczenia się położenia maksimum skanowanego profilu linii o $\Delta\theta$. Przesunięcie refleksu jest całkowitym błędem systematycznym, który musi być uwzględniony, aby wyznaczona wartość parametru sieciowego a była wartością rzeczywistą [17]:

$$\Delta\theta = \Delta\theta_{ref} + \Delta\theta_{HD} + \Delta\theta_{VD} + \Delta\theta_{S} + \Delta\theta_{AC} + \Delta\theta_{A} + \Delta\theta_{B} + \ldots$$

gdzie: kolejne człony oznaczają wpływ : $\Delta\theta_{ref}$ - załamania, $\Delta\theta_{HD}$ - rozbieżności poziomej (w płaszczyźnie obrotu), $\Delta\theta_{VD}$ - rozbieżności pionowej (osiowej), $\Delta\theta_{S}$ - członu wolno zmieniającego się z θ i z λ (dyspersja, całkowite odbicie), $\Delta\theta_{AC}$ - absorpcji w krysztale, $\Delta\theta_{A}$ - absorpcji w materiale ogniska, okienkach i powietrzu, $\Delta\theta_{B}$ - absorpcji w ognisku lampy. Zestawienie wzorcowych wartości parametrów sieciowych monokryształów Si przedstawiono w Tabeli 3.

Tabela 3. Wartości parametrów sieciowych monokryształów krzemu przeliczone dla długości fali CuKα_1 według Hölzera λ=0,15405929±5·10^{-7} nm [10].

Metoda pomiarowa	Parametr sieciowy [nm]	Literatura
Bond	0,543 098 32	[19]
Interferometryczna	0,543 099 65	[6]
Bond	0,543 098 99	[20]
Bond	0,543 098 89	[21]
Bond	0,543 097 49	[22]
Bond	0,543 098 39	[16]

Monokryształy krzemu posiadają wartości parametrów sieciowych bardziej wiarygodne i mogą być wykorzystywane jako kryształy wzorcowe w wielu innych technikach. W naszym laboratorium począwszy od 1986 roku kryształ wzorcowy, nazwany Si$_{KAT,}$ mierzony był wielokrotnie na dyfraktometrze Bonda. Monokryształ ten został otrzymany metodą Czochralskiego w ITME w Warszawie. Wyznaczone wartości parametrów sieciowych tego monokryształu przedstawione są w Tabeli 4. Wartości te są korygowane do temperatury 20ºC zgodnie z [21].

Tabela 4. Parametry sieciowe wzorca Si$_{KAT.}$ Długość fali CuKα_1 wg. Hölzera λ=0,15405929±5·10^{-7} nm [10], refleks 444.

Pomiar	Parametr sieciowy wzorca Si$_{KAT}$ [nm]
1986 rok – Katowice	0,543 098 9 ± 7·10^{-7}
1987 rok – Katowice	0,543 099 ± 7·10^{-6}
1990 rok – Katowice	0,543 099 6 ± 5·10^{-7}
1995 rok – Katowice	0,543 099 1 ± 3·10^{-7}
2003 rok – Katowice	0,543 099 ± 1·10^{-6}
2007 rok - Katowice	0,543 099 ± 2·10^{-6}

4. Podsumowanie

Przedstawiony w pracy przegląd literaturowy wykazał możliwość zastosowania krzemu, zarówno w polikrystalicznej jak i monokrystalicznej postaci, jako materiału wzorcowego umożliwiającego wyznaczanie parametrów sieciowych z wysoką precyzją. Pomimo zastosowania wyrafinowanych technik pomiarowych i obliczeniowych występuje ewidentna, przy tej skali

dokładności, różnica Δa = 2,10·10^{-4} nm pomiędzy wartościami parametrów sieciowych wzorca polikrystalicznego, a monokrystalicznego. Różnica ta może mieć związek z obecnością zanieczyszczeń w badanych kryształach. W przypadku pomiarów parametrów sieciowych monokryształów stosowane wzorce posiadają jedynie niewielkie ilości atomów zanieczyszczeń. Są nimi przede wszystkim tlen i węgiel. Dla najlepszych monokryształów, takich jak WASO 9 koncentracja zanieczyszczeń jest rzędu N_C = 9·10^{15} cm^{-3} atomów węgla i N_O = 2·10^{15} cm^{-3} atomów tlenu. Daje to względną zmianę parametrów sieciowych Δa=7·10^{-8} nm. Monokryształy otrzymywane metodą Czochralskiego są znacznie bardziej zanieczyszczone i mogą one zawierać 2·10^{17} – 1,5·10^{18} cm^{-3} atomów tlenu, powodując w efekcie zmiany parametrów sieciowych o Δa = 4,8·10^{-7} – 3,6·10^{-6} nm. Różnica w parametrach sieciowych polikryształów i monokryształów może wynikać również z samej specyfiki pomiaru. W metodach polikrystalicznych wartość parametru sieciowego jest wartością uśrednioną z większej ilości krystalitów, które mogą pomiędzy sobą się różnić, pod względem zawartości zanieczyszczeń. Dlatego też monokryształy krzemu znalazły liczne zastosowanie, przede wszystkim do wyznaczania wielu stałych fizycznych: wyznaczono dzięki nim nową wartość stałej Avogadro N_A = 6,0221353(20) · 10^{23} mol^{-1} [24], wprowadzono nowy wzorzec masy (kg), jak również udokładniono wartość stałej Plancka h = 6,626 075 5(40) · 10^{-34} Js [25]. Należy również zwrócić uwagę na zastosowanie wzorcowych, bezdefektowych monokryształów krzemu w badaniach synchrotronowych, a szczególnie w monochromatyzacji promieniowania synchrotronowego. Dzięki użyciu odpowiednio dobranych monochromatorów krzemowych typu Bartelsa Si (111) dwu – lub czteroodbiciowych możliwe jest uzyskanie ściśle monochromatycznej wiązki promieniowania synchrotronowego. Pozwoli to na bardziej subtelną charakteryzację stechiometrii badanych materiałów i wpływu defektów na ich właściwości.

Literatura:

[1] E. Gałdecka, "X-ray diffraction methods: single crystals", *International Tables for Crystallography, T.* C**,** rozdz. 5.3, (2006) 505-536.

[2] J. Kucytowski, K. Wokulska, "Lattice parameter measurements of boron doped Si single crystals", *Cryst. Res. Technol.* **40** (2005) 424-428.

[3] C.R. Hubbard, H.E. Swanson, F.A. Mauer, "A silicon powder diffraction standard reference material", *J. Appl. Crystallogr.* **8** (1975) 45-48.

[4] C.R. Hubbard, "Certification of Si powder diffraction standard reference material 640a", *J. Appl. Crystallogr.* **16** (1983) 285-288.

[5] L. Kieffer, R. McKenzie, C.R. Hubbard, C. Robbins, N. Wong, *National Bureau of Standards Certificate: SRM 640b,* National Bureau of Standards, Gaihersburg, MD 20899, USA (1987) 1-4.

[6] R. Deslattes, A. Henins, "X-ray to visible wavelength ratios", *Phys. Rev. Lett.*, **31** (1973) 972-975.

[7] J.P.Cline, R.D. Deslattes, J-L. Staudenmann, E.G. Kessler, L.T. Hudson, A. Henins, R.W. Cheary, *NIST Certificate: SRM 640c*, NIST, Gaithersburg, MD 20899, USA (2000) 1-4.

[8] D.Y. Short, "On a small error in SRM640, SRM640a and SRM640b lattice parameters", *J. Appl. Crystallogr.* **26** (1993) 272-276.

[9] A. Bergamin, G. Cavagnero, G. Mana, G. Zosi, "Lattice parameter and thermal expansion of monocrystalline silicon", *J. Appl. Phys.* **82** (1997) 5396-5400.

[10] G. Hölzer, M. Fritsch, M. Deutsch, J. Härtwig, E. Förster, "K$\alpha_{1,2}$ and K$\beta_{1,3}$ x-ray emission lines of the 3*d* transition metals", *Phys. Rev. A* **56** (1997) 4554-4568.

[11] *International Tables for Crystallography*, T.3 (Kynoch Press, Birmingham 1962).

[12] J.A. Bearden, "X-Ray Wavelengths", *Rev. Mod. Phys.* **39** (1967) 78-124.

[13] J. Härtwig, S. Groβwig, P. Becker, D. Windisch, "Remeasurement of the CuKα_1 emision X-ray wavelength in the metrical system (present stage)", *phys. stat. sol. (a)* **125** (1991) 79-89.

[14] P. Becker, K. Dorenwendt, G. Ebeling, R. Lauer, W. Lucas, R. Probst, H.J. Rademacher, G. Reim, P. Seyfried, H. Siegert, "Absolute measurement of the (220) lattice plane spacing in a silicon crystal", *Phys. Rev. Lett.* **46** (1981) 1540-1543.

[15] D. Windisch, P. Becker, "Silicon Lattice Parameters as an Absolute scale of length for high precision measurements of fundamental constants", *phys. stat. sol. (a)* **118** (1990) 379-387.

[16] J. Härtwig, J. Bąk-Misiuk, H. Berger, H.-G. Brühl, Y. Okada, S. Groβwig, K. Wokulska, J. Wolf, "Comparison of lattice parameters obtained from an internal silicon monocrystal standard", *phys. stat. sol. (a)* **142** (1994) 19-26.

[17] K. Wokulska, Precyzyjny pomiar parametrów sieciowych i jego zastosowanie do badania struktury kryształów roztworów stałych, Wydawnictwo Uniwersytetu Śląskiego, Katowice 1997.

[18] W.L. Bond, "Precision lattice constant determination", *Acta Crystalogr.* **13** (1960) 814-818.

[19] R.L. Barns, "A survey of precision lattice parameter measurements as a tool for the characterization of single-crystal materials", *Mat. Res. Bull.* **2** (1967) 273-282.

[20] C.R. Hubbard, F.A. Mauer, "Precision and Accuracy of the Bond Method as Applied to Small Spherical Crystals", *J. Appl. Crystallogr.* **9** (1976) 1-8.

[21] K. Łukaszewicz, D. Kucharczyk, M. Malinowski, A. Pietraszko, "New model of the Bond diffractometer for precise determination of lattice parameters and thermal expansion of single crystals", *Kristall Techn.* **13** (1978) 561-567.

[22] Y. Okada, "A high-temperature attachment for precise measurement of lattice parameters by Bond's method between room temperature and 1500 K", *J. Phys. E: Sci. Instrum.* **15** (1982) 1060-1063.

[23] Y. Okada, Y. Tokumaru, "Precise determination of lattice parameter and thermal expansion coefficient of silicon between 300 and 1500 K", *J. Appl. Phys.* **56** (1984) 314-320.

[24] P. Becker, H. Bettin, H-U. Danzebrink, M. Gläser, U. Kuetgens, A. Nicolaus, D. Schiel, P. Bièvre, S. Valkiers, P. Taylor, "Determination of the Avogadro constant via the silicon route", *Metrologia*, **40** (2003) 271-287.

[25] E.R. Cohen, B.N. Taylor, "The 1986 CODATA Recommended Values of the Fundamental Physical Constants", *J. Res. Natl. Bureau Stand.* **92** (1987) 1-14.

NEWS FROM THE POLISH SYNCHROTRON RADIATION SOCIETY

Almost one year ago we met at *the 7th National Symposium of Synchrotron Radiation Users* (7th KSUPS) held in Poznań on 24th – 26th September 2007 and organised by the Polish Synchrotron Radiation Society in co-operation with the Adam Mickiewicz University. The Symposium gathered 73 participants. The programme included 9 invited lectures, 10 oral contributions, and 51 posters.

The lectures touched on many subjects, structural studies of different objects, from single crystals to biological matter, by means of various metods. There were also presentations of the project of the synchrotron light source in Cracow, the POLFEL project to be built in Świerk, and the European X-ray Free Electron Laser in Hamburg.

For me two lectures were of particular interest. In first, Dr Gilski of the Center for Biocrystallographic Research of the Polish Academy of Sciences in Poznań presented a remote synchrotron data collection from ESRF in Grenoble, France, via internet. On the monitor screen the audience could see a researcher from ESRF staff going to the laboratory in synchrotron center, mounting a sample which has been sent from Poland, and making the synchrotron experiment. After a few minutes results in the form of diffraction paterns and results of the data processing were shown. It was a very exciting experience, indeed.

Figure 1. A visit of the meteorite at the symposium.

(Fot. by W. Paszkowicz)

Figure 2. The excursion of the symposium participants to the Morasko nature reserve.

(Fot. by J. Pełka)

Figure 3. The General Meeting 2007 – Wojciech Wierzchowski takes the floor.

(Fot. by W. Paszkowicz)

The second lecture concerned a meteorite discovered in Morasko near Poznań in XIX century. Prof. Muszyński of the Adam Mickiewicz University described the results of investigations of the meteorite origin and structure, and showed us a part of the biggest one. We could touch (Fig. 1) a visitor from the universe. After the lecture we had an excursion to Morasko (Fig. 2). It was a didactic and pleasant walk.

Selected Symposium presentations will be published as regular papers in a special issue of *Acta Physica Polonica A* (vol. 114 (2008) No 1) prepared by Maciej Kozak and Wojciech Paszkowicz as the guest editors.

The last Annual General Meeting of the Polish Synchrotron Radiation Society was held in Poznań on the 25th of September 2007. The first item of the agenda was connected with the PSRS membership. Three new members were registered. The reports for the period of June 2006 – September 2007 were the next point of the agenda. Krystyna Jabłońska, the President, and Wojciech Kwiatek, the Treasurer, presented the meritorious and financial reports, respectively. Wojciech Wierzchowski, the Head of the Auditing Commission, read out the minutes (Fig. 3). After a discussion, all reports were received with favour by the General Assembly.

Then, the President described the current Polish access to European sources. The Polish membership (with the annual dutes of 1% of the budget and in an advisory capacity) in the European Synchrotron

Radiation Facility in Grenoble is realised due to a special grant coordinated by Prof. Jabłońska. Poland makes efforts to set up a consortium together with Austria, Israel and Portugal, contributing now also 1 % share because a consortium such as this with 4 % fee comes into prominence and it will be a co-owner of the research intra-structure. As well the negotiations on a Polish contribution to the construction and operation of European X-ray Free Electron Laser (XFEL) in Hamburg are also carried on.

The last item of the agenda concerned *the 9th International School and Symposium on Synchrotron Radiation in Natural Science* in hotel "Ameliówka" in Mąchocice Kapitulne near Kielce in June 2008.

From September 2007 till June 2008 two sessions of the Council of the PSRS were held.

The Council fixed attention on the extension of Polish possibilities of modern research and it is why it decided to promote and actively participate in works of the National Centre of Synchrotron Radiation in Cracow as well as to support an idea of the construction of a Polish free electron laser POLFEL. For the latter, owing to efforts of the President of the PSRS, a consortium XFEL-Polska, consisting of 18 Polish institutions, was created for this goal. Refering to the former, recently, on the 8th of April 2008, a bilateral agreement between the Polish Synchrotron Radiation Society and the National Centre of Synchrotron Radiation was signed.

The 8th National Symposium of Synchrotron Radiation Users (8th KSUPS) will be held in Cieszyn on 24th – 25th September 2009 and organised by the Polish Synchrotron Radiation Society in co-operation with the University of Silesia.

At present (June 2008), just before the General Meeting, the Polish Synchrotron Radiation Society has 131 members: 1 honorary member, 110 full members, and 20 associate members (among them 10 foreigners).

Danuta Żymierska

/Secretary of the Polish Synchrotron Radiation Society/

CENTRAL LABORATORY OF X-RAY AND ELECTRON MICROSCOPY AT THE INSTITUTE OF PHYSICS OF THE POLISH ACADEMY OF SCIENCES, WARSAW [1*)]

D. Żymierska

Institute of Physics of the Polish Academy of Sciences, al. Lotników 32/46, PL 02-668 Warsaw, Poland

e-mail: zymier@ifpan.edu.pl

The beginning and history of the Central Laboratory of X-ray and Electron Microscopy at the Institute of Physics of the Polish Academy of Sciences in Warsaw is described. Then, recent scientific achievements are presented. Organising activities of the Laboratory staff are also mentioned.

1. History

The Central Laboratory of X-ray and Electron Microscopy at the Institute of Physics of the Polsh Academy of Sciences in Warsaw has a long history. In 2008 it celebrates a jubilee of 35th anniversary. In fact, a background is much longer because the crystal structure research was carried out at the University of Warsaw by a group headed by Professor Stefan Pieńkowski. In 1953 the Institute of Physics of the Polish Academy of Sciences was founded with departments located not only in Warsaw, but also in Wrocław, Poznań, Kraków, and Toruń [1]. Prof. Pieńkowski was appointed to a director of the Institute and Prof. Leopold Infeld to a chairman of the Scientific Council. The development of the Institute was fast. As a continuation of the work at the University of Warsaw, in 1966 the Department for X-ray Physics was organised in Warsaw, and Prof. Julian Auleytner was established as its leader.

In 1973 the Institute of Physics was reorganised. In Warsaw the research topics were concentrated in three scientific divisions and two central laboratories. The Department of X-ray Physics was turned into the Central Laboratory of X-ray and Electron Microscopy, created for a double purpose: scientific investigations concerning a development of material characterisation, and scientific expertises for other groups of the Institute and for other research institutions as well as of medicine and industry.

Prof. Julian Auleytner took up a leadership of the Laboratory and he was its head for twenty years. In the period of 1993-1999 Prof. Tadeusz Figielski was a head of the Laboratory. Since 2000 Prof. Krystyna Jabłońska is its leader.

Initially, the Laboratory included three scientific groups: the Group for Real Structure Research and X-ray Spectroscopy, the Group of Physics of Defects in Semiconductors, and the Group of Electron Microscopy, as well as the Technical Support Group. At that time the Laboratory was equipped with modern X-ray and electron analytical tools. From the beginning the Laboratory has collaborated with many foreign scientific groups.

In 1986 The Group of Applied Crystallography was established. Next, the Technical Support Group was closed down, whereas the Group of X-ray Fluorescence and Electron Microprobe was created which was then transformed into the Group of X-ray Spectroscopy and Microanalysis. In late nineties the Group of Secondary Ion Mass Spectrometry was founded. In 2000 the Group of Physics of Defects in Semiconductors moved to the Scientific Division of Physics of Semiconductors and simultateously the Group of X-ray Optics was established which in 2004 joined the Group for Real Structure Research, creating together the Group of X-ray Optics and Atomic Structure Research. At the same time the Group of SIMS was taken in by the Group of X-ray Spectroscopy and Microanalysis and the Group of Biological Physics was founded.

At present, in 2008, the Laboratory consists of five scientific groups: the Group of X-ray Optics and Atomic Structure Research, the Group of X-ray Spectroscopy and Microanalysis, the Group of Applied Crystallography, the Group of Electron Microscopy, and the Group of Biological Physics.

---

[1] *) In this issue we begin a presentation of Polish research groups involved in synchrotron radiation investigations and workers of which are active members of the Polish Synchrotron Radiation Society. We start with the Central Laboratory of X-Ray and Electron Microscopy at the Institute of Physics of the Polish Academy of Sciences in Warsaw.

Figure 1. Laboratory staff and visitors gathered at the Institute entrance during the celebration of the 30th anniversary in 2003

As the result of the 35 year-scientific activity of the Laboratory, over 1500 papers were published in the international scientific journals and 28 research workers received the PhD degree. At present, five PhD students are preparing their theses at the Laboratory.

Several persons of the staff went abroad, and actually they work at the scientific institutions in Federal Republic of Germany, the USA, Canada, and Australia. Two young researchers are holders of post-doc scholarships in the USA and Germany.

The researches of the Laboratory were winners of several prizes [1]. These of the greatest prestige were two international awards: in 1976 the Polish Academy of Sciences and Academy of Sciences of German Democratic Republic awarded an international prize to Prof. J. Auleytner and Prof. J. Heydenreich, and their co-workers for development of X-ray and optical method for solid state physics and in 1985 the Scientific Secretaries of the Polish Academy of Sciences and Bulgarian Academy of Sciences to Prof. J. Auleytner and Prof. G. Grigorov, and their coworkers for investigations of adsorption properties of metallic surfaces. Five times members of the staff were given prizes of the Scientific Secretary of the PAS: in 1972 the group directed by Prof. J. Auleytner, in 1979 the group headed by Prof. T. Figielski, in 1984 the group of Dr. G. Jasiołek, in 1988 Dr E. Sobczak and Prof. J. Auleytner, and in 1989 the group directed by Dr J. Bąk-Misiuk in co-operation with the Institute of Electronic Materials Technology.

The establishment in 2002 the Centre of Excellence CEPHEUS (Centre of Photon, Electron and Ion Advanced Methods for Natural Science) with the European Commission support for 3 years under the direction of Prof. K. Jabłońska, the leader of the Laboratory, was also a great achievement.

2. Equipment

Studies of the solid state require a good technology for preparing samples (crystals, thin films, low dimantional objects) and a research equipment for a characterisation of them as well as an understanding their crystal and defect structure. At early years the structures were characterised using commercial cameras, diffractometers, and spectrometers. In the Department of X-ray Physics, self-made cameras and high resolution diffractometers were built, among them an X-ray camera with oscillating crystal and film [2] and a moving slit for X-ray automonochromatization [3], and used here and at other institutes.

After the creation of the the Central Laboratory of X-ray and Electron Microscopy, at early seventies of the

20th century, it received respectable amount of money for purchase of several modern pieces of apparatus: an electron probe micro-analyser JXA-50A with scanning electron microscope and X-ray energy dispersive spectrometer LINK (JOEL), a double axis X-ray diffractometer of Bond type with temperature chamber, equipped with a four crystal monochromator of Bartels type, an X-ray powder diffractometer with secondary monochromator for high sensitivity phase analysis (SIEMENS Kristalloflex 4 made in Germany), a soft X-ray grating spectrometer RSM-500 (made in USSR), an electron diffractometer (RHEED, TED) ENR-102 (made in USSR), and a metallographic microscope Reichert MeF2. Several devices were projected and constructed by the staff of the Laboratory: an automated diffractometer for powders and single crystals, an automated diffractometer for powders, and a bremsstrahlung isochromat spectrometer.

After a long time of use these devices became old and inadequate to nowadays tasks of the Laboratory. Therefore the leaders and staff made great efforts to upgrate an equipment. In late eighties a high-resolution electron transmission microscope JEM 2000 EX (JEOL) was bought for the finest structure studies at the nano- and atomic scale. In nineties the Laboratory was equipped in various facilities permiting for the structure and composition determination, in particular with two modern high-resolution diffractometers Philips MRD and X'Pert MPD and with powder diffractometer/ reflectometer X'Pert MRD with semiconductor linear position-sensitive detector as well as a secondary ion mass spectrometer IMS 6f (CAMECA, France) for an analysis of atomic composition of materials, determination of mass spectra and element's depth profiles.

At present a variety of materials are studied, *e.g.* single crystals grown by the Bridgman, Czochralski, chemical transport and vapour methods and thin layers and multilayers prepared by MBE, MOCVD and sputtering methods as well as minerals and biomedical materials. Nowadays, the experimental methods at laboratory are either completed or replaced by methods provided at the synchrotron beamlines. Starting from early nineties, the scientists of the Laboratory usually get more than ten weeks of beam-time at the experimental stations of various synchrotrons, what helps to solve various scientific tasks. Many research projects have been performed for several years in co-operation with the European and American laboratories owing the national synchrotron radiation sources.

3. Recent scientific activities

The research activity of the Laboratory has an interdisciplinary approach and concerns the comprehensive characterisation of matter. Over the past years, numerous techniques were developed which determine, on an atomic scale, the structure of the matter and which enable the physicists to describe, with increasing precision, basic interactions between the component atoms.

The recent scientific activity of **the Group of X-ray Optics and Atomic Structure Research** is focused on investigations of an interaction of intense extreme ultraviolet (XUV) and X-ray synchrotron beams with solids. In particular, damage processes induced on solid surfaces with XUV-FEL femtosecond pulses are studied, as well as resistance to the damage for the materials applicable in the optical components for the new radiation sources is determined. Experimental studies are compared to simulations of the propagation in solids of strong electromagnetic pulsed beams within the XUV and soft X-ray radiation (SXR) wavelength. The propagation models are computed in function of the intensity and pulse duration in the ranges up to 10^{14} W/cm^2, and down to 30 fs, respectively [4, 5]. A significant part of experimental results has been achieved with a unique experimental station FELIS (Free Electron Laser - Interaction with Solids) designed and constructed by the scientists and engineering staff of the group to study interactions of intense femtosecond vacuum ultaviolet (VUV) pulses with matter at TTF1 Free Electron Laser in Hamburg [6]. Apart the XUV-FEL directly related work, surface modifications and defect structures induced by other damage processes, such as ion implantation, or ablation with picoseconds pulses generated by optical lasers are also investigated [7]. The surface modifications are studied with a variety of techniques, that includes optical interference-polarization microscopy, RHEED, X-ray scattering methods with synchrotron radiation, raman spectroscopy, and the others. The above mentioned main scientific interests of the group are supplemented with structural research of low dimensional structures and nanomaterials by means of methods employing intense X-ray beams of synchrotron radiation. An example here can be a determination of structure and electrical properties of thin films composed of gold nanoparticles spaced by dithiols of various length [8].

Figure 2. Ablation crater created on Si surface by a few shots of femtosecond free-electron laser pulses (interference-polarizing microscope with Nomarski contrast).

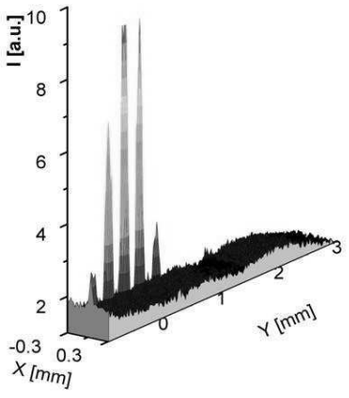

Figure 3. X-ray diffraction map showing strain distribution around points on Si (001) surface irradiated by a few FEL pulses. The map was obtained at BM-20 beamline at the ESRF, Grenoble.

The activity of **the Group of X-ray Spectroscopy and Microanalysis** is devoted to charactersation of the variety of materials independently of their states (liquid, glasses, amorphous or crystals). The techniques used for this purpose are X-ray absorption spectroscopy (XAS), electron probe microanalysis (EPMA), and secondary ions mass spectroscopy (SIMS). By means of these methods the content of given element in the materials is estimated, mapping element distribution and depth profile are determined. Exploiting the advanced analysis of XAS the local atomic structure around elements, as well as their chemical bonds and ionic state is determined. Analysis of the EXAFS oscillations is a source of information on a short-range order in the samples. This is of particular value in the case of investigation of buried low dimensional structures or dopants in semiconductors. The example of application of this technique to study of strains and Si concentration inside Ge quantum dots formed in silicon is presented in the paper [9] and the location of Mn implanted into Si crystals in the paper [10]. Due to the fact, that the shape of the XANES spectra depends on the density of the unoccupied states in a given compound, XANES can be used for testing the solid state theory applied for estimation of other physical properties of matter. The examples of this kind of comprehensive studies were published for III-V family of semiconductors [11]. Recent interests of the group is devoted to the biomaterials. The local atomic structure of di-alanine amino acid derivative of protoporphyrin IX used in the photodynamic diagnostic and therapy of cancers was investigated to find the location of Fe atoms [12]. The location of Fe in the chitosans was found using complementary XAS and magnetic studies [13]. Chitosan and its derivatives have a variety of current and potential applications e.g. in biomedical products, cosmetics, food processing and removal of metallic impurities from wastewaters.

For phase analysis, crystal structure refinement of polycrystals, and for understanding the defect structure of bulk crystals, thin films and multilayered samples, **the Group of Applied Crystallography** uses various high resolution and powder X-ray diffraction as well as scattering methods. A large part of studies are performed under extreme conditions (low/high temperature, high pressure) or after a high-pressure-high-temperature treatment. The scientific activity of the group includes the determination of the thermal expansion and compressibility for semiconductor materials, determination of the influence of carriers, dopant atoms and defects on the lattice parameters in semiconductor thin films. Examples of the activities concern the structure refinement using the Rietveld method [14], thermal expansion for spinel-type silicon nitride [15] (Fig. 4), multiple diffraction effect in strained thin ZnSe film [16] (Fig. 5). Recently the group is also involved in the studies of strained GaAs thin films [17]. Moreover, the structure of potential spintronics materials, *e.g.* diluted ferromagnetic GaMnAs semiconductor, GaAs films with embedded MnAs magnetic nanoclusters as well as silicon implanted with Mn is investigated. In particular, small precipitates within the Si:Mn near-surface region as well as changes in the lattice after introduction of magnetic inclusions have been characterised [18].

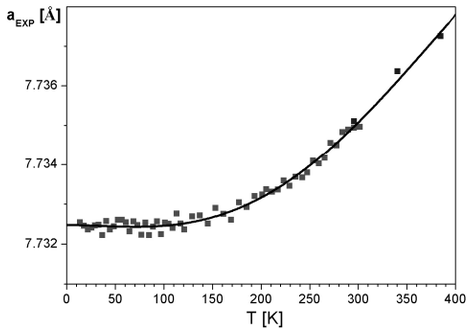

Figure 4. Temperature dependence of the lattice parameter of spinel-type Si_3N_4 [14]. The low temperature data are obtained at B2 beamline (Hasylab).

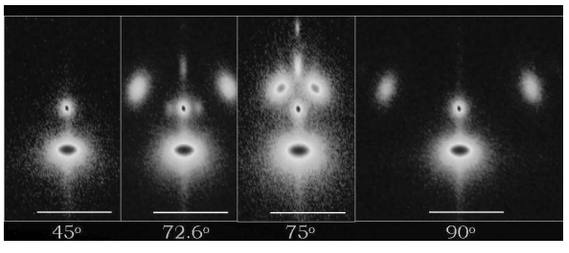

Figure 5: Reciprocal space maps for 002 reflection of ZnSe (1 μm thick) relaxed layer on GaAs (001), for various azimuthal angles, φ = 45, 72, 75 and 90, of the sample [15]. Additional spots are observed in the vicinity of the main reciprocal lattice point, due to the multiple diffraction effect. The azimuthal angle related to [100] direction on the surface is indicated below each image. Analysis of such effects permits for analysis of the strain state of the layer.

The Group of Electron Microscopy is involved in the structure characterisation of semiconductors, metaloxides, supercoductors and fullerenes nano-objects. Computer aid methods of analysis and simulation of diffraction patterns and transmission electron microscopy images are developed and applied to solve the structure of new materials [19, 20] and to a quantitative determination of strain fields and chemical composition at atomic level in semiconductors' heterostructures [21].

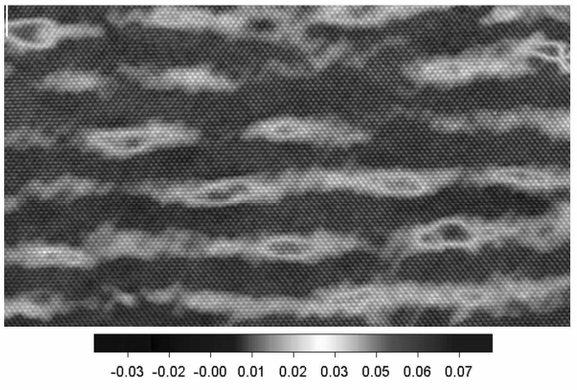

Figure 6. Cross-sectional HRTEM image in 110-zone axis of stacked ZnTe/CdTe QDs structures. Colors illustrate the relative local lattice parameter values measured from the image of CdTe/ZnTe superlattices.

The youngest group, **the Group of Biological Physics** participates in interdisciplinary studies, experimental and theoretical, which involve physics, biology, chemistry, and bioinformatics. One domain of the research is focused on molecular mechanisms of regulation of eukaryotic protein biosynthesis and mRNA turnover [22, 23], in particular, structure - function relationships for the specific ligands of the proteins involved in these processes and also thermodynamic aspects of intermolecular recognition. The main experimental techniques used are: emission spectrosopy, surface plasmon resonance, and atomic force microscopy. The members of the group work also on toxicity mechanisms of the β-amyloids in the context of the Alzheimer disease [24] as well as they study ways to generate optimal biodegradable drug transporters and diagnostic sensors that could enter live biological cells. The leader of the group, Marek Cieplak, uses computer simulations to elucidate mechanisms concerning single protein manipulations (such as stretching by using the atomic force microscope) [25], protein folding, and effects of confinement and hydrodynamic interactions on proteins. He is also involved in providing biological interpretation of data obtained by using the genetic micoarrays on the genetic activity of all genes in an organisms such as yeast [26].

4. Organising activities

From the very beginning, the staff of the Laboratory was very active in the organisation of national and international meetings concerning the variety of X-ray and electrons based methods. During the period of thirty five years of the activity one Congress, two series of international conferences, and one series of national symposia were organised. In 1978 the XIth International Congress on Crystallography for 1650 participants was organised in Warsaw by the staff of the Laboratory and the Institute for Low Temperature and Structure Research of the PAS, Wroclaw. The Congress was the great success of Polish organisers. In the period 1964-1992 the Laboratory organised eight *International Schools and Symposia on Defects in Crystals*. Due to these schools the Polish scientists had an opportunity to be in touch with colleagues from the West and East. It was very important at that time when the distribution of scientific information was hidebound.

Recognising the importance of synchrotron radiation for X-ray physicists, Laboratory decides to disseminate actively the knowledge about these new sources of radiation as well as the scientific achievements among the scientific community in Poland and Central and Eastern Europe (CEE). In 1991 the Polish Synchrotron Radiation Society (PSRS) was created by the scientists of the Laboratory together with researchers of other scientific institutions in Poland with the main goal to organise national and international synchrotron radiation schools. Till now, nine *International Schools and Symposia on Synchrotron Radiation in Natural Science* and seven *National Symposia of Synchrotron Radiation Users* were organised. The Proceedings of these meetings were published in *Acta Physica Polonica A* and *J. Alloys and Compounds*. Scientific workers of the Laboratory have been the chairmen and main organisers of symposia of European Materails Research Society Fall Meetings in Warsaw since 2003, and many other meetings and workshops, among them *East European Meeting on Synchrotron Radiation and Free Electron Laser Sources* in Kraków-Przegorzały in 1999*, Workshop on Extended X-ray Absorption Fine Structure Analysis* in Warsaw in 2001, *Workshop on New Methods of Low-Dimensional Structures Characterisation: VUV and X-ray Free Electron Lasers* in Warsaw in 2002*, Workshop on Advanced Methods for Interpretation of TEM, X-ray and SIMS Measurements in Nano and Atomic Scale* in Warsaw in 2005, and *Workshop on Application of X-ray Absorption for Determination the Local and Electron Structure of Materials* in Warsaw in 2006.

The scientists of the Laboratory are on the go in the Polish Synchrotron Radiation Society; they promote and actively participate in works of the National Centre of Synchrotron Radiation in Cracow as well as support an idea of the construction of a Polish free electron laser POLFEL in Świerk. The Polish access to the European Synchrotron Radiation Facility in Grenoble is realised due to a special grant coordinated by Prof. Jabłońska, the President of the PSRS and the head of the Laboratory.

References

[1] *Kronika Pięćdziesięciolecia 1953-2003*, Instytut Fizyki PAN, Warszawa 2003.

[2] S. Szarras, L. Bonkowski, J. Auleytner, "X-ray camera with oscillating crystal and film for studies of single crystals", *J. Sci. Instrum.* **40** (1963) 20-22.

[3] J. Auleytner, "A method of X-ray automonochromatization bya moving slit to investgate the real structure of crystals", *Acta Phys. Polon. A* **39** (1971) 379-383.

[4] J. Krzywinski, R Sobierajski, M. Jurek, R. Nietubyc, J.B. Pelka, L. Juha, M. Bittner, V. Létal, V. Vorlíček, A. Andrejczuk, J. Feldhaus, B. Keitel, E.L. Saldin, E.A. Schneidmiller, R. Treusch, M.V. Yurkov, "Conductors, semiconductors, and insulators irradiated with short-wavelength free-electron laser", *J. Appl. Phys*. **101** (2007) 043107.

[5] S.P. Hau-Riege, H.N. Chapman, J. Krzywinski, R. Sobierajski, S. Bajt, R.A. London, M. Bergh, C. Caleman, R. Nietubyc, L. Juha, J. Kuba, E. Spiller, S. Baker, R. Bionta, K. Sokolowski-Tinten. N. Stojanovic, B. Kjornrattanawanich, E. Gullikson, E. Plönjes, S. Toleikis, T. Tschentscher, "Sub-nanometer-scale measurements of the interaction of ultrafast soft x-ray free-electron-laser pulses with matter", *Phys. Rev. Lett*. **98** (2007) 145502.

[6] R. Sobierajski, J. Krzywiński, A. Andrejczuk, U. Hahn, M. Jurek, D. Klinger, R. Nietubyć, J.B. Pełka, H. Reniewicz, M. Sikora, W. Sobala, R. Treusch, "Experimental station to study the interaction of intense femtosecond vacuum ultraviolet pulses with matter at TTF1 free electron laser", *Rev. Sci. Instrum.* **76** (2005) 13909.

[7] D. Klinger, E. Łusakowska, D. Żymierska, "Nano-structure formed by nanosecond laser annealing on amorphous Si surface", *Materials Science in Semiconductor Processing* **9** (2006) 323-326.

[8] J.B. Pełka, M. Brust, P. Gierłowski, W. Paszkowicz, N. Schell, "Structure and conductivity of self-assembled films of gold nanoparticles", *Appl. Phys. Lett.* **89** (2006) 063110.

[9] I.N. Demchenko, K. Lawniczak-Jablonska, S. Kret, A.V. Novikov, J.-Y. Laval, M. Zak, A. Szczepanska, A.N. Yablonskiy, Z.F. Krasilnik, "The effect of local atomic structure on the optical properties of GeSi self-assembled islands buried in silicon matrix*", Nanotechnology* **18** (2007) 115711.

[10] A. Wolska, K. Lawniczak-Jablonska; M. Klepka; M.S. Walczak, A. Misiuk, "Local structure around Mn atoms in Si crystals implanted with Mn^+ studied using x-ray absorption spectroscopy techniques", *Phys. Rev. B* **75** (2007) 113201.

[11] K. Lawniczak-Jablonska, T. Suski, I. Gorczyca, N.E. Christensen, K.E. Attenkofer; E.M. Gullikson, J.H. Underwood, D.L. Ederer, R.C.C. Perera, Z. Liliental-Weber, "Electronic states in valence and conduction bands of group-III nitrides: Experiment and theory", *Phys. Rev. B* **61** (2000) 16623.

[12] M.S. Walczak, K. Lawniczak-Jablonska, A. Sienkiewicz, M. Czuba, M. Klepka, A. Graczyk, "The local atomic structure of di-alanine amino acid derivative of protoporphyrin IX", *J. Phys.: Condens. Matter* **19** (2007) 285214.

[13] M.T. Klepka, N. Nedelko, J.-M. Greneche, K. Lawniczak-Jablonska, I.N. Demchenko, A. Slawska-Waniewska, C.A. Rodrigues, A. Debrassi, C. Bordini, "Local atomic structure and magnetic ordering of iron in Fe−chitosan complexes", *Biomacromolecules* (2008), in press.

14] W. Paszkowicz, S. Podsiadlo, R. Minikayev, "Rietveld-refinement study of aluminium and gallium nitrides", *J. Alloys Compds* **382** (2004) 100-106.

[15] W. Paszkowicz, R. Minikayev, P. Piszora, M. Knapp, C. Bahtz, J.M. Recio, M. Marques, P. Mori-Sanchez, L. Gerward, J.Z. Jiang, "Thermal expansion of spinel-type Si_3N_4", *Phys. Rev. B* **69** (2004) 52103-1-4.

[16] S.L. Morelhao J.Z, Domagala, **"**Hybrid reciprocal space for X-ray diffraction in epitaxic layers", *J. Appl. Crystallogr* **40** (2007) 546-551.

[17] A. Shalimov, J. Bak-Misiuk, V.M. Kaganer, M. Calamiotou, A. Georgakilas, "Strain nonuniformity in GaAs heteroepitaxial films on Si(001) studied*", J. Appl. Phys.* **101** (2007) 013517.

[18] J. Bąk-Misiuk, E. Dynowska, P. Romanowski, A. Shalimov, A. Misiuk, S. Kret, P. Dłużewski, J. Domagala, W. Caliebe, J. Dabrowski, M. Prujszczyk, "Srtucture of magnetically Ordered Si:Mn", *Solid State Phen*om.**131-133** (2008) 327

[19] P. Dłużewski, J. Górecka, M. Kozłowski, W. Paszkowicz, A. Yamaguchi, "Transmission electron microscopy and X-ray diffraction studies of Al_2CO microcrystals", *Mater Chem. Phys*. **81** (2003) 383-386.

[20] P. Dłużewski, J. Górecka, W. Paszkowicz, A. Yamaguchi,, "Transmission electron microscopy and X-ray diffraction study of aluminium oxycarbide α'-Al_2CO", *J. Phys. IV* **11** (2001) 273-275.

[21] S. Kret, P. Dłużewski, A. Szczepańska, M. Żak, R. Czernecki, M. Kryśko, M. Leszczyński, G. Maciejewski,, "Homogenous indium distribution in InGaN/GaN laser active structure grown by LP-MOCVD on bulk GaN crystal revealed by transmission electron microscopy and x-ray diffraction", *Nanotechnology*. **18** (2007) 465707.

[22] I. Rutkowska-Wlodarczyk, J. Stepinski, M. Dadlez, E. Darzynkiewicz, R. Stolarski, A. Niedzwiecka, "Structural changes of eIF4E upon binding to the mRNA 5′ monomethylguanosine and trimethylguanosine cap", *Biochem.* **47** (2008) 2710-2720.

[23] P. Nilsson, N. Henriksson, A. Niedzwiecka, N. A. A. Balatsos, K. Kokkoris, J. Eriksson, A. Virtanen, "A multifunctional RNA recognition motif in poly(A)-specific ribonuclease with cap and poly(A) binding properties"**,** *J. Biol. Chem.* **282** (2007) 32902-32911.

[24] M. Brzyska, K. Trzesniewska, T. Gers, D. Elbaum, "Discrete conformational changes as regulators of the hydrolytic properties of beta-amyloid (1–40)", *FEBS J.* **273** (2006) 5598.

[25] J.I. Sulkowska, M. Cieplak, "Stretching to understand proteins - A survey of the Protein Data Bank", *Biophys. J.* **94** (2008) 6-13.

[26] T.R. Lezon, J.R. Banavar, M. Cieplak, A. Maritan, N. Fedoroff, "Using the principle of entropy maximization to infer genetic interaction networks from gene expression patterns", *Proc. Natl. Acad. Sci. (USA)* **103** (2006) 19033-19038.

9th International School and Symposium on Synchrotron Radiation in Natural Science June 15-20, 2008 Ameliówka, Poland

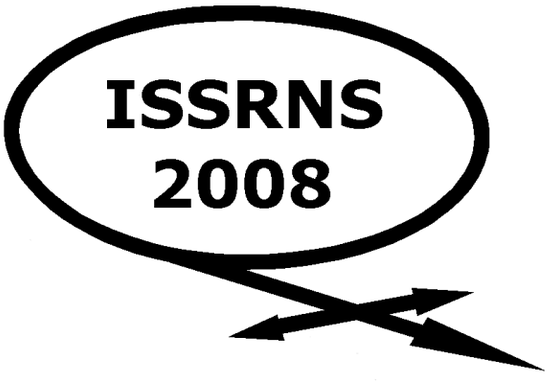

Organized by Polish Synchrotron Radiation Society
in cooperation with Institute of Physics PAS

Sponsors:
Ministry of Science and High Education - special project no. ESRF/73/2006
International Radiation Detectors (IRD) Inc.
Softrade Sp. z o.o. (representative of Pfeiffer Vacuum)
PANalytical
Huber Diffraktionstechnik GmbH & Co. KG
Urząd Marszałkowski Województwa Świętokrzyskiego w Kielcach

	Monday 16.VI	**Tuesday 17.VI**
8.00-9.00	breakfast	breakfast
9.00-9.45	opening 9.00-9.30	**Hermann Dürr** Electron and spin correlations in complex materials on nm length and fs time scales
9.45-10.15	9.30 **José Baruchel** Advances and trends in hard X ray SR-base imaging	**Vladimir Cháb** Intra-atomic charge re-organization at the Pb-Si interface: binding mechanism at low coverage
10.15-10.45	coffee break	coffee break
10.45-11.15	**Daniele Pelliccia** Advancement in x-ray waveguides and their applications in coherent diffraction imaging	**Elżbieta Guziewicz** Localized and itinerant 5f states in actinide materials as seen by photoemission spectroscopy
11.15-11.45	**Jung Ho Je** Imaging in the nanoworld	**Aurelien Gourrier** Revealing the nanostructure of biological materials using scanning x-ray imaging with SAXS contrast
11.45-11.55	break	break
11.55-12.25	**Paweł Korecki** Real-space imaging of atomic structure	**Bogdan Pałosz** Nanocrystals under high pressure
12.25-12.55	**Maya Kiskinova** Imaging and spectromicroscopy of micro- and nanomaterials	**Thomas Tschentscher** Scientific Applications of X-ray Free-Electron Laser Sources
13.00-14.00	lunch	lunch
14.00-14.20	excursion	**Tomasz Wysokinski** Developing modern biomedical imaging and therapy facility at the synchrotron; challenges and unknowns
14.20-14.40		**Paweł Grochulski** Towards full automation at the Canadian macromolecular crystallography facility
14.40-15.00		**Paweł Piszora** In-situ high-pressure observation of Jahn-Teller effect in lithium-manganese oxides
15.00-15.20		**Jerzy Pełka** Damage of solids exposed to intense XUV free electron laser single shots.
15.20-15.40		**Helena Grigoriew** Non-typical, including structural transition, gelation process of monosaccharides
16.00-18.00		**POSTER SESSION**
18.00-19.00	dinner	
19.00-19.20	**Dénes Nagy** Synchrotron Mössbauer Reflectometry Observation and Cellular Automaton Simulation of Domain Formation and Transformation in Antiferromagnetically Coupled Fe/Cr Multilayers	conference dinner
19.20-19.40	**Andrzej Wojtowicz** VUV luminescence of BaF_2:Er and (Ba,La)F_2:Er	
19.40-20.00	**Wojciech Tabiś** Structural changes at the Verwey transition in Fe_3O_4	
20.00-22.00	**POSTER SESSION**	

Wednesday 18.VI	**Thursday 19.VI**	**Friday 20.VI**
breakfast	breakfast	breakfast
Claus M. Schneider Magnetism in nanoscience, spin-polarized photoemission, x-ray magnetooptics, photoemission microscopy	**Bruce Ravel** EXAFS studies of the metal binding site in catalytic DNA sensors	**Andy Fitch** High resolution powder diffraction
Pieter Glatzel Hard X-Ray Photon-In-Photon-Out Spectroscopy with Lifetime Resolution; XAS, XES, RIXS and HERFD	**Carlo Meneghini** Recent Advances in X-ray Absorption Spectroscopy	**Daniel Rolles** Imaging nanoscale objects by femtosecond x-ray diffraction with a soft x-ray free electron laser
coffee break	coffee break	coffee break
Jorma Holsa Synchrotron radiation studies of persistent luminescence materials	**Christian Bressler** Femtosecond and picosecond X-ray spectroscopy studies	**György Vankó** Temperature and pressure-induced spin-state transitions: applications of high-resolution x-ray spectroscopy
Tolek Tyliszczak Application of Scanning Transmission X-ray Microscopy in natural sciences	**Rachid Belkhou** Nanospectroscopy – XPEEM applied to nanomagnetism	**Krzysztof Polewski** Temporal structure of SR - application to study biomolecules in UV and visible range
break	break	break
Edmund Welter A Monolithic 7 Cell Silicon Drift Detector Module for X-Ray Spectroscopy	**Maurits Haverkort** Soft X-ray absorption spectroscopy and magnetic circular and linear dichroism in thin films	**Andrzej Burian** Determination of partial structure factors using 3th generation synchrotron source: In-Se amorphous films
special presentation	**Edward Görlich** Proposed technical concepts and time scenario for Polish synchrotron light source	closing remarks
lunch	lunch	lunch
excursion	**Jan Michalik** X-MCD in the Cr-Re and Fe-Re based double perovskite at high pulsed magnetic fields	
	Marcin Sikora Nanocrystalization in Vanadium doped carbon films studied by means of X-ray Emission Spectroscopy	
	Marcin Klepka XAFS determination of local atomic arrangement of iron in Fe-chitosan complexes	
	Dariusz Zając X-ray absorption spectroscopy study of platinum chloride complex ions in aqueous solutions	
	Monika Walczak XANES and EXAFS studies of malarial pigment's substitutes in reaction with antimalarial drug	
	PTPS General Assembly (or integration)	
dinner		
Iwona Kowalik Electronic structure and magnetic properties of self-organized MnSb and MnAs dots grown by MBE on GaN surface	bonfire	
Mieczysław Pietrzyk Comparison of the valence band of the Mn/GeTe, Mn/GeMnTe and Mn/GeEuTe layers		
Marek Pajek Application of a high-resolution grazing-emission x-ray fluorescence in material sciences		
POSTER SESSION		

WELCOME to the 9th ISSRNS

On behalf of the Programme and Organizing Committees we would like to welcome you to the 9th International School and Symposium on Synchrotron Radiation in Natural Science organized by the Polish Synchrotron Radiation Society (PTPS) in cooperation with the Institute of Physics, Polish Academy of Sciences.

The ISSRNS takes place in Poland every two years. From the very first meeting organized in 1992, the idea of dissemination of knowledge on synchrotron radiation applications in Poland and integration of the community of Polish synchrotron radiation users proved to be very popular and successful. Nowadays, when Polish scientists carry out experiments in many synchrotron laboratories all over the world and have become members of the international community of synchrotron radiation users, these conferences transformed into a forum of sharing new results, new ideas of experiments and starting collaboration. Nevertheless, it partly retained its original character of "first step to synchrotron radiation" for young generations of scientists.

This year we meet in the Ameliówka hotel, in the middle of the Świętokrzyskie (Saint Cross) Mountains, a wooded mountain range in central Poland covered by remnants of a primeval forest with beautiful rivers, caves and hundreds of unique relics of the past. Not only Nature is of interest there - just in this central region some hundreds year ago, early metallurgy and industry started to develop, and traces of this activity can be found in a number of local museums in the region. Mostly known are the oldest objects: five thousand years old unique flint stone mine in Krzemionki Opatowskie, and the thousands of furnaces discovered in the region where for several hundred years starting from 2nd century B.C. iron was massively produced.

However, not only the neighbourhood is interesting. We made an effort to ascertain a large variety of subjects to be presented at the meeting. The lecturers come from the best synchrotron laboratories in Europe, Asia and America and from university laboratories using the intense radiation sources.

We would like to thank all lecturers for accepting our invitations to show the results of their exciting research. We also thank all the participants for preparing oral and poster presentations. We hope that the participation in the conference will be fruitful and stimulating for all of you. We wish you good time with excellent science amid nature's splendor.

The Organizers

L1

ADVANCES AND TRENDS IN HARD X-RAY SR-BASE IMAGING

José Baruchel

European Synchrotron Radiation Facility, BP 220, 38043 Grenoble, France

Keywords: x-ray imaging, resolution, rocking curve, tomography, microscopy, diffraction

X-ray imaging techniques are increasingly used in modern SR facilities [1], and constitute, for instance, one of the five priority topics retained for the Upgrade Program of the ESRF [2]. The common feature to all these techniques is that they apply to inhomogeneous samples, where it is important to measure "locally" a given property, which can be, for instance, the density, the composition, the chemical state or the distortion. These techniques take advantage of most of the photon-matter interactions: absorption, wavefront modification, diffraction, scattering, photoemission, … An increasing part of the experimental results obtained at modern SR-facilities can now be considered, in this way, as "X-ray images" *i.e*. maps in two, or, increasingly, in three dimensions, over the sample of the "local" value of a physical quantity. In this case "local" does not mean atomic level (whereas in some cases atomic information can be extracted from the images) but corresponds to the very important 10^{-3}-10^{-8} m range, where many biological and materials science phenomena occur.

The availability of very efficient lenses in the hard X-ray range (2-100 keV) [3-6] led to a dramatic progress of the scanning version of X-ray imaging (**microbeam based imaging**). This is used for structural and chemically–selective X-ray imaging (high spatial resolution fluorescence maps, or chemical state using energy dispersive micro-spectroscopy) [7, 8].

Techniques are clearly heading towards fulfilling the nanoscale challenge, this implying **higher spatial resolution** X-ray imaging. This is a clear requirement originating from many different scientific communities, which include materials science, but also soft condensed matter, biology, and cultural heritage. High spatial resolution, beyond the detector resolution, is being achieved by nanofocused beams or by lensless coherent diffraction imaging, with a generalized use of phase retrieval procedures, like the iterative determination of the phase of the scattering amplitude in coherent diffraction imaging [9-14].

A second obvious trend is the **improvement of temporal resolution**, made possible by the specific development of X-ray detectors and computing upgrades, which offer new scientific opportunities to follow a system evolving with a short time constant (ms-s range) [15, 16]. Recent developments exploit the **coherence** of the synchrotron X-ray beams for sophisticated phase contrast imaging or coherent diffraction imaging. These techniques rely on improvements of detectors and algorithms, in particular for the reconstruction of "holotomographic" images [17, 18].

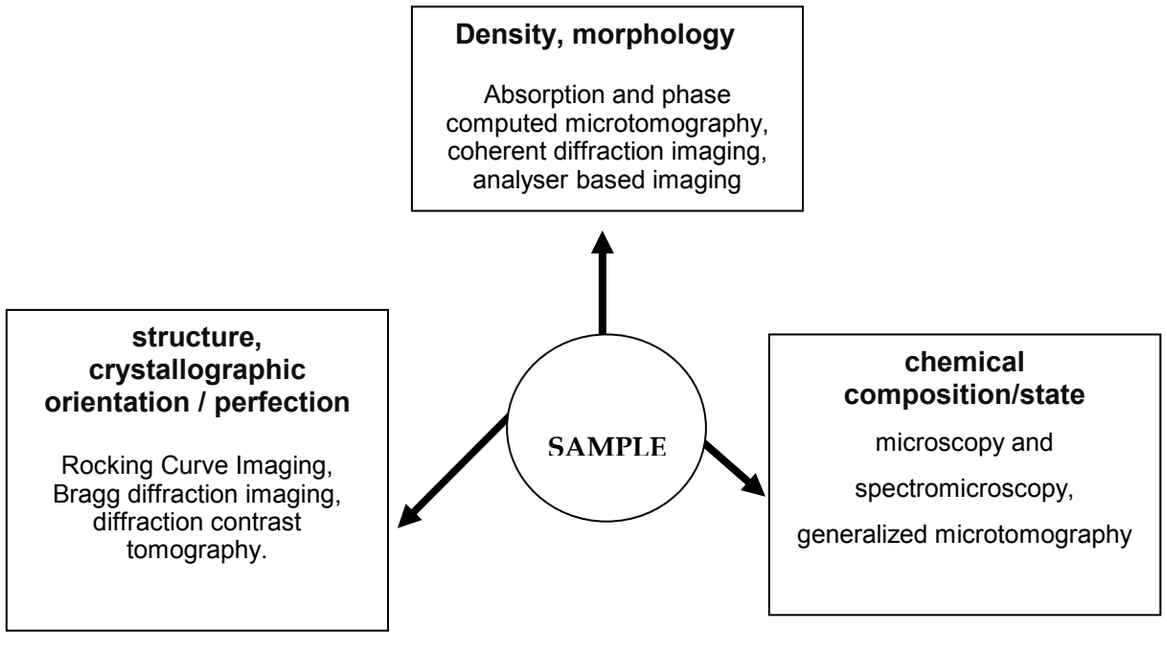

Figure 1: information accessible by using X-ray imaging, and some corresponding SR-based techniques.

L1

The **combination of techniques** can substantially improve the scientific information that can be obtained on a given topic [19]. An example is Diffraction Contrast Tomography, which provides both the shape and orientation of the grains in a polycrystalline, and the fracture path when this sample is submitted to a tensile stress [20, 21].

These new opportunities will be discussed and illustrated by examples of applications to a wide variety of materials, which reveal features not observable otherwise.

References

[1] J. Baruchel, P. Bleuet, A. Bravin, P. Coan, E. Lima, A. Madsen, W. Ludwig, P. Pernot, J. Susini, "Advances in synchrotron hard X-rays based imaging", *CR. Physique* (2007), in press doi:10.1016/j.crhy.2007.08.003.

[2] http://www.esrf.fr/AboutUs/Upgrade/purple-book/

[3] C. Schroer, B. Lengeler, "Focusing hard X-rays to nanometer dimensions by adiabatically focusing lenses", *Phys. Rev. Lett*. **94** (2005) 054802.

[4] O. Hignette, P. Cloetens, G. Rostaing, P. Bernard, C. Morawe, "Efficient sub 100 nm focusing of hard x-rays", *Rev. Sci. Instrum.* **76** (2005) 063709

[5] H. Kang, J. Maser, G. Stephenson, C. Liu, R. Conley, A. Macrander, S. Vogt, "Nanometer linear focusing of hard X-rays by a mulilayer Laue lens", *Phys. Rev. Lett*. **96** (2006) 127401.

[6] H. Hidekazu Mimura, H. Yumoto, S. Matsuyama, Y. Sano, K. Yamamura, Y. Mori, M. Yabashi, Y. Nishino, K. Tamasaku, T. Ishikawa, K. Yamauchi, "Efficient focusing of hard x rays to 25 nm by a total reflection mirror", *Applied Physics Letters* **90** (2007) 051903.

[7] F. Adams, L. Van Vaeck, R. Barrett, "Advanced analytical techniques: platform for nano materials science", *Spectrochim. Acta B* **60** (2005) 13.

[8] J. Susini, M. Salomé, R. Tucoulou, G. Martinez-Criado, S. Bohic, D. Eichert, P. Bleuet, I. Letard, M. Cotte, J. Cauzid, B. Fayard, R. Baker, S. Labouré, "X-Ray Micro-Analysis Activities at the ESRF", Proc. 8th International Conference on X-ray Microscopy, *IPAP (The Institute of Pure and Applied Physics) Conf. Series* **7** (2006) 18.

[9] J. Baruchel, J.-Y. Buffière, P. Cloetens, M. Di Michiel, E. Ferrie, W. Ludwig, E. Maire, L. Salvo, "Advances in synchrotron radiation microtomography", *Scripta Mater*. **55** (2006) 41.

[10] P. Cloetens, R. Mache, M. Schlenker, L. Lerbs-Mache, "Quantitative phase tomography of Arabidopsis seeds reveals intercellular void network", *Proc. Natl. Aced. sci. (USA)* **103** (2006) 14626.

[11] R. Mokso, P. Cloetens, E. Maire, W. Ludwig, J.Y. Buffière, "Nanoscale zoom tomography with hard X rays using Kirkpatrick-Baez optics", *Appl. Phys. Lett*. **90** (2007) 144104.

[12] M.A. Pfeifer, G.J. Williams, I.A. Vartanyants, R. Harder, I.K. Robinson, "Three-dimensional mapping of a deformation field inside a nanocrystal", *Nature* **442** (2006) 63.

[13] S. Eisebitt, J. Lüning, W.F. Schlotter, M. Lörgen O. Hellwig, W. Eberhardt, J. Stöhr, "Lensless imaging of magnetic nanostructures by X-ray spectro-holography", *Nature* **432** (2004) 885.

[14] J.M. Rodenburg, A.C. Hurst, A.G. Cullis, B.R. Dobson, F. Pfeiffer, O. Bunk, C. David, K. Jefimovs, I. Johnson, "Hard-x-ray lensless imaging of extended objects", *Phys. Rev. Lett.* **98** (2007) 034801.

[15] Y.J. Wang, K.-S. Im, K. Fezzaa, W.K. Lee, J. Wang, P. Micheli, C. Laub, "Quantitative X-ray phase contrast imaging of air-assisted water sprays with high Weber numbers", *Appl. Phys. Lett*. **89** (2006) 151913.

[16] N. Limodin, E. Boller, L. Salvo, M. Suéry, M. DiMichel, "In-situ fast X-ray tomography investigation of microstructural changes occurring during partial remelting and solidification of Al-Cu alloys", in: *Proceedings of the 5th International Conference on Solidification Processing*, Sheffield, 2007, pp 316-320.

[17] S. Zabler, P. Cloetens, J.-P. Guigay, J. Baruchel, M. Schlenker, Optimization of phase contrast imaging using hard X-rays, *Rev. Sci. Instr*. **76** (2005) 1.

[18] J.P. Guigay, M. Langer, P. Cloetens, R. Boistel, "Mixed transfer function and transport of intensity approach for phase retrieval in the Fresnel region", *Optics Lett*. **32** (2007) 1617.

[19] B. Golosio, A. Somogyi, A. Simionovici, P. Bleuet, J. Susini, L. Lemelle, "Nondestructive three-dimensional elemental microanalysis by combined helical X-ray microtomographies", *Appl. Phys. Lett*. **84** (2004) 2199.

[20] W. Ludwig, S. Schmidt, E.M. Lauridsen, H.F. Poulsen, "Diffraction contrast tomography: A novel technique for 3D grain mapping in polycrystals", Part I: direct beam case, *J. Appl. Cryst.* **41** (2008) 302.

[21] G. Johnson, A. King, M. Gonzalves-Hoennicke, W. Ludwig, "Diffraction contrast tomography: a novel technique for 3D grain mapping in polycrystals. Part II: The combined case", *J. Appl. Cryst.* **41** (2008) 310.

L2

ADVANCEMENT IN X-RAY WAVEGUIDES AND THEIR APPLICATIONS IN COHERENT DIFFRACTION IMAGING

D. Pelliccia [1*], C. Giannini [2], L. De Caro [2], A. Cedola [3], I. Bukreeva [3], and S. Lagomarsino [3]

[1] *Institut für Synchrotronstrahlung – ANKA Forschungszentrum Karlsruhe*
Herman-von-Helmholtz-Platz 1, D-76344 Eggenstein-Leopoldshafen, Germany
[2] *Istituto di Cristallografia - CNR, Via Amendola 122/O, 70126 Bari, Italy*
[3] *Istituto di Fotonica e Nanotecnologie - CNR, Via Cineto Romano 42, 00156 Roma, Italy*

Keywords: x-ray waveguides, x-ray imaging, coherent x-ray diffraction

**) e-mail: daniele.pelliccia@iss.fzk.de*

X-ray planar waveguides are currently used tools, in synchrotron radiation facilities, to produce a coherent beam with dimension of nanometer size. The properties of waveguided beams such as divergence and coherence will be reviewed for different coupling methods of the radiation field with the waveguide channel. Results obtained with both synchrotron radiation and laboratory source will be presented.

Due to the high degree of coherence of the exiting beam, x-ray waveguides can be successfully exploited in Coherent Diffraction Imaging experiments. We present results concerning Fresnel coherent diffraction imaging experiments with hard x-rays, using planar waveguides as optical elements in one and two dimensions. This method offers a route for fast and reliable phase retrieval in x-ray coherent diffraction.

References

[1] D. Pelliccia, I Bukreeva, M. Ilie, W. Jark, A. Cedola, F. Scarinci, S. Lagomarsino, "Computer simulations and experimental results on air-gap x-ray waveguides", *Spectrosc. Acta B* **62** (2007) 615.

[2] I. Bukreeva, A. Popov, D. Pelliccia, A. Cedola, S. Dabagov, S. Lagomarsino, "Wave field formation into an hollow x-ray waveguide", *Phys. Rev. Lett*. **97** (2006) 184801.

[3] L. De Caro, C. Giannini, A. Cedola, D. Pelliccia, S. Lagomarsino, W. Jark, "Phase retrieval in x-ray coherent Fresnel projection-geometry diffraction", *Appl. Phys. Lett*. **90** (2007) 041105.

[4] L. De Caro, C. Giannini, D. Pelliccia, C. Mocuta, T.H. Metzger, A. Guagliardi, A. Cedola, I. Bukreeva, S. Lagomarsino, "In-line holography and coherent diffractive imaging with x-ray waveguides"**,** *Phys. Rev. B* **77** (2008) 081408(R).

L3

X-RAY IMAGING IN MICRO-TO-NANO WORLD

J.H. Je [1*], B.M. Weon [1], S.K. Seol [1], J.M. Yi [2], Y. Hwu [3], and G. Margaritondo [4]

[1] *X-ray Imaging Center, Pohang University of Science and Technology San 31 Hyojadong, 790-784 Pohang, Korea*

[2] *Advanced Photon Source, Argonne National Laboratory, Argonne, Illinois 60439, USA*

[3] *Institute of Physics, Academia Sinica, Taipei 115, Taiwan*

[4] *Ecole Polytechnique Fédérale de Lausanne (EPFL), CH-1015, Switzerland*

Keywords: radiography, phase contrast, x-ray imaging, synchrotron, bright field imaging

**) e-mail: jhje@postech.ac.kr*

In recent years, X-ray imaging has been literally revolutionized by the exploitation of the unique characteristics of synchrotron sources. In particular, the high spatial coherence of the radiation significantly contributes to the development of advanced and powerful X-ray imaging. The results are very high quality microradiology and microtomography images and movies - taken with a limited X-ray dose – that find a variety of applications in materials science, biology and medical research. In this talk we review basic theory and selected applications of phase contrast X-ray imaging to materials and biomedical sciences. Furthermore we introduce a new strategy of combining phase contrast radiology and diffraction X-ray microscopy to visualize atomic level defects such as misfit dislocations and micropipes in semiconductor single crystals. Finally phase contrast X-ray imaging in nanometer-resolution (< 30 nm) will be demonstrated.

1. Introduction

X-ray imaging methods based on phase contrast radiology are becoming important analytical tools for real-time processes in materials science, life science, medicine, physics, chemistry and other disciplines [1-4]. Even though theoretical background and the practical implementation were discussed recently [5], most of results had limitation in dynamic studies owing to significant losses of X-ray flux by using monochromatic X-rays.

In comparison we introduce white beam phase contrast X-ray imaging, enabling time-resolved dynamic studies in millisecond time resolution. We review basic imaging mechanism of white beam phase contrast imaging and demonstrate several applications in materials and biomedical sciences.

To further enhance spatial resolution in nanoscales, the development of X-ray nanoscopy based on using Fresnel zone-plates is discussed [6]. Furthermore we introduce a new concept of X-ray microscopy, bright-field X-ray microscopy, which has been for the first time developed in our group by combining phase contrast radiology and diffraction topography [7, 8].

2. Technical background

Coherence is the property of a wave that enables to produce visible diffraction and interference effects. For the X-rays traveling though a pinhole, the diffraction pattern may or may not be visible on the detector depending on the source size, its angular divergence and its wavelength bandwidth. The condition to see the edge diffraction fringes is $\Delta\lambda/\lambda < \sqrt{2}$. This condition is already satisfied without using any monochromator for synchrotron hard X-rays. The equivalent condition for "refraction" radiology is much more relaxed. This results in many consequences of the limited need for time coherence. First of all, no monochromator is necessary for phase contrast radiology. In other words white or "pink" beamlines are enough for phase contrast X-ray imaging. Therefore there is no monochromator-related X–ray flux loss, enabling time-resolved experiments with time resolution of 1 msec. Finally high time resolution together with high (better than 1 micrometer) lateral resolution can be achieved [9].

As for X-ray nanoscopy, Fresnel zone plates (FZPs) are widely used as focusing and magnifying optics devices and offer the highest imaging resolution in the entire electromagnetic spectrum. A FZP consists of concentric rings with decreasing width and increasing radius - and the outermost zone width approximately sets the resolution.

X-rays can yield bright-field (BF) images of crystalline systems similar to transmission electron microscopy (TEM); such images carry information both from diffraction/scattering phenomena and from absorption and phase contrast. For a strong reflection of (0001) 4H-SiC wafers in the Laue (transmission) geometry, synchrotron X-ray transmission micrographs simultaneously yield diffraction-based information on lattice distortions and radiographic information on structural inhomogeneities.

3. Applications in materials and biomedical sciences

The fabrication of 3D conducting polymer structures with high aspect ratios remains a challenge. Such structures are particularly important in a broad range of device applications in microelectronics, biomedical devices, and micro-systems such as actuators and sensors.

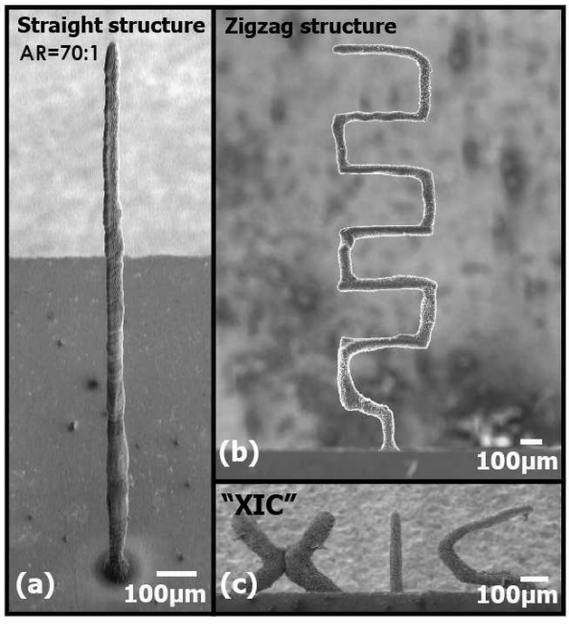

Figure 1. FESEM images of freestanding PPy HAR microstructures with dense and smooth morphology. The images show: a) a wire-like straight structure with aspect ratio = 70; b) a zigzag structure; c) a complex structure corresponding to the letters "XIC".

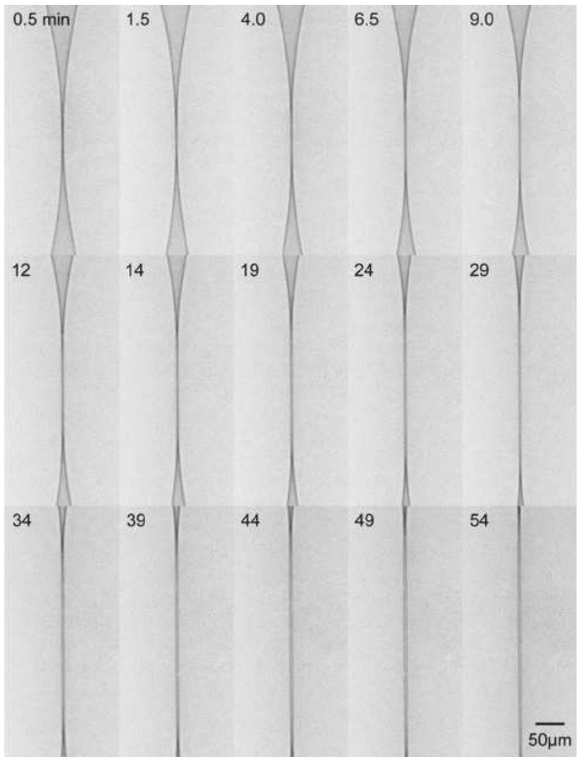

Figure 2. Sequence of phase contrast images revealing the evolution of the water film during X–ray irradiation.

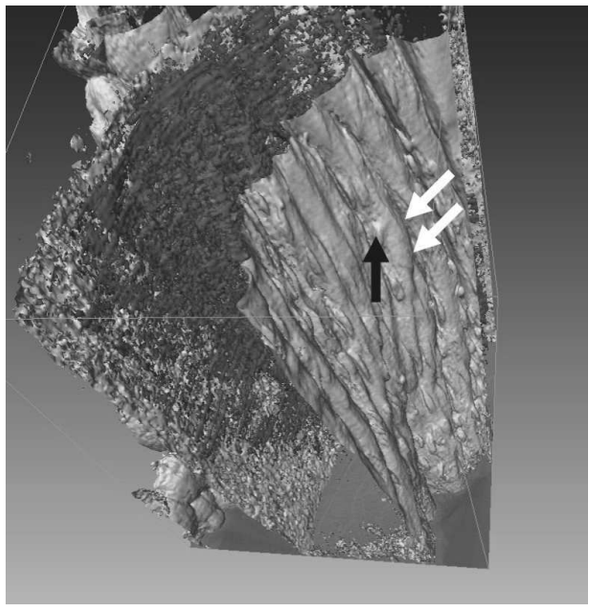

Figure 3. The volume-rendered 3D structure of a piece of mouse aorta. Scale bar is 50 μm.

Figure 1 shows several successful fabrication tests of freestanding polypyrrole(PPy) high-aspect-ratio microstructures with different shapes: straight (a), zigzag (b), and a complex geometry (c) using real-time monitoring of localized electropolymerization of 3D PPy growth [10].

In spite of the strong fundamental and applied interest in water microstructure, so far, no technique was able to produce stable freestanding pure-water thin films, mostly due to rapid rupture caused by the very low viscosity and high surface tension of pure water. As can be demonstrated in Fig. 2 that shows real-time fabrication process of stable free standing thin films of pure water, we were for the first time able to fabricate free standing water film with a lifetime of 1 h after 54 min irradiation [11].

Figure 3 demonstrates the volume-rendered 3D structure of a piece of mouse aorta. The white arrows point to borders between neighboring cells, whereas the black arrow points to a cell nucleus that extrudes from the surface and whose outline is well preserved in the 3D reconstruction analysis. In this case, the imaging capability goes beyond the mere imaging of the outline and shape of the individual cell and provides subcell information [12].

4. Conclusions

White beam phase contrast X-ray imaging is expected to be significantly applied in a variety of sciences in the near future.

L4

REAL-SPACE IMAGING OF ATOMIC STRUCTURE

P. Korecki *

Institute of Physics, Jagiellonian University, ul. Reymonta 4, 30-059 Krakow, Poland

Keywords: x-ray absorption anisotropy, real-space imaging, tomography

**) e-mail: pawel.korecki@uj.edu.pl*

The majority of x-ray methods for crystal structure investigations are based on diffraction phenomena and sample the information in the reciprocal space.

In this talk we will discuss the possibility of x-ray imaging of the atomic structure directly in the real-space [1]. This distinct and novel approach is possible by recording and analysing the absorption anisotropy of polychromatic, so called "white" x-rays. In this approach, the interference between the incident x-ray beam and the secondary waves coherently scattered inside the specimen modifies the x-ray wave field at the position of the absorbing atoms. Thus, the absorption cross-section is effectively modulated by the x-ray scattering. For a white x-ray beam, the wave field variations cancel out by energy integration for all directions, except for the near forward scattering components, coinciding with the incident beam. Therefore, a two-dimensional pattern of absorption anisotropy can be interpreted as a real-space projection of atomic structure. In this sense, the method lies aside from the traditional x-ray diffraction and closer to the forward scattering of electrons or ion beam channelling. However, its description can be made in the frame of a straightforward first Born approximation, which makes the data interpretation much easier.

We will present two algorithms for direct structure imaging from x-ray absorption anisotropy data. The first one allows for full three-dimensional imaging of crystal structure and it is similar to tomography [2]. The second one uses spherical wavelet transform to determine the bond directions in the local neighbourhood of the absorbing atoms.

Both approaches were tested on the experimental data recorded in HASYLAB for GaP(111) and InAs(001) samples, using a white x-ray radiation from a bending magnet [3]. In order to monitor the x-ray absorption anisotropy we measured total electron yield as the function of the orientation of the sample relative to the incident beam direction. Examples of the recorded data and the three-dimensional reconstruction of atomic structure are shown in Fig. 1.

In future experiments we plan to obtain chemically resolved x-ray anisotropy patterns for element specific imaging. This will be possible with a new experimental setup containing polycapillary optics for collimation of the secondary x-ray fluorescence.

Acknowledgements: This work was supported by Polish Ministry of Science and Higher Education (grant no. N202 012 32/0628). Synchrotron experiments at HASYLAB/DESY were financially supported by the European Community-Research Infrastructure Action under the FP6 "Structuring the European Research Area" Program (Integrating Activity on Synchrotron and Free Electron Laser Science; project: contract RII3-CT-2004-506008).

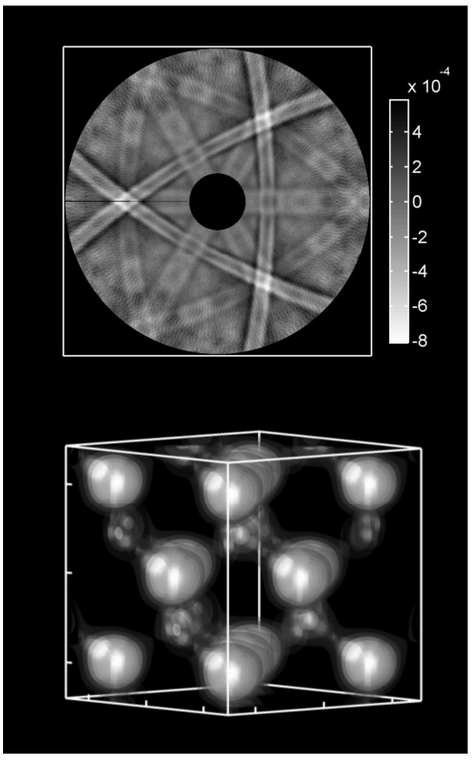

Figure 1. Top: white x-ray absorption anisotropy recorded for GaP(111) crystal. The visible bands correspond to real-space projections of atomic planes. Bottom: structure of GaP recovered with a tomographic algorithm form the data.

References

[1] P. Korecki, G. Materlik, "Real-space imaging of atomic structure with white x-rays", *Phys. Rev. Lett.* **86** (2001) 2333.

[2] P. Korecki, M. Tolkiehn, D.V. Novikov, G. Materlik, M. Szymonski, "X-ray tomographic imaging of crystal structure at atomic level", *Phys. Rev. Lett.* **96** (2006) 035502.

[3] P. Korecki, M. Tolkiehn, D.V. Novikov, G. Materlik, M. Szymonski, "Directional fine structure in absorption of white x-rays: a tomographic interpretation", *Phys. Rev. B* **74** (2006) 184116.

L5

IMAGING AND SPECTROMICROSCOPY OF MICRO- AND NANO-MATERIALS

Maya Kiskinova *

Sincrotrone Trieste, Area Science Park, 34012 Trieste, Italy

Keywords: spectromicroscopy, nanomaterial, imaging, photoelectron spectroscopy

**) e-mail: kiskinova@elettra.trieste.it*

The complementary capabilities of different microscopy approaches in terms of imaging, spectroscopy, spatial and time resolution are strongly requested by the multi-disciplinary research programs at the synchrotron facilities and have motivated continuous investments in development of instrumentation for imaging with spectroscopic analysis. ELETTRA has very extensive programs in the field of spectromicroscopy, which have significantly contributed to advancing the frontiers of surface, material and life science [1].

The major part of the lecture will be focused on the potential of modern x-ray photoelectron microscopes in chemical imaging and micro-spot photoelectron spectroscopy [2]. Among the selected research topics are (i) addressing the surface properties of the individual C and oxide nanostructures and supported catalyst micro and nano-particles (ii) mass transport driven self-reorganization processes which can introduce lateral heterogeneity in the composition and reactive properties of surfaces and (iii) identification of degradation processes in organic light devices.

The final part will briefly illustrate the most recent achievements in combining the potential of soft x-ray scanning transmission x-ray microscopy with multiple contrast approaches and fluorescence analysis.

References

[1] D. Eichert, L. Gregoratti, B. Kaulich, A. Marcello, P. Melpignano, L. Quaroni, M. Kiskinova, *Anal. Bioanal. Chem.* **389** (2007) 1121.

[2] S. Günther, B. Kaulich, L. Gregoratti, M. Kiskinova, *Prog. Surf. Sci.* **70** (2002) 187.

L6

SYNCHROTRON MÖSSBAUER REFLECTOMETRY OBSERVATION AND CELLULAR AUTOMATON SIMULATION OF DOMAIN FORMATION AND TRANSFORMATION IN ANTIFERROMAGNETICALLY COUPLED Fe/Cr MULTILAYERS

D.L. Nagy [1*], L. Bottyán [1], A.I. Chumakov [2], L. Deák [1], E. Harth [1], M. Major [1], J. Meersschaut [3], D.G. Merkel [1], R. Rüffer [2], E. Szilágyi [1], F. Tanczikó [1], and D. Visontai [1]

[1] *KFKI Research Institute for Particle and Nuclear Physics, P.O.B. 49, H-1525 Budapest, Hungary*

[2] *European Synchrotron Radiation Facility, BP 220, F-38043 Grenoble, France*

[3] *Instituut voor Kern- an Stralingsfysica, K.U. Leuven, Celestijnenlaan 200 D, B-3001 Leuven, Belgium*

Keywords: nuclear resonant scattering, reflectometry, magnetic domains, multilayers, cellular automaton

**) e-mail: nagy@rmki.kfki.hu*

1. Introduction

Antiferromagnetically (AF) coupled metallic multilayers (ML) have received much attention in recent years due to their relevance in fundamental science and magnetic recording technology alike. The performance of magnetoresistive devices is strongly affected by the ML domain structure [1]. Both plane-perpendicular and lateral magnetic structure of AF coupled metallic MLs can be efficiently studied by two closely related nuclear scattering techniques, viz. synchrotron Mössbauer reflectometry (SMR) [2, 3] and polarised neutron reflectometry (PNR) [4]. Here we present SMR studies of the magnetic-field-history-dependent formation and transformation of magnetic domains in strongly AF-coupled epitaxial MLs. One of the observed transformations will be described by a Monte Carlo simulation using a cellular automaton algorithm.

2. Experimental

An epitaxial MgO(001)/[^{57}Fe(2.6 nm)/Cr(1.3 m)]$_{20}$ ML was fabricated by MBE technique and was characterised reflection high-energy electron diffraction (RHEED), Rutherford backscattering (RBS), x-ray reflectometry, magneto-optical Kerr effect (MOKE), vibrating sample magnetometry (VSM), conversion electron Mössbauer spectroscopy (CEMS), conversion electron Mössbauer polarimetry (CEMP), specular PNR and specular SMR experiments. The room-temperature (RT) saturation field of the ML of fourfold in-plane anisotropy was found from the specular intensity of the SMR AF reflections to be H_S = 0.85 T and 1.05 T along the easy and hard axes, respectively. The easy-axis saturation field increased to H_S = 1.55 T at T = 15 K. A bulk-spin-flop (BSF) transition took place at RT when a magnetic field of 14 mT was applied along the easy axis in which the layer magnetisations actually lay [5, 6].

Diffuse SMR experiments were performed at the nuclear resonance beamline ID18 of the European Synchrotron Radiation Facility, Grenoble. The ML was placed in a liquid helium cryostat equipped with a superconducting solenoid and a variable temperature inset. The photons reflected from the ML were detected by an avalanche photo diode (APD).

3. Diffuse synchrotron Mössbauer reflectometry

The off-specular (diffuse) nuclear resonant reflectivity of synchrotron radiation (diffuse SMR) probes the in-plane component q_x of the scattering vector. In the kinematical approximation, the q_x-scan width at the AF Bragg peak (*i.e.*, at fixed q_z) is $\Delta q_x = 1/\xi$ where ξ is the in-plane correlation length ξ of the magnetisation, *i.e.*, the 'size' of the AF domains. A more accurate theory of diffuse SMR relating the diffuse scatter to the structural and/or magnetic autocorrelation function of the ML in terms of a distorted-wave approximation has been given recently [7].

4. Domain formation and ripening

Starting with a strongly AF-coupled ML in magnetic saturation and then gradually decreasing the field, two kinds of AF patch domains differing only in the sense of rotation of the magnetisation in their odd and even layers are spontaneously formed [8]. The patch domain formation is the consequence of the reduced stray field and the freedom of the AF-coupled regions in selecting the sense of rotation of their top-layer magnetisation during unsaturation [9]. On further decreasing the field and, thereby, increasing the domain-wall angle, the size of the domains is expected to spontaneously increase in order to decrease the domain-wall energy per unit area of the ML [10]. We observed this *domain ripening* with SMR. At RT, the native domain size of ξ = 370 nm did not change down to 200 mT while it spontaneously increased to ξ = 800 nm between 200 and 100 mT. No further increase of ξ was found down to remanence. The domain ripening was found to be an irreversible process and was followed by an apparent change in the shape of the diffuse SMR scattering peak. No ripening took place

at $T = 15$ K, probably a consequence of the temperature dependence of the coercivity [11]. However, the ripening was observed with SMR when the temperature was raised to RT. Domain ripening was not sensitive to the orientation of the external field relative to the magnetic easy axes.

5. Domain coarsening

A dramatic increase of ξ from 800 nm to at least 5 μm, *i.e.*, a *coarsening* of the AF domains was observed in the same multilayer [12] both with SMR and with PNR when it passed the BSF transition provided that the external easy-axis magnetic field was previously decreased from magnetic saturation to zero. In contrast to ripening, a domain-wall-energy-driven and coercivity-limited process, the explosion-like coarsening is driven by the Zeeman and the anisotropy energies and is not associated with any long-range domain-wall movement. Also coarsening was found to be irreversible as long as the applied field did not reach the saturation region.

6. Supersaturation memory effect

We observed an apparent *supersaturation memory effect* in the field history of the same Fe/Cr ML. At RT, we had to apply at least $H_{SS} = 1.30$ T in either easy or hard directions to erase the 'ripened' or 'coarsened' domain structure, *i.e.*, to convert the ML domains into their native size and shape. At $T = 15$ K, H_{SS} increased to a value as high as 3.60 T. A comparison with the behaviour of other Fe/Cr MLs suggests that this effect was the consequence of the presence of a small fraction of very strongly coupled regions in the first ML [13].

7. Cellular automaton simulation

Although the physical bases of these transformations are quite clear, so far no model has been able to quantitatively describe the observed details. In the following, we will present a simple model of the domain walls and of the domain-wall movement in strongly AF-coupled MLs. We will show that a cellular automaton simulation based on this model is able to describe all the observed details of domain transformations.

We describe the ML as consisting of AF domains, that are much bigger than the domain walls. The model magnetisation of the domains obeys a two-sublattice behaviour characterised by the opening angle 2φ calculated from the minimum condition for the bilinear layer-layer coupling and the Zeeman energy as $\varphi = \arccos H/H_s(\boldsymbol{r})$. We assume that the layer-layer coupling and, consequently, the saturation field $H_S(\mathbf{r})$ follow a certain (*e.g.*, Gaussian) distribution the expectation value and standard deviation of which are free parameters of the model. The domain-wall energy is supposed to be proportional to the square of the domain-wall angle with a coupling coefficient D having no lateral distribution. In addition, the coercivity H_c of the FM layers is considered constant for the whole ML but allowed to depend on the temperature T.

A micromagnetic simulation of the domain structure in a volume of the ML, which is large enough for calculating the autocorrelation function of the magnetisation with the accuracy necessary for determining the diffuse SMR scatter would include 10^{12}–10^{13} spins. This is technically not feasible and, therefore, the number of degrees of freedom has to be reduced considerably.

The Monte Carlo simulation starts with generating random values of $H_s(\boldsymbol{r})$ on a lattice of 'pixels' that will be the lattice points of a cellular automaton. One pixel is an area of the ML smaller than a domain (*i.e.*, the correlation length of the top-layer magnetisation) and bigger than a domain wall. One pixel consists of about 10^8 strongly coupled spins of the ML stack; the whole simulation includes 10^4–10^5 lattice points. The domain-wall energy of the ML is calculated as the sum of the next-neighbour pixel domain-wall energies with non-vanishing contribution only from pairs of opposite sense of rotation of the top-layer magnetisation. Should a pixel jump from one sense of rotation to the other, half of its full hysteresis loss, *i.e.*, $2H_cM \sin\varphi$ will be dissipated (M is the saturation magnetisation of one pixel).

The cellular automaton rule is to minimise the total energy of the lattice in monotonically changing external magnetic field or monotonically changing coercivity. The Hamiltonian contains a nearest-neighbour domain-wall energy term as well as the dissipative penalty term describing the hysteresis loss. Further terms of the Hamiltonian, *i.e.*, the Zeeman energy and the bilinear layer-layer interaction of random lateral distribution are replaced by the logical condition $\varphi = 0$ for $H \geq H_s$ and $\varphi \neq 0$ for $H < H_s$. Indeed, both terms are independent of the sense of rotation.

The movies of the domain dynamics with varying H or T (*i.e.*, H_c) to be shown in the presentation consist of pictures. Subsequent pictures of the calculation always differ from each other only by the sense of rotation of a single pixel (the saturation state being considered to have a third, 'neutral' sense of rotation). On gradually changing H or H_c, a pixel will change its sense of rotation if the new state, taken into account the domain-wall energy and the hysteresis loss, will be energetically more favourable. Thus, the simulation depends from D and H_c only through their ratio D/H_c. The simulation of domain ripening reproduces the observed, relatively sudden transition. This is attributed to the fact that the pixel model properly accounts for the local character of the domain-wall interaction. Therefore ripening is seen in the movies as a smoothing out of the domain walls and vanishing of small enclosures of the opposite sense of rotation. Other H-dependent simulations fairly well describe the supersaturation behaviour in case of a broad distribution of $H_s(\mathbf{r})$. Starting from the native state, and decreasing H_c (*i.e.*, increasing T) [11] the temperature-induced ripening is well simulated.

8. Conclusion

In conclusion, we have shown that the domain structure of a ML of strong AF coupling depends on the history of the external magnetic field and of the coercivity of the

L6

ferromagnetic layers (*i.e.*, of the temperature). This results in a great variety of domain formation and transformation processes. The cellular automaton algorithm based on the rough 'pixel model' of the domains depending only on a very small number of free parameters is able to properly reproduce the main features of domain ripening and domain memory supersaturation in AF-coupled MLs.

Acknowledgements: The authors thank F. Iglói, Yu.N. Khaidukov, L. Lovász, Yu.V. Nikitenko, A.V. Petrenko, V.V. Proglyado and Gy. Szabó for stimulating discussions. Provision of synchrotron radiation by the European Synchrotron Radiation Facility as well as financial support by the Hungarian National Fund (OTKA) and by the European Community under the respective contract Nos. T047094 and STREP NMP4-CT-2003-001516 (DYNASYNC) is gratefully acknowledged.

References

[1] H.T. Hardner, M.B. Weissmann, S.S.P. Parkin, "History dependent domain structures in giant-magnetoresistive multilayers", *Appl. Phys. Lett.* **67** (1995) 1938-1940.

[2] L. Deák, L. Bottyán, D.L. Nagy, H. Spiering, "The coherent forward scattering amplitude in transmission and grazing incidence Mössbauer spectroscopy", *Phys. Rev. B* **53** (1996) 6158-6164.

[3] D.L. Nagy, L. Bottyán, L. Deák, E. Szilágyi, H. Spiering, J. Dekoster, G. Langouche, "Synchrotron Mössbauer reflectometry", *Hyperf. Interact.* **126** (2000) 353-361.

[4] G.P. Felcher, S.G.E. te Velthuis, A. Rühm, W. Donner, "Polarized neutron reflectometry: recent developments and perspectives", *Physica B* **297** (2001) 87-93.

[5] L. Bottyán, L. Deák, J. Dekoster, E. Kunnen, G. Langouche, J. Meersschaut, M. Major, D.L. Nagy, H.D. Rüter, E. Szilágyi, K. Temst, "Observation of the bulk spin-flop in an Fe/Cr superlattice", *J. Magn. Magn. Mat.* **240** (2002) 514-516.

[6] F. Tanczikó, L. Deák, D.L. Nagy, L. Bottyán, "Conversion electron Mössbauer spectroscopy with a linearly polarized source", *Nucl. Instr. Meth. B* **226** (2004) 461–467.

[7] L. Deák, L. Bottyán, D.L. Nagy, H. Spiering, Yu.N. Khaidukov, Y. Yoda, "Perturbative theory of grazing-incidence diffuse nuclear resonant scattering of synchrotron radiation", *Phys. Rev. B* **76** (2007) 224420-1-13.

[8] M. Rührig, R. Schäfer, A. Hubert, R. Mosler, J.A. Wolf, S. Demokritov, P. Grünberg, "Domain observations on Fe-Cr-Fe layered structures", *phys. stat. sol. A* **125** (1991) 635-656.

[9] N. Persat, H.A.M. van den Berg, A. Dinia, "Domain-phase transformations in antiferromagnetically coupled Co/Cu sandwiches", *J. Magn. Magn. Mat.* **165** (1997) 446-449.

[10] D.L. Nagy, L. Bottyán, L. Deák, B. Degroote, O. Leupold, M. Major, J. Meersschaut, R. Rüffer, E. Szilágyi, J. Swerts, K. Temst, A. Vantomme, "Specular and off-specular synchrotron Mössbauer reflectometry: Applications to thin film magnetism", *phys. stat. sol. A* **189** (2002) 591-598.

[11] J. Hauschild, H. Fritzsche, S. Bonn, Y. Liu, "Determination of the temperature dependence of the coercivity in Fe/Cr (110) multilayers", *Appl. Phys. A* **74** (2002) S1541-S1543.

[12] D.L. Nagy, L. Bottyán, B. Croonenborghs, L. Deák, B. Degroote, J. Dekoster, H.J. Lauter, V. Lauter-Pasyuk, O. Leupold, M. Major, J. Meersschaut, O. Nikonov, A. Petrenko, R. Rüffer, H. Spiering, E. Szilágyi, "Coarsening of antiferromagnetic domains in multilayers: The key role of magnetocrystalline anisotropy", *Phys. Rev. Lett.* **88** (2002) 157202-1-4.

[13] M. Major, L. Bottyán, J. Meersschaut, D.L. Nagy, A.V. Petrenko, F. Tanczikó, "Supersaturation of antiferromagnetically coupled multilayers: A comparative polarised neutron reflectometry study", *Physica B* **397** (2007) 53–55.

VUV LUMINESCENCE OF BaF_2:Er AND (Ba,La)F_2:Er

A.J. Wojtowicz [1*] and S. Janus [1]

[1] *Institute of Physics, Nicolaus Copernicus University, ul. Grudziadzka 5, 87-100 Torun, Poland*

Keywords: VUV luminescence, Er, BaF_2:Er, (Ba,La)F_2:Er

**) e-mail: andywojt@fizyka.umk.pl*

New applications such as fast scintillators, VUV solid state lasers and mercury free phosphors have generated a surge of interest in the VUV luminescence of rare earth activated wide bandgap materials. It is interesting to note that the so-called "extended Dieke's" diagram has been established only recently [1]. Lack of experimental and theoretical data on energies of the higher lying levels of the $4f^n$ and $4f^{n-1}d$ configurations and availability of excellent synchrotron facilities devoted to VUV (Superlumi and HIGITI stations, Hasylab, DESY, Hamburg) provide additional factors attracting attention of many researchers.

In this communication we present luminescence and luminescence excitation spectra of Er-activated BaF_2 and (Ba,La)F_2. Preliminary, low resolution results on BaF_2:Er have been published by Drozdowski *et al*. [2]. Since their interpretation did not take into account higher lying energy levels of the $4f^{11}$ configuration [2], we have planned and performed new experiments in August 2007. These experiments were designed to clarify the role of the $^2F_{5/2}$, $^2G_{7/2}$ and $^2G_{9/2}$ $4f^{11}$ states in the VUV and UV emissions following excitation into spin-allowed $4f^{10}5d$ levels of the Er^{3+} ion in BaF_2 and (Ba,La)F_2.

Surprisingly, the dominant VUV emissions in these two closely related materials, shown in Figs. 1 and 2, are different. The emission of BaF_2:Er, peaking at 163.5 nm, is slow, as reported earlier [2,3], and similar to VUV emissions from other Er-activated fluorides [4]. The emission of (Ba,La)F_2:Er, peaking at 162.5 nm is, unexpectedly, relatively fast (35 ns at room temperature and 45 ns at 10 K). Also, as showin in Figs. 1 and 2, the relative intensities of the longer wavelengths bands are different.

We explain these results by proposing that in BaF_2:Er the emitting level is, as expected, the lowest, high spin (HS) *d*-level, $(HS)4f^{10}5d(e)$. The transition to the lowest energy $4f^{11}$ level ($^4I_{15/2}$) is spin forbidden, hence slow. Fast relaxation from the higher energy low spin level $(LS)4f^{10}5d(e)$ is facilitated by an intermediate $4f^{11}$ state, $^2F_{5/2}$. In (Ba,La)F_2:Er *d*-levels are shifted and the corresponding, spin forbidden emission, at 170 nm, is much weaker. The likely reason is that the intermediate $^2F_{5/2}$ state levels in (Ba,La)F_2 overlap the LS *d*-band at 158.7 nm leaving a relatively large energy gap between this and the lowest energy HS level corresponding to the *d*-band at 165 nm. Since both of these bands correspond to the same electronic configuration $(4f^{10}5d(e)$, a change in configuration coordinate must be small and, consequently, the relaxation of the ion in the higher energy LS state to the lower energy HS spin state, must be relatively slow. Slow relaxation promotes build up of the population of the LS level, from which the spin-allowed transitions to the $^4I_{15/2}$ ground state originate, producing the dominant VUV band at 162.5 nm. The longer wavelengths VUV and UV bands, shown in Figs. 1 and 2, originate in spin-forbidden (BaF_2) and spin-allowed ((Ba,La)F_2) transitions terminating at the excited states of the $4f^{11}$ multiplet, ^4I_J. It is not clear why, in (Ba,La)F_2, the relative intensities of these bands are higher than in BaF_2.

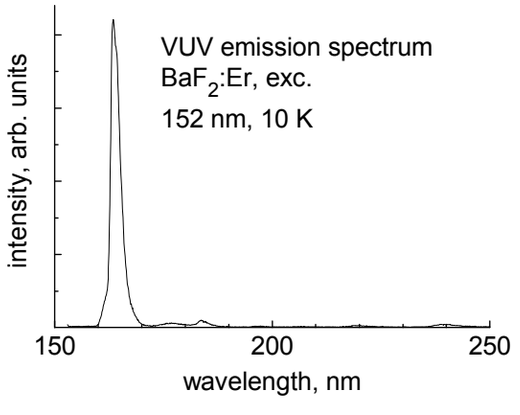

Figure 1. Time integrated VUV emission spectrum of BaF_2:Er. Excitation wavelength 152 nm (*d*-band), temperature 10 K.

Acknowledgements: The authors are grateful to Prof. Georg Zimmerer and Dr. G. Stryganyuk of Hasylab for their support and assistance at Superlumi. This work was supported by DESY and the European Community under contract RII3-CT-2004-506008 (IA-SFS).

L7

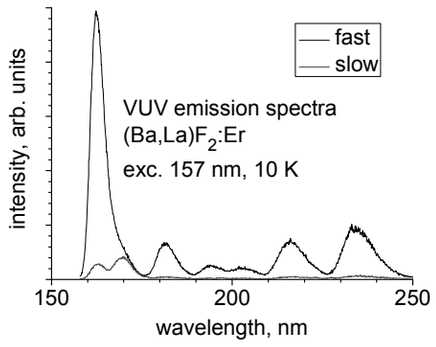

Figure 2. Time resolved emission spectra of $(Ba,La)F_2$:Er. Excitation wavelength 157 nm (*d*-band), temperature 10 K.

References

[1] R.T. Wegh, A. Meijerink, R.J. Lamminmäki, J. Hölsa, "Extending Dieke's diagram", *J. Lumin.* **87-89** (2000) 1002-1004.

[2] W. Drozdowski, J. Glodo, A.J. Wojtowicz, *Hasylab Annual Report*, Hamburg, 1999 (hasyweb.desy.de/science /annual_reports/1999_report/part1/contrib/42/621.pdf).

[3] A.J. Wojtowicz, "VUV spectroscopy of BaF_2:Er", *Optical Mater.*, in print.

[4] R.T. Wegh, H. Donker, A. Meijerink, "Spin-allowed and spin-forbidden *fd* emissions from Er^{3+} and $LiYF_4$", *Phys. Rev. B* **57** (1998) R2025-R2028.

L8

STRUCTURAL CHANGES AT THE VERWEY TRANSITION IN Fe_3O_4

Wojciech Tabiś [1]*, Joachim Kusz [2], Nhu Kim-Ngan Tarnawska [3], Zbigniew Tarnawski [1], Federico Zontone [4], Zbigniew Kąkol [1], and Andrzej Kozłowski [1]

[1] *AGH University of Science and Technology, Faculty of Physics and Applied Computer Science, Al. Mickiewicza 30, 30-059 Kraków, Poland*

[2] *Institute of Physics ,University of Silesia ,Uniwersytecka 4, 40-007 Katowice, Poland*

[3] *Institut of Physics, Pedagogical University, Kraków, Poland*

[4] *European Synchrotron Radiation Facility, P.B. 200, F-38043 Grenoble, France*

Keywords: metal-insulator phase transition; magnetite; photon correlation spectroscopy, crystal strucrure

**) e-mail: wtabis@agh.edu.pl*

The aim of the experiment (HS3274, June 2007, ESRF, ID10A) was to observe the temporal changes of magnetite Fe_3O_4 lattice symmetry occurring at the Verwey transition and to study the fluctuations of the lattice close and at the transition using X ray photon correlation (XPCS) technique.

At the Verwey transition at T_V = 125 K, a large latent heat manifests the abrupt change of major physical characteristics; *e.g.*, the crystal symmetry that turns from monoclinic (space group *Cc*) below T_V to cubic *Fd*-3*m*. Despite 60 years of interest the transition is still not entirely understood. In view of that, we have set up the project [1, 2] aimed to simultaneously observe how magnetic susceptibility χ_{AC}, electrical resistivity ρ and the specific heat change exactly at the transition. Due to large latent heat of transition, the time of this observation may be largely extended. In the present experiment we added yet another characteristics, crystal lattice symmetry, that can be observed simultaneously with others mentioned above, while the transition develops.

Two samples of stoichiometric magnetite ("110 sample" and "553 sample"), each ca. 0.5 g, were measured with the *E*=7.1 keV radiation and the superlattice peaks' (2 2 ½) and (1 1½ 2) dynamics was observed by CCD camera with the partially coherent beam. Sample temperature was monitored by the miniature Pt thermometer glued on the sample. AC susceptibility χ_{AC} was measured simultaneously by the setup within the sample holder.

The most important results are:

1. The superstructure peak disappears in the first one third part of the transition, as observed on heating (Fig. 1), (1 1½ 2) peak of "553" sample), *i.e.* where both *T* profile-plateau and a χ_{AC} step still signal the undergoing processes, ultimately leading to a high T phase. Since this result is valid also for cooling (the superlattice peak always appears close to low-T site of a transition), it may reflect the general fact that the Verwey transition is caused by the structural changes that trigger the transformation of other subsystems.

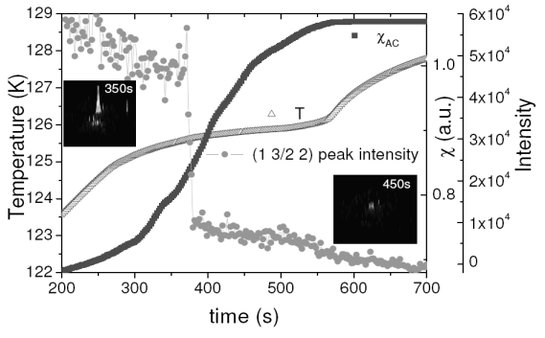

Figure 1. "553" sample. Temporal changes of the integrated (1 3/2 2) peak intensity (integrated over main part of CCD screen), sample temperature and χ_{AC} across the Verwey transition on heating.The insets show characteristic CCD intensity profiles.

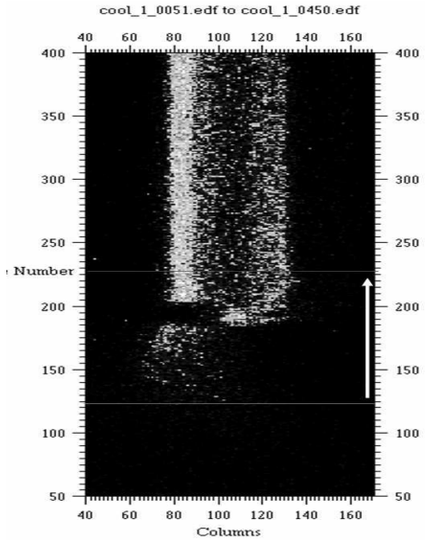

Figure 2. "553" sample. Temporal changes of the CCD screen representative section for (1 1½ 2) peak on cooling (contrary to Fig. 1). Note that no peak is observed for Time<120 and that the peak changed its center of gravity from, initially, column 80, to 105 (180<Time<200) and, finally, again to 80.

L8

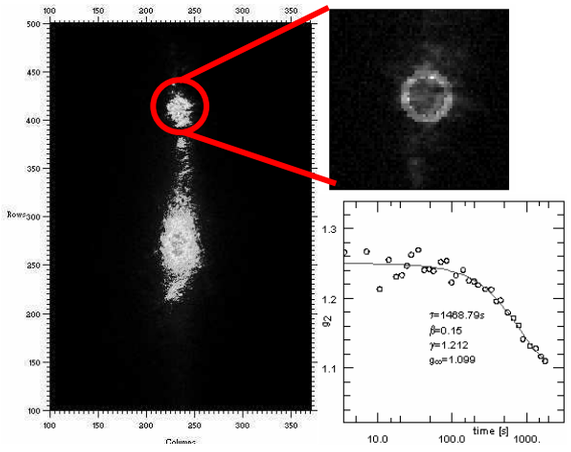

Figure 3. The streched exponential fit to the one time correlation function calculated for part of the (2 2 ½) superstructure reflection in "110" sample. For this analysis, circular peak shape was assumed.

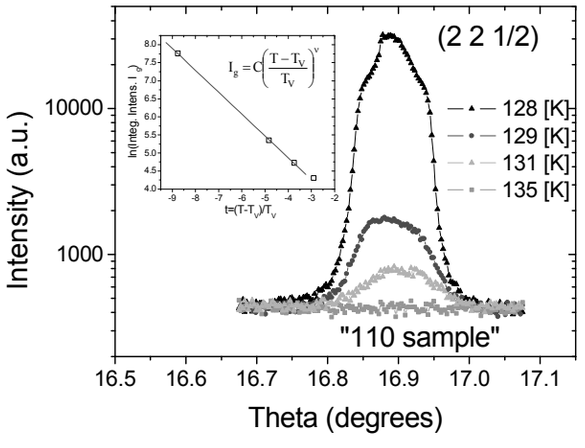

Figure 4. Theta scan of the superstucture reflection for "110" sample at T just above the Verwey transition. Ln from the "integrated" intensity (surface below the peak) is plotted vs $t = (T\text{-}T_V)/T_V$ (where T_V = 127.98 K) suggests critical behavior.

2. The jumps of the (1 1½ 2) peak center of gravity in "553" sample (observed on CCD camera and shown on Fig. 2) are most probably due to structural twins dynamics occurring both at the temperature very close to the transition (Fig. 2), but also ca. 10K below T_V. This last result, observed also for (2 2 ½) peak of "110" sample, was found ca 2 hours after the low T phase was established.
3. Some long lasting speckle dynamics was found for part of (2 2 ½) reflection for "110" sample (Fig. 3) with the characteristic time τ declining with increasing Q values (radius of the circle). Here, due to very low peak intensity, the circular peak profile was assumed.
4. Characteristic diffuse scattering was found for "110" sample just above the transition (see Fig. 4), despite the fact that the transition is discontinuous. The critical exponent for the integrated intensity $I_g = C((T\text{-}T_V)/T_V)^V$ relation (see the inset of Fig. 4) was ν =-0.606. This resembles the neutron measurements results in [3] and will be the subject of the next proposal for the beamtime in ESRF.

Summarizing, both fast dynamics, as with the phenomenon shown on Fig. 2, or very slow, lasting hundreds of seconds (even longer than that on Fig. 3) have been observed by our XPCS experiment. These studies and the data analysis will be continued.

Acknowledgements: Support of the Polish Ministry of Education and Science Grant No. 1P03 B01530 is acknowledged.

References

[1] Z. Tarnawski, A. Wiecheć, M. Madej, D. Nowak, D. Owoc, G. Król, Z. Kąkol, L. Kolwicz-Chodak, A. Kozłowski, "Studies of the Verwey transition in magnetite", *Acta Phys. Polon. A* **106** (2004) 771.

[2] W. Tabiś, Z. Tarnawski, Z. Kąkol, G. Król, A. Kołodziejczyk, A. Kozłowski, A. Fluerasu, J.M. Honig, "Magnetic and structural studies of magnetite at the Verwey transition", *J. Alloys Compds* **442** (2007) 203.

[3] S.M. Shapiro, M. Iizumi, G. Shirane, "Neutron scattering study of the diffuse critical scattering associated with the Verwey transition in magnetite", *Phys. Rev. B* **14** (1976) 200.

L9

ELECTRON AND SPIN CORRELATIONS IN COMPLEX MATERIALS ON nm LENGTH AND fs TIME SCALES

Hermann A. Dürr

BESSY GmbH, Albert-Einstein-Str. 15, 12489 Berlin, German

Keywords: spin correlation, femtosecond scale, angle-resolved photoemission

BESSY is operating Europe's largest third generation synchrotron user facility for the VUV and soft X-ray range. A brief description of the facility will be given, accompanied by highlights of research in the field of magnetic and correlated electron materials. The high brightness of the source enables studies with highest spatial, spectral and temporal resolution. Microscopy applications of magnetic systems are quite important since the soft X-ray range covers 3*d* transition metal L-edges. Soft X-ray resonant magnetic scattering is a unique tool for probing electronic and magnetic ordering phenomena on the nm length scale. High resolution angle resolved photoemission spectroscopy allows unprecedented insights into quasiparticle interactions in complex materials. Ultrafast time resolved studies of laser induced phase transitions are enabled by the <1 ps pulse length in the low-a mode of operation or by using the 100 fs pulses delivered by the fs slicing facility.

L10

INTRA-ATOMIC CHARGE RE-ORGANIZATION AT THE Pb-Si INTERFACE: BONDING MECHANISM AT LOW COVERAGE

Martin Švec [1], Viktor Dudr [1], Martin Vondráček [1], Pavel Jelínek [1], Pingo Mutombo [1], Vladimír Cháb [1], František Šutara [2], Vladimír Matolín [2], and Kevin C. Prince [3,4]

[1] *Institute of Physics, Academy of Science of the Czech Republic, Cukrovarnická 10, 162 53, Prague, Czech Republic*

[2] *Department of Electronics and Vacuum Physics, Charles University, V Holešovičkách 2, 180 00, Prague, Czech Republic*

[3] *Sincrotrone Trieste, Strada Statale 14, km 163.5, 34012 Basovizza-Trieste, Italy*

[4] *INFM, Laboratorio TASC, in Area Science Park, Strada Statale 14, km 163.5, 34012 Basovizza-Trieste, Italy*

Keywords: lead, interface, adsorption, intra-atomic bonding, density functional theory (DFT)

Many studies of adsorption of group IV elements on the group IV substrates have been reported in the past decade, but many questions are still open. The most curious and intriguing system is Pb on a Si(111) surface, which shows phase transitions and phase co-existence, in-commensurate structures and similar effects that depend extremely strongly on Pb coverage[1]. If the structure of (√3 ×√3)R30° (denoted as (√3 hereafter) with 1/3 monolayer (ML) of Pb coverage has a unit cell that contains one metal atom located at the T_4 site of the Si(111) surface, it is conventionally called β phase (denoted as). When cooled, the layer transforms to the incomplete (3×3) structure, with three metal atoms per unit cell in two different chemical states[2]. The two states were identified by core level photoemission experiments for both the √3 and (3×3) structures. A widely accepted model is based on different vertical heights of metal atoms above the surface resulting in charge redistribution between these distinct states and the presence of surface soft phonons. On reducing the coverage to 1/6ML – to the γ- phase (hereafter), an alloy with the same symmetry – the √3 – is found containing 1/6 ML of Si and 1/6 ML of Pb atoms in a single chemical state. The Si and Pb atoms forming the chemically disordered phase occupy the same T_4 position. The γ phase is found to be more stable than the β experimentally. The relation between the single chemical state in the phase and two states in the β phase is crucial for a full understanding of the charge transfer effect in the system and the bonding character in particular phases. The model based on different vertical heights of Pb atoms at T_4 sites was successfully introduced with ab initio calculations for the Pb/Si(111) system [3]. The height of the Pb atoms above the T_4 site calculated by Density Functional Theory (DFT) pseudopotential method depends strongly on the valence band electronic configuration of an applied Pb pseudopotential. In particular, the pseudopotential including 6*s*2 6*p*2 states in the valence band produces the β with atoms at constant height above the substrate. Involving the shallow 5*d* outer core levels in the valence states of the pseudopotential produces an arrangement of one Pb atom up and two down in the (3×3) unit cell, which is the ratio found with photoemission[4]. This effect underlines the importance of the 5*d* electrons in the charge transfer and screening. DFT calculations of the charge redistribution in real space are needed to get an insight into the formation of the √3 phase on the Si(111) surface and to understand the bonding of Pb with an isoelectronic substrate. This point is extremely important as two competing models, soft phonons and charge density waves, are based on the redistribution of charge between the Pb and Si atoms. The one up and two down arrangement of Pb atoms is understood as a dynamic exchange of up and down positions keeping the ratio between them constant. The process is too fast for the time resolution of the STM (Scanning Tunneling Microscope), which gives an image of atomic position averaged over micro to milliseconds. The experimental characterization of an adsorption site on a fast time scale we did using photoemission and photoelectron diffraction (PhD). The spectrum reflects the local arrangement of neighbouring atoms with a time resolution of femtoseconds. The fit of experimental PhD patterns we did with the Van Hove code. In this contribution, we present experimental and theoretical studies of the 1/3 ML and the 1/6 ML Pb/Si(111) phases by means of energy scanned photoelectron diffraction and DFT calculations. We found that the "one up and two down" model is a good description of the β phase. DFT calculations show a localized rearrangement of charge at particular Si atoms in the second layer participating in the Pb-Si bonding.

The measurements were carried out at the Czech Materials Science Beamline, Elettra synchrotron light

source, Trieste, Italy. The desired coverage of Pb was achieved by evaporating several monolayers (ML) of Pb at room temperature onto the clean (Si(111)–7×7 surface, and then progressively desorbing the Pb by annealing at constant temperature for fixed time intervals [4]. The Pb 5*d* and Si 2*p* signals were measured at photon energies (and resolution) of 73.0 (0.1) and 150.0 (0.18) eV, respectively. The PHOIBOS 150 hemispherical analyzer used here has an angular acceptance of half cone angle up to 8°. The photoemission spectra were used to monitor the quality of the β and γ phases and ensure that they had stoichiometric coverage of 1/3 and 1/6 ML. The Pb 5*d* lines were sharpest at coverage of 1/6 ML or less, while a clear two-component doublet was observed for 1/3 ML. The LEED (Low Energy Electron Diffraction) pattern was checked and found to give the best (√3×√3) patterns for these coverage. We measured photoelectron diffraction spectra of the Pb 5*d* core levels for the β and γ phases. The variation of peak intensities was measured as a function of photon energy and the data were acquired as Energy Distribution Curves (EDC) in three basic geometries (polar angle): normal emission (NE), off-normal emission (28°) and grazing emission (55°) at a fixed angle of 60° between the analyser and the incident beam. The azimuthal angle was kept constant and for off-normal conditions was approximately along the Γ – K direction of the Si(111)–(1×1) surface Brillouin zone. The angular resolution of the analyser was kept at ±4° The photon energy was changed by steps of 1 eV in the interval 50–150 eV producing Pb 5*d* photoelectrons with kinetic energy in the range 30 to 130 eV.

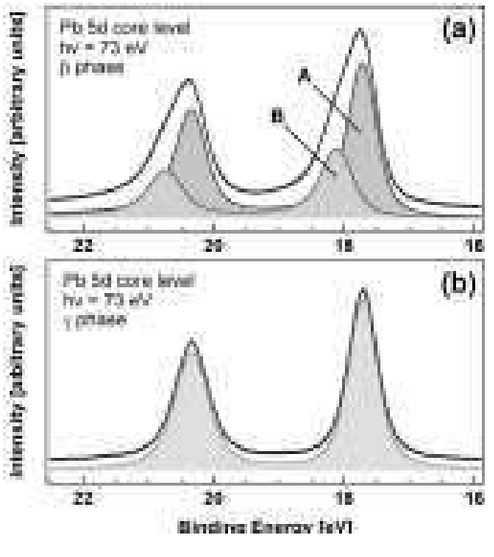

Figure 1. Core level spectra for the Pb/Si(111) β and γ phases measured at NE geometry. One of the two states in the β phase is identical with the single state of the γ phase.

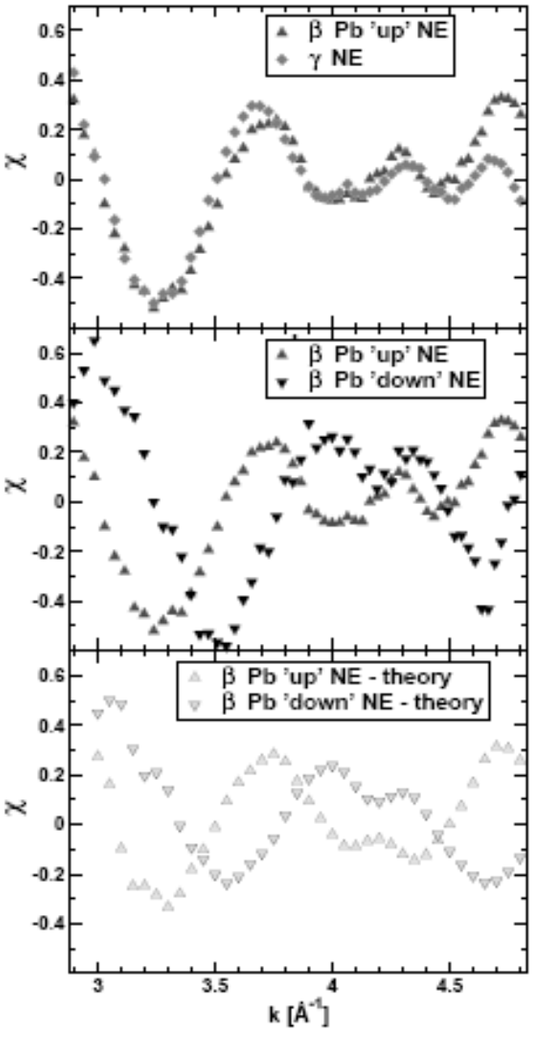

Figure 2. 5*d* core level diffraction in the NE geometry of the Pb atoms on the γ phase and up and down Pb atoms on the β phase with theoretical simulation.

We used the pseudopotential local orbital Fireball code [5] based on density functional theory (DFT). This code was developed with the aim of providing a very favourable accuracy/efficiency balance if an atomic-like basis set is chosen appropriately. The valence wavefunctions are expanded in the Fireball orbitals, a set of strictly localized pseudoatomic orbitals (they are exactly zero for distances larger than the cut-off radius (RC). In our case, Si valence states were represented by a basis set including *s*, *p* and *d* Fireball orbitals with the following parameters: RC (Si, *s*-orbital) = 4.8 Å, RC (Si, *p*-orbital) = 5.4 Å. and RC (Si, *d*-orbitals) = 5.2 Å. This basis set yields a very good description of the bulk properties of Si, as well as the Si(111)–(7×7) reconstruction; for the bulk diamond structure we obtained a lattice parameter a = 5.46 Å and a bulk modulus *B* = 105 GPa (experiment: a = 5.40 Å, *B* = 100 GPa). For Pb, we used a pseudopotential involving the 6*s*2 6*p*2 5*d*10 states of Pb in the valence band electronic configuration. We applied this particular configuration to optimize electronic structure according to the local

L10

atomic arrangement.. The Fireball orbitals of the Pb atom had the following parameters: RC (Pb, *s*-orbital) = 5.4 Å, RC (Pb, *p*-orbital) = 5.9 Å and RC (Pb, *d*-orbitals) = 5.2 Å In our calculations, we have used a supercell approach to model the Pb/Si(111) – √3 surface. First we have considered a (3×3) periodic slab that includes 3 Pb adatoms, 6 Si layers underneath and hydrogen atoms saturating the bonds of the deeper Si layer. The last two layers of the slab, the deeper Si and passivated H layer, were kept fixed during the relaxation process. The supercell contained 66 atoms, in total.

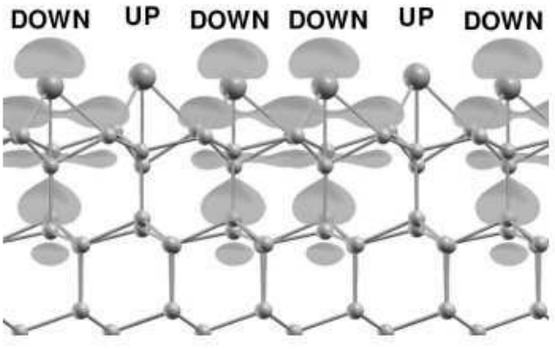

Figure 3. Surfaces of constant charge density 0.01 eV integrated over the range -0.1..0.1 eV around EF are projected onto the ball-and-stick model of the calculated 3×3 structure with the up and down Pb atoms. The surfaces are transparent yellow, Pb atoms are blue and Si grey. The absence of charge density on the Pb up and on the underlying Si atoms is apparent.

To understand better the electronic structure of the system, we plot a surface of constant real-space density of states near EF in Fig. 3. The figure displays the different charge distribution on the β surface with the up and down Pb atoms with particular triangular bipyramids. For the Pb down position, a considerable amount of the charge is located between a Pb atom and a SiT_4 one near the Fermi level. This feature is missing for the SiT_4 atom beneath the up Pb atom indicating a weak interaction between these two atoms. The dangling bonds of the up Pb adatoms are pushed deeper into the valence band and the triangular bipyramid shows a semiconducting character. To summarize, the movement of Pb atoms up or down causes the redistribution of the charge within a covalent bond, not between the dangling bonds, contrary to the case of the Sn p3 structure. The redistribution is limited to the triangular bipyramids and it lacks the extended character of charge density waves. The proximity of the Pb-SiT_4 distance to the ideal Si-Pb bond length gives rise to a special type of binding in the bipyramid.

We found that the Pb/Si(111)–β is stabilized with the dynamic, intra-atomic charge redistribution as an interplay between the band structure and elastic deformation energy. It is the result of the interaction between the adsorbed unsaturated Pb atom and saturated underlying Si atom in the T_4 position. The extra bonding between them is localised in the triangular bipyramid. The dynamics occurs by the flipping of the Pb atoms between the up position, characteristic in the γ phase, and the down position. The effect causes the switching of a triangular bipyramid between metallic and semiconductor states in the agreement with experimental data. The combined study of PhD and ab initio DFT calculations contributes significantly to the understanding of the bonding of the two iso-electronic elements Si and Pb. Influence of defects on the stability of the β phase has been analysed using DFT calculations. The direct correction between the local electronic state and vertical position of Pb adatoms has been identified.

Acknowledgments: The work was supported from grants No. IAA1010413, AV0Z10100521 and IAA100100616.

References

[1] E. Ganz, I.-S. Hwang, F. Xiong, S.K. Theiss, J. Golovchenko, *Surf. Sci.* **257** (1991) 256.

[2] H.H. Weitering, D.R. Heslinga, T. Hibma, *Phys. Rev. B* **45** (1992) 9126.

[3] I. Brihuega, O. Custance, R. Perez, J.M. Gomez-Rodrıguez, *Phys. Rev. Lett.* **94** (2005) 046101.

[4] V. Dudr, N. Tsud, S. Fabık, M. Vondracek, V. Matolın, V. Chab, K.C. Prince, *Phys. Rev. B* **70** (2004) 155334.

[5] P. Jelınek, H. Wang, J.P. Lewis, O.F. Sankey, J. Ortega, *Phys. Rev. B* **71** (2005) 235101.

L11

LOCALIZED AND ITINERANT 5*f* STATES IN ACTINIDE MATERIALS AS SEEN BY PHOTOEMISSION SPECTROSCOPY

Elżbieta Guziewicz [1*], Tomasz Durakiewicz [2], John J. Joyce [2], and Clifford G. Olson [3]

[1] *Institute of Physics, Polish Academy of Sciences, Warsaw, Poland*
[2] *Los Alamos National Laboratory, Los Alamos, NM 87545, USA*
[3] *Ames Laboratory, Iowa State University, Ames, Iowa 50011, USA*

Keywords: actinides, synchrotron radiation, photoemission, angle resolved photoemission sepctroscopy

[*]) *e-mail: guzel@ifpan.edu.pl*

Photoemission spectroscopy (PES) is a direct and powerful probe of the occupied electronic structure, chemical properties of surfaces, and bonding in solids. The angle-resolved version of the technique (ARPES) gives unique information concerning $E(k)$ relation in the solid. ARPES studies of uranium compounds provides extensive insight into the electronic structure and are crucial for comprehension of the wide range of ground state properties found in actinide materials such as magnetism or enhanced mass. PES techniques are capable of providing information regarding the binding energy of the 5*f* band, as well as the dispersion and hybridization with the conduction band and are a valuable tool for evaluation of the various theoretical models that forms the foundation for a comprehensive understanding of complex solids.

We present photoemission results of layered tetragonal compounds: antiferromagnet UAsSe and ferromagnet USb_2 that present an intriguing electronic structure in which both relatively dispersive and narrow 5*f* bands are found. ARPES studies reveal a very sharp photoemission peak in the vicinity of the Fermi edge we found, which is a fingerprint of the 5*f* density of states. Dispersion of this peak along the Γ to Z direction of the Brillouin zone (20 meV for UAsSe and 10 meV for USb_2) proves that neither UAsSe nor USb_2 have purely two-dimensional electronic structure and these compounds are indeed quasi-2D. We have also found a broader, hybridized *f*-character bands with a dispersion of several hundred meV along the Γ to X direction in the Brillouin zone. Narrow and dispersive bands in these U-based magnetic materials are reminiscent of band magnetism previously found in Cr and Fe, but for these uranium compounds the band widths and dispersions are two orders of magnitude smaller.

Photoemission studies also provide an evidence of a very close relationship between the electronic structure and magnetic properties in actinide compounds. The results obtained for cubic uranium, neptunium and plutonium compounds and layered uranium materials show that ordered magnetic moments and/or magnetization is closely correlated with binding energy of valence band photoemission features. For ferromagnetic UTe a Stoner-like mechanism and simple mean-field explanation is proposed.

Acknowledgements: The author (E.G.) was supported by the Polish grant of Ministry of Science and Higher Education No. N202 140 32/3877.

References

[1] E. Guziewicz *et al.*, *Phys. Rev.B* **73** (2006) 155119.
[2] T. Durakiewicz *et al.*, *Phys. Rev. B* **70** (2004) 205103.
[3] E. Guziewicz *et al.*, *Phys. Rev. B* **69** (2004) 045102.
[4] T. Durakiewicz *et al.*, *Phys. Rev. Lett.* **93** (2004) 267205.

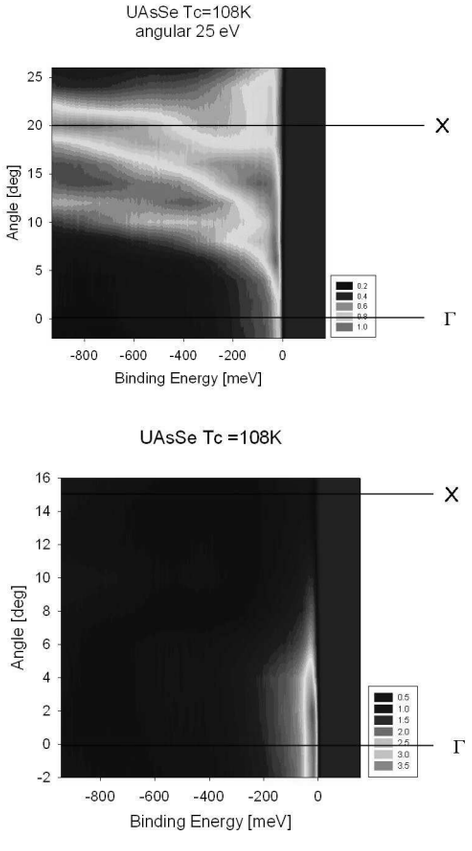

Figure 1. Angle-resolved PES spectra of UAsSe taken for $h\nu = 25$ eV (a) and 44 eV (b). Both data are taken along the Γ to X direction of the Brillouin zone.

L12

REVEALING THE NANOSTRUCTURE OF BIOLOGICAL MATERIALS USING SCANNING X-RAY IMAGING WITH SAXS CONTRAST

A. Gourrier [1,2*], C. Riekel [2], and J. Doucet [1]

[1] *Laboratoire de Physique des Solides, Bat. 510, Université Paris-Sud, 91405 Orsay Cedex, France*
[2] *ESRF, 6 rue Jules Horowitz, 38043 Grenoble cedex, France*

Keywords: biological materials, biomineralization, nanostructure, X-ray imaging, SAXS, microbeam

**) e-mail: gourrier@lps.u-psud.fr*

Biological materials often exhibit complex structures generally extending over several length scales. This essentially results from the optimization of the growth processes to attain the desired function within a given set of restricted environmental conditions [1, 2]. Despite of the great variety of structures found in nature, at the fundamental level, hard materials usually show common patterns of organic macromolecules embedded in a mineral phase. Thus, the most basic events in biomineralization occur at the nanometer level through self-assembly processes [3]. More recently, it was recognized that natural (and synthetic) composites with nanometer-sized features (particles, layers...) could achieve exceptional properties [4]. These observations are therefore currently driving a widespread effort in the direction of a better understanding of the structure of biomineralized materials at the nanoscale.

Due to the heterogeneous nature of the mineralized tissues, the difficulty of a precise characterization lies in the necessity to correlate the shape and organization of the nanoscale features with the microstructure. Typical film/particle thicknesses in, *e.g.* shells, bones and teeth, are in the order of 1-10 nm arranged in larger structures of up to tens of mm^2 in cross-section. In most cases several techniques therefore need to be combined since there is always a trade-off between the resolution that is needed to measure the nanoscopic heterogeneities and the field of view required to image the microstructure.

Synchrotron facilities have provided extremely powerful tools to address such questions. In this respect, small- and wide-angle X-ray scattering (SAXS/WAXS) experiments now constitute one of the major classes of synchrotron experiments in biology. This technique allows bridging the gap between the information obtained at the atomic/molecular level by macromolecular crystallography or spectroscopy and this of the cells or tissues by imaging. The growing impact of SAXS/WAXS methods essentially results from the increase in brightness by orders of magnitude in second and third-generation sources as the ESRF as compared to conventional X-ray laboratory equipment. The first benefit of using such sources comes from the considerable increase in data collection rate which ultimately allows real-time studies.

A second important development stems from the recent advances in X-ray optics which have paved the way for position-resolved measurements [5]. Scanning SAXS/WAXS therefore allows mapping structural parameters related to the atomic and molecular order as well as average shape, size and orientation of nanometre-sized heterogeneities within the region probed by the beam. This enables the reconstruction of images where each pixel is a representation of the local value of a nanostructural parameter obtained from the analysis of the scattering pattern. The lateral resolution of this image is thus given by the beam size in first approximation. However, this method relies on a systematic analysis of the scattering patterns, which becomes rather tedious as the number of frames increases by orders of magnitude due to smaller beam sizes and faster detector read-out time, allowing larger areas to be covered.

This work intends to demonstrate how this technique could be further developed in the direction of more standard full-field X-ray imaging techniques using small angle scattering as source of contrast.

The first example chosen to illustrate this technique is this of the eggshell (Fig. 1), a model for biomineralization studies. Eggshell is a composite that forms by deposition of calcite on the inner protein membrane which further directs the overall growth of the shell [7]. At present, the intimate relationship between the original protein matrix and the mineralizing phase is still poorly understood. In this study, a region of interest on the mammillary layer of the eggshell section was selected by optical microscopy (box in Fig. 1a). This layer is responsible for the initial spherulitic growth processes.

A sample section was scanned at the ID13 beamline of the ESRF using a focussed beam of $1\times1\mu m^2$ over an area of 130×100 μm^2 ($h\times v$) in steps of 2×5 μm^2 ($h\times v$). The transmitted intensity shown in Fig. 1b was measured at each scan point using a photodiode. It appears higher in the mammillary membrane and darker in the mineralized part, *i.e.* regions II and III respectively. This information is qualitatively equivalent to a classical radiography of the sample where the contrast is due to a higher X-ray absorption by the mineral phase. Note that the decrease in intensity in region I of the image is due to absorption by the embedding resin, PMMA.

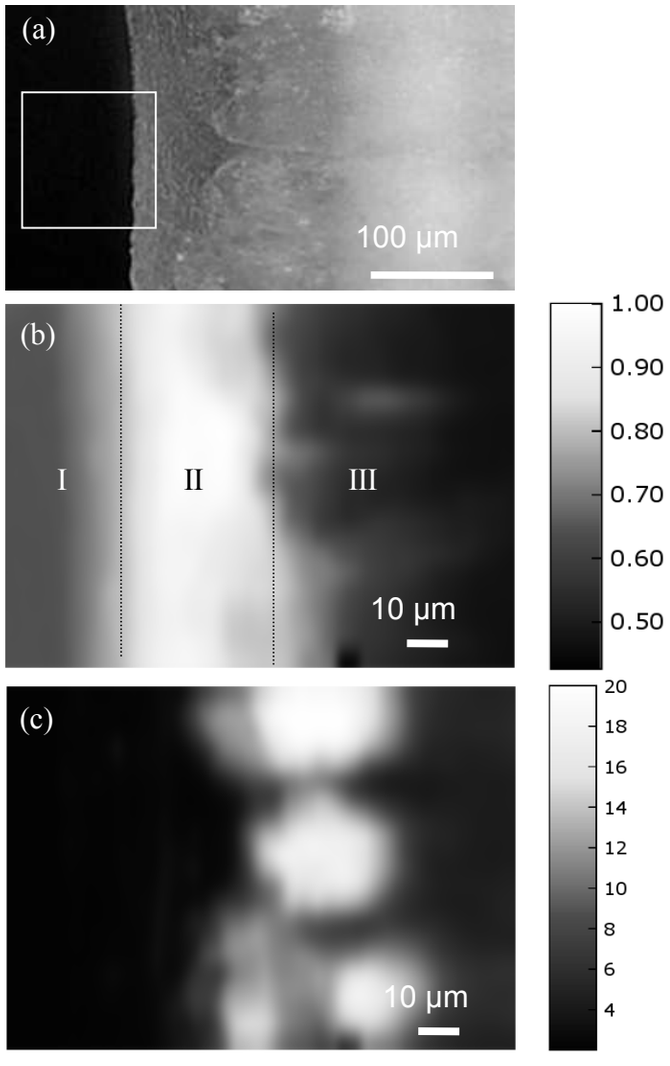

Figure 1. (a) Optical microscopy images of the inner surface of a 110 µm thick eggshell section showing the membrane on the left and mammillary spherulitic layer on the right; (b) X-ray transmission image of the region indicated by the box in (a) obtained using a 1 µm diameter beam with a scan step of 2 µm horizontally and 5 µm vertically; (c) integrated SAXS intensity (arbitrary units) of the same region [6].

The image of the integrated SAXS intensity (Fig. 1c) reveals strikingly different features in the form of three very intense microscopic focal discs stacked vertically. The upper and lower discs appear at the positions of the nucleating knobs observed in the optical image (Fig. 1a), close to the interface between the organic membrane (II) and mineral part (III). The difference of integrated intensity between the nucleating knob and the remaining mineralized layer was attributed to a decrease in the volume fraction of the organic content from the centre to the outside of the knob [7], as observed in other studies [8].

The second example is this of Bone, well known for it's sophisticated hierarchical architecture resulting in exceptional mechanical properties. At the fundamental level, bone is a composite composed of calcium phosphate nanoparticles at least partly embedded in collagen fibrils. At the next structural level, the fibrils are ordered into a variety of structures such as the osteons shown in Fig. 2a. These structures essentially result from the remodelling processes constantly renewing bone throughout the lifetime. They consist of cylindrical layers of ~ 3 µm in thickness which differ in the orientation of the collagen fibrils. However, the fine arrangement of the collagen macromolecules is still an open matter of debate. This is particularly important since it is well known that the mechanical properties of the osteons usually differ from the rest of the tissue.

L12

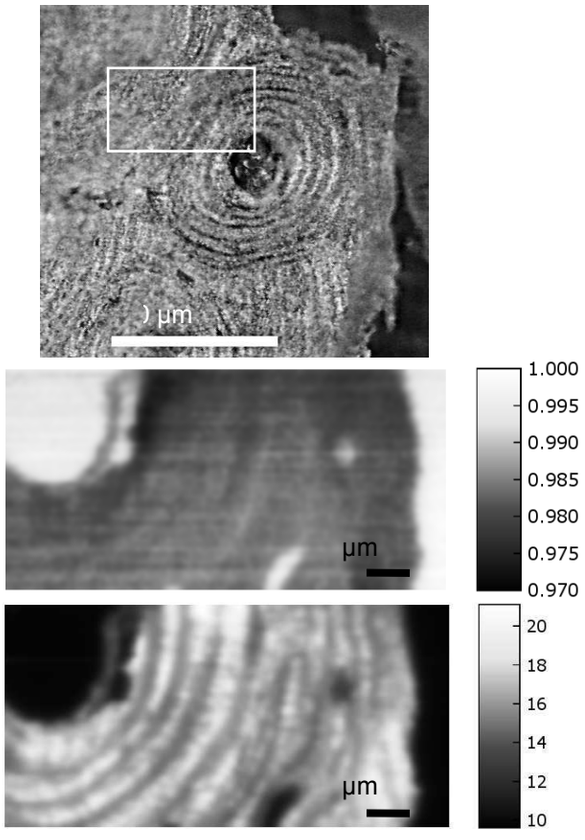

Figure 2. Optical microscopy images of a 5 µm thick human bone section taken in the dense cortical part of the femoral midshaft of a healthy human female; (b) X-ray transmission scan of the region indicated by the box in (a), obtained using a 1 µm diameter beam with 1 µm scan steps in both directions; (c) image of the SAXS intensity (arbitrary units) using the same scan parameters [6].

In the framework of a general study of the intra-lamellar structure, a thin sample section was analyzed under the same conditions as the eggshell. An area of 100×50 µm^2 (h×v) was covered in steps of 1 µm in both directions. The transmitted intensity shown in Fig. 2b appears to be uniform throughout the bone section which implies that the mineral density is constant. However, similar to the case of the eggshell, the image of the integrated SAXS intensity (Fig. 2c) clearly reveals features which could not be observed in the transmission image. In this case, alternating concentric rings appear, strongly reflecting the lamellar structure also seen in the light micrograph (Fig. 2a). The contrast in the SAXS image was attributed to changes in orientation of the mineral particles and thus the fibrils as demonstrated in other studies [9, 10].

These examples demonstrate the potential of this technique to image nanometer-sized heterogeneities in bulk samples. Although the main examples are biological materials, it will be shown that this method could be used for other domains of materials science.

References

[1] G. Jeronimidis, A.G. Atkins, "Mechanics of biological materials and structures – Nature's lessons for the engineer", *J. Mech. Eng. Sci.* **209** (1995) 221–235.

[2] P. Fratzl, "Biomimetic materials research: What can we really learn from nature's structural materials?", *J. R. Soc. Interface* **4** (2007) 637–642.

[3] S. Mann, S. Weiner, "Biomineralization: Structural questions at all length scales", *J. Struct. Biol.* **126** (1999) 179–181.

[4] H. Gao, B. Ji, I.L. Jager, E. Artz, P. Fratzl, "Materials become insensitive to flaws at nanoscale: Lessons from nature", *Proc. Nat. Acad. Sci. USA* **100** (2003) 5597–5600.

[5] C. Riekel, "New avenues in x-ray microbeam experiments", *Rep. Prog. Phys.* **63** (2000) 233-262.

[6] A. Gourrier, W. Wagermaier, M. Burghammer, D. Lammie, H.S. Gupta, P. Fratzl, C. Riekel, T.J. Wess, O. Paris "Scanning X-ray imaging with small-angle scattering contrast", *J. Appl. Crystallogr.* **40** (2007) 78-82.

[7] Y. Nys, M.T. Hincke, J.L. Arias, J.M. Garcia-Ruiz, S.E. Solomon, "Avian eggshell mineralization", *Poult. Avian Biol. Rev.* **10** (1999) 143-166.

[8] D. Lammie, M.M. Bain, S.E. Solomon, T.J. Wess, "Scanning microfocus small angle X-ray scattering study of the avian eggshell", *J. Bionic Eng.* **3** (2006) 11-18.

[9] W. Wagermaier, H.S. Gupta, A. Gourrier, O. Paris, P. Roschger, M. Burghammer, C. Riekel, P. Fratzl, "Scanning texture analysis of lamellar bone using microbeam synchrotron X-ray radiation", *J. Appl. Crystallogr.* **40** (2007) 115-120.

[10] W. Wagermaier, H.S. Gupta, A. Gourrier, M. Burghammer, P. Roschger, P. Fratzl, "Spiral twisting of fiber orientation inside bone lamellae", *Biointerfaces* **1** (2006) 1-5.

L13

NANOCRYSTALS UNDER HIGH PRESSURE

B. Palosz, E. Grzanka, S. Gierlotka, and S. Stelmakh

Institute of High Pressure Physics, Polish Academy of Sciences, ul. Sokolowska 29/37, 01 142 Warszawa, Poland

Keywords: high pressure, nanocrystal, strain distribution, bulk modulus, Bragg reflection

e-mail: palosz@unipress.waw.pl

This work concerns application of high-pressure X-ray diffraction to examination of the structure of nanocrystalline materials. In general, high pressure is a unique tool for investigation of interatomic interactions: high pressure suppresses the interatomic distances and, thus, "forces the material" to show the nature of interactions between its components like atoms/ions or lattice defects [1]. A tentative model of a nanocrystal assumes that it has a non-homegenous structure [2]. High-pressure diffraction technique can serve for determination of different elastic properties of inner and surface parts of the nanocrystalline grains, which relate directly to different lengths of the atomic bonds in the interior and at the surface of the grains. Here, application of *in situ* high pressure powder diffraction technique for examination of specific structural properties of nanocrystals is demonstrated for nanocrystalline powders of diamond and SiC having the average grains dimension from several to several tens of nm in diameter. Limitations and capabilities of the experimental techniques themselves and methods of diffraction data elaboration applied to nanocrystals with very small dimensions (< 30 nm) are discussed.

High-pressure in situ diffraction experiments were performed in DAC at Station F3 under the pressure of up to 40 GPa. The high pressure, high temperature experiments were performed in the six-anvil cubic press MAX80 at Station F2.1, HASYLAB at DESY, Hamburg. The measurements of *micro*- and *macro*-strains were performed for dry powders and in different pressure media.

Examination of polycrystals under pressure using diffraction methods is a well established technique. For polycrystalline materials high pressure studies are dedicated to studies on phase transformation, mesurements of physical parameters like compressibility, characterization of microstructural behaviour like deviatoric stresses, *micro*-strains, yield strength, etc. In this work, dedicated to nanocrystalline powders of diamond, SiC and GaN, we attempt to find out if there are any specific properties of these materials which are dependent on, and correlated with, (1) the grain dimensions and, (2) the surface of the crystallites. For "ordinary polycrystals" both such effects can be ignored, but may be significant in nanocrystalline materials. In the analysis of the lattice compression one finds, that the lattice parameters determined from the positions of Bragg reflections do not have the usual meaning of a constant. What one calculates for individual reflections are "apparent lattice parameters", *alp*, the value of which depends on the reflection [2]. This is due to a complex structure of a nanocrystal constituting a two-phase, core/surface shell system, for which a unique value of the lattice parameter loses its meaning. In consequence, no unique compressibility coefficient can satisfactorily describe the behaviour of nanocrystals under pressure. We offer a tentative interpretation of the distribution of *macro*- and *micro*-strains in nanoparticles of different grain size.

Because a nanocrystalline specie constitutes a two-phase (core-shell) system, Fig. 1, there is an obvious uncertainity as to the real meaning of the measured values of the apparent lattice parameters as determined from the Bragg reflections. This causes that evaluation of the elastic properties of nanocrystals requires a new approach. In this work we attempt to determine the type of the real structure of nanocrystals in comparison with conventional polycrystalline samples. We conclude that nanocrystalline samples should be characterized by two moduli (that of the core and that of the shell). Similar dilemnia concerns the yield strength of nanocrystals.

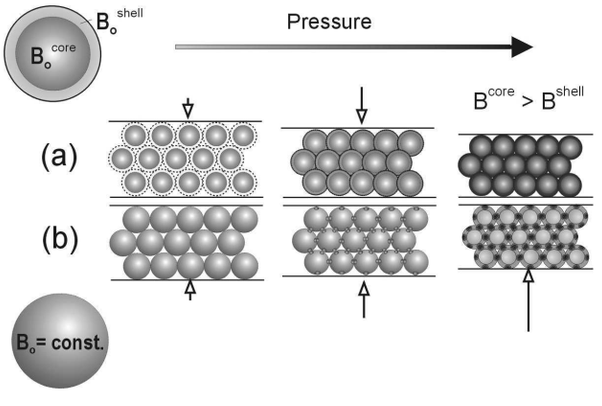

Figure 1. Compression of (a) core-shell structure of a nanocrystal and (b) a perfect small single crystal

Acknowledgements: The authors are indebted to staff of F3 and F2.1 Stations at HASYLAB by DESY for continuos support during numerous experiments there performed.

References

[1] B. Palosz, S. Stel'makh, E. Grzanka, S. Gierlotka, R. Pielaszek, U. Bismayer, S. Werner, and W. Palosz, *J. Phys.: Condens. Matter* **16** (2004) S353-S377.

[2] B. Palosz, S. Stelmakh, E. Grzanka, S. Gierlotka, W. Palosz, *"Nanocrystallography", in: Z.Kristallography*. **222** (2007) 580-594.

L14

SCIENTIFIC APPLICATIONS OF X-RAY FREE-ELECTRON LASER SOURCES

Th. Tschentscher

European XFEL, Deutsches-Eektronen Synchrotron DESY, Notkestrasse 85, D-22607 Hamburg, Germany

Keywords: x-ray free-electron lasers, ultrafast dynamics, coherent diffraction, extreme conditions, coherent x-ray optics, x-ray instrumentation

e-mail: thomas.tschentscher@xfel.eu

Present-day scientific applications using x-rays from synchrotron radiation sources show very high performance in a broad range of science areas. However, even the newest and most performing sources are limited intrinsically in their pulse duration, photon flux per pulse and coherence properties. A variety of scientific problems therefore cannot be investigated at present. Amongst these are the investigation of dynamics of matter and of extremely short-living states, both at ultrafast time-scales, and the imaging of nanoscale systems with atomic or at least sub-nanometer resolution. Recently proposed free-electron lasers (FEL) for x-ray radiation will provide radiation with many orders of magnitude higher peak brilliance. These sources promise to overcome the present-day limitations and will allow a broad range of new x-ray scientific applications.

For short-wavelength radiation of the order 0.1 nm using the self-amplifed spontaneous emission (SASE) principle is the most reliable way to generate high FEL gain [1-3]. The FEL process depends critically on the emittance of a high-energy electron beam of very high peak current that can be generated by linear accelerators only. Spontaneous emission of synchrotron radiation in a very precise undulator magnetic field is used to create an electro-magnetic field co-propagating with the electron bunch through the undulator. The interaction of the electro-magnetic field with the electron bunch leads to the characteristic exponential gain process. The emitted FEL radiation is characterized by typically 100 femtosecond duration, a peak flux of $10^{12} – 10^{14}$ photons per pulse, and high degree of coherence. The best appreciation of this combination of properties gives the peak brilliance of an XFEL reaching about nine orders of magnitude higher than present-day sources. As the FEL process starts from noise the radiation output shows statistical fluctuations in output power, temporal and spectral distribution. Experiments using FEL radiation therefore will require specific diagnostics of the radiation, in many cases on a shot-by-shot basis.

The first short-wavelength FEL facility, providing FEL radiation of 6-100 nm wavelength is FLASH at DESY, Hamburg [4-6]. The facility is operational since 2006 and provides FEL radiation for scientific experiments of a broad user community. At the same time many new developments in the areas of accelerator, FEL technology and scientific instruments are pursued at FLASH. The first facility operating in the hard x-ray range will be the LCLS at SLAC, Stanford, scheduled to start operation by 2009. Another hard x-ray facility, the European XFEL, launched in June 2007 and scheduled for first beam in 2014, is based on a super-conducting accelerator enabling acceleration of a large number of electron bunches during a single radio-frequency pulse [7]. Likewise the total number of x-ray pulses available to the experiments can be increased significantly (up to 30,000 per second). On the one hand, this significant increase in average brilliance compared to other FEL facilities enables new science, facilitates the parallel operation of many instruments and leads to improved stability of the electron beam. On the other hand, the high intensity and the high repetition rate lead to new requirements for x-ray optics and x-ray diagnostics. These requirements will be discussed in relation to the scientific instruments which have been proposed for the European XFEL facility.

X-ray FEL radiation in the photon energy regime from a few 100 up to 15000 eV will enable to address new scientific problems in the areas of physics, materials science, chemistry and biology. The particular properties of hard x-ray FEL radiation, these are the short wavelength, the short pulse duration, the high degree of transverse and longitudinal coherence and the high pulse intensities, will provide outstanding conditions for the investigation of ultrafast dynamics on the femtosecond level, of properties of nanoscale systems including biological samples and matter under extreme conditions energy density. In the lecture examples of proposed investigations and the current state-of-the-art using e.g. soft x-ray FEL radiation at FLASH or low intensity pulses provided by the Sub-Picosecond-Pulse-Source at SLAC will be discussed.

The initial layout of the European XFEL foresees the construction of three SASE FEL beamlines. Figure 1 shows a layout of the photon beam distribution with two electron and three photon beam lines. Additional space for two further undulators and photon beamlines is provided. The first six scientific instruments have been determined recently and are listed in Table 1. These instruments will allow covering the most exciting science fields and could be complemented with further instruments in the future.

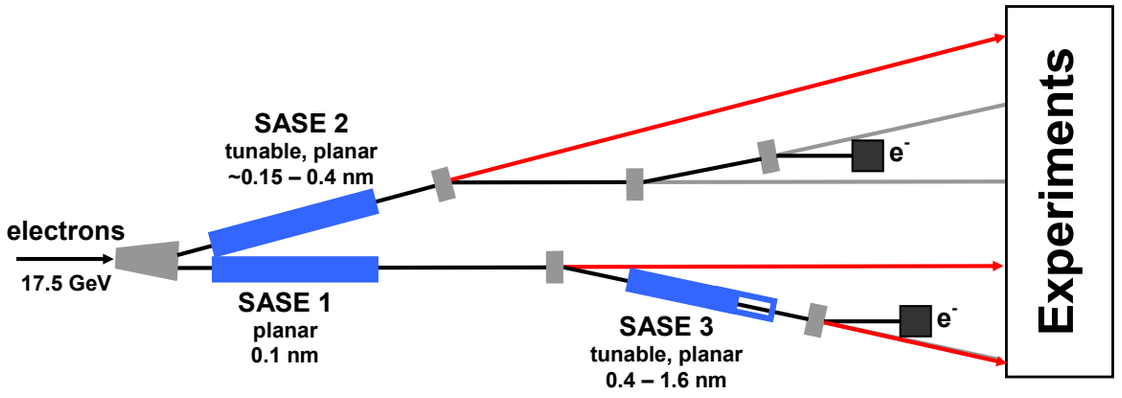

Figure 1. Layout of the European XFEL photon beam distribution. Two electron beam lines serve initially three SASE FEL undulators.

Table 1. Description of the initial scientific instruments of the European XFEL

Name	Description
SPB	**Ultrafast Coherent Diffraction Imaging of Single Particles, Clusters, and Biomolecules –** Structure determination of single particles: atomic clusters, bio-molecules, virus particles, cells.
MID	**Materials Imaging & Dynamics** – Structure determination of nano-devices and dynamics at the nanoscale.
FDE	**Femtosecond Diffraction Experiments –** Time-resolved investigations of the dynamics of solids, liquids, gases.
HED	**High Energy Density Matter –** Investigation of matter under extreme conditions using hard x-ray FEL radiation, *e.g.* probing dense plasmas.
SQS	**Small Quantum Systems –** Investigation of atoms, ions, molecules and clusters in intense fields and non-linear phenomena.
SCS	**Soft x-ray Coherent Scattering** – Structure and dynamics of nano-systems and of non-reproducible biological objects using soft X-rays.

Acknowledgements: The author is indebted to the authors and collaborators of the Technical Design Report for the European XFEL and to the staff at FLASH for excellent experimental conditions. Funding by the European Commission is acknowledged (Grant Pre-XFEL, No. 211604).

References

[1] A.M. Kondratenko, E.L. Saldin, "Generation of coherent radiation by a relativistic electron beam in an undulator", *Sov. Phys. Dokl.* **24** (1979) 986; *Part. Accelerators* **10** (1980) 207.

[2] R. Bonifacio, C. Pellegrini and L.M. Narducci, "Collective Instabilities and high-gain regime in a free-electron laser", *Opt. Commun*. **50** (1984) 373.

[3] R. Bonifacio, F. Casagrande, L. De Salvo Souza, "Collective variable description of a free-electron laser", *Phys. Rev. A* **33** (1986) 2836.

[4] J. Andruszkow *et al.*, "First 6bservation of self-amplified spontaneous emission in a free-electron laser at 109 nm wavelength", *Phys. Rev. Lett*. **85** (2000) 3825-3829.

[5] V. Ayvazyan *et al.*, "Generation of GW radiation pulses from a VUV free-electron laser operating in the femtosecond regime", *Phys. Rev. Lett.* **88** (2002) 104802.

[6] W. Ackermann *et al.*, "Operation of a free-electron laser from the extreme ultraviolet to the water window", *Nature Photon.* **1** (2007) 336-342.

[7] *The European X-Ray Free-Electron Laser: Technical Design Report*, M. Altarelli *et al.* (eds.), DESY 2006-097, (Hamburg, 2006).

L15

DEVELOPING MODERN BIOMEDICAL IMAGING AND THERAPY FACILITY AT THE SYNCHROTRON – CHALLENGES AND UNKNOWNS

T.W. Wysokinski [1*], D. Chapman [2], E. Hallin [1], and M. Renier [3]

[1] *Canadian Light Source, Saskatoon, SK, Canada*
[2] *Anatomy and Cell Biology, University of Saskatchewan, Saskatoon, SK, Canada*
[3] *European Synchrotron Radiation Facility, Grenoble, France*

Keywords: synchrotron radiation, biomedical research, x-ray imaging, x-ray therapy

**) e-mail: tomasz.wysokinski@lightsource.ca*

The BioMedical Imaging and Therapy (BMIT) laboratory will provide a world class facility with unique synchrotron-specific imaging and therapy capabilities. The facility consists of the Insertion Device (ID) beamline 05ID-2 and the bend magnet (BM) beamline 05B1-1. These beamlines are designed for imaging and therapy research primarily in biomedical systems, as well as tissue specimens including plants. The experimental methods available include: Microbeam Radiation Therapy (MRT), Synchrotron Stereotactic Radiation Therapy (SSRT) and imaging (KES, DEI, projection and computed tomography) [1].

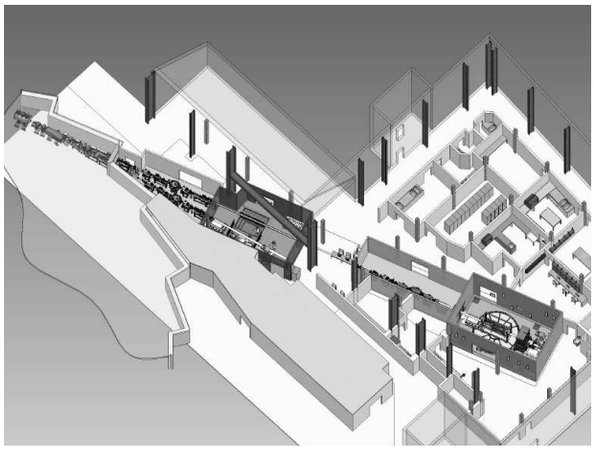

Figure 1. Top view of the BMIT hutches and laboratories.

Proposed research program defines the technical requirements for the facility [2] that includes the hutches and accompanying laboratories including patient and animal preparation rooms. Biomedical programs in general require wide and uniform beam (10-20 cm required, up to 40-50 cm is preferred), which in turn necessitates either very wide beam (the maximum horizontal photon beam angle for 05B1-1 is 19.54 mrad of which the BM beamline utilizes 10 mrad) or a large distance from the source (60 meters for the 05ID-2 line). Such wide beams require specialised imaging device – cameras.

Samples can vary from very small to very large and heavy (hundreds of kilograms). They need to be restrained, which requires a variety of different holders and restraint systems. Large samples require very large hutches and preparation areas with the appropriate entrances and doors. When dealing with live subjects one has to minimise the delivered dose, in case of imaging, cameras with very fast readout times are needed.

The therapy experiments on the other hand, require delivery of dose as high as 3000 Gy/s (MRT program). To generate such dose in BMIT case a custom multi-pole superconductive 4.3 T wiggler is required; it can generate 30 kW of radiative power (500 mA, 2.9 GeV).

This paper describes the pathway for the development of BMIT facility as well as challenges faced during development, such as space requirements for the positioning system than can handle hundreds of kilograms loads with the required accuracy.

Most challenging components of the beamlines are identified: Insertion Device, filters, shutters including collimators and beam-stops, monochromators, X-ray windows, positioning systems and the cameras. An important part of the project is the personnel and patient safety system.

When starting the biomedical program of such scale all the regulatory issues related to facility design and operation need to be reviewed. As it turned out, the cost of implementing the proper air handling system was one of the main cost driving factors for this project.

Acknowledgements: This project is supported by an Infrastructure Grant from the Canada Foundation for Innovation, the Province of Saskatchewan and more than 19 other private and public granting agencies.

References

[1] D. Chapman, *BioMedical Imaging and Therapy Beamline Conceptual Design Report*, CLS Design Note 26.2.1.1, Rev. 0 (2006).

[2] D. Chapman, *Biomedical Imaging and Therapy Beamline Preliminary Design Report*, CLSI Document No. 26.2.1.2 Rev. 0 (2006).

[3] T.W. Wysokinski, D. Chapman, G. Adams, M. Renier, P. Suortti, W. Thomlinson, *Nucl. Instrum. Meth. Phys. Res. A* **582** (2007) 73–76.

L16

TOWARDS FULL AUTOMATION AT THE CANADIAN MACROMOLECULAR CRYSTALLOGRAPHY FACILITY

P. Grochulski [1*], M. Fodje [1], N. Strynadka[2], and L. Delbaere [3]

[1] *Canadian Light Source Inc., University of Saskatchewan, 101 Perimeter Rd, Saskatoon, SK S7N 4S2, Canada*
[2] *Department of Biochemistry, University of British Columbia, Vancouver, BC V6T 1Z3, Canada*
[3] *Department of Biochemistry, University of Saskatchewan, Saskatoon, SK S7N 5E5, Canada*

Keywords: macromolecular crystallography, automation, structural biology

**) e-mail:pawel.grochulski@lightsource.ca*

The Canadian Macromolecular Crystallography Facility (CMCF) which serves more than 60 protein crystallographers located across Canada consists of two beamlines [1]. The first, an insertion device beamline (08ID-1) is capable of satisfying the requirements of the most challenging and diverse crystallographic experiments, *i.e.* physically small crystals with large unit cell dimensions. The second, the 08B1bending magnet beamline is being constructed and has been designed for high-throughput data collection, capable of being accessed remotely.

The primary method of access to CMCF beamlines will be remotely via the CA•Net research network. In what is commonly referred to in the field as 'Mail-in Crystallography', scientists will be able to send prefrozen crystals to the facility and be able to setup experimental parameters as well as inspect, evaluate and download their data from their home laboratories via the internet. To facilitate remote access the SAM robots [2] are being built for both beamlines (Fig. 1). The robot is used in combination with Universal Puck (Uni-Puck), a single sample holding cassette standard among facilities in North America. With the Uni-Puck, the robot can hold 192 samples, sufficient for a shift of screening and data collection.

Features of the final software will include automatic alignment and configuration of the beamline hardware, automatic crystal mounting and centering of crystals in the X-ray beam, automatic measurement of fluorescence spectra for MAD experiments, automatic screening and analysis of crystals in order to assess crystal quality and determine optimum parameters and strategies for data collection, automatic data collection and data processing. Centering of the crystals, automatic performance of MAD experiments and automatic data processing from raw images to processed reflection files, including automated indexing, space group selection, integration and file format conversion with minimal user's input has been implemented at the 08ID-1 beamline (Fig. 2). All software development is focused on the XDS package [3] however other popular data processing software is also available at the beamlines (HKL2000, CCP4).

References

[1] P. Grochulski, I. Blomqvist, L. Delbaere, "Status of the Canadian Macromolecular Crystallography Facility: Design and commissioning of the 08ID-1 beamline at the Canadian Light Source", *Phys. Can.* **62** (5) (2006) 301-304.
[2] A.E. Cohen, S.E. McPhillips, J. Song, M.D. Miller, "Automation of high-throughput protein crystal screening at SSRL", *Synchr. Radiat. News* **18**N2 (2005) 28-35.
[3] W. Kabsch, "Automatic processing of rotation diffraction data from crystals of initially unknown symmetry and cell constants", *J. Appl. Crystallogr.* **26** (1993) 795-800.

Figure 1. SAM robot at the CMCF.

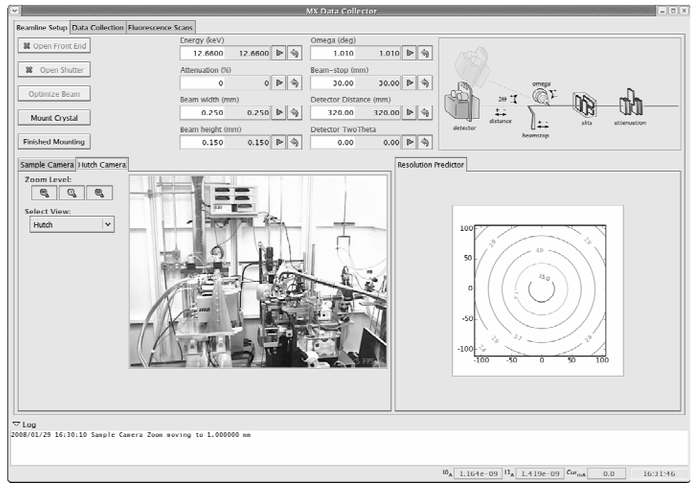

Figure 2. CMCF Users' software.

L17

IN-SITU HIGH-PRESSURE OBSERVATION OF JAHN-TELLER EFFECT IN LITHIUM-MANGANESE OXIDES

P. Piszora [1*], W. Nowicki [1], J. Darul [1], S. Carlson [2], and Y. Cerenius [2]

[1] *Dept of Materials Chemistry, Faculty of Chemistry, A.Mickiewicz University, Grunwaldzka 6, PL-60780 Poznań*
[2] *MAX-lab, Lund University, SE-22110 Lund, Sweden*

Keywords: high pressure, $LiMn_2O_4$, $Li_4Mn_5O_{12}$, cathode materials

**) e-mail: pawel@amu.edu.pl*

A secondary battery is a crucial part of portable and high-performance electrical devices such as personal computers, mobile phones, digital cameras, and video movies. The high cost and high toxicity of cobalt has created enormous interest in development of less expensive, environmentally benign manganese-based cathodes as an alternative to cobalt-based cathodes for rechargeable lithium batteries. The spinel oxides, $Li_xMn_{3-x}O_4$ are being intensively pursued in this regard.

$LiMn_2O_4$ shows two plateaus in voltage versus capacity plots. For one of them, around 3 V, one can observe drastic capacity fading upon cycling due to the macroscopic volume change associated with a cooperative Jahn-Teller distortion. The cyclability can be improved by increasing the average oxidation state of manganese through a substitution of lithium for manganese in $Li_{1+x}Mn_{2-x}O_4$. Such substitutions suppress Jahn-Teller distortions. $Li_4Mn_5O_{12}$ is known to show better cyclability in the 3 V region than $LiMn_2O_4$. Likewise, a cubic symmetry can be preserved at low temperature due to lithium insertion into the manganese lattice sites.

Table 1. Selection of the high-pressure experiments and the average valency of manganese.

Li-Mn oxides	Mn valency	HP Ref.
$LiMn_2O_4$	3.5	[1, 2]
$LiMnO_2$	3	[3]
$Li_xMn_{3-x}O_4$	3.35 - 3.50	[4]
$Li_{0.92}Mn_2O_4$	3.54	[5]
$Li_4Mn_5O_{12}$	4	–

The relevance of the lithium manganese oxides to electrochemistry and to many another applications merits a deeper understanding of the materials. Among several kinds of lithium manganese oxides, the high pressure (HP) properties of the end member of the spinel structure type, $Li_4Mn_5O_{12}$, is of high interesting. In compounds with average valency of manganese less than 4, Mn^{3+} ions give a Jahn-Teller distortion to the regular MnO_6 octahedron, as Mn^{3+} ions are in a high-spin state with the electronic configuration $t_{2g}^3 e_g^1$. The cooperative Jahn-Teller distortion due to Mn^{3+} ions plays a significant role in determining the high-pressure crystal structure of many lithium-manganese oxides (Table 1). $Li_4Mn_5O_{12}$ is in this context an ideal reference material for the high-pressure experiments (Fig. 1).

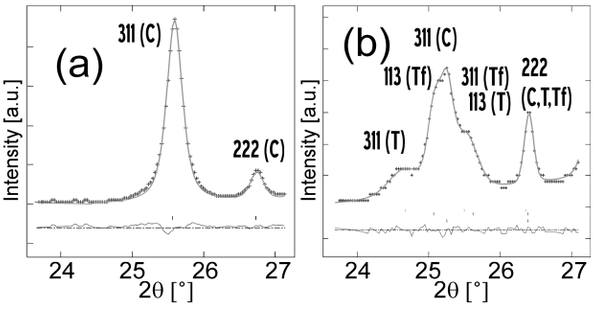

Figure 1. The most representative 2Θ region of the Rietveld refinement of $Li_4Mn_5O_{12}$ (a) and $LiMn_2O_4$ (b) at 7.5 GPa. Indices refer to *Fd*3*m* (C) and $F4_1/ddm$ (T and Tf) space groups.

Acknowledgements: The authors are grateful for the support from EC - Research Infrastructure Action under the FP6 "Structuring the European Research Area" Programme (through the Integrated Infrastructure Initiative "Integrating Activity on Synchrotron and Free Electron Laser Science") by MAX-Lab.

References

[1] A. Paolone, A. Sacchetti, P. Postorino, R. Cantelli, A. Congeduti, G. Rousse, C. Masquelier, "Stabilization of an orthorhombic phase in $LiMn_2O_4$ by means of high pressure", *Solid State Ionics* **176** (2005) 635-639.

[2] P. Piszora, "*In-situ* investigations of $LiMn_2O_4$ at high pressure", *Z. Kistallogr.* **S26** (2007) 387-392.

[3] J. Sugiyama, T. Noritake, T. Hioki, T. Itoh, T. Hosomi, H. Yamauchi, "A new variety of $LiMnO_2$: high-pressure synthesis and magnetic properties of tetragonal and cubic phases of $Li_xMn_{1-x}O$ (x~0.5)", *Mat. Sci. Eng. B* **84** (2001) 224–232.

[4] P. Piszora, W. Nowicki, J. Darul, "High-pressure metaelastic properties of $Li_xMn_{3-x}O_4$ (x=0.87; 0.94; 1.00)" *J. Mater. Chem.* **18** (2008) 2447-2452.

[5] K. Yamaura, Q. Huang, L. Zhang, K. Takada, Y. Baba, T. Nagai, Y. Matsui, K. Kosuda, E. Takayama-Muromachi, "Spinel-to-$CaFe_2O_4$-type structural transformation in $LiMn_2O_4$ under high pressure", *J. Am. Chem. Soc.* **9** (2006) 9449-9456.

L18

DAMAGE OF SOLIDS EXPOSED TO INTENSE XUV FREE ELECTRON LASER SINGLE SHOTS. *POST-SITU* CHARACTERIZATION BY X-RAY MICRODIFFRACTION, OPTICAL MICROSCOPY AND *AFM*

J.B. Pelka [1*], R. Sobierajski [1], W. Paszkowicz [1], J. Krzywinski [1], D. Klinger [1], M. Jurek [1], D. Zymierska [1], A. Wawro [1], L. Juha [2], V. Hajkova [2], H. Wabnitz [3], S. Toleikis [3], T. Tschentscher [3], K. Sokolowski-Tinten [4], R. London [5], S. Hau-Riege [5], C. Riekel [6], R. Davies [6], M. Burghammer [6], E. Dynowska [1], W. Szuszkiewicz [1], W. Caliebe [3], and R. Nietubyc [7]

[1] *Institute of Physics, Polish Academy of Sciences, Al. Lotnikow 32/46, 02-668 Warsaw, Poland*
[2] *Institute of Physics, Academy of Sciences of the Czech Republic, Na Slovance 2, 182 21 Prague 8, Czech Republic*
[3] *HASYLAB / DESY, Notkestrasse 85, D-22603 Hamburg, Germany*
[4] *Institut für Exp. Physik, Universität Duisburg-Essen, Lotharstr. 1, 4748 Duisburg, Germany*
[5] *Lawrence Livermore National Laboratory, 7000 East Avenue, Livermore, CA 9455, USA*
[6] *European Synchrotron Radiation Facility, 6 rue Jules Horowitz, BP 220, 38043 Grenoble, France*
[7] *Andrzej Soltan Institute for Nuclear Studies, PL-05400 Swierk, Poland*

Keywords: XUV FEL, radiation damage, ablation, structure modification, X-ray diffraction

**) e-mail: pelkay@ifpan.edu.pl*

The irradiation of solids with short-wavelength femtosecond pulses delivered by the XUV free electron laser creates states of strong electronic excitation with a highly reduced influence of optical nonlinearities at frequencies in between the plasma frequency and the frequency of the inner shell absorption edge. The absorption depth for most of materials can be therefore much longer, as compared to femtosecond optical pulses, boosting creation of well-defined excitation conditions in relatively large sample volumes [1, 2].

In the present work, we report on results obtained on three materials: the insulating α-SiO_2, the semiconducting monocrystalline silicon and the metallic films of gold deposited on sapphire substrate. The samples were irradiated by single pulses, of 25 fs FWHM, at the FLASH facility in HASYLAB (Hamburg), operating at a wavelength of 32.5 nm. The applied fluency has been kept in the range of 100-2000 mJ/cm^2.

After irradiation, the samples were examined by several techniques, including optical microscopy with Nomarski contrast and AFM, as well as by X-ray diffraction and reflectometry at W-1 beamline of DORIS storage ring (Hamburg). Finally, the microstructure was probed at ID-13 beamline in ESRF, Grenoble, with the X-ray submicrometer beam of size of 250 nm. 2D diffraction patterns were recorded in transmission mode while the samples were step-scanned along chosen paths throughout places irradiated with laser pulses of various fluencies.

Ablation craters of well defined edges with smooth interiors were found in the materials for virtually all applied fluencies. Pronounced embankments and columnar structures around ablation craters, induced at intermediate fluencies, were revealed in silicon. In α-SiO_2 a typical diffraction pattern of an amorphous material was observed without any traces of irradiation-initiated crystallization. A step-like, complete removal of the gold film was evidenced inside of damaged areas, with only small gold residues in central part of craters exposed to higher fluencies. Polycrystalline phase of gold was found in thin leafs 200-300 nm thick, set upright as walls up to few micrometers high and outlining the crater boundaries.

The observed features are compared with results of a damage induced at other wavelength between 13.4 nm and 98 nm and related to models of ablation [2, 3].

Acknowledgments This work has been partially supported the grant of Ministry of Science and Higher Education of Poland, SPB nr. DESY/68/2007. Irradiation with FLASH has been performed within the framework of the *Peak-Brightness-Collaboration* [project II-20022049 EC]. Support from the PBC and the operators of the FLASH facility is gratefully acknowledged. The synchrotron measurements at HASYLAB, Hamburg were supported by the RIA FP6 Contract RII3-CT-2004-506008 of the European Community, The microdiffraction study has been done at the ID-13 beamline at ESRF, Grenoble.

References

[1] N. Stojanovic, U. Zastrau, R. Sobierajski, F. Perner, R. Nietubyc, *et. al*.; "Ablation of solids using a femtosecond XUV free electron laser"; *Appl. Phys. Lett.* **89** (2006) 241909.

[2] S.P. Hau-Riege, R.A. London, R.M. Bionta, M.A. McKernan, S.L. Baker, J. Krzywinski, R. Sobierajski**,** R. Nietubyc, J.B. Pelka, *et. al*., "Damage threshold of inorganic solids under free-electron-laser irradiation at 32.5 nm wavelength"; *Appl. Phys. Lett.* **90** (2007) 173128.

[3] J. Krzywinski, R Sobierajski, M. Jurek, R. Nietubyc, J.B. Pelka, L. Juha, M. Bittner, V. Létal, V. Vorlíček, A. Andrejczuk, J. Feldhaus, B. Keitel, E.L. Saldin, E.A. Schneidmiller, R. Treusch, M.V. Yurkov, "Conductors, semiconductors, and insulators irradiated with short-wavelength free-electron laser"*; J. Appl. Phys*. **101** (2007) 043107.

L19

NON-TYPICAL, INCLUDING STRUCTURAL TRANSITION, GELATION PROCESS OF MONOSACCHARIDES

H. Grigoriew

Institute of Nuclear Chemistry and Technology, Dorodna 14, 03-195 Warsaw, Poland

Keywords: structural transsition, gelation, monosaccharide

e-mail: hgrigori.ichtj.pl

During gelation process, ruled by self-assembling, aggregates built of bonded and/of polymerized molecules are formed. Through the gelation process their size increases monotonically until a great supramolecular structure is formed.

The monosaccharide gelators can form physical, weak organogels of very low gelator concentration. The small, compact molecules of gelators can be held together only by weak, non-covalent interactions, and many aspects of these materials gelation are still unclear. One of the existing opinions, formed on the basis SEM pictures of the gels, is, that the gelator and solvent molecules form a homogenous mixture into sol phase, and, at the gelation point, they separate, forming an infinite fibril-like structure of the gelator in the medium. But SEM uses dried samples, and results of our study of these gels in wet and dried state showed that drying process caused a great structural changes in monosaccharide gels [1].

The experimental studies performed by us at SAXS beamlines of Hasylab and Elettra synchrotrons were as follows. (i) In situ studies of gelation of galactose-based gelator with benzene as a solvent, in room temperature, using time resolved mode [2]. (ii) Temperature influenced gelation of galactose-based gelator with dipphenyl ether as a solvent, also using time-resolved mode [3]. (iii) Study of dependence of glucofuranose gels (with toluene as a solvent) structure on the gelator concentration [4]. The glucofuranose-based gelators molecules are larger, than galactose-based and each includes three (not two) free –OH groups.

The obtained experimental data, $I(q)$ [2-4], were analyzed using a row of methods:

a/ *Fractal structures* were identified for SAXS curves [log(I) vs log(q)] through appearance of straight-line segments in q ranges related to one of fractal type: 1/ for larger q, after the Porod bend - to surface fractal of primary particle, of dimension $d_s = 6$ – segment slope, with values change from 2 – for smooth surface, to 3 – for very irregular and rough one, and 2/ for smaller q - to mass fractal of average aggregate, d_m, of dimension equal to value of the slope, not exceeding three.

b/ *Distance distribution function, p(r)* in real space, which is connected with SAXS scattering data by Fourier transform (where $s = q$):

$$p(r) = \frac{1}{2\pi^2}\int_0^\infty sr(Is)\sin(sr)ds$$

c/ *Radius of gyration, R_g.* It is a shape-independent value, presented size of aggregate calculated from $p(r)$,

d/ *Aggregate model* built by Monte Carlo method through fitting its pair function with the experimental one.

The analyses results, obtained for sets of data in Refs. [2-4] were compared. The subsequent increase of gelator concentration [4] was compared with progressing stages of gelation [2, 3].

The run of gelation process of galactose-based gel with benzene as a solvent [2], showed in Fig. 1,2 and Table I, is as follows: for sol structure (Figs. 1a, 2a and Table I, meas. No. 2) aggregates exixt, and are loose, of the largest size, oval-type shape, and without determined surface (lack d_s). At measurement No. 4, the big decreasing of R_g and rough but defined aggregate surface (Table 1) are detected. For the next measurements aggregate become denser, of rod-like shape (Fig. 1b and 2b) and mainly smoothness of the surface is more and more smooth (d_s in Table 1).

The similar run of structural changes during temperature-influenced galactose-based gelatotion, with diphenyl-ether as a solvent was registered [3].

During subsequent increase of glucofuranose-based gelator concentration [4], the structural changes registered in Table II are: for gel of the smallest concentration, the aggregate is the largest and, as above, only one fractal dimension is visible (Table 2). However, it is surface fractal. This seems to be caused by a change of two free –OH groups in galactose molecule for three such groups in glucofuranose one. Then, each gelator molecule can form 2twohydrogen bonds for galactose, *i.e*. one-dimensional chain, but 3 hydrogen bonds for glucofuranose can form 2-dimensional surface. In this way we found a confirmation, that hydrogen bonds are formed in these gels durjng gelation.

For increasing concentrations of glucofuranose can be observed: at 0.5 %–an appearance of second kind of aggregates with smooth surface, which become the only for biggest concentration (two d_s values). Also the gradual decrease in aggregate size is observed (Table II). Besides, the shape of aggregate change from the oval- like for the smallest concentration to rod-like for the largest one.

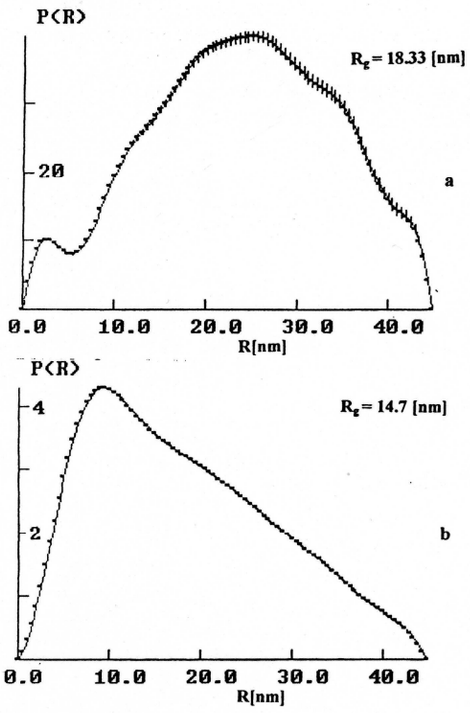

Figure 1. Pair curves, p (r), for the sol (a) and the gel (b) [2].

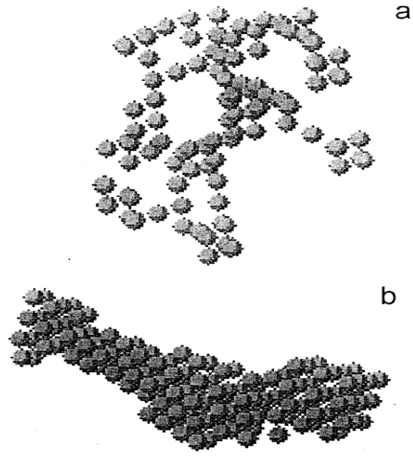

Figure 1. The aggregate model, for the sol (a) and the gel (b) [2].

Table 1. Structural parameters through gelation of galactose [2]

No. of Measurement	d_m	d_s	R_g
2	1.58	-	18.33
3	1.79	-	17.72
4	1.79	2.90	14.88
10	1.84	2.29	14.56

Table 2. Structural parameters of concentration dependent glucofuranose gels [4].

Concentration %[g/mL]	d_m	d_s	R_g
0.1	-	2.9	61.9
0.5	2.7	2.2 -2.7	60.7
1.0	2.6	2.2	57.4
3.0	2.8	2.2	49.7

The observed structural changes do not agree with aggregation ruled by self-assembling [5], and can be explained only by taking into account a structural transition, takes place after the initial stage of the aggregation.

Conclusions:

The gelator aggregates of fractal type exist also in a sol state. Supramolecular structure of studied sols and gels seems to be dependent on level of participation of the aggregates: i/ *small participation*- aggregates are of rounded, oval-type shape and loose, simple fractal structure including medium, ii/ *big participation* – aggregates are denser, partly occupy volume and are of rod-like shape and well-definied surface. The change of the aggregate structure from: i/ to ii/ is of structural transformation type.

The number of free –OH groups in the sugar molecule influences the formation of mass or surface fractals.

References

[1] H. Grigoriew, D. Chmielewska, J. Gronkowski, "SAXS structural study of Xerogels and Aerogels formed from small-molecule organic gelators", *J. Physics: Conf. Series*, in print.

[2] H. Grigoriew, R. Luboradzki, S. Cunis, "In situ studies of monosaccharide gelation using the small-angle X-ray scattering time-resolved method", *Langmuir* **20** (2004) 7374-7377.

[3] S. Bernstorff, H. Grigoriew, D. Chmielewska, "Structural change induced by temperature increase in monosaccharide gel", *Annual Report* (2006), SAXS beamline at ELETTRA, pp. 101-102.

[4] H. Grigoriew, R. Luboradzki, J. Gronkowski, "USAXS studies of monosaccharide gels I. Dependence of glucofuranose-based gel structure on the gelator concentration", *J. Non-Cryst.* Solids **352** (2006) 3052-3057

[5] H. Grigoriew, J. Gronkowski, "USAXS study of monosaccharide gels II. The common features of structural changes", *J. Non-Cryst. Solids* **352** (2006) 5492-5497

L20

INVESTIGATING SPINTRONICS THIN FILM SYSTEMS WITH SYNCHROTRON RADIATION

C.M. Schneider [1*], I. Krug [1], M. Müller [1], F. Matthes [1], S. Cramm [1], F. Wegelin [2], A. Oelsner [2], S.A. Nepijko [2], A. Krasyuk [2], C.S. Fadley [3], and G. Schönhense [2]

[1] *Institut f. Festkörperforschung IFF-9, Forschungszentrum Jülich, D-52425 Jülich, Germany*

[2] *Institut f. Physik, Joh.-Gutenberg Universität Mainz, D-55099 Mainz, Germany*

[3] *Physics Department, University of California Davis, Davis, USA*

Keywords: magnetism, spin-polarized photoemission, photoemission microscopy

**) e-mail: c.m.schneider@fz-juelich.de*

I. Introduction

Complex layered structures and and nanomagnets are the main building blocks for current and future spintronics applications. The electronic, magnetic and magneto-transport properties of these layered systems are determined not only by the characteristics of the individual layers, but even more so by the boundaries between them. Magnetic coupling phenomena and spin-dependent transport are sensitively affected by the atomic arrangement, electronic states and the magnetic nanostructure of the individual constituents at the interfaces. In addition, not only the static magnetic properties are of interest, but also the dynamic response. A controlled and fast magnetization reversal determines the functionality of magnetic devices and therefore, the details of the magnetic switching mechanisms and the limiting timescales involved are of great interest.

Synchrotron radiation provides a convenient and versatile approach to the study of magnetism. Magnetic sensitivity can be achieved by a proper choice of circular or linear polarization. The synchroton light also combines element selectivity with time-resolution due to the broad tuning range and intrinsic time-structure. It is therefore ideally suited to address both static and dynamic issues in thin film and nanomagnetism on the basis of a variety of spectroscopy and microscopy techniques. In the following, we will focus on the application of photoelectron spectroscopy and microscopy techniques with synchrotron radiation to magnetic thin films.

In the first part of this contribution, we will discuss recent results of our studies on the electronic and magnetic states in two spintronic model systems: MgO/Fe(001) and NiO/Fe_3O_4(011). A particular emphasis is laid on the role of the interfaces. The second part is devoted to pump-probe investigations of the magnetodynamics in magnetic microstructures by means of time-resolved photoemission microscopy.

II. Electronic States in MgO/Fe(001)

The Fe/MgO system is well known by now for its high tunneling magnetoresistance effects [1,2], presumably caused by coherent tunneling through matched electronic states across the interfaces. Little is known, however, about the electronic states at the MgO/Fe interface and the influence of the chemical composition and defects, respectively. Using spin-polarized photoemission spectroscopy, we have studied the spin-split electronic states in Fe(001) upon deposition of ultrathin MgO films of variable stoichiometry [3,4]. The band gap of MgO ensures that the Fe-related spectral features can still be observed through the MgO overlayer (Fig. 1). In our experimental geometry we are sensitive to electronic states of both Δ_1 and Δ_5 spatial symmetry. We find that for stoichiometric MgO overlayers the Fe spectral features and the spin polarization at the Fermi level remain unchanged.

On the other hand, overoxidation of the Mg leads to a clear reduction of the Fe spin polarization, caused by the formation of interfacial FeO. This can also be confirmed by the evolution of an exchange-splitting in the O 2*p* states. An oxygen deficiency in the MgO layer, however, causes a significant increase of the Fe spin polarization, which may be explained through the electronic interaction with O vacancies and the resulting charge transfer.

III. Magnetic proximity effects in NiO/Fe_3O_4(001)

The interface between antiferromagnets (AF) and ferromagnets (FM) gives rise to the phenomenon of exchange bias, which is often used to define a magnetic reference in spintronics. The combination NiO (AF) and Fe_3O_4 (FM) represents an interesting model system, as oxidic interfaces promise higher structural and magnetic quality than metallic ones. In our studies we addressed the magnetic coupling of ultrathin NiO overlayers on Fe_3O_4 single crystal surfaces by means of soft x-ray photoemission microscopy. By exploiting circular (XMCD) and linear (XMLD) magnetodichroic contrast mechanisms, we can address the magnetic microstructure of the ferrimagnet and the antiferromagnet separately (Fig. 2). From a comparison of the domain structures and a detailed analysis of the angular dependence of the XMLD contrast we can deduce the details of the coupling at the interface.

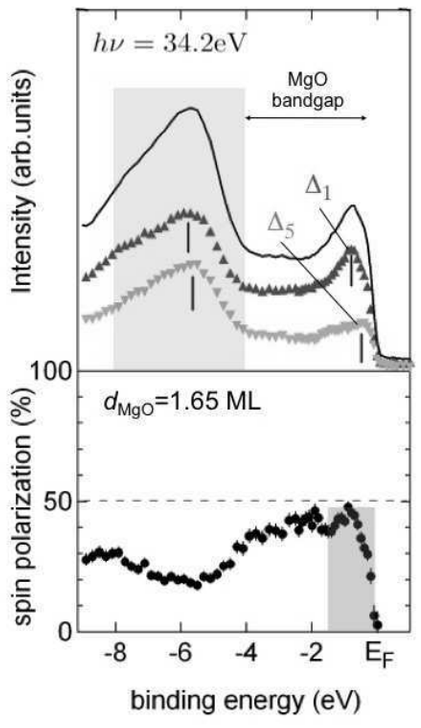

Figure 1. Spin-resolved photoemission spectra of a 1.65 monolayer (ML) MgO-films on Fe(001) at 34.2 eV photon energy. The spin-up (red) and spin-down (green) spectra can be interpreted in terms of the Fe bulk band structure. The broad feature below -4 eV binding energy results from MgO. The spin polarization (bottom) of ~50% close to the Fermi level corresponds to that of clean Fe(001) at the same experimental parameters.

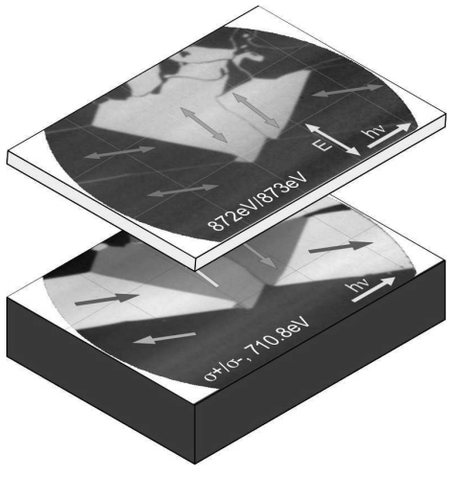

Figure 2. Element-selective magnetic domain imaging in the $NiO/Fe_3O_4(011)$ system exploiting XMCD at the Fe L_3 and XMLD at the Ni L_2 edges. The magnetic domain structure in the ferrimagnet (FM) Fe_3O_4 (bottom) is characterized by four magnetization axes (arrows). In the NiO film the micromagnetic structure is replicated, but exhibits only two different contrast levels, corresponding to two different spin quantization axes in the antiferromagnet (AF). This corresponds to a collinear coupling of FM and AF.

The ideal (011)-surface of NiO is spin-compensated, *i.e.* there is no net magnetic moment in this lattice plane. According to the theoretical considerations of Koon [5], this situation should lead to a 90° (spin-flop) coupling between AF and FM For the (011)-oriented interface, we find clear evidence for a spin-flip coupling, which may be mediated through the superexchange interaction across the interface. In addition, we observe a proximity effect on the NiO-side of the interface, leading to a sizable ferromagnetic response and XMCD signal of the interfacial NiO layer [6].

A similar behavior, *i.e*. spin-flip coupling is found for the (111) axis. The (001) orientation, which in the ideal case is also spin-compensated behaves differently and exhibits the expected spin-flop coupling. The difference of the interfacial coupling between the various crystalline orientations can be understood on the basis of the bonding mechanisms at the specific interface. Further analysis reveals that also magnetoelastic interactions have to be taken into account.

IV. Time-resolved studies of magnetization dynamics

Understanding the microscopic mechanisms and limits of fast magnetic switching processes is of high fundamental as well as of vital technological importance. This task asks for a real-space mapping of transient magnetization structures with high lateral and time resolution. Stroboscopic soft x-ray PEEM (XPEEM) studies exploiting the intrinsic picosecond time structure of the syn- chrotron light are ideally suited for this purpose by [7, 8]. In our pump-probe approach we excite the magnetic system with synchronized magnetic field pulses via a coplanar waveguide and probe the magnetodynamics via the transient state imaged by selected synchrotron light pulses. The time resolution obtained ranged between 10 and 70 ps, depending on the operational mode of the storage ring.

In our studies on small Permalloy and Co platelets we observe a variety of microscopic processes, which affect the reversal modes, for example, incoherent and coherent rotation events (Fig. 3). Domain magnetizations which are oriented perpendicular to the magnetic field pulse undergo a coherent rotation. Incoherent magnetization rotation occurs, if the driving pulse field opposes the sample or domain magnetization direction. These transient states are characterized by a strip-like domain pattern, which forms in selected domains along the rising edge of the pulse (region I in Fig. 3). Such a structure is associated with sizable magnetic stray fields, proving the importance of the magnetization torque in these fast processes. On the pulse plateau, the transient structure stabilizes and the system assumes a new dynamic equilibrium (region II). This has a peculiar consequence at the falling edge of the pulse. The reduction of the magnetic field is acting on the system like a magnetic field in the opposite direction. This leads to a formation of the strip-like domains also in other domains (region III). The domain walls, which have been created in this process, are rather stable causing the transient state to

L20

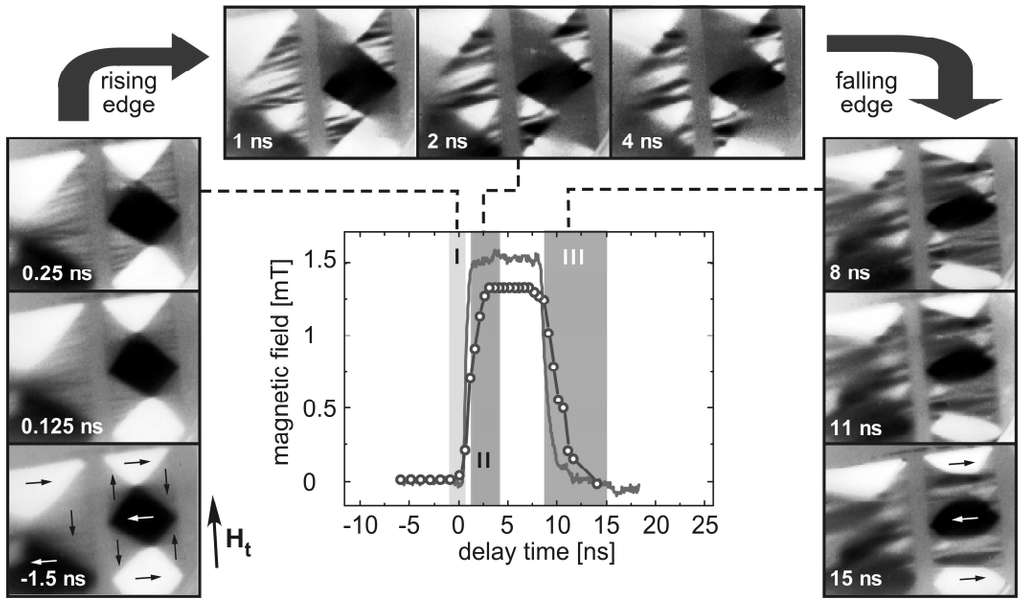

Figure 3. Time-resolved photoemission microscopy from rectangular Permalloy microstructures. The ground state (-1.5 ns) corresponds to a simple Landau flux closure pattern (magnetization directions marked by arrows). The images correspond to the transient domain configuration obtained from XMCD contrast along the field pulse (center) at different delay times (in ns).

relax only slowly (on the time scale of 20-30 ns) back into the ground state.

In addition to domain wall motion and rotation events, we also find collective excitations of the magnetization. These precessional modes have frequencies in the GHz regime and are determined by the shape of the platelets and the domain configurations [9]. By exciting the system close to the mode resonance, we can even generate quasistatic modifications of the magnetic domain structure.

Acknowledgements: Financial support through Deutsche Forschungsgemeinschaft (SFB 491) is gratefully acknowledged. The authors are indepted to the staff at BESSY (Berlin), ESRF (Grenoble) and SLS (Villingen) for their technical support during the beamtimes.

References

[1] S. Yuasa T. Nagahama, A. Fukushima, Y. Suzuki, K. Ando, "Giant room-temperature magnetoresistance in single-crystal Fe/MgO/Fe magnetic tunnel junctions", *Nature Mater.* **3** (2004) 868-871.

[2] S.S.P. Parkin, C. Kaiser, A. Panchula, P.M. Rice, B. Hughes, M. Samant, S.-H. Yang, "Giant tunnelling magnetoresistance at room temperature with MgO (100) tunnel barriers", *Nature Mater.* **3** (2004) 862-867.

[3] M. Müller, F. Matthes, C.M. Schneider, "Photoemission study of the Fe(001)/MgO interface for varying oxidation conditions of magnesium oxide", *J. Appl. Phys.* **101** (2007) 09G519.

[4] M. Müller, F. Matthes, C.M. Schneider, "Spin polarization at ferromagnet-insulator interfaces: The important role of stoichiometry in MgO/Fe(001)", *Europhys. Lett.* **80** (2007) 17007.

[5] I.P. Krug, F.U. Hillebrecht, H. Gomonaj, M.W. Haverkort, A. Tanaka, L.H. Tjeng, C.M. Schneider, "Magnetic coupling in highly ordered NiO/Fe_3O_4(110): Ultrasharp magnetic interfaces vs. long-range magnetoelastic interactions", *Europhys. Lett.* **81** (2008) 17005.

[6] N.C. Koon, "Calculations of exchange bias in thin films with ferromagnetic/antiferromagnetic interfaces", *Phys. Rev. Lett.* **78** (1997) 4865-4868.

[7] A. Krasyuk, A. Oelsner, S. Nepijko, A. Kuksov, C.M. Schneider, G. Schönhense, "Time-resolved photoemission electron microscopy of magnetic field and magnetisation changes", *Appl. Phys. A* **76** (2003) 863-868.

[8] J. Vogel W. Kuch, M. Bonfim, J. Camarero, Y. Pennec, F. Offi, K. Fukumoto, J. Kirschner, A. Fontaine, S. Pizzini, "Time-resolved magnetic domain imaging by x-ray photoemission electron microscopy", *Appl. Phys. Lett.* **82** (2003) 2299-2301.

[9] G. Schönhense, H.-J. Elmers, S.A. Nepijko, C.M. Schneider, "Time-resolved photoemission electron microscopy", in: *Advances in Imaging and Electron Physics,* vol. 142, P.W. Hawkes (ed.), *(Academic Press 2006)* 157-323.

[10] F. Wegelin, D. Valdaitsev, A. Krasyuk, S.A. Nepijko, G. Schönhense, H.J. Elmers, I. Krug, C.M. Schneider, "Magnetization dynamics in microscopic spin-valve elements: Shortcomings of the macrospin picture", *Phys. Rev. B* **76** (2007) 134410.

L21

HARD X-RAY PHOTON-IN-PHOTON-OUT SPECTROSCOPY WITH LIFETIME RESOLUTION – OF *XAS, XES, RIXSS* AND *HERFD*

Pieter Glatzel*

European Synchrotron Radiation Facility (ESRF), BP22, 6 rue Jules Horowitz, 38043 Grenoble, France

Keywords: photon-in-photon-out spectroscopy, spectrometer, x-ray emission, x-ray absorption

**) e-mail: Glatzel@esrf.fr*

A photon-in-photon-out technique using hard x-rays is most suitable for applications where the sample environment cannot be chosen freely, *i.*e. UHV conditions necessary for photoemission experiments are not possible, or when a truly bulk sensitive probe is desired. The preferred X-ray spectroscopy technique to study element specifically electronic structure and local coordination is X-ray absorption spectroscopy (XAS). The near edge structure (XANES) is mainly used to obtain oxidation states, even though XANES also contains information on the local geometry and coordination. A detailed analysis of the XANES structure is a complex task because of the numerous interactions that contribute to its shape. The spectroscopy using the extended range (EXAFS) is well developed theoretically and experimentally but the technique has its inherent limitations (*e.g.* differentiation of elements close in atomic number Z) and the ideal experimental conditions (*e.g.* sample thickness, homogeneity) for a correct EXAFS analysis are not always given. It is thus desirable to introduce other techniques that either provide a mean to verify the results obtained from XAS or yield additional information on the sample in particular with respect to electronic structure.

An X-ray spectrometer based on perfect crystal Bragg optics opens up new possibilities for X-ray spectroscopy. Detecting the emitted X-rays with an instrumental energy bandwidths on the order of the core hole lifetime broadening enables to resolve fine structure in the X-ray emission spectrum. This fine structure contains information on the electronic configuration and chemical environment of the emitting atom that is complementary to what can be obtained in XAS [1, 2]. Such a secondary monochromator provides an additional tunable energy detection to the primary monochromator of the synchrotron radiation source. X-ray emission spectroscopy (XES) thus adds a dimension to XAS. The techniques arising from such an experimental setup have been named non-resonant XES, resonant XES or resonant inelastic X-ray scattering (RIXS) spectroscopy and high-energy-resolution fluorescence detection (HERFD). They will be discussed in this contribution. Another technique, non-resonant X-ray Raman scattering, will be left out to be discussed by others [3].

The experimental setup requires monochromatization of the emitted X-rays using perfect Bragg optics. Many instruments use a Rowland geometry with spherically bent Si or Ge wafers either in Johann or Johansson geometry (Fig. 1). An energy scan can be performed either point-by-point or single shot where the emission energy is dispersed over a position sensitive detector [4].

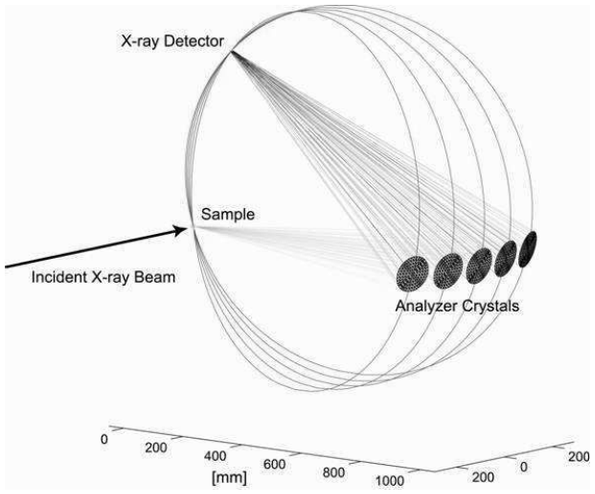

Figure 1. Setup for x-ray emission spectroscopy. Five spherically bent analyzer crystals monochromatize and focus the X-rays on a photon counting detector. The Rowland circles that define the focusing condition are shown.

An important feature and difference to standard XAS of x-ray emission detection with lifetime resolution is the strong sensitivity to electronic structure. The emission lines just below the Fermi level reflect the projected density of occupied electronic states (Fig. 2). The final states electron configuration is formally identical to valence band photoemission even though different selection rules yield different relative spectral intensities. A comparison between absorption and emission spectra can provide an element specific band gap. This is routinely done in soft x-ray spectroscopy and will now be combined with hard x-rays in order to have more freedom

L21

with respect to sample environment and to have access to a larger range of momentum transfer. Bergmann and co-workers showed the sensitivity of the Kβ cross-over peak to the atomic charge of the ligand [5]. It is thus possible to distinguish between O, N and F as ligands to the metal atom which is difficult or impossible using other techniques.

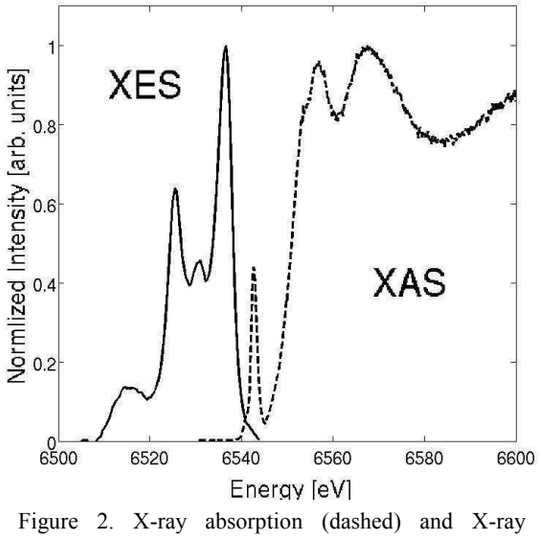

Figure 2. X-ray absorption (dashed) and X-ray emission spectra (full) in a Mn(III) nitrido complex.

The 3*p* to 1*s* transitions (Kβ main lines) in 3*d* transition metals at lower energies have been used by many authors to address the metal atom spin state[6, 7]. The spin-sensitivity in the emission can also be exploited to record spin-selective absorption spectra [8]. This can be used to elucidate the origin of the spectral features in the K absorption pre-edge. Based on this technique, it was straight forward to prove the existence or absence of a $3d^4$ high-spin configuration, *i.e.* a high-spin Fe(IV) species, in catalytic systems [9] and the presence of a non-local excitation in hematite (Fe_2O_3) [10].

In a seminal study, Hämäläinen showed that spectral features with a broadening that is lower than the absorption core hole lifetime broadening can be obtained using high energy resolution fluorescence detected (HERFD) absorption spectroscopy [11]. More then 10 years later, this technique found its way to the applied sciences and was for example used to study the chemical behaviour of Au nanoparticles in the oxidation of carbon monoxide (Fig. 4) [12]. For this technique to yield spectra that can be analyzed using the theory of X-ray absorption it is necessary that final state effects in the X-ray emission process can be neglected. This is fortunately the case for the Lα decay channels in 5*d* transition elements.

Many pitfalls can surprise the scientist who uses high energy resolution emission detection. Some of them have been first pointed out by Carra, Fabrizio and Thole [13]. Based on this paper the problems have been illustrated by the present author and it is strongly recommended to record full intensity planes with incident and emitted energy as energy axes in order to unequivocally identify the origin of a spectral feature (*cf.* Fig. 3 and Ref. [1]) Many years of experience does not prevent erroneous assignment of spectral features as the present author had to experienced.

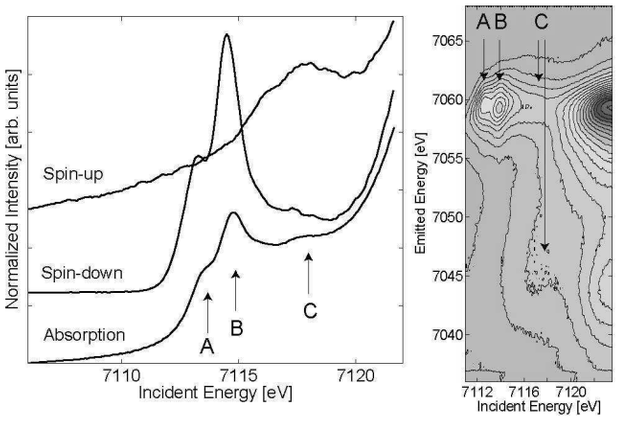

Figure 3. Left: Total and spin-selective absorption in Fe_2O_3 for ε ⊥ c. Right: 1*s*3*p* RXES plane for polycrystalline Fe_2O_3. The spin-up and spin-down excitations occur around 7045 and 7059 eV emitted energy, respectively.

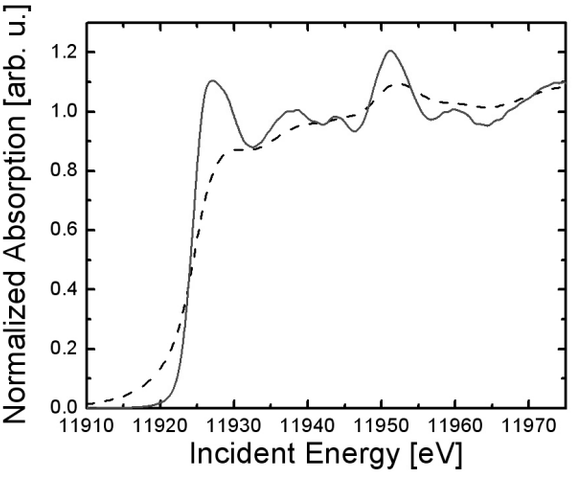

Figure 4. The L_3 absorption edge of a Au foil detected in transmission mode (dotted) and using the HERFD technique (solid).

The fundamental problem and hold-up in the progress of X-ray spectroscopy to study electronic structure is the theoretical modelling of the spectra. While the interpretation of EXAFS to obtain structural information is well developed, only few experiments that address the electronic structure are well understood based on an established theoretical framework. This is mainly due to the complexity of the problem. There are excellent research groups who do theoretical spectroscopy and

produce outstanding results. However, this is by far not enough to match the ever growing number of experimental spectra that require interpretation. X-ray emission spectrometers are either planned or being constructed at all of the new European synchrotron radiation sources. At first this will aggravate the problem but also gives rise to the hope that a larger user community will push for greater efforts in theoretical modelling in order to have more resources devoted to this field.

Acknowledgement: The author would like to thank the ID26 staff, the ESRF support groups and all users of beamline ID26 for valuable input and fruitful discussions.

References

[1] P. Glatzel, U. Bergmann, "High resolution 1s core hole x-ray spectroscopy in 3*d* transition metal complexes - Electronic and structural information", *Coord. Chem. Rev.* **249** (2005) 65-95.

[2] P. Glatzel, U. Bergmann, J. Yano, H. Visser, J.H. Robblee, W.W. Gu, F.M.F. de Groot, G. Christou, V.L. Pecoraro, S.P. Cramer, V.K. Yachandra, "The electronic structure of Mn in oxides, coordination complexes, and the oxygen-evolving complex of photosystem II studied by resonant inelastic X-ray scattering", *J. Am. Chem. Soc.* **126** (32) (2005) 9946-9959.

[3] U. Bergmann, O.C. Mullins, S.P. Cramer, "X-ray raman spectroscopy of carbon in asphaltene: light element characterization with bulk sensitivity", *Anal. Chem.* **72** (11) (2000) 2609-2612.

[4] H. Hayashi, M. Kawata, R. Takeda, Y. Udagawa, Y. Watanabe, T. Takano, S. Nanao, N. Kawamura, "A multi-crystal spectrometer with a two-dimensional position-sensitive detector and contour maps of resonant K beta emission in Mn compounds", *J. Electron Spec. Rel. Phen.* **136** (1-2) (2004) 191-197.

[5] U. Bergmann, C.R. Horne, T.J. Collins, J.M. Workman, S.P. Cramer, "Chemical dependence of interatomic x-ray transition energies and intensities – a study of Mn Kb" and $Kb_{2,5}$ spectra", *Chem. Phys. Lett.* **302** (12) (1999) 119-124.

[6] G. Vanko, T. Neisius, G. Molnar, F. Renz, S. Karpati, A. Shukla, F.M.F. de Groot, "Probing the 3*d* spin momentum with X-ray emission spectroscopy: The case of molecular-spin transitions", *J. Phys. Chem. B* **110** (24) (2006) 11647-11653.

[7] J. Badro, G. Fiquet, F. Guyot, J.P. Rueff, V.V. Struzhkin, G. Vanko, G. Monaco, "Iron partitioning in Earth's mantle: Toward a deep lower mantle discontinuity", *Science* **300** (5620) (2003) 789-791.

[8] K. Hämäläinen, C.C. Kao, J.B. Hastings, D.P. Siddons, L.E. Berman, V. Stojanoff, S.P. Cramer, "Spin-dependent X-ray absorption of MnO and MnF_2", *Phys. Rev. B* **46** (21) (1992) 14274-14277.

[9] G.D. Pirngruber, J.D. Grunwaldt, J.A. van Bokhoven, A. Kalytta, A. Reller, O.V. Safonova, P. Glatzel, "On the presence of Fe(IV) in Fe-ZSM-5 and $FeSrO_{3-x}$ - unequivocal detection of the 3*d*(4) spin system by resonant inelastic X-ray scattering", *J. Phys. Chem. B* **110** (37) (2006) 18104-18107.

[10] P. Glatzel, A. Mirone, S.G. Eeckhout, M. Sikora, G. Giuli, "Orbital hybridization and spin polarization in the resonant 1s photoexcitations of alpha-Fe2O3", *Phys. Rev. B* **77**(11) (2008) -.

[11] K. Hämäläinen, D.P. Siddons, J.B. Hastings, L.E. Berman, "Elimination of the inner-shell lifetime broadening in X-ray- absorption spectroscopy", *Phys. Rev. Lett.* **67**(20) (1991) 2850-2853.

[12] J.A. van Bokhoven, C. Louis, J. T Miller, M. Tromp, O.V. Safonova, P. Glatzel, "Activation of oxygen on gold/alumina catalysts: In situ high-energy-resolution fluorescence and time-resolved X-ray spectroscopy", *Angew. Chem. - Intern. Ed.* **45**(28) (2006) 4651-4654.

[13] P. Carra, M. Fabrizio, B.T. Thole, "High-resolution X-ray resonant Raman-scattering", *Phys. Rev. Lett.* **74**(18) (1995) 3700-3703.

L22

SYNCHROTRON RADIATION STUDIES OF PERSISTENT LUMINESCENCE MATERIALS

J. Hölsä [1*], M. Kirm [2], T. Laamanen [1,3], M. Lastusaari [1], and J. Niittykoski [1]

[1] *Department of Chemistry, University of Turku, FI-20014 Turku, Finland*
[2] *University of Tartu, Institute of Physics, EE-51014 Tartu, Estonia*
[3] *Graduate School of Materials Research, Turku, Finland*

Keywords: persistent luminescence, UV-VUV excitation, band gap, europium, rare earth, valence state

**) e-mail: jholsa@utu.fi*

The persistent luminescence is obtained continuously from materials for even tens of hours after ceasing the irradiation – either with the UV radiation or, preferably, with the visible light [1]. This requires extensive storage of the exciting radiation for a very long but not for too a long time. The energy stored is required to be released from the traps without an input of artificial energy, so the temperature should do the job. This means that the traps must be rather shallow, of the order of less than 1 eV. At first, this seems totally incompatible with the high energies used in the synchrotron radiation studies of materials, but more and more frequently the phenomena dealing with the band structure of the host lattice are studied – and this is done most easily with the synchrotron radiation UV-VUV excitation spectroscopy [2]. Moreover, with the trapping and release of the charge carriers – either electrons or holes (or both), the question whether a change – a real or a virtual one – in the valence state of the dopant takes place becomes a critical question. In this context, the synchrotron radiation methods as EXAFS and XANES become interesting in probing the valence of the species present in the persistent luminescence materials.

The persistent luminescence materials with very good performance are usually oxidic compounds as alkaline earth aluminates (MAl_2O_4) or disilicates ($M_2MgSi_2O_7$) which are doped with divalent europium (Eu^{2+}). The broad band $4f^6 5d^1 \rightarrow 4f^7$ emission from this dopant ensures efficient conversion of the energy stored into visible – usually blue or green – light. In order to make these materials even more efficient, these are customarily co-doped with trivalent lanthanides (R^{3+}). The presence of at least one (Eu^{2+}/ Eu^{3+}) but maybe a second (R^{2+}/ R^{3+}/ R^{IV}) set of ions, too, capable of undertaking redox reactions – real or virtual, no importance at the moment – has intrigued the minds of the researchers from the very beginning of the modern persistent luminescence era – that means from the mid 1990s.

In this work, the synchrotron radiation source of HASYLAB (Hamburg, Germany) with the SUPERLUMI beamline was used to study the band gap energies of the aluminate and disilicate persistent luminescence materials. In addition, the Eu^{2+} $4f^7 \rightarrow 4f^6 5d^1$ excitation band structure was monitored as a function of the temperature from 10 K to ambient. The band gap energy of *ca.* 7 eV together with the Eu^{3+} charge transfer band energy of *ca.* 5 eV leaves no doubt about the concept that the persistent luminescence mechanism is based on the electron transfer from the Eu^{2+} dopants to the traps *via* the conduction band. The holes – if present – thus play only a minor role. Even if the exciton structure was not observed for the Eu^{2+} doped materials – probably due to the too high Eu^{2+} concentration – the defect luminescence of the non-doped materials indicates the presence of defects in these materials.

The XANES measurements carried out in the MAX-lab (Lund, Sweden) with the beamline I811 for the Eu^{2+},R^{3+} co-doped $SrAl_2O_4$ and $Sr_2MgSi_2O_7$ materials indicated the presence of both the Eu^{3+} and Eu^{2+} ions in all materials. For the $Sr_2MgSi_2O_7$ host, the relative amount of Eu^{3+} was observed to increase upon increasing exposure to X-rays, whereas for $SrAl_2O_4$ there was very little or no change. For the Dy and Yb co-dopants, only trivalent species were observed. On the other hand, traces of tetravalent cerium were present in the Eu,Ce co-doped materials. Nevertheless, the redox behaviour of the dopant and the co-dopants seem to be rather complicated, and thus the present XANES results are so far inconclusive and more work is needed to elaborate the persistent luminescence materials.

Acknowledgements: The financial support from the Academy of Finland, the foundations of the Turku University as well as of Jenny and Antti Wihuri is gratefully acknowledged.

References

[1] T. Aitasalo, J. Hölsä, H. Jungner, M. Lastusaari, J. Niittykoski, "Thermoluminescence study of persistent luminescence materials: Eu^{2+} and R^{3+} doped calcium aluminates, $CaAl_2O_4$:Eu^{2+},R^{3+}", *J. Phys. Chem. B* **110** (2006) 4589-4598.

[2] Y. Chen, B. Liu, M. Kirm, Z. Qi, C. Shi, M. True, S. Vielhauer, G. Zimmerer, "Luminescent properties of blue-emitting long afterglow phosphors $Sr_{2-x}Ca_xMgSi_2O_7$:Eu^{2+}, Dy^{3+} (x=0, 1)", *J. Lumin.* **118** (2006) 70-78.

L23

APPLICATION OF SCANNING TRANSMISSION X-RAY MICROSCOPY IN NATURAL SCIENCE

Tolek Tyliszczak

Advanced Light Source, Lawrence Berkeley National Laboratory, MS-6-2100, 1 Cyclotron Rd. Berkeley, CA, 94720, USA

Keywords: STXM, spectromicroscopy, x-ray absorption, magnetism

e-mail: tolek@lbl.gov

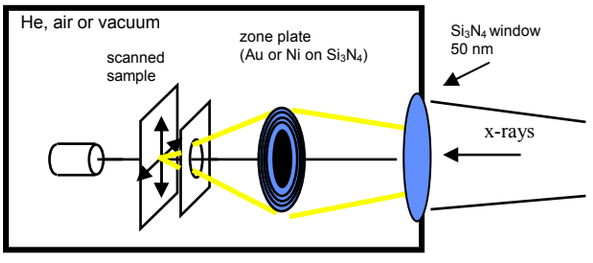

Figure 1. STXM basics.

Scanning x-ray transmission microscope (STXM) became during last few years an important tools in applying soft x-ray spectroscopy to many scientific disciplines. When STXM is placed on a modern beamline of the third generation synchrotron it allows for chemical characterization of materials and processes on 20 nm scale. It is a microscope, thus it produces images, but its strength is ability to do high quality spectroscopy on that scale.

In STXM x-rays are focused using a Fresnel zone plate and the sample is mechanically scanned in the zone plate focal plane. Transmitted x-rays are detected by a single element detector and the detector signal as a function of the sample position constitutes an image. Recording images at different x-ray energies around absorption edges of a given element allows obtaining spectroscopic information for each of image pixels [1].

At the Advanced Light Source there are three STXMs. One is placed on a bending magnet beamline and operates between 250 eV and 600 eV. The most versatile one is on the 11.0.2 beamline with an elliptically polarizing undulator as a source and operates between 80 eV and 2100 eV. This x-ray range covers absorption edges of most common elements. The third STXM is a portable microscope which can be used on many different beamlines.

Resolution of a STXM depends on the used zone plates. Current ALS zone plates can resolve details smaller than 20 nm. Samples preparation can be similar to that for a TEM, but because the sample can be at full atmospheric pressure of He (or air for some x-ray energies) they can be "wet", fully hydrated, a huge advantage for biological or environmental sample studies.

The 11.0.2 STXM can take advantage of elliptically polarized light. Magnetic sensitivity is provided by the X-ray Magnetic Circular Dichroism (XMCD) effect of resonance x-ray absorption at the absorption edges. As such, it is an element specific magnetization measurement with high sensitivity. It is possible to measure a single monolayer of element with full spatial resolution. This is well illustrated in studies of ferromagnetic effect of carbon [2]. Elemental specificity of the measurements allow on separate characterization of different layers in complex structures. By measuring a sample in few different orientations with respect to the x-ray beam it is possible not only to obtain a value of magnetic moment but also its direction on scale of 20 nm.

The x-ray beam has a time structure of bursts with a duration of 70 ps and frequency 500 MHz. Fast, direct x-ray photon detection using an avalanche photodiode results in about 100 ps time resolution of the measurements. The magnetization dynamics studies on sub-micrometer complex samples are one of the most unique applications of the STXM. Detail motion of vortex core under various excitations can be observed [3]. Imaging of spin transfer switching gave new insights into a combined role of spin transfer and charge current in the switching process.

STXM found a very wide application in polymer science, where a high chemical sensitivity combined with a good spatial resolution and relatively low radiation damage makes it a very important tool in studies today's complex polymers. Other common applications are environmental studies, especially of a role of bacteria.

References

[1] A.L.D. Kilcoyne, T. Tyliszczak, W.F. Steele, S. Fakra, P. Hitchcock, K. Franck, E. Anderson, B. Harteneck, E.G. Rightor, G.E. Mitchell, A.P. Hitchcock, L. Yang, T. Warwick, H. Ade, "Interferometer controlled scanning transmission X-ray microscopes at the advanced light source", *J. Synchrotr. Radiat*. **10** (**2003**) 125.

[2] H. Ohldag, T. Tyliszczak, R. Höhne, D. Spemann, P. Esquinazi, M. Ungureanu, T. Butz, "π-electron ferromagnetism in metal-free carbon probed by soft X-ray dichroism", *Phys. Rev. Lett.*, **98** (2007) 187204.

[3] B. Van Waeyenberge, A. Puzic, H. Stoll, K.W. Chou, T. Tyliszczak, R. Hertel, M. Fähnle, H. Brückl, K. Rott, G. Reiss, I. Neudecker, D. Weiss, C.H. Back, G. Schütz, "Magnetic vortex core reversal by excitation with short bursts of an alternating field", *Nature* **444** (2006)461-465.

L24

A MONOLITHIC 7 CELL SILICON DRIFT DETECTOR MODULE FOR X-RAY SPECTROSCOPY

E. Welter [1*], K. Hansen [2], Chr. Reckleben [2], and I. Diehl [2]

[1] *Hamburger Synchrotron Strahlungslabor am Deutschen Elektronen Synchrotron, Notkestraße 85, D 22607 Hamburg, Germany*

[2] *Deutsches Elektronen-Synchrotron, Notkestraße 85, D-22607 Hamburg, Germany*

Keywords: Silicon Drift Diode Detector, fl-XAFS, Energy-Dispersive X-ray Detector

**) e-mail: edmund.welter@desy.de*

Energy-dispersive semiconductor detectors find widespread application in the registration of fluorescence-yield X-ray absorption fine structure spectroscopy (fl-XAFS). Today mostly high purity Ge and Si(Li) diode detectors are used for this purpose. Silicon-Drift Detectors (SDD) were first introduced in 1984 [1]. They are based on high-resistivity n-type silicon. The bulk volume of the SDD is completely depleted by application of relatively small voltages - compared to standard diode detector - between p^+ contacts at the front and at the back side and a small n^+ anode in the centre of the detector cell. The electrical field in the SDD is shaped in a way that the generated charge carriers are drifting towards the small read out anode [2]. This design offers several advantageous properties:

- The small read out anode has a very small capacitance thus minimising rise time and noise.
- The SDD can be operated at or near room temperature.
- With a signal rise time of the order of 100 ns the SDD can work at very high count rates up to 1 MHz.

Based on a monolithic 7-cell SDD chip which was manufactured by PNsensors, Munich, Germany, we developed a complete SDD module including a specially developed read-out chip and housing. The complete module is shown in Fig. 1. The read out chip was designed to reach count rates of several 100 kHz and a spectral resolution of 250 - 600 eV (FWHM Mn-K_α), depending on the count rate. The SDD chip has 7 hexagonally shaped cells with integrated JFET in the centre of each cell. The JFET is the first transistor of the signal amplification chain. The read-out ASIC is located behind a radiation protection shield. The housing for the SDD and read-out chip is completely made from pure AlN. The hexagonal rod behind the detector head is made from Cu which provides very good thermal conductivity for the heat transport form the hot side of a Peltier element which is used to cool the read-out ASIC and the SDD down to temperatures between 0° and 10°C.

Spatially resolved test measurements like line scans with a 4×4 µm² pencil beam had shown that the signal-to-noise ratio (S/N) can be improved by a factor of ~10 by covering the cell borders and the JFET in the centre of each cell with a mask. The reason for this effect is that

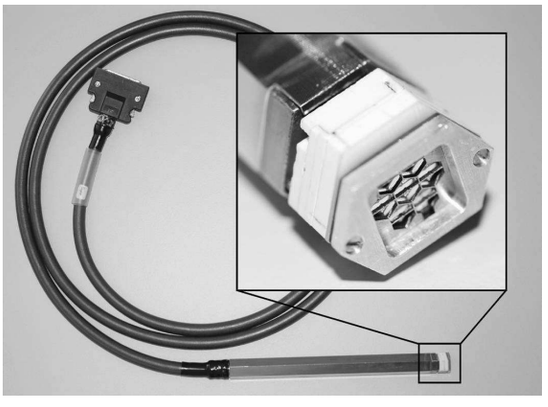

Figure 1. Photograph of a complete detector module, the inset shows the head of the detector with the AlN housing (white) and a Zr mask in front of the SDD chip.

the charge which is produced by photons which are absorbed in these regions is split between neighbouring cells or partly lost. We have chosen Zr metal as material for the mask, because the window between the L and K emission lines corresponds well with the foreseen operation range of the detector modules.

Without light tight entrance windows in front of the SDD chip these modules are used in the vacuum and under strict exclusion of any visible light. Operation in vacuum allows working at very small distances from the sample and thus achieving a high coverage of the total solid angle with a small detector. Meanwhile the first modules were used for test experiments and during a number of user experiments at HASYLAB XAFS beamlines.

The influence of the mask on the S/N ratio is visualised in Fig. 2. It shows fluorescence spectra of a gold foil (Goodfellow, Germany) exited at 12 keV. The beam spot on the foil has a size of 10×1 mm². It is clearly visible that with increasing distance between sample and SDD the escape peak becomes better visible due to the increased S/N ratio. The mask is working more effective if the distance becomes larger, because the number of photons which pass under the mask from the side decreases.

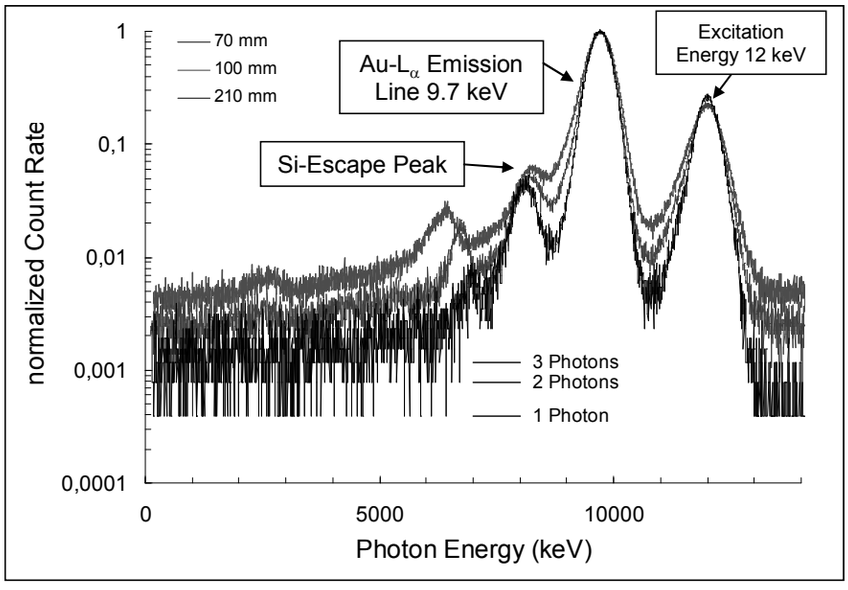

Figure 2. Au-L fluorescence spectra measured at differing distances between detector and sample.

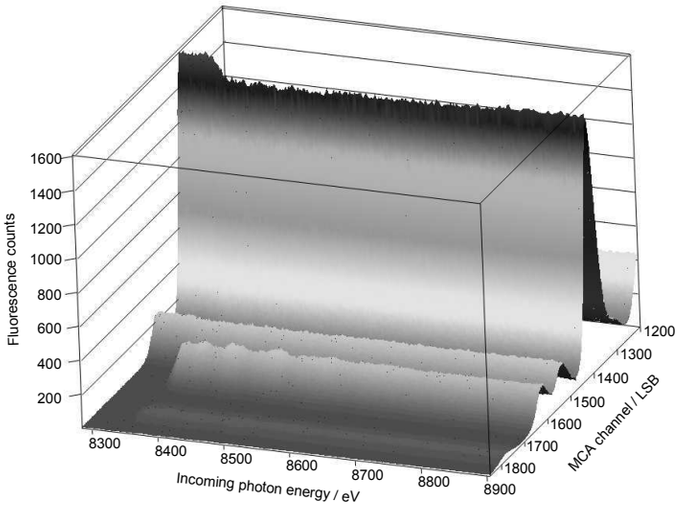

Figure 3. Fluorescence spectra registered during an EXAFS scan over the Ni-K edge of a stainless steel sample.

Figure 3 shows a pseudo 3-d plot of a Ni-K edge EXAFS scan of a stainless steel foil (Cr17FeNi11, Goodfellow, Germany). The Ni-K_α emission line with the edge and the first XAFS oscillations is visible in the front of the graph. The extracted EXAFS spectrum is shown in figure 4 together with the simultaneously registered transmission EXAFS spectrum. Samples like this stainless steel foil which produce a large number of mostly background photons are a typical application for a detector which enables very large count rates per mm^2 active area.

The quality of the EXAFS signal is only limited by photon-counting statistic. This was shown in test scans without changes of the incoming photon energy. The standard deviation of the count rates within the pre-set energy window was always equal to the square radix of the average count rate.

L24

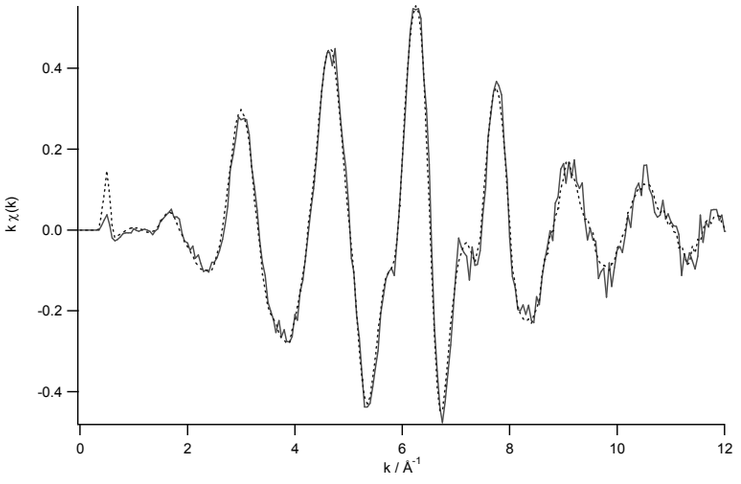

Figure 4. Ni-K edge EXAFS spectra measured on a stainless steel foil in transmission (blue) and SDD-detected fluorescence (red) mode XAFS.

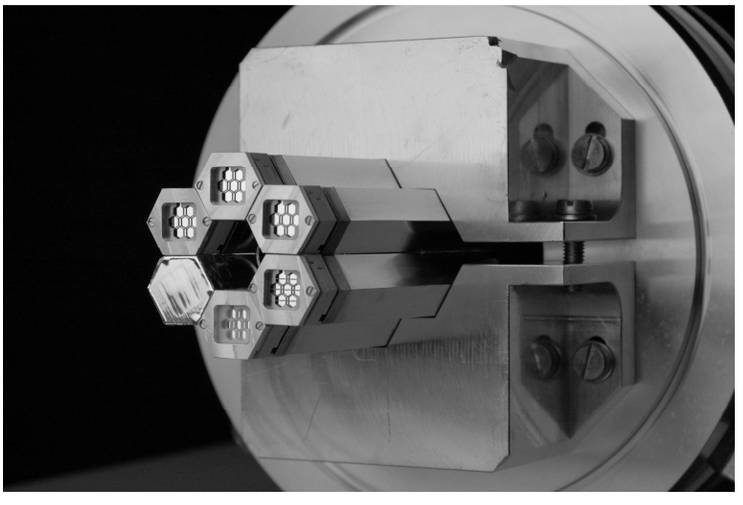

Figure 5. Holder for up to 7 detector modules.

Outlook

Figure 5 shows a special holder for up to 7 modules. With the help of this holder it is possible to work with a 49-cell detector system which is able to achieve count rates of several MHz with an energy resolution around 300 eV (FWHM Mn-K_α). Obviously with a bundle of seven of our presently available detector module there is a lot of insensitive area between the detectors. It would however be very easy to use the read-out ASIC together with different - larger - SDD sensor arrays.

References

[1] E. Gatti, P. Rehak, "Semiconductor drift chamber - an application of a novel charge transport scheme", *Nucl. Instrum. Meth. Phys. Res. A* **225** (1984) 608-621.

[2] L. Strüder, P. Lechner, "Silicon drift detector - the key to new experiments", *Naturwissenschaften* **85** (1998) 539–543.

ELECTRONIC STRUCTURE AND MAGNETIC PROPERTIES OF SELF-ORGANIZED MnSb AND MnAs DOTS GROWN BY MBE ON GaN SURFACE

I.A. Kowalik [1,2*], B.J. Kowalski [1], M. Sawicki [1], M. Pietrzyk [1], J. Sadowski [1,2], E. Łusakowska [1], I. Grzegory [3], and S. Porowski [3]

[1] *Institute of Physics, Polish Academy of Sciences, Al. Lotników 32/46, PL-02-668 Warszawa, Poland*

[2] *MAX-lab, Lund University, Box 118, SE-22100 Lund, Sweden*

[3] *Institute of High Pressure Physics, Polish Academy of Sciences, Sokołowska 29/37, PL-01-142 Warsaw, Poland*

Keywords: manganese arsenide, manganese antimony, quantum dots, resonant photoemission, electronic structure, magnetic properties,

**) e-mail: iwona.kowalik@maxlab.lu.se*

Ferromagnetic/semiconductor hybrid structures have acquired a considerable attention recently because of a growing necessity to integrate magnetism into the contemporary semiconductor technology. To achieve this, semiconductors compatible ferromagnets are required, which will retain their ferromagnetic properties at above room temperature. Among many possible materials manganese-based magnetic compounds, such as MnSb and MnAs, are one of the most promising candidates. MnSb is characterized by a Curie temperature of 590 K, much higher than the one of MnAs (320 K). Another important advantage of MnSb is the possibility of growing high quality epitaxial films on different *III-V* semiconductor substrates. It was already shown that MnSb dots can be applied for high sensitivity magnetic field detectors, due to the huge magnetoresistance effect occurring at room temperature [1].

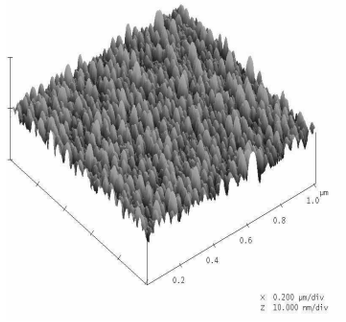

Figure 1. MnSb/GaN surface morphology obtained by Atomic Force Microscopy.

In this paper we summarize our comparative studies of photoemission and magnetic properties of self-organized MnAs and MnSb quantum dots (QD). The MBE growth is performed stepwise on clean, high quality GaN(000$\underline{1}$)-(1×1) surfaces, *in situ* prepared by Ar^+ ion sputtering and annealing.

The 3D growth is confirmed *in situ* by RHEED observations and *ex situ* by AFM characterization. A deposition of 6 ML of MnSb resulted in dots with typical diameter of 40-50 nm and height of 3-3.5 nm. 6 and 8 ML of MnAs produced dots with similar or smaller dimensions, depending on the initialization of the growth mode [1]. The electronic structure of the dots was determined by the analysis of resonant photoemission data. The photoemission measurements were carried out for photon energies close to the Mn 3*p*→3*d* transition to observe the changes of the Mn 3*d* states distribution. The difference between EDC curves obtained at resonant and antiresonant conditions clearly shows the Mn 3*d* states contribution to the valence band region and the CIS analysis indicates a single Fano profile.

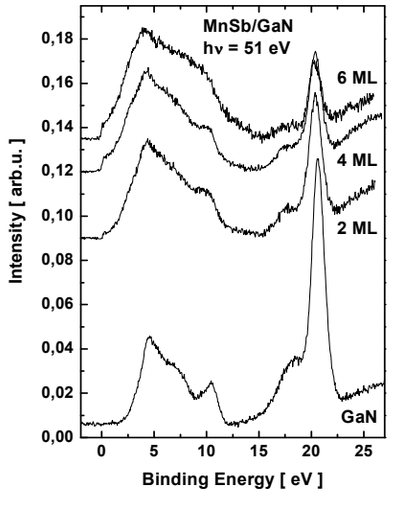

Figure 2. EDC set obtained for photon energy 51 eV (resonance conditions) for MnSb/GaN after each stage of MnSb growth.

L25

The MnSb dots exhibit metallic character while MnAs dots, grown by the same manner, have half-metallic character characteristic of zinc-blende MnAs. Thus, the observed previously formation of half-metallic MnAs in self-organized dots seems to be exceptional in the family of manganese pnictides. We connect this to the crystal lattice misfit and different strains at the MnAs/GaN and MnSb/GaN interfaces.

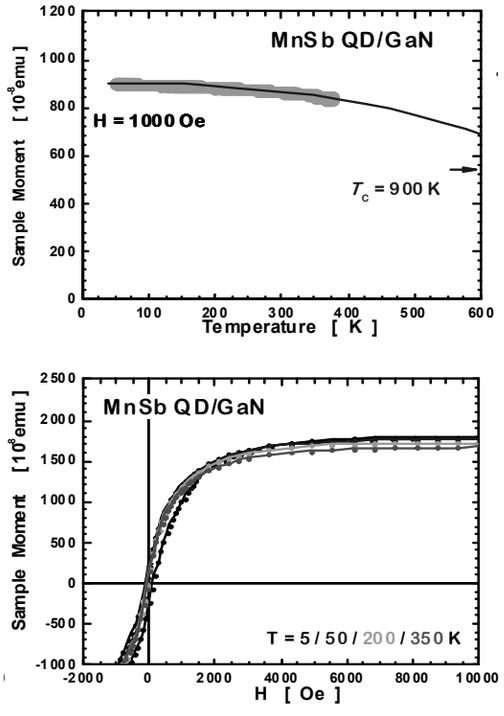

Figure 3. Magnetic (SQUID magnetometry) investigation of MnSb dots on GaN substrate. (Left) Green points: temperature dependence of the magnetic moments at 1000 Oe; blue line: Brillouin function 'fitted' to the data indicates a possible T_C of about 900 K. (Right) M-H dependency at various temperatures indicates a superparamagnetic-like collective behaviour of the dots. The presence of increasing apparent coercivity upon lowering the temperature or remanence indicates the existence of a blocking mechanism.

Magnetic properties of the MnSb dot array were measured using a SQUID magnetometer. The measurements confirm the granular character of the layers, as the basic magnetic characteristics of both systems are typical of a blocked superparamagnet with an average size of the magnetic moment of the single magnetic 'molecule' corresponding nicely to the average volume of the dot. More importantly, despite electronic and crystallographic differences, both systems shows considerably enlarged, approximately 50-100% (well beyond our current experimental limit), T_C. Such an increase of T_C in self-organized magnetic QD, if confirmed in other systems, could be of a profound importance in the search for functional materials for future spintronics applications.

Acknowledgments: The support of EU - Research Infrastructure Action under the FP6 "Structuring the European Research Area" Programme (through the Integrated Infrastructure Initiative "Integrating Activity on Synchrotron and Free Electron Laser Science") and Polish Ministry of Science and Higher Education (grant N202 101 31/0749) is acknowledged.

References

[1] H. Akinaga, "Metal-nanocluster equipped GaAs surfaces designed for high-sensitive magnetic field sensors", *Surf. Sci.* **514** (2002) 145.

[2] I.A. Kowalik, B.J. Kowalski, R. Iwanowski, K. Kopalko, E. Lusakowska, M. Sawicki, J. Sadowski, M. Adell, I. Grzegory, S. Porowski, "MnAs dots grown on GaN(000-1) –(1x1) surface", *Phys. Rev. B* **75** (2007) 235303.

L26

COMPARISON OF THE VALENCE BAND OF THE Mn/GeTe, Mn/GeMnTe AND Mn/GeEuTe LAYERS

M.A. Pietrzyk [1*], B.J. Kowalski [1], B.A. Orlowski [1], W. Knoff [1], T.Story [1], and R.L. Johnson [2]

[1] *Institute of Physics, Polish Academy of Sciences, Al. Lotnikow 32/46, 02-668 Warsaw, Poland*

[2] *Institute of Experimental Physics, University of Hamburg, Luruper Chaussee 149, D-22761 Hamburg, Germany*

Keywords: photoemission spectroscopy, synchrotron radiation, IV-VI semiconductors, Fano resonace

**) e-mail: pietrzyk@ifpan.edu.pl*

Resonant photoemission spectroscopy (RPES) belongs to experimental techniques developed thanks to access to sources of synchrotron radiation. Wide, continuous spectrum of SR enables studying photoemission for photon energies close to a particular intra-system transition. RPES is particularly useful for studying contribution of partly filled shells (*d* or *f*) of transition metals or rare earth elements to the electronic structure of a system. This technique is based on the Fano effect in which rare earth (RE) 4*f* and transition metal (TM) 3*d* electrons are locally and selectively excited when the photon energy is tuned to the RE 4*d*→4*f* and TM 3*p*→3*d* transition. The photoemission intensity in the resonance region is described by the Fano line shape [1], which consists of a resonance maximum and an antiresonance minimum. Comparison of the spectra measured for these two photon energies allows determination of *f*- and *d*-related emission.

The comparison of the experimental results, which have been received in the photoemission study of electronic structure of GeTe doped with Mn and/or Eu, is presented in this work. The IV-VI crystals are known to form solid solutions not only with magnetic ions with uncompletely filled 3*d* shell (*e.g.* Mn, Fe), but also with the elements with uncompletely filled 4*f* shell (*e.g.* Eu, Gd) [2]. Eu-doped IV-VI crystals can be effectively applied for the construction of mid-infrared tunable detectors and lasers. In Eu-doped IV-VI crystals, Eu ions interact ferromagnetically via the RKKY mechanism. The substitutional europium ions occur as Eu^{2+}, however, sometimes Eu^{3+} can also be detected, especially at disordered surfaces. Presence of Eu^{3+} related spectra features indicates a deviation from stechiometry.

$Ge_{1-x}Mn_xTe$ becomes ferromagnetic with a relatively high Curie temperature - 140 K. T_C of $Ge_{1-x}Mn_xTe$ depends strongly on Mn concentration [3]. However the introduction of Eu ions to the system leads to a similar Curie temperature but for markedly lower Mn contents [4]. Therefore, the properties of $Ge_{1-x}Mn_xTe$ and related systems attract considerable interest, due to possible applications of IV-VI-based systems for fabrication of spintronic devices.

However, $Ge_{1-x}Mn_xTe$ and related solid solutions can be obtained as policrystalline bulk sample or monocristalline epilayers. Monocrystalline samples of $Ge_{1-x-y}Mn_xEu_yTe$ are not available yet. In order to carry out a thorough, comparative study of all these systems, a set of GeTe, $Ge_{0.9}Mn_{0.1}Te$ and $Ge_{0.98}Eu_{0.02}Te$ layers was prepared. The samples were grown on BaF_2 (111) substrates by an MBE method with the use of effusion cells as GeTe, Eu, Te_2 and Mn sources. The substrate temperature was 400-450°C. The content of Mn in $Ge_{0.9}Mn_{0.1}Te$ and Eu in $Ge_{0.98}Eu_{0.02}Te$ were checked by energy dispersive X-ray fluorescence analysis. After first photoemission studies of GeTe, $Ge_{0.9}Mn_{0.1}Te$, $Ge_{0.98}Eu_{0.02}Te$, Mn atoms were introduced into the surface layer of the samples by Mn deposition at room temperature and annealing the sample in ultra high vacuum. In particular, the $Ge_{1-x-y}Mn_xEu_yTe$ surface alloy were prepared by this method. Then, the valence bands of the surface alloys were investigated by means of RPES.

The photoemission measurements were performed at the FLIPPER II beamline (E1) in HASYLAB (Germany). The spectra of GeTe, $Ge_{0.9}Mn_{0.1}Te$, $Ge_{0.98}Eu_{0.02}Te$ were measured for the photon energy range of 130 - 160 eV (corresponding to Eu 4*d*→4*f* resonance for both Eu^{2+} and Eu^{3+}) and 30-60 eV (Mn 3*p*→3*d*).

Fig. 1 shows a typical set of energy distribution curves taken at photon energies 50 eV near to the Mn 3p-3d resonance for clean GeTe, $Ge_{0.9}Mn_{0.1}Te$ and $Ge_{1-x}Eu_xTe$ samples, after deposition of manganese and after annealing. In the case of the $Ge_{0.98}Eu_{0.02}Te$ the peak located around 2.0 eV below the Fermi level in the clean sample can be associated with the Eu^{2+} 4*f* final state multiplet contribution to the emission from the valence band. The Mn 3*d* states contribution occurred in the upper part of the valence band, with a maximum at the binding energy of about 4.6 eV. Its shape corresponded to that expected for Mn^{2+} ions surrounded by six Te ions in the octahedral coordination. Deposition of Mn and annealing the system led to an increase of Mn 3*d* feature intensity without any change in its shape. This proved

L26

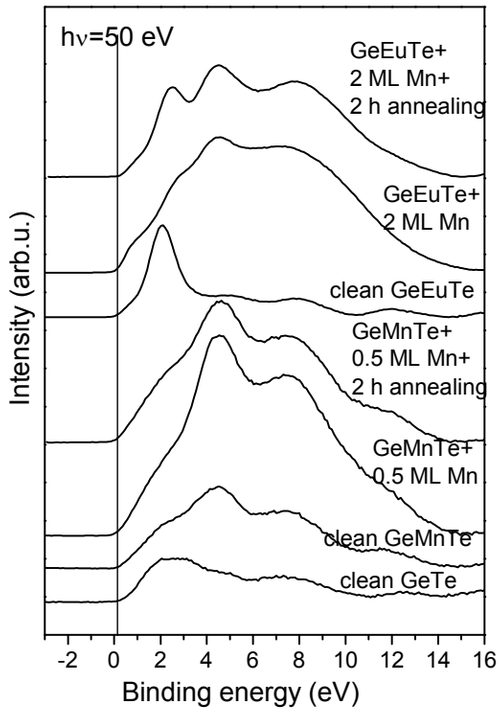

Figure 1. The valence band spectra of GeTe, $Ge_{0.9}Mn_{0.1}Te$ and $Ge_{0.98}Eu_{0.02}Te$ measured for clean samples, after deposition of manganese and after annealing, for photon energies 50 eV.

that diffusing Mn ions occupied the same sites in the lattice as those introduced during the layer growth. Increase of Mn contents in the subsurface layer correlates with increase of the sample magnetization. Its relation with magnetic properties of the system is discussed.

For $Ge_{1-x-y}Mn_xEu_yTe$, the valence band density of states distribution was determined for the first time, to our knowledge. The Mn 3*d* contribution to the electronic structure of the system was revealed and changes in the Eu-related feature corelated with presence of Mn ions were analyzed.

Acknowledgements: The authors acknowledge support by MSHE (Poland) grants N202 101 31/0749 and DESY/68/2007 as well as by the European Community via the Research Infrastructure Action under the FP6 "Structuring the European Research Area" Programme (through the Integrated Infrastructure Initiative "Integrating Activity on Synchrotron and Free Electron Laser Science") at DESY.

References

[1] U. Fano, *Phys. Rev. B* **23** (1961) 1866.

[2] G. Bauer, H. Pascher, W. Zawadzki, *Semicond. Sci. Technol.* **7** (1992) 703.

[3] Y. Fukuma, T. Murakami, H. Asada, T. Koyanagi, *Physica E* **10** (2001) 273.

[4] W. Dobrowolski, M. Arciszewska, B. Brodowska, V. Domukhovski, V.K. Dugaev, A. Grzęda, I. Kuryliszyn-Kudelska, M. Wójcik, E.I. Slynko, *Sci. Sinter.* **38** (2006) 109.

L27

APPLICATION OF A HIGH-RESOLUTION GRAZING EMISSION X-RAY FLUORESCENCE IN MATERIAL SCIENCES

A. Kubala-Kukuś [1], D. Banaś [1], W. Cao [2], J.-Cl. Dousse [2], J. Hoszowska [2], Y. Kayser [2], M. Pajek [1*], J. Szlachetko [1,3], M. Szlachetko [2], M. Salomé [3], and J. Susini [3]

[1] *Institute of Physics, Jan Kochanowski University, Świętokrzyska 15, PL25-406 Kielce, Poland*

[2] *Department of Physics, University of Fribourg, Chemin du Musée 3, CH-1700 Fribourg, Switzerland*

[3] *European Synchrotron Radiation Facility (ESRF), 6 rue Jules Horowitz, BP220, F-38043 Grenoble, France*

Keywords: synchrotron radiation, grazing–emission x-ray fluorescence, high-resolution x-ray spectroscopy, GEXRF

**) e-mail: pajek@pu.kielce.pl*

In recent experiments [1, 2] performed at the ESRF beamline ID21 we have demonstrated that the grazing emission x-ray fluorescence (GEXRF) technique combined with synchrotron radiation excitation and high-resolution x-ray detection offers new attractive possibilities for application of synchrotron radiation to study the distribution of low-level contamination on the surface of materials. The GEXRF technique benefits from the grazing emission observation angle (*i.e.* below the critical angle) of the x-ray fluorescence excited by a narrow and intense x-ray photons beam and from high-resolution (~1 eV) detection by means of a diffraction von Hamos spectrometer [3]. This technique can be effectively used for detailed surface studies of different materials, including ultra-low concentration ($\sim 10^{10}$ atoms/cm^2) contamination and its depth and lateral distribution in the nanometer and micrometer scale, respectively.

In the GEXRF method [4] the excited x-ray fluorescence is observed at a small, grazing emission angle ($\varphi < \varphi_c$) below a critical angle φ_c , being usually below 1°. The grazing emission geometry results in a relative enhancement of the characteristic fluorescence emission from surface impurities with respect to substantially suppressed x-ray fluorescence from the bulk material, which for grazing emission angles are limited to the evanescent x-ray waves [4] propagating along the surface. In this way the x-ray fluorescence from the substrate is limited to the very shallow surface layer of about few nm. Consequently, the GEXRF is a kind of an "inverse" of the total reflection x-ray fluorescence (TXRF) method [5], both techniques having similar detection limits. In the GEXRF measurements, to fulfill the grazing emission condition $\varphi < \varphi_c$, the samples were tilted close to the direction of observation of x-rays, defined by the Bragg angle. For such geometry the photon beam spot on the target is viewed by the x-ray spectrometer as a very narrow line, allowing its slitless operation mode resulting in an increased detection sensitivity.

The GEXRF method is well suited for elemental 2D mapping with a resolution given by the size of the x-ray photon beam, while the depth distribution of the surface contamination can be extracted from the measured dependence of the x-ray fluorescence intensity on the emission angle with respect of the surface. The high-resolution x-ray detection leads to a drastic improvement of the selectivity of elemental analysis and it allows for a substantial reduction of the x-ray "background" from the Raman scattering process. Furthermore, by using a linearly polarized x-ray photon beam and a polarization sensitive diffraction spectrometer the x-ray background from elastic scattering of primary photons can be substantially reduced.

In this paper the following detailed aspects of the high-resolution GEXRF method will be discussed: measurements of the low-level Al impurities on Si wafers, reduction of the resonant Raman scattering "background" below Si K-edge, 2D-mapping of Cr pattern on Si, and Al depth profiling in Si for film-like and ion-implanted samples. Due to ultra-low detection limits, the 2D mapping and depth profiling capabilities, the GEXRF technique is well suited for future applications in nanotechnology.

References

[1] A. Kubala-Kukuś, M. Pajek, D. Banaś, J.-Cl. Dousse, J. Hoszowska, J. Szlachetko, M. Szlachetko, Y. Kayser. W. Cao, M. Salomé, J. Susini, "High resolution grazing emission x-ray fluorescence studies of Al impurities in silicon", presented at the *XXV International Conference on Photonic, Electronic, and Atomic Collisions (ICPEAC)*, 25-31 July 2007, Freiburg, Germany.

[2] J. Szlachetko, J-Cl. Dousse, J. Hoszowska, M. Pajek, R. Barrett, M. Berset, K. Fennane, A. Kubala-Kukuś, M. Szlachetko, "High-resolution study of x-ray resonant Raman scattering at the K edge of silicon", *Phys. Rev. Lett*. **97** (2006) 073001.

[3] J. Hoszowska, J.-Cl. Dousse, J. Kern, Ch. Rhême, "High-resolution von Hamos crystal spectrometer", *Nucl. Instr. Meth. Phys. Res. A* **376** (1996) 129.

[4] H.P. Urbach, P.K. de Bokx, "Calculations of intensities in grazing-emission x-ray fluorescence", *Phys. Rev. B* **53** (1996) 3752.

[5] R. Klockenkämper, *Total Reflection X-ray Fluorescence Analysis* (Wiley, New York 1997).

L28

EXAFS STUDIES OF THE METAL BINDING SITE IN CATALYTIC DNA SENSORS

Bruce Ravel [1], Scott Slimmer [2], Xiangli Meng [2], and Yi Lu [2]

[1] *National Institute of Standards and Technology, 100 Bureau Drive, Stop 1070, Gaithersburg, MD 20899-1070, USA*
[2] *University of Illinois, Urbana-Champaign, USA*

Keywords: EXAFS, DNA sensor, fluorophore, quenchers, catalysis

Catalytic sensors based on in vitro-selected, metal-specific, catalytic DNA have been produced with high selectivity for specific metals and sensitivity rivaling laboratory analytical equipment. These sensors work by binding fluorophores and quenchers to the ends of the catalytic DNA segments. When activated by exposure to the metal, the strand is cleaved and the fluorophore emits a photon. This technology can ultimately be deployed as a field-ready, hand-held device for contaminant identification in real-world aqueous systems. Despite extensive success in producing DNA-based sensors for many metals on the periodic table, very little is known about the interaction of the metal with the cleavage site. In this work, we present results of EXAFS measurements on several metal systems. In the most successful case, EXAFS can identify the bonding position on the nucleotide. In this talk, we demonstrate an approach to the analysis of EXAFS data on a complicated system about which very little is initially known. The analytical techniques discussed are easily generalized and may be applied to a wide variety of EXAFS problems.

L29

RECENT ADVANCES IN X-RAY ABSORPTION SPECTROSCOPY

C. Meneghini * **and S. Mobilio**

Dip. Di Fisica, University of Rome ROMA TRE, via della Vasca Navale 84, I-00146 Rome, Italy

**) e-mail: meneghini@fis.uniroma3.it*

X-ray absorption spectroscopy (XAS) is a well established technique to obtain direct information about local atomic structure and electronic state of the absorbing ions. The elemental specificity and local sensitivity, being largely independent on the aggregation state of the system, make XAS based techniques suited in several research fields ranging from fundamental condensed matter physics, material science, biology, chemistry. Moreover the relative simplicity of the experimental set-up makes XAS particularly suited in studying materials in extreme conditions: high temperature, high pressure, high magnetic fields and ultra-diluted systems. In the recent years enormous progresses have been made in XAS, both in the experimental methods, in theory, in data analysis and interpretation methods.

The absorption spectra are usually distinguished, as a function of the information can be obtained and of the analysis methods, into two main regions: the extended (EXAFS) the near-edge (XANES) regions. At the origin of the ample popularity of EXAFS is the relative simplicity of the theoretical formula, which is well suited for intuitive and accurate experimental data refinement as a function of structural parameters (*i.e.*: coordination numbers, interatomic distances and disorder factors). The high brilliance of 3rd generation synchrotron radiation (SR) sources, coupled with the improved experimental set-up, greatly enhanced the quality of the EXAFS data pushing, for example, the metrical precision down to the *pm* and even *fm* scale. Such a great accuracy on experimental data has permitted to go beyond the simple Gaussian approximation exploiting the cumulant expansion to investigate anharmonic effects in the atomic distribution functions. This approach allowed, for example, to deeply probe the static and dynamic disorder in crystals to shed light on phenomena such as negative thermal expansion in bulk or in nanosized clusters.

From a technical point of view *micro-focus* and *time resolution* are keywords in development of SR facilities. The μ-XAS technique, available on micro focused SR beamlines is providing a unique probe for in-situ chemical analysis probing not only the elemental map in a sample (as X-ray μ-fluorescence) but also the chemical form of the ions; such information being relevant in biology, medicine, environmental science and cultural heritage. Time resolved XAS (TR-XAS) is reaching the *fs* time resolution so probing fast time scale electron transfer processes, transient states and structural dynamics, which are crucial phenomena in chemistry, biology as well in technological devices.

Due to the strong interaction between photoelectrons and atomic potentials, it is not sufficient to restrict the interpretation of the XAS data to single scattering processes; even in the EXAFS region multiple scattering (MS) effects must be taken into account. MS terms probes simultaneously the relative disposition of several ions around the absorber providing topological information through. The sensibility *n*-atoms distribution functions makes the XAS a very special probe in condensed matter complementary, for example, to X-ray and neutron scattering techniques which are intrinsically limited to pair distribution functions. Progresses have been made to quantitatively interpret the *n*-body distributions which are particularly relevant, for example, in amorphous and liquids systems in which the absence of long range order constraints allows structural degree of freedom absent in their crystalline counterparts.

Modelling and interpretation of XANES data is generally complex due to the large amount of structural and electronic information condensed in the near edge region, and to the long computation time usually required for *ab-initio* theoretical calculations. This often limits the XANES analysis to a qualitative or semi-quantitative stage. The recent evolution in XANES analysis improved the theory and developed experimental data refinement techniques. Progress in theoretical calculation include self consistent algorithms and full-potential methods to go beyond the muffin-tin (MT) approximation. Failure of MT approximation, in fact, is specially evident dealing with asymmetric local environment and in the very near edge regions of the spectra, where the low kinetic energy makes the photoelectron sensitive to the details of the electronic structure. The increasing computational velocity on dedicated workstations and/or code parallelization methods have favoured the development of packages addressing the problem of quantitative refinement of XANES data such as the *MXAN* code, for ab-initio data refinement as a function of structural and electronic degree of freedom, or *FitIt* which uses a reduced set of *ab-initio* models and a multidimensional interpolation algorithm to reduce the computation time.

Light elements like oxygen, carbon, nitrogen play an essential role in life, chemistry and material science. However, the application of XAS dealing with light absorbers is strongly limited by experimental constraints imposed by the low energies of the K edges involved. X-ray Raman scattering (XRS) offers a valid method to overcome these constraints. The high brilliance available on last generation SR facilities is making XRS set-up routinely available.

L30

FEMTOSECOND AND PICOSECOND X-RAY SPECTROSCOPY STUDIES

C. Bressler [1,2*], R. Abela [2], and M. Chergui [1]

[1] *Laboratoire de Spectroscopie Ultrarapide (LSU), Ecole Polytechnique Fédérale de Lausanne (EPFL), BSP, CH-1015 Lausanne, Switzerland*

[2] *Swiss Light Source, Paul Scherrer Institut, CH-5232 Villigen-PSI, Switzerland*

Keywords: ultrafast x-ray absorption spectroscopy, chemical dynamics, spin crossover

**) e-mail: christian.bressler@epfl.ch*

Time-resolved x-ray absorption fine structure (XAFS) spectroscopy with picosecond temporal resolution is a new method to observe electronic and geometric local structures of short-lived reaction intermediates [1]. While it adds to the information available by established ultrafast laser spectroscopies, the combination of both methodologies to the system under investigation can deliver a rather complete picture of the underlying mechanisms. We have implemented ultrafast XAFS at a synchrotron and successfully applied it to different condensed phase chemical systems.

The basic experimental setups used at the Advanced Light Source and at the Swiss Light Source (SLS) have been described previously [2-5], and will be only summarized here for the SLS setup. Briefly, x-rays from a Si(111) monochromator enter the experimental hutch, where they are focused to ca. 50 μm diameter onto the sample with a pair of Kirkpatrick Baez (KB) mirrors (Fig. 1). X-ray signals are detected with 4 large-area avalanche photodiodes (APD), one each for transmission (I_1) and for the incident signal scattered off a thin metal (Cr) foil (I_0), and via two fluorescence APDs (I_{F1}, I_{F2}) for the x-ray fluorescence emitted from the sample. The sample consists of a free-flowing liquid jet (with an adjustable thickness in the 0.1-0.5 mm range), which is excited by an amplified fs laser system. Spatial overlap (including a measurement of the spot sizes) on the sample between both laser and x-ray beams is set via steering the laser beam onto the x-ray spot on sample and monitored with an imaging CCD camera. The amplified laser used for sample excitation is synchronized to one specific x-ray pulse from the storage ring [4,5] at 1 kHz repetition rate. For femtosecond XAFS experiments we exploit so called time-sliced x-radiation, which delivers ca. 160 fs x-ray pulses at 2 kHz into the beamline [6].

Electronic structure modifications can be observed in charge transfer processes via XANES. Fig. 2 shows the example for aqueous $Ru(bpy)_3$, in which a laser photon promotes a metal-centered electron from the crystal field split and fully occupied $4d(t_{2g})$ level onto the bpy ligand system in a metal-to-ligand charge transfer (MLCT) process. For the x-ray probe process this opens up a new absorption channel, $2p_{3/2,1/2}$ (L_3, L_2 edges, respectively) → $4d(t_{2g})$ (labeled *A'* in Fig. 2b), right below the $2p_{3/2,1/2}$ → $4d(e_g)$ absorption (labeled *B*, *B'* for the ground and excited state absorptions, respectively).

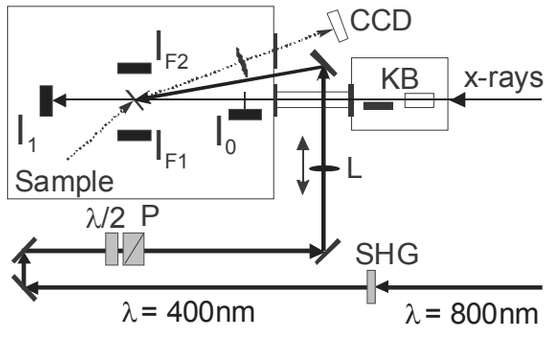

Figure 1. Top view of the experiment with overlapping laser pump and x-ray probe beams on the liquid sample sheet. 4 detectors (I_0, I_1, I_{F1}, I_{F2}) are used for measuring the XAFS, and an imaging CCD detector monitors spatial overlap and beam sizes. 400 nm light (after frequency-doubling (SHG) the 800 nm fundamental beam) is adjusted for pulse energy with a $\lambda/2$ waveplate and polarizer (P) combination before being focused (with the lens L) onto the sample with spot sizes typically around 100-500 μm. The x-ray beam is focused to ca. 50 μm diameter with the KB optics.

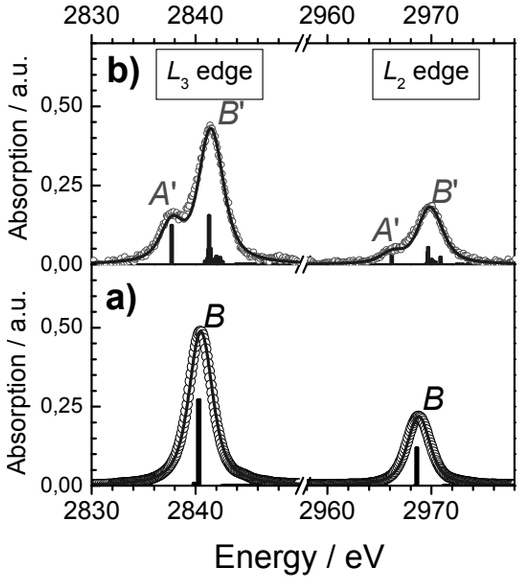

Figure 2. a) $L_{2,3}$ edge XAFS of aqueous $[Ru^{II}(bpy)_3]^{2+}$ in its ground state (open circles) together with a simulation (vertical bars) for the bound-bound transitions, which were convoluted with the lifetime width of Ru (blue curve). b) same as in a), but 50 ps after laser excitation.

From this study we also obtained the crystal-field splitting of the 4*d* levels in the excited state for the first time, and exploited this value to derive the geometric structure (here: the Ru-N distance), which is slightly shorter than in the ground state species [7].

Time-resolved XANES can also serve to observe (optically) dark species. We have probed the population of nascent I^0 species, by X-ray absorption spectroscopy at the L_1 and L_3 edges, 50 ps, and later, after electron detachment from I^- by the pump laser [8]. At the L_1 edge (Fig. 3a) one observes a small blue shift of the first transient peak around 5186 eV shown in Fig. 3b with increasing delay time. Since we know that iodine radicals react towards more complex products on a diffusion-governed time scale, we have to take these processes into account, and the following reactions also occur on the pico- to nanosecond time scales following photoionization:

$$I^- + h\nu \rightarrow I^0 + e^- \quad (1)$$

$$I^0 + I^- \rightarrow I_2^- \quad (2)$$

$$I_2^- + I_2^- \rightarrow I_3^- + I^- \quad (3)$$

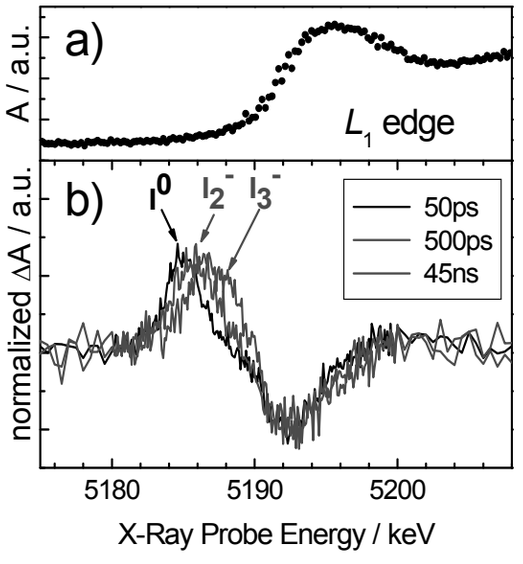

Figure 3 a) Static x-ray absorption spectrum of aqueous iodide. b) Transient absorption spectra of photoexcited iodide after 50 ps (black), 500 ps (red), and 45 ns (green), showing nascent atomic radicals, and subsequent bimolecular products.

As a last example we have observed the ultrafast magnetization process in photoexcited aqueous $Fe(bpy)_3$ (Fig. 4) exploiting time-sliced x-radiation at the microXAS beamline of the Swiss Light Source [6]. $[Fe^{II}(bpy)_3]^{2+}$ represents the simplest molecule of iron-based light-induced spin-cross over complexes, itself being a typical example of a low spin (LS) compound, which can undergo a spin change to a high spin (HS) quintet state upon irradiation [9]. The optical absorption spectrum of aqueous $[Fe^{II}(bpy)_3]^{2+}$ is characterized by an intense broad band centred at 520 nm due to the singlet Metal-to-Ligand-Charge-Transfer (^{1}MLCT) state. Photoexcitation into this band (or to higher energies) is followed by a cascade of intersystem crossing (ISC) steps through singlet, triplet and quintet MLCT and ligand-field (LF) states, which brings the system to the lowest-lying (HS) quintet state, $^5T_2$, with almost unit quantum yield in ca. 1-2 ps [10]. This state relaxes non-radiatively to the LS ground state within 0.6 ns in aqueous solutions at room temperature. Using picosecond XAS, we recently determined that in the HS state, an elongation of ca. 0.2 Å of the Fe-N bond distances occurs [11].

However, the pathway and time scale of the cascade from the intitially excited ^{1}MLCT to the $^5T_2$ state are still not known, as ultrafast optical spectroscopy can neither resolve the intermediate steps nor determine their structures. In order to address these issues and to probe the relaxation processes, we have implemented femtosecond XANES spectroscopy.

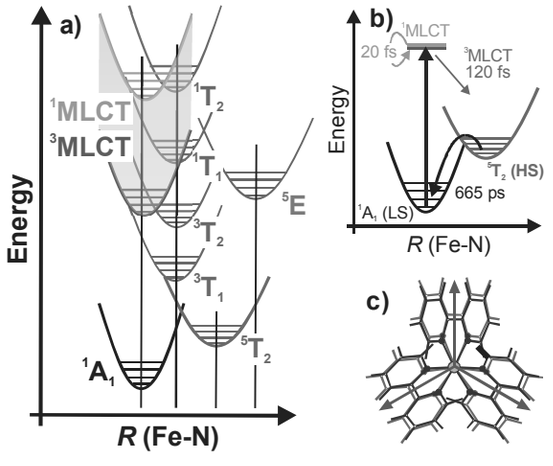

Figure 4 Generic potential energy curves of Fe(II)-SCO complexes as a function of the Fe-N bond distance (a)- The manifold of metal-to-ligand-charge-transfer (MLCT) states is shown by a shaded area. The metal-centred (MC) states are represented by their symmetry character (T and E) in the D_3 group of $[Fe(bpy)_3]^{2+}$. The LS $^1A_1$ ground state has a completely filled t_{2g}^6 subshell, while the antibonding e_g level is empty. For each electron that is promoted from the t_{2g} subshell to the e_g orbital the metal-ligand bond length increases. For the $[Fe(bpy)_3]^{2+}$ complex in its low-spin $^1A_1(t_{2g}^6)$ ground state, the bond length is 1.97 Å (Fe-N), in its high-spin $^5T_2$ ($t_{2g}^4 e_g^2$) the bond length increases by ca 0.2 Å (c), as measured in picosecond XAS experiments. The arrows (b) show the relaxation cascade as determined by ultrafast laser spectroscopy.

Hereby the strongest absorption change at a multiple scattering edge feature near 7126 eV (not shown here) reflects the altered Fe-N bond distance (and thus the molecular structure), which increases by 0.2 Å in the HS state [11]. We therefore used this feature to investigate

the temporal evolution of the relaxation process from the ^{1}MLCT to the $^5T_2$ by scanning the laser-x-ray time delay, which also confirms that this process terminates below 300 fs (Fig. 5). In order to quantify the time required for this spin crossover process, we have calculated the rate equations for this process. Hereby the following reaction cycle using the input from our optical studies [10] (Fig. 4b) was applied (using the indicated lifetimes and an overall cross correlation time of 250 fs [6]):

$$^1\text{GS} + h\nu\ (400\ \text{nm}) \rightarrow {}^1\text{MLCT}\ (20\ \text{fs}) \rightarrow {}^3\text{MLCT}\ (120\ \text{fs}) \rightarrow {}^5\text{T}\ (665\ \text{ps}) \rightarrow {}^1\text{GS} \quad (4)$$

With this we calculated the population dynamics of all intermediate states given above, and determined the final HS signal, which is shown in Fig. 5 together with the data. In addition, we fit the final arrival time to the ^{5}T state (previously fixed to the ^{3}MLCT departure time of 120 fs) yielding 130 (60) fs. This result implies that the electron back transfer from the ligand system simultaneously triggers the excitation of a second electron from the bonding t_{2g} orbital, so that both electron spins are parallel in the antibonding e_g orbital, together with two unpaired electrons ramaing from the bonding t_{2g} orbitals (thus changing the spin by $\Delta S = 2$). Any possible intermediate steps (in the metal-centered states) are considerably faster than 60 fs according to this fit procedure.

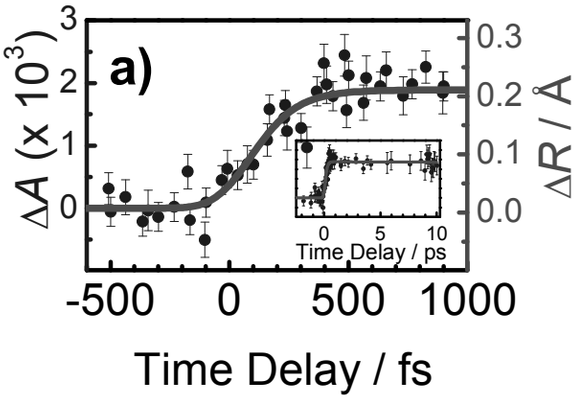

Figure 5. Transient x-ray absorption signal of photoescited aqueous $Fe(bpy)_3$, measured near the Fe K edge, together with a simulation to its ultrafast magnetization from the reactant low spin to the high spin states. The right axis shows the Fe-N bond elongation during this process, which is roughly proportional to the absorption change (and amounts to 0.2 Å in the HS state). The inset shows an expanded time scale out to 10 ps.

Acknowledgements: This work was funded by the Swiss National Science Foundation (FNRS), via contracts 200020 – 116023, PP002 – 110464, 200021 – 107956, 620-066145, and 200021-105239.

References

[1] C. Bressler, R. Abela, M. Chergui, "Exploiting EXAFS for time-resolved molecular structures in liquids", *Z. Kristallogr.* ***223*** (2008) 307-321.

[2] M. Saes, R. Abela, D. Grolimund, S.L. Johnson, P.A. Heimann, C. Bressler, M. Chergui, "Ultrafast time-resolved x-ray absorption spectroscopy of chemical systems", *Synchr. Rad. News* **16** (2003) 12-20.

[3] M. Saes, F. van Mourik, W. Gawelda, M. Kaiser, M. Chergui, C. Bressler, D. Grolimund, R. Abela, T.E. Glover, P.A. Heimann, R.W. Schoenlein, S.L. Johnson, A.M. Lindenberg, R.W. Falcone, "A setup for ultrafast time-resolved x-ray absorption spectroscopy", *Rev. Sci. Instrum.* **A75** (2004) 24-30.

[4] W. Gawelda, C. Bressler, M. Saes, M. Kaiser, A. N. Tarnovsky, D. Grolimund, S. L. Johnson, R. Abela, M. Chergui, "Picosecond Time-resolved x-ray absorption spectroscopy of solvated organometallic complexes", *physica scripta* T**115** (2005) 102-106.

[5] W. Gawelda, V.-T. Pham, A. El Nahhas, M. Kaiser, Y. Zaushitsyn, S.L. Johnson, D. Grolimund, R. Abela, A. Hauser, C. Bressler, M. Chergui, "Capturing transient electronic and molecular structures in liquids by picosecond x-ray absorption spectroscopy", *AIP Conf. Proc.* **882** (2007) 31-36.

[6] G. Ingold, R. Abela, P. Beaud, S. L. Johnson, U. Staub, "Towards pump-probe resonant x-ray diffraction at femtosecond undulator sources", *Z. Kristallogr.* **223** (2008) 292-306

[7] W. Gawelda, M. Johnson, F. M. F. deGroot, R. Abela, C. Bressler, M. Chergui, "Electronic and molecular structure of photoexcited $[Ru^{II}(bpy)_3]^{2+}$ probed by picosecond x-ray absorption spectroscopy", *J. Am. Chem. Soc.* **128** (2006) 5001-5009.

[8] V.-T. Pham, W, Gawelda, Y. Zaushitsyn, M. Kaiser, D. Grolimund, S. L. Johnson, R. Abela, C. Bressler, M. Chergui, "Observation of the solvent shell reorganization around photoexcited atomic solutes by picosecond x-ray absorption spectroscopy", J. *Am. Chem. Soc.* **129** (2007) 1530-1531.

[9] A. Hauser, C. Enachescu, M.L. Daku, A. Vargas, N. Amstutz, "Low-temperature lifetimes of metastable high-spin states in spin-crossover compounds: The rule and exceptions to the rule", *Coord. Chem. Rev.* **250** (2006) 1642-1652.

[10] W. Gawelda, A. Cannizzo, V.-T. Pham, F. Van Mourik, C. Bressler, M. Chergui, "Ultrafast nonadiabatic dynamics of [FeII(bpy)3]2+ in solution". *J. Am. Chem. Soc.* **129** (2007) 8199-8206.

[11] W. Gawelda, V.-T. Pham, M. Benfatto, Y. Zaushitsyn, M. Kaiser, D. Grolimund, S.L. Johnson, R. Abela, A. Hauser, C. Bressler, M. Chergui, "Structural determination of a short-lived excited iron(II) complex by picosecond x-ray absorption spectroscopy", *Phys. Rev. Lett.* **98** (2007) 057401.

L31

X-PEEM NANOSPECTROSCOPY APPLIED TO NANOMAGNETISM

R. Belkhou

Synchrotron SOLEIL, L'Orme des Merisiers Saint-Aubin, 91192 Gif-sur-Yvette, France

e-mail: Belkhou@synchrotron-soleil.fr

The recent progress in the fabrication of nanostructures requires the development in parallel of new techniques to characterize these materials at the nanoscopic level. This is particularly the case for magnetic and semiconducting technologies, where the interest for submicrometric range devices has been rapidly increasing during the last decade. Moreover, many of these new materials are used for dynamic applications (magnetic recording heads, memories, sensor *etc*…). A technique which could study them combining good spatial (few nm) and time (submicrosecond) resolution would be of primordial importance.

The high brightness of third generation synchrotron radiation sources has opened the way to surface and interface imaging with resolution in the 10 nm ranges with further instrument improvements in the 1 nm range [1]. Experimentally there are two different approaches. The first uses a well focused photon beam which is scanned across the sample's surface. The second employs parallel imaging techniques making use of special electron optics (X-PEEM), and will be the main subject of this lecture.

X-PEEM (X-ray PhotoEmission Electron Microscopy) spectromicroscopy is a derivative of the classical PEEM. If a photon energy just above the photothreshold is used, the photoelectron yield is mainly determined by the differences in the work function ϕ of the sample. The local variations of ϕ result in images with high contrast. This UV-PEEM mode of operation is ideally suited to study surface chemical reactions in real time [2]. With the advent of high brilliance synchrotron radiation from storage rings, a wide and tunable energy range of photons of the illuminating beam has become available, allowing to access well established techniques like Ultraviolet Photoemission Spectroscopy (UPS), X-ray Photoemission Spectroscopy (XPS) and X-ray absorption spectroscopy (XAS) at the nanoscopic level, and thus leading to element selective imaging. Moreover, information on the spatial distribution of the electronic structure, chemical composition and nature, or the local magnetization at the surface can be obtained. Dedicated beamlines with high brilliance, variable photon polarization (both circular and linear) and a broad energy range have become recently available at several facilities (ELETTRA, ESRF, ALS, BESSY II…). This opens a wide research area for the X-PEEM [3] including surface magnetism, surface and interfaces, surface chemistry, tribology *etc.*

In particular, the interest in magnetic domain imaging in the nanometer range has been rapidly increasing during the last decade. A considerable impetus is coming from the development of high-density magnetic storage devices and from the forthcoming achievement of spin electronics. In order to tailor the magnetic behavior of these systems to specific needs, for instance a certain response to magnetization reversal, a detailed understanding of the structure and of the dynamics of magnetic domains is mandatory. In addition, the thin film nature of such devices emphasizes the surface aspect of magnetism. This situation requires magnetic domain-imaging techniques which combine surface sensitivity and high spatial resolution. Moreover, for many applications element specificity is even more important than high lateral resolution. Magnetic storage media or building elements of spintronics devices are often composed of several chemical elements or intermetallic compounds, each of which distinctly contributes to the magnetic behaviour [4] (Fig. 1). All these requirements pose a considerable challenge to conventional magnetic domain imaging techniques such as magneto-optical Kerr microscopy, Lorentz microscopy, scanning electron microscopy (SEMPA) *etc.*.

X-PEEM magnetic microscopy is today a good candidate for an ideal surface magnetic imaging technique, as it combines the magnetic sensitivity and element selectivity with a spatial resolution below the size of the magnetic domains. One may identify three important length scales for magnetic imaging which consecutively decrease by a factor of 100. The first one is about 1 μm, set by the size of lithographically manufactured magnetic cells such as in spin valve heads or magnetic memory cells. The second one is about 10 nm, corresponding to the crystallographic grain size of typical magnetic materials. The last one is 0.1 nm, i.e. the atomic size. A spatial resolution of 22 nm using synchrotron radiation has already been achieved [5] and further improvements of this resolution may allow access to the second characteristic length scale of 10 nm.

The elemental specificity in X-PEEM magnetic microscopy arises from the characteristic binding energies of the atomic core electrons. Both X-ray absorption (XAS) and X-ray photoelectron spectroscopy (XPS) can be used. The X-ray absorption spectrum directly exhibits the characteristic absorption edges of the elements in the sample. At the absorption thresholds of the elements the spectrum shows strong resonances arising from transitions to unfilled valence band states.

L31

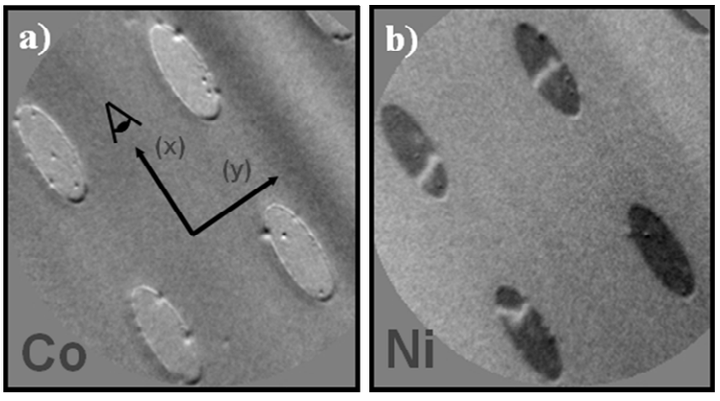

Figure 1. X-PEEM images of 4 magnetic tunnel junction ellipses ($Co/Al_2O_3/FeNi$) recorded at the Co edge (a) and at the Ni edge (b). The photons incidence direction is aligned with the ellipses long axis from the top left corner. The white and black contrasts correspond to magnetizations aligned along the long ellipses axis, parallel or antiparallel to the saturating field [4].

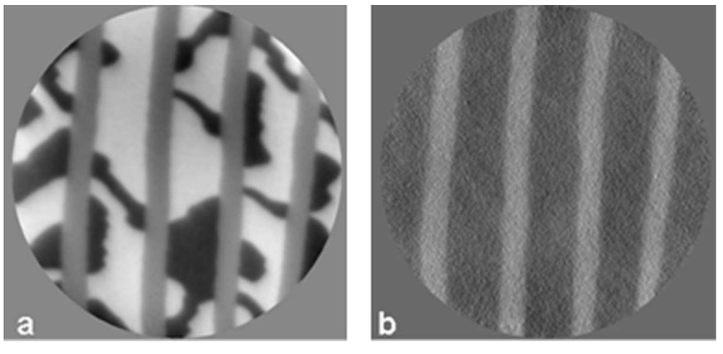

Figure 2: a) XMCD-PEEM image, and (b) XMLD-PEEM image of a 300 nm thick MnAs film on GaAs (100) at room temperature. (a) shows the magnetic domain structure in the ferromagnetic phase: alpha phase (b) the coexisting antiferromagnetic phase: beta phase. The XMCD image is obtained using right/left circular polarised light at the L_3 Mn edge. The XMLD is obtained using the linear dichroism asymmetry associated with the multiplets structure of the Mn L_3 edge. Field of view 5 μm [6].

The use of polarized synchrotron radiation enables studies of the electronic and magnetic anisotropies [7], and thus allows magnetic contrast for the X-PEEM [8]. A simple description of the photon polarization by a biaxial vector for linear polarization and a vector for handed circular polarization is the physical basis for probing various anisotropies of the sample. In general, linearly polarized light can only detect anisotropy of electronic charge. In contrast, handed circularly polarized light can measure a dipolar or vector quantity, in our case the size and direction of the electron angular moment and spin.

For magnetic spectromicroscopy, X-ray magnetic circular dichroism (XMCD) in the total photoyield mode is exploited. Using XMCD we can determine the size, the direction and the anisotropy of the atomic magnetic moments (see Fig. 2a) .The black and white regions in the image reflect the domains where the magnetic axis is aligned parallel or anti parallel to the direction of the light at fixed polarization. The grey area corresponds to domains where the magnetic axis is perpendicular to the direction of the light. To distinguish the orientation of the domains in this grey region we have simply to turn the sample in a way to align the magnetic axis parallel and antiparallel to the light.

The study of antiferromagnetic (AFM) surfaces and interfaces has posed an even larger challenge because conventional techniques are mainly bulk sensitive. This limitation was overcome recently by the use of XMLD spectroscopy. In contrast to XMCD which directly measures the magnetic moment, XMLD measures the expectation value of the square of the magnetic moment. XMLD can therefore be applied for all uniaxial magnetic system, *i.e.* antiferromagnets as well (Fig. 2.b). Recently it was shown that XMLD spectroscopy in conjunction

with X-PEEM microscopy is capable of imaging the detailed antiferromagnetic domain structure of a surface and interface [9].

A new feature that is actually under extensive development is to add temporal resolution to magnetic spectromicroscopy. The dynamics of the magnetization reversal in thin magnetic films has become a matter of high interest for the future of magnetic recording and non-volatile magnetic memories. Parallel to the evolution toward smaller magnetic bits and memory cells, writing and reading times approaching the ns range will be required in a few years from now. A complete understanding of the magnetization dynamics in these structures requires the ability to probe the magnetization of the individual layers as well as their mutual interaction. It has been recently shown, using time-resolved XMCD, that the coupling between the magnetic layers can be very different in static and dynamical measurements [10]. This is probably due to different reversal processes which play a role in the magnetization reversal at low (mainly domain wall propagation) and high (mainly nucleation of reversed domains) field sweep rates, but time-resolved X-PEEM measurements would be decisive in confirming this hypothesis. Time-resolved X-PEEM measurements are very challenging, since the secondary electrons that are used for the image are strongly perturbed by the magnetic field necessary to switch the magnetization direction. For the time resolved XMCD measurements, dedicated copper microcoils have been developed, capable of providing a relatively strong magnetic field (up to 5000 Oe) during a short time period (20-50 ns). These magnetic pulses can be synchronized with the X-ray pulses coming from the storage ring to perform dynamic measurements in a pump-probe scheme. X-PEEM images cannot be acquired during the field pulses, but the relatively slow dynamics (some ns) occurring after the pulse could be measured.

In this lecture, we will present a review of recent results obtained using X-PEEM microscopy, focusing mainly on the magnetic imaging part. After a short overview of the X-PEEM principles and capabilities, the basic magnetic contrast used in X-PEEM will be reviewed. Finally a selection of recent scientific case will be developed in the field of magnetic imaging of surfaces and nanostructures.

References

[1] For a detailed review see *J. Electron Spectrosc. Related Phenom.* **84** (1997).

[2] M. Mundschau *et al.*, *Surface Sci.* **227** (1990) 246.

[3] Several beamlines are presently operating or under development: PEEM3 (ALS), SMART (BESSY II), Nanospectroscopy beamline (ELETTRA), Surface/interface microscopy beamline (SLS), Soft X-ray microscopy beamline (SOLEIL).

[4] M. Hehn, D. Lacour, F. Montaigne, J. Briones, R. Belkhou, S.El Moussaoui, F. Maccherozzi, N. Rougemaille. *Appl. Phys. Lett.* **92** (2008) 072501.

[5] Th. Schmidt, *et al*., *Surf. Rev. Lett.* **5** (1998) 1287.

[6] E. Bauer, R. Belkhou, S. Cherifi, A. Locatelli, A. Pavlovska, N. Rougemaille, *J. Vac. Sci. Technol. B* **25** (2007) 1470.

[7] J. B. Kortright e*t al*., *J. Magn. Magn. Mat.* **207** (1999) 7.

[8] J. Stöhr *et al*., *Science* **259** (1993) 658.

[9] J. Stöhr *et al*., *Phys. Rev. Lett.* **83** (1999) 1862, H. Ohldag et al, *Phys. Rev. Lett.* **86** (2001) 2878.

[10] M. Bonfim *et al*., *Phys. Rev. Lett.* **86** (2001) 3646.

L32

SOFT X-RAY ABSORPTION SPECTROSCOPY AND MAGNETIC CIRCULAR AND LINEAR DICHROISM IN THIN FILMS

M.W. Haverkort [1]

[1] *Max Planck Institute for Solid State Research, Heisenbergstraße 1, D-70569 Stuttgart, Germany*

Keywords: Soft X-ray absorption, circular dichroism, linear dichroism, spin state, thin film

**) e-mail: M.W.Haverkort@fkf.mpg.de*

X-ray absorption spectroscopy (XAS) is a spectroscopic technique whereby one excites a core electron into the valence bands. Depending on the edge the core-hole valence interaction can be very strong and for the transition metal $L_{2,3}$ edge and the rare-earth $M_{4,5}$ edges the spectra is strongly excitonic. The spectroscopy of these edges has developed into maturity in the last 25 years and the pioneering work of Fink, Thole, Sawatzky and Fugle, who used electron energy loss spectroscopy on narrow band and impurity systems has been very important for the development of soft x-ray absorption spectroscopy. They recognized, that the observed multiplet structures can provide an extremely detailed information about the local electronic structure of the ground and lower excited states of the system [1-3].

In this talk I will start by reviewing some of the aspects of XAS and show by examples from the literature how it can be used to probe the element specific magnetic spin and orbital moments, spin directions in anti-ferromagnets, valence, spin-states, orbital occupations and crystal fields. In the second half of the talk I will concentrate on work done in the group of L.H. Tjeng (Cologne) and discus the measurements of magnetic properties of thin films. With the use of linear dichroism, Csiszar *et al.* [4] have shown how one can, by applying different strain to the CoO thin film, tune the spin direction of the Co ion. They furthermore showed [5] how one can transfer the preferred spin direction from a film with high magneto anisotropy (CoO in this case) to a film with low magneto anisotropy (MnO). These are important findings for the field of exchange bias where one tries to pin the spin direction of a ferromagnet by an adjoined anti-ferromagnet.

References

[1] B.T. Thole, R.D. Cowan, G.A. Sawatzky, J. Fink, J.C. Fuggle, *Phys. Rev. B* **31** (1985) 6856.

[2] J. Finkt, T. Mueller-Heizerling, B. Scheerer, W. Speiier, F.U. Hillebrecht, J.C. Fuggle, J. Zaanen, G.A. Sawatzky, *Phys. Rev. B* **32**, 4899.

[3] J. Fink, *Advances in Electrons and Electron Physics* **75** (1989) 121.

[4] S.I. Csiszar, M.W. Haverkort, Z.Hu, A. Tanaka, H.H. Hsieh, H.-J. Lin, C.T. Chen, T. Hibma, L.H. Tjeng, *Phys. Rev. Lett.* **95** (2005) 186401.

[5] S.I. Csiszar, M.W. Haverkort, T. Burnus, Z. Hu, A. Tanaka, H.-H. Hsieh, H.-J. Lin, C.-T. Chen, T. Hibma, L.H. Tjeng, submitted to *Phys. Rev. B.*

L33

PROPOSED TECHNICAL CONCEPTS AND TIME SCENARIO FOR POLISH SYNCHROTRON LIGHT SOURCE

Edward A. Görlich [1,2]

[1] *M. Smoluchowski Institute of Physics, Jagiellonian University, ul. Reymonta 4, PL 30-059 Krakow, Poland*
[2] *Centrum Promieniowania Synchrotronowego Sp. z o.o., ul. Reymonta 4, PL 30-059 Krakow, Poland*

Keywords: synchrotron light source, booster synchrotron, storage ring lattice, beamline

e-mail: ufgoerli@cyf-kr.edu.pl

The exceptional properties of the electromagnetic radiation obtained at the synchrotron light sources have proved indispensable for application of advanced modern experimental techniques in numerous fields of research. The notion is best supported by the fact of an enormous increase in 'investigation power' of synchrotron radiation facilities worldwide in the last ten years due both to emerging new centres and to modernisation of existing ones. It refers not only to traditional economic strongholds (like USA, Japan, Western Europe) but also to rapidly developing countries like Brazil, China or India. The simple observation leads to a conclusion that Poland and, in general, East Central Europe deserves such a facility. The very concept was put forward a decade ago but the important step occurred at the turn of 2006 when the project of the synchrotron light source in Poland was included in a national list of the high-priority research infrastructure, opening a possible access to the European structural funds. The act was a positive reaction to the document presented at the Ministry of Science and Higher Education in June 2006 by 45 Polish scientists from 22 leading research institutions.

In April 2008 thirty-three leading universities and research institutes of Poland formed the Consortium 'Polish Synchrotron' ('Polski Synchrotron') to actively support the idea and to collaborate at the realisation of the project.

About a year ago there appeared a new circumstance connected with an initiative of the Czech Republic to build a synchrotron facility, being basically a copy of the Spanish design in Barcelona (to be commissioned in 2009), at Brno. The situation led to the involvement of European Commission institutions and subsequently to a requirement of the complementarity of the two facilities, in Kraków and in Brno.

In the present talk, in view of this new situation, the proposed solutions for the lattice design of a storage ring of the Polish synchrotron light source will be given. Assumed basic characteristics defining the scale of the facility remain unaltered with respect to the preliminary concept presented at the national conference in October last year at Poznań (7KSUPS): electron energy 2.5 – 3.0 GeV, circumference ca. 260~m, low-emittance, top-up mode of operation. The preferred solution will be indicated and supported by arguments.

The advanced research techniques for various disciplines will become available thanks to the specialized beamlines. The satellite meeting "IInd National Conference on Experimental Lines at the Polish Synchrotron" ("II^{-ga} Krajowa Konferencja: Polski Synchrotron – Linie Eksperymentalne") [1] immediately following the present Conference (and in the same location) will be concerned in more detail with individual line proposals [1] both of those seven included in a first phase of the general project as well as the 'independent' experimental line proposals.

The organisational matters related to institutional and financial bases of the project will be commented.

Finally, the updated schedule will give the main courses of action and their time frames.

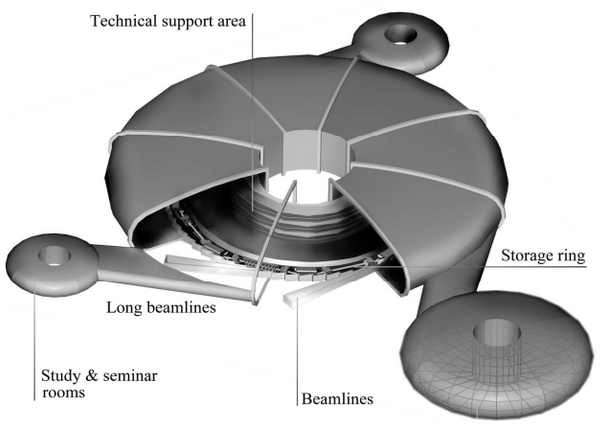

Figure 1. The architectural concept (by Studio AW) for the Polish synchrotron light source.

References

[1] http://synchrotron.pl

L34

X-MCD IN THE Cr-Re AND Fe-Re BASED DOUBLE PEROVSKITE AT HIGH PULSED MAGNETIC FIELDS

J.M. Michalik [1,2], M. Sikora [3], Cz. Kapusta [1,*], J.M. De Teresa [2], and O. Mathon [3]

[1] *Department of Solid State Physics, AGH University of Science and Technology, 30-059 Krakow, Poland*
[2] *Instituto de Ciencia de Materiales de Aragón, Universidad de Zaragoza-CSIC, 50009 Zaragoza, Spain*
[3] *European Synchrotron Radiation Facility, BP 220, 38043 Grenoble Cedex, France*

Keywords: dichroism, high magnetic field, double perovskite, orbital moment

**) e-mail: kapusta@uci.agh.edu.pl*

Oxide half metals, *i.e.* materials with only one spin direction present in the Fermi level either parallel or antiparallel to the magnetization direction are being actively studied due to their potential applications in Spin Electronics. Among them, ferromagnetic double perovskites (DP's) have attracted a lot of interest due to their high Curie temperature (T_C) and predicted half-metallicity [1, 2]. Re-based compounds are the most promising among the (DP's) family, exhibiting T_C as high as 610 K in the case of Sr_2CrReO_6.

Recently we have performed several experiments using high pulsed and static magnetic fields measuring the bulk magnetization of the Re-based double perovskites [3-5]. Magnetism of these materials was primarily explained on the basis on a spin-only model by the double-exchange-like interaction between Fe (or Cr) and Re ions via the unoccupied oxygen 2*p* orbital. However, a large Re orbital moment of the order of one third of the Re spin moment was revealed by the X-ray Magnetic Circular Dichroism (XMCD) in the A_2FeReO_6 series (A=Sr, Ca and Ba) [6]. Its presence is due to a strong spin-orbit coupling in the Re ion being 5*d* element. It was confirmed that the Re orbital moment contributes significantly to the saturation magnetization of the Re based double perovskites, which makes the spin-only ionic model insufficient for a proper description of the magnetic and transport properties of this kind of compounds [3-5].

We present the results of the first, to our knowledge, XMCD study under high magnetic field (up to 26T) generated using pulsed technique. The measurements were performed on CrRe and FeRe based samples using recently improved set-up installed at dispersive XAFS beamline, ID24, at ESRF [7]. The derived orbital contribution to the magnetic moment proves the higher than spin-only-value of the saturation magnetization to be consistent with the models including spin-orbit coupling in the heavy Rhenium ion (see Fig. 1). In our study we compare the results obtained under low and high magnetic field for the FeRe based compounds being an interesting approach having in mind that only large applied magnetic field allows the magnetic saturation of the material. The data collected also allows the comparison of the orbital moment contribution in Cr and Fe based materials each having different electronic band structure.

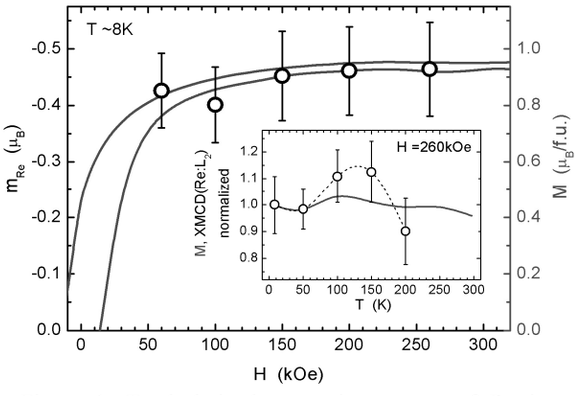

Figure 1. Total derived magnetic moment of Re ion obtained from Sum Rules analysis (left axis, open circles) and the bulk magnetization (right axis, green line) of Sr_2CrReO_6 compound. In the inset the temperature dependence of the normalized L_2 XMCD and bulk magnetization (average value), both measured at 26T.

Acknowledgements: We acknowledge the Spanish Ministry of Science, the Aragon Regional Government and Polish Ministry of Science and Higher Education for the financial support, the European Synchrotron Radiation Facility for provision of beamtime through the peer reviewed project MI739 and inhouse research time as well as Dr. J. Blasco and R. Córdoba for the sample synthesis.

References

[1] K.-I. Kobayashi, T. Kimura, H. Sawada, K. Terakura, Y. Tokura, *Nature* **395** (1998) 677.
[2] D. Serrate, J.M. De Teresa, M.R. Ibarra, *J. Phys.: Condens. Matter* **19** (2007) 023201.
[3] J.M. Michalik, J.M. De Teresa, C. Ritter, J. Blasco, D. Serrate, M.R. Ibarra, C. Kapusta, J. Freudenberger, N. Kozlova, *Europhys. Lett.* **78** (2007) 17006.
[4] J.M. De Teresa, J.M. Michalik, J. Blasco, P.A. Algarabel, M.R. Ibarra, C. Kapusta, U. Zeitler, *Appl. Phys. Lett.* **90** (2007) 252514.
[5] J.M. Michalik, J.M. De Teresa, J. Blasco, P.A. Algarabel, M.R. Ibarra, Cz. Kapusta, U. Zeitler, *J. Phys.: Condens. Matter* **19** (2007) 506206.
[6] M. Sikora, Cz. Kapusta, M. Borowiec, C.J. Oates, V. Prochazka, D. Rybicki, D. Zajac, J.M. De Teresa, C. Marquina, M.R. Ibarra, *Appl. Phys. Lett.* **89** (2006) 062509.
[7] O. Mathon, P. van der Linden, T. Neisius, M. Sikora, J.M. Michalik, C. Ponchut, J.M. De Teresa, S. Pascarelli, *J. Synchotr. Radiat.* **14** (2007) 409.

L35

NANOCRYSTALIZATION IN VANADIUM DOPED CARBON FILMS STUDIED BY MEANS OF X-RAY EMISSION SPECTROSCOPY

M. Sikora [1,2*], C. Adelhelm [3], M. Balden [3], K. Schneider [2], Cz. Kapusta [2], and P. Glatzel [1]

[1] *European Synchrotron Radiation Facility, 6 rue Jules Horowitz, 38043 Grenoble, France*

[2] *AGH University of Science and Technology, Al. Mickiewicza 30, 30-059 Cracow, Poland*

[3] *Max-Planck-Institut für Plasmaphysik, EURATOM Association, D-85748 Garching, Germany*

Keywords: X-ray spectroscopies, metal-doped amorphous carbon films, crystallization

**) e-mail: sikora@esrf.fr*

We report on an *in-situ* study of thermally induced nanocrystallization in the series of vanadium doped carbon films by means of valence-to-core X-ray emission spectroscopy.

Nanostructured metal-doped amorphous carbon films show excellent tribological properties, high hardness and increased electrical conductivity. In future fusion devices like ITER [1], the application of carbon (CFC) together with metals as plasma facing material will lead to the formation of undesired metal-containing hydrocarbon layers during operation. Compared to pure carbon they show higher erosion resistance against hydrogen. A systematic investigation of the influence of doping on the erosion process was studied using a model system: metal-doped carbon films produced by magnetron sputtering.

The structure of carbon films doped with low amounts of Ti, V, Zr and W was studied by XRD, RBS and EXAFS [2]. It revealed that the 'as-deposited' layers have an amorphous, disordered surrounding which already starts to order after annealing at temperatures below 1000 K, when a carbide and (possibly) some amount of oxide clusters are created.

In order to monitor the course of annealing process and simultaneous evolution of the local surrounding of vanadium species *in-situ* temperature dependent measurements of V $K\beta''$ and $Kb_{2,5}$ emission spectra were carried out. They provide bulk sensitive, element selective way to identify the type of ligand in a transition metal compound [3] since the energy separation between $K\beta_{2,5}$ and $K\beta''$ corresponds roughly to the energy difference between the ligand 2*s* and 2*p* levels (Fig. 1).

XES measurements performed at the ESRF ID26 beamline proved the feasibility of such an experiment both from a surface and buried layers. The spectra obtained reveal a nice temperature correlation between $K\beta_{2,5}$ area and the amplitude of EXAFS oscillations reflecting the formation of nanocrystals. Moreover, both carbide and oxide contributions to the $K\beta''$ are observed in samples annealed at high temperatures. They appear at the temperature of order-disorder transition, while their further temperature evolution (and annealing dynamics) is qualitatively different from that of $K\beta_{2,5}$. Since the two parts of XES spectra have a different range of sensitivity, this technique, supported by the cluster calculations of electronic structure, may be used to derive size of nanocrystals of unlike kind.

The results of quantitative analysis of the average size of crystalline clusters of both kinds at different doping levels and annealing temperatures and their comparison to the XRD derived estimations will be presented.

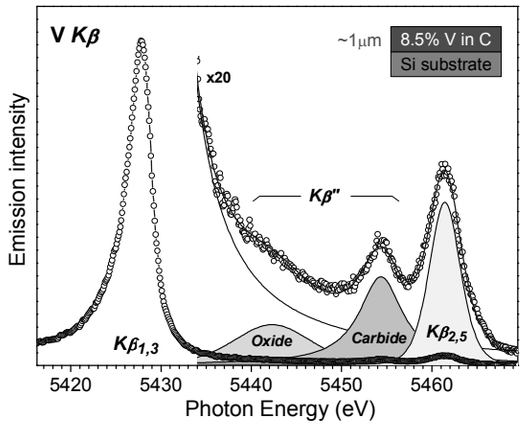

Figure 1. Vanadium $K\beta$ emission spectrum of ~ 1 μm thick layer of 8.5% V in amorphous carbon upon annealing at 1300 K. The $K\beta''$ of oxide and carbide ligands and $K\beta_{2,5}$ peak are fitted using Voigtian profiles and are magnified by factor 20.

Acknowledgements: The authors acknowledge European Synchrotron Radiation Facility for provision of beamtime and B. Gorges for construction of the high temperature oven.

References

[1] R. Aymar, "ITER status, design and material objectives", *J. Nucl. Mater.* **307** (2002) 1-9.

[2] M. Balden, C. Adelhelm, M. Sikora, "Thermal stability and nano-structure of metal-doped carbon layers", *J. Nucl. Mater.* **367-370** (2007) 1458-1462.

[3] S. Fazinić, M. Jakšić, L. Mandić, J. Dobrinić, "Chemical dependence of second-order radiative contributions in the $K\beta$ x-ray spectra of vanadium and its compounds", *Phys. Rev. A* **74** (2006) 062501.

L36

XAFS DETERMINATION OF LOCAL ATOMIC ARRANGEMENT OF IRON IN Fe-CHITOSAN COMPLEXES

M.T. Klepka*, K. Lawniczak-Jablonska, and I.N. Demchenko

Institute of Physics, Polish Academy of Sciences, Al. Lotnikow 32/46, PL–02668 Warsaw, Poland

Keywords: XAFS, chitosan, coordination

**) e-mail: mklepka@ifpan.edu.pl*

The widespread study of metallo-organic chelating compounds is inspired by perspectives of biomedical, ecological and industrial applications. One type of metallo-organic materials are transition metal - chitosan complexes [1]. Presented studies were focused on iron-chitosan complexes. Most new materials used in biomedicine is based on natural materials, mainly polymers, because of their biocompatibility, bioactivity and easy biodegradation. One of them is chitosan, N-deacetylated product of chitin which is obtained in large quantities from crustacean shells (waste products of seafood processing industries). Both materials are significant natural polymers. Chitosans exhibit attractive for nowadays technology physical and mechanical properties. From the application point of view a very important aspect is their ability to chelate metal ions, including heavy and toxic ones [1]. Chitosans have better ability to chelate transition metal ions than other polymers. This skill is correlated with free amino ($–NH_2$) groups [2] (Fig. 1) or other as *e.g.* carboxyl (-COOH) in case of caboxylmethyl chitosan [3] (Fig. 2).

Chitosan, since its discovery in 1859, was wide`ly studied and found adaptation in many applications *e.g.* in water treatment, food processing or as a dietary supplement. Nowadays, the iron containing biopolymers have been examined as possible drug carriers and controlled release beads for various models of drugs. To achieve this goal a lot of attempts were undertaken to increase the sorbent functionality of the chitosan. The prospective method for this seems to be the crosslinking of polymer chains with metal ions (Ch-Fe-CL) or the insertion of carboxylic functional group in chitosan (N-CM-Ch-Fe).

In spite of wide interest of chitosan with 3d metals there is a lack of information about metal coordination, especially in case of Fe-chitosan complexes. Knowing the usefulness of XAFS (EXAFS and XANES) for studies of non-crystalline materials, we have applied this technique for investigation of local atomic order around Fe atoms in different chitosan complexes. Measurements of Fe K-edges were performed in HASYLAB at station A1 in fluorescence mode of detection at liquid nitrogen temperature.

At the beginning, Fe valence was investigated and was qualitatively estimated using XANES. Set of reference iron oxides were measured and energy position of first derivative was compared with Ch-Fe-CL and N-CM-Ch-Fe. In both chitosans dominant part of iron atoms exists as Fe^{3+} ions (Fig. 3).

Investigation of the first coordination sphere in Ch-Fe-CL using EXAFS indicated that two Fe positions are equally possible, consist of two subshells and correspond to *(i)* three oxygen and two nitrogen atoms; *(ii)* two oxygen and three nitrogen atoms. Furthermore, one Fe atom at distance of around 3 Å and at least three more at distance of around 3.5 Å were identified in the second coordination sphere. Third coordination sphere consists of six oxygen or nitrogen atoms. Knowing that the amine group should came from the single chitosan monomer, at least two or three monomers (or even polymers) should be bonded to each Fe atom and each of this polymer has in turn built-in another Fe atom.

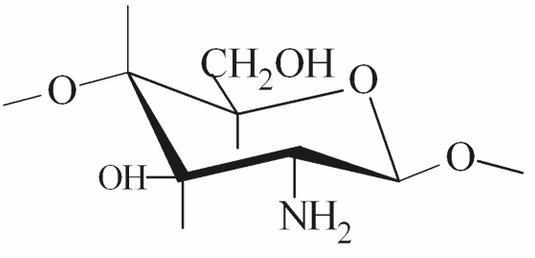

Figure 1. Monomer of chitosan structure.

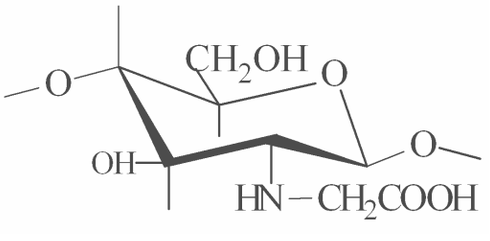

Figure 2. Monomer of N-carboxylmethyl chitosan structure.

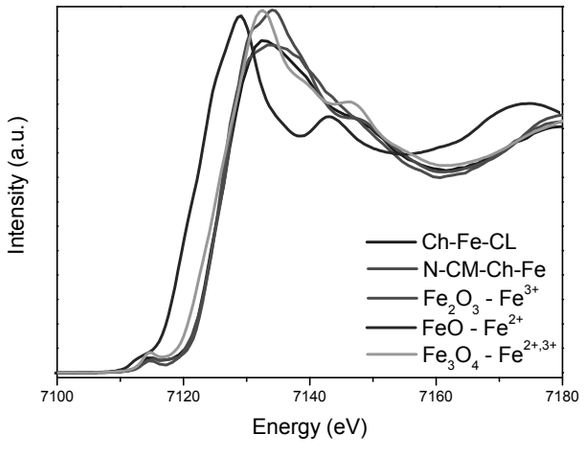

Figure 3. Experimental XANES spectra of Fe-chitsans and reference oxides.

In the case of N-CM-Ch-Fe only one Fe coordination was identified with two subshells consist of three oxygen and two nitrogen atoms. Other Fe atoms were identified neither in first nor in second coordination sphere, but third coordination sphere indicated the presence of Fe atoms. In the second coordination sphere three carbon and two oxygen atoms were identified. This provides the evidence that carboxyl group is an active one and Fe atoms showed a high ability to be chelated by polymers with this group. The detected two nitrogen atoms came from two monomers (or separated polymers), only 20% of monomers contain the carboxyl group, and the additional monomer (at least one) should have –COOH group.

A similarity of first coordination sphere and the differences between further coordination spheres for both chitosans are clearly visible in R space (Fig. 4).

The XANES analysis confirmed that in the considered Fe-chitosans the dominant part of the iron atoms exists as Fe^{3+} ions, which share three electrons in covalence bonding with at least two polymers or monomers. The EXAFS analysis indicated that Fe in both chitosans is penta-coordinated and local atomic structure up to third coordinataion sphere was determined. Obtained results are in agreement with recent magnetic and Mössbauer studies on these chitosans [4].

Acknowledgements: This work was partially supported by national grant of Ministry of Science and High Education N202-052-32/1189 and by DESY and the EC under Contract RII3-CT-2004-506008 (IA-SFS)

References

[1] N.V. Majeti, R. Kumar, "A rewiew of chitin and chitosan applications", *Reac. & Function. Polym.* **46** (2000) 1-27.

[2] B.E. Gamblin, J.G. Stevens, K.L. Wilson, "Structural investigation of chitin and chitosan complexed with iron or tin", *Hyperfine Interact.* **112** (1998) 117-122.

[3] A.J Varma, S.V. Deshpande, J.F. Kennedy, "Metal complexation by chitosan and derivatives: A review", *Carbohyd. Polym.* **55** (2004) 77-93.

[4] M. Klepka, N. Nedelko, J.M. Greneche, K. Lawniczak-Jablonska, I.N. Demchenko, A. Slawska-Waniewska, C.A. Rodrigues, A. Debrassi, C. Bordini, "Local atomic structure and magnetic ordering of iron in Fe-chitosan complexes", *Biomacromolec.,* accepted (2008).

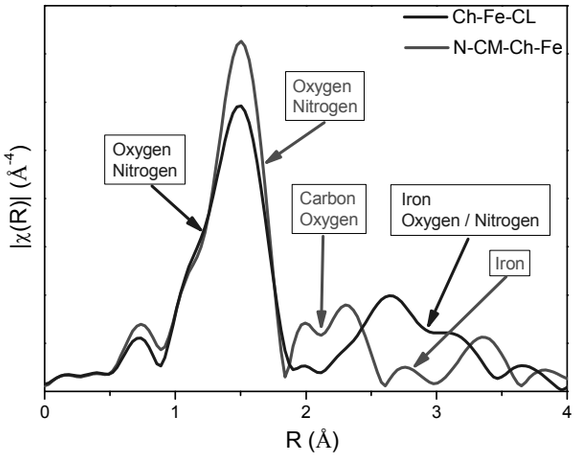

Figure 4. Comparison of Fourier transformed experimental EXAFS spectra for Ch-Fe-CL (blue line) and N-CM-Ch-Fe (red line).

L37

X-RAY ABSORPTION SPECTROSCOPY STUDY OF PLATINUM CHLORIDE COMPLEX IONS IN AQUEOUS SOLUTIONS

D.A. Zając [1,2*], K. Pacławski [3], Cz. Kapusta [4], and K. Fitzner [3]

[1] *Hasylab at DESY, Notkestrasse 85, 22607 Hamburg, Germany*
[2] *H. Niewodniczański Institute of Nuclear Physics of PAN, Radzikowskiego 152, 31-342 Kraków, Poland*
[3] *Faculty of Non-Ferrous Metals, AGH University of Science and Technology, Mickiewicza 30, 30-059 Kraków, Poland*
[4] *Department of Solid State Physics, Faculty of Physics and Applied Computer Science, AGH University of Science and Technology, Mickiewicza 30, 30-059 Kraków, Poland*

Keywords: XAS, EXAFS, platinum, chloride complex, aqueous solution, UV-Vis

**) e-mail: dariusz.zajac@desy.de*

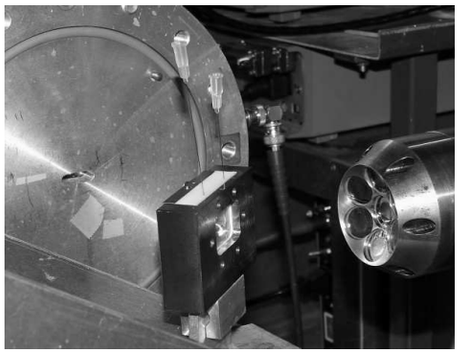

Figure 1. Sample holder for liquids mounted at the beamline X1 in the standard experimental set-up for absorption and fluorescence mode. Behind the sample holder the second ionisation chamber is visible, on the right side – 7 pixel fluorescence detector.

The investigations of noble metals chloride ions (*e.g.* Au, Pt or Ag) in the aqueous solutions are interesting due to the different reaction types involved (*e.g.* substitution, redox, complex) as well as due to the possibility for the synthesis of many valuable products. However, the reaction processes are not fully understood yet. Additionally, the standard experiments techniques, which have been used to investigate such reaction (*e.g.* spectrophotometry UV-Vis), in many cases are not able to detect the progress of the reaction as well as the change in the reactant structure. The example is the redox reaction of *e.g.* Pt, which can not be investigated by spectrophotometry, due to the precipitation of metal nanoparticles. Thus, the combination of X-ray absorption spectroscopy (XAS), in absorption and fluorescence detection, appears to be a suitable tool to investigate mechanism of the reaction.

In this paper we present first results of novel experiments at platinum chloride complex ions in aqueous solution under different pH conditions. Experiments have been performed at the beamline X1 at Hasylab/DESY, Hamburg. The standard absorption setup together with 7 pixel fluorescence detector has been used. A special stopped-flow sample holder for liquids has been constructed. The sample holder is presented in Fig. 1 together with the experimental set-up.

First, the experiment on 7.63×10^{-3}M H_2PtCl_6 in aqueous solutions (pH ≈ 2.5) has been performed in order to check that the sample is not influenced by the irradiation with X-rays. The repeated scans have shown that the Pt:L_3 edge position and shape, as well as the nearest neighbors' peak position and intensity do not change. The experiments have also shown no qualitative difference between EXAFS and QEXAFS (Quick EXAFS) spectra in the absorption mode. Thus, the QEXAFS could be exploitet with the benefit of relatively short measurement time.

Next, experiments on 7.63×10^{-3}M H_2PtCl_6 in aqueous solution with different pH have been performed. Results for pH of 2.5, 5 and 12 show the unchanged position and intensity of the nearest neighbors' peak. The effect could be studied in more details in the experiment on 7.63×10^{-3}M H_2PtCl_6 + 1M NaOH (pH = 14), where a decrease of the intensity of the nearest neighbors' peak is observed after few hours experiment, Fig. 2. We conclude that the hydrolysis of Pt is very slow and the reaction progresses during several hours.

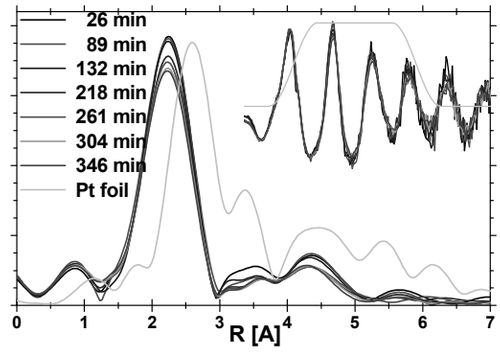

Figure 2. The Fourier transforms of the Pt:L_3 EXAFS functions for different time of hydrolysis of 7.63×10^{-3}M H_2PtCl_6 + 1M NaOH.

L38

XANES AND EXAFS STUDIES OF MALARIAL PIGMENT'S SUBSTITUTES IN REACTION WITH ANTIMALARIAL DRUG

M.S. Walczak [1*], K. Ławniczak-Jabłońska [1], A. Wolska [1], M. Sikora [2], A. Sienkiewicz [3], L. Suárez [4], A. Kosar [4], M.J. Bellemare [4], and D.S. Bohle [4]

[1] *Institute of Physics, PAS, Al. Lotników 32/46, 02-668 Warsaw, Poland*

[2] *European Synchrotron Radiation Facility, 6 rue Jules Horowitz, Boîte Postale 220, 38043 Grenoble, France*

[3] *Institute of Physics of Complex Matter, Ecole Polytechnique Fédérale de Lausanne, Lausanne, CH-1015, Switzerland*

[4] *Department of Chemistry, McGill University, 801 Sherbrooke Street West, Montreal, Canada*

Keywords: malaria, hemozoin, β-hematin, X-ray absorption spectroscopy

**) e-mail: mwalczak@ifpan.edu.pl*

Malaria remains the world's most prevalent vector-borne disease, which causes severe health problem particularly in African and Asiatic countries. Today, over 40% of the world's population, especially in the tropics, is at risk [1, 2]. The most severe form of malaria is caused by a protozoan parasite, *Plasmodium falciparum* (*Pf*), which lately has become resistant to traditional therapies. The intraerythrocytic stage of *Pf* involves hemoglobin proteolysis as the primary nutrient source and detoxify heme into an inert crystalline material, called malarial pigment, or hemozoin [3]. The crystal structure of hemozoin has been solved by X-ray powder diffraction [4] in the last years and its synthetic analogue, β-hematin was synthesized. The X-ray absorption spectroscopy (XAS) measurements performed on solid hemozoin and β-hematin samples confirmed that the radial distributions of atoms around the iron centers in these compounds are very similar but differ in the level of ordering. These studies also pointed to the presence of the trivalent iron atoms (FeIII) in both materials [5].

Understanding of all possible interactions and chemical structures related to malarial pigments become now critically important in respect the commonly used drugs based on chloroquine are not longer effective on many tribes of parasite.

In presented work we are especially interested in drug-induced perturbations of the dimer structures of soluble β-hematin-like compounds, iron(III) (meso-porphyrin-IX anhydride) and iron(III) (deuteron-porphyrin-IX anhydride). Similarly to their insoluble parent compound, β-hematin, *i.e.* Iron(III) (protoporphyrin-IX anhydride), these compounds are also built of dimers.

The XAS measurements were performed at ESRF (station ID26). The high resolution XANES and EXAFS spectra enabled us to reveal the differences in local environment of Fe atoms before and after drug addition. The results of EXAFS χ–function analysis for hemozoin' substitutes as compare to monomeric reference compounds, will be presented. The indicated changes in 1*s*-3*d* preedge feature of XANES spectra point on symmetry changes in nearest iron neighborhood and degree of bonds covalency. The shape of that feature depends strongly on used solvent. In solution of dimethyl sulfoxide (DMSO) differences after adding antimalarial drug to dimmer as well as to corresponding monomer are well noticeable.

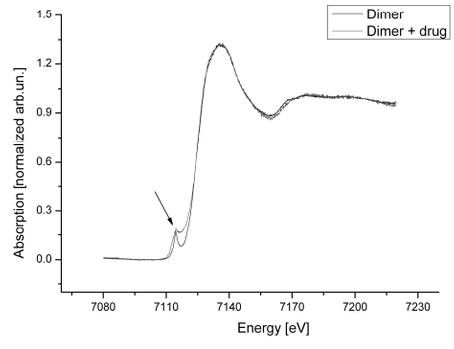

Figure 1. Comparison of XANES spectra of dimer before and after interaction with antimalarial drug in solution of DMSO.

Acknowledgements: This work was partially supported by research grant No. N20205332/1197 from the Ministry of Science and High Education. We acknowledge also the European Synchrotron Radiation Facility ESRF.

References

[1] L.H. Miller, D.I. Baruch, K. Marsch, O.K. Duombo, *Nature* **415** (2002) 673-679.

[2] World Health Organization, The World Malaria Report 2005, http://www.who.int/malaria.

[3] A. Dorn, R. Stoffel, H. Matile, A. Bubendorf, R.G. Ridley, *Nature* **374** (1995) 269-271.

[4] S. Pagola, P.W. Stephens, D.S. Bohle, A.D. Kosar, S.K. Madsen, *Nature* **404** (2000) 307-310.

[5] M. Walczak, K. Ławniczak-Jabłońska, A. Sienkiewicz, I.N. Demchenko, E. Piskorska, G. Chatain, D.S. Bohle, *Nucl. Instrum. Meth. Phys. Res. B* **238** (2005) 32-38.

L39

HIGH RESOLUTION POWDER DIFFRACTION

A.N. Fitch

ESRF, BP220, 38043 Grenoble Cedex, France

Keywords: powder diffraction, high resolution, beamline, peak shape

e-mail: fitch@esrf.fr

High resolution powder X-ray diffraction beam lines operate at many synchrotron radiation sources, exploiting the very high intensity, vertical collimation and wavelength tunability of the beam. At ESRF in Grenoble, a powder diffraction beam line has operated since May 1996. Originally built on the BM16 bending magnet source [1], the diffractometer was transferred six years ago to a new location at ID31, where it is powered by three 11-mm minimum gap undulators, to give very intense beams in the operational range of 6 keV – 60 keV (wavelength ≈2 Å – 0.2 Å). The diffractometer, shown in Figure 1, is equipped with a bank of post-sample analyser crystals, Figure 2, to give very high angular resolution as well as accuracy. An analyser crystal, rather than inferring the 2θ angle of diffraction from the position of a slit or pixel on a PSD, defines a true angle of diffraction, and thereby removes a number of systematic aberrations in the peak positions that affect standard configurations.

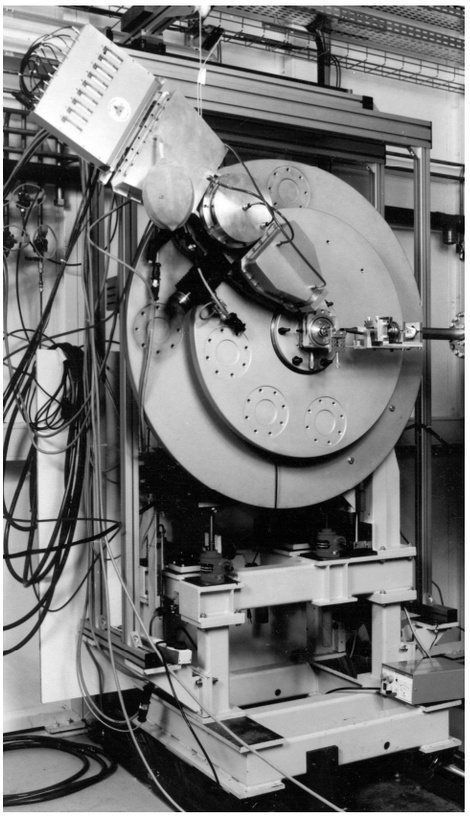

Figure 1. ID31's high resolution powder diffractometer, equipped with the nine crystal multianalyser stage.

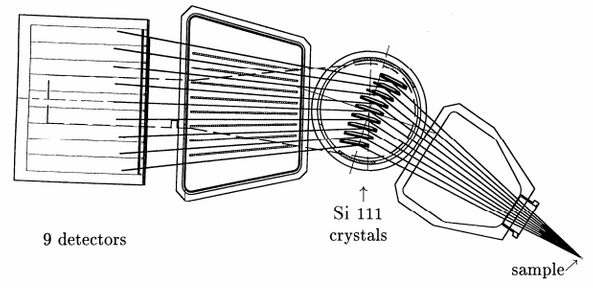

Figure 2. Nine channel Si 111 multianalyser stage [2]. Each channel is offset from the next by ≈2º. As the detector arm is scanned, nine high resolution powder diffraction patterns are collected in parallel, and these are subsequently combined and normalised in a data reduction step [3].

A wide range of sample environments is available, allowing measurements at temperatures from 3 K to 1600°C, and under a variety of atmospheres. A robotic sample changer permits up to 50 samples to be processed automatically. Typical uses of the beam line include;

- Structural studies: the solving and refining of crystal structures, exploration of the structure of glasses, and atomic pair distribution function (PDF) analysis;
- *In-situ* studies: observation of structures or materials evolving with temperature, time, voltage, etc. during phase transitions, solid-state chemistry, electrochemistry, *etc.*;
- Anomalous scattering: tuning to an absorption edge to help distinguish between elements with similar atomic number in a material;
- High throughput studies: involving many samples synthesised with different compositions, or under varied preparation conditions, *etc.*;
- Quantitative analysis: diffraction patterns from complex mixtures with many contributing phases can be analysed; the detection of phases present in very low proportions is possible;
- Microstructure: analysis of peak shapes yields microstructural information about a material. Since the instrumental contribution is very small, the peak shapes are dominated by sample effects;
- Residual strain: Measurements of residual strain, either by the traditional $sin^2\psi$ technique, or by mapping peak positions from within the bulk and surface of a sample, *etc.*;

- Diffraction at grazing incidence and reflectivity: measurements from thin films and surfaces.

The accessibility of high 2θ resolution at short wavelengths is a particular strength of the beam line. Thus a wide range of absorbing materials can be investigated using spinning-capillary sample geometry. The use of a spinning capillary can greatly reduce preferred orientation effects, which are hard to avoid when using a flat-plate powder specimen, thus improving the accuracy of the measured diffraction intensities. Hard energies, 30 keV and above, also allow measurements to high values of $Q = 4\pi \sin\theta / \lambda$ for investigation of the atomic pair distribution function $G(r)$ of a material. The PDF is obtained by Fourier transforming the normalised scattered X-ray intensity and is a measure of the number of atoms in a spherical shell of radius r about a reference atom. Thus peaks in $G(r)$ represent characteristic distances between pairs of atoms in the structure, and the method can be applied to crystalline and non-crystalline samples alike [4]. This allows structural characterisation of poorly crystalline and disordered materials that lack the translational periodicity of a good crystal. The analyser crystals help the quality of the PDF analysis by suppressing background contributions to the diffraction pattern coming from fluorescence and Compton scattering [5]. However scanning the analyser crystals requires several hours to collect data of sufficient statistical quality, and it is often advantageous to use a lower resolution arrangement with very hard X-rays (90 keV) and a two dimensional detector to record the whole scattering pattern in a single exposure [6], which may be a matter of less than a second. This approach is extensively used at the APS (Argonne National Laboratory).

In the development of new materials, analysis of the diffraction peak shapes can yield important chemical or microstructural information. For example, in the search for new hydrogen storage materials, cycling hydrogen between lithium nitride Li_3N, lithium imide Li_2NH, lithium amide $LiNH_2$ has been investigated [7]. Three samples that had undergone various cycles of hydrogen adsorption and desorption were examined on ID31. As well as a complex mixture of phases identified in sample I, including the unexpected new phase $Li_{1.15}NH_{1.85}$ (composition from the refined Li occupancy), some remarkable peak shapes were apparent in samples II and III, Figure 3, implying complex microstructural behaviour. The broad Bragg peaks of the dominant cubic Li-N-H phase are highly structured and follow a strain-broadening dependence on diffraction angle, indicative of a pronounced variation in stoichiometry. Detailed analysis of the pattern using the remarkable Rietveld refinement program TOPAS [8] allowed the range of non-stoichiometry to be evaluated. The peak shape was modelled as a sum of 11 phases, $Li_{1+x_n}NH_{2-x_n}$, with uniformly varying stoichiometry (x_n) and lattice parameter (a_n), refining the stoichiometric and lattice-parameter limits, x_0, x_{10}, a_0, a_{10}, and the amount of each phase present. Thus the compositional variation represented by the complex peak profile can be obtained, which allowed a mechanism for hydrogen storage and release to be proposed.

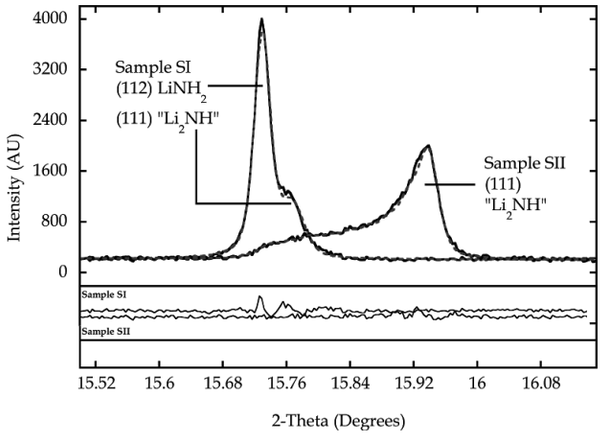

Figure 3. Some of the remarkable powder diffraction peak shapes seen from samples produced by hydrogen cycling in the lithium nitride-imide-amide system, and the fit using the Rietveld refinement program TOPAS, from Ref. [7].

With very high 2θ resolution, the question arises as to just how big a structure can be analysed from a powder diffraction pattern, and measurements with protein samples have been pioneered by Von Dreele working at the NSLS (Brookhaven) [9, 10] and APS [11]. One of the bottlenecks in protein structure analysis is growing a suitable single crystal and modern screening approaches often produce polycrystalline material instead. Protein structures can be refined by the Rietveld method employing extensive stereochemical restraints to preserve the molecular structure, and even solved by molecular replacement *e.g.* for a variant of the T_3R_3 human insulin-zinc complex produced by grinding [10].

Remarkable progress has been made in the field, reviewed by Margiolaki and Wright [12]. Recently reported was the solution by molecular replacement of the structure of the second SH3 domain of the muscle protein Ponsin, with 67 amino acids in the chain, via a model with only 38% amino-acid sequence homology [13]. The analysis exploited multiple data sets with radiation-induced anisotropic shifts in peak positions to improve the amount of structural information that could be extracted from the powder data. Anisotropic peak shifts mean that peaks overlapping in one pattern may be better (or differently) resolved in another. By fitting simultaneously to the multiple data sets, the deleterious effects of peak overlap can be alleviated, to some extent at least. Anisotropic shifts in peak positions, reflecting underlying lattice strains, can be induced via changes in temperature [14], or for proteins via crystallisation at different pH values [15], with different solvents, or as a result of radiation damage in the very intense synchrotron X-ray beam [11, 13].

L39

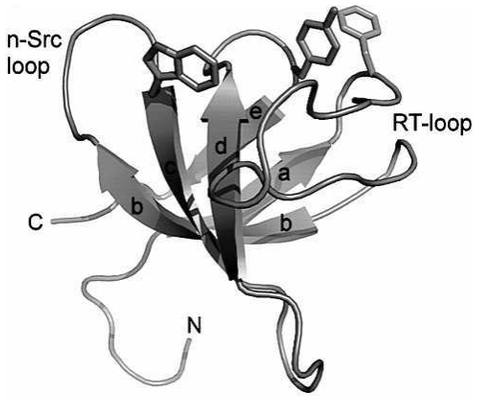

Figure 4. Ribbon representation of the structure of the second SH3 domain of Ponsin determined by high resolution powder diffraction [13].

References

[1] A.N. Fitch, "The high resolution powder diffraction beam line at ESRF", *J. Res. Natl. Inst. Stand. Technol.* **109** (2004) 133-142.

[2] J.-L. Hodeau, P. Bordet, M. Anne, A. Prat, A.N. Fitch, E Dooryhée, G. Vaughan, A. Freund, "Nine crystal multi-analyser stage for high resolution powder diffraction between 6 and 40 keV", *Proc. SPIE* **3448** (1998) 353-361.

[3] J.P. Wright, G.B.M. Vaughan, A.N. Fitch, "Merging data from a multi-detector continuous scanning powder diffraction system", *IUCr Computing Commission Newsletter* **1** (2003) 92-96, (http://www.iucr.org/iucr-top/comm/ccom/newsletters/2003jan/index.html).

[4] M.G. Kanatzidis, S.J.L. Billinge, "Beyond crystallography: the study of disorder, nanocrystallinity and crystallographically challenged materials with pair distribution functions", *Chem. Commun.* (2004) 749-760.

[5] S. Brühne, E. Uhrig, K.-D. Luther, W. Assmus, M. Brunelli, A.S. Masadeh, S.J.L. Billinge, "PDF from X-ray powder diffraction for nanometer-scale atomic structure analysis of quasicrystalline alloys", *Z. Krist*. **220** (2005) 962-967.

[6] P.J. Chupas, K.W. Chapman, P.L. Lee, "Applications of an amorphous silicon-based area detector for high-resolution, high-sensitivity and fast time-resolved pair distribution function measurements", *J. Appl. Crystallogr.* **40** (2007) 463-470.

[7] W.I.F. David, M.O. Jones, D.H. Gregory, C.M. Jewell, S.R. Johnson, A. Walton, P.P. Edwards, "A mechanism for non-stoichiometry in the lithium amide lithium imide hydrogen storage reaction", *J. Am. Chem. Soc.* **129** (2007) 1594-1601.

[8] A. Coelho, TOPAS Academic, see http://members.optusnet.com.au/alancoelho/.

[9] R.B. Von Dreele, "Combined Rietveld and stereochemical restraint refinement of a protein crystal structure", *J. Appl. Crystallogr.* **32** (1999) 1084-1089.

[10] R.B. Von Dreele, P.W. Stephens, G.D. Smith, R.H. Blessing, " The first protein crystal structure determined from high-resolution X-ray powder diffraction data: a variant of T_3R_3 human insulin-zinc complex produced by grinding", *Acta Crystallogr. D* **56** (2000) 1549-1553.

[11] R.B. Von Dreele, "Multipattern Rietveld refinement of protein powder data: an approach to higher resolution", *J. Appl. Crystallogr.* **40** (2007) 133-143.

[12] I. Margiolaki, J.P. Wright, " Powder crystallography on macromolecules", *Acta Crystallogr. A* **64** (2008) 169-180.

[13] I. Margiolaki, J.P. Wright, M. Wilmanns, A.N. Fitch, N. Pinotsis, "Second SH3 domain of ponsin solved from powder diffraction", *J. Am. Chem. Soc.* **129** (2007) 11865-11871.

[14] K. Shankland, W.I.F. David, D.S. Sivia, "Routine *ab initio* structure determination of chlorothiazide by X-ray powder diffraction using optimised data collection and analysis strategies", *J. Mater. Chem*. **7** (1997) 569-572.

[15] S. Basso, A.N. Fitch, G.C. Fox, I. Margiolaki, J.P. Wright, "High-throughput phase-diagram mapping *via* powder diffraction: A case study of HEWL *versus* pH", *Acta Crystallogr. D* **61** (2005) 1612-1625.

L40

IMAGING NANOSCALE OBJECTS BY FEMTOSECOND X-RAY DIFFRACTION WITH A SOFT-X-RAY FREE ELECTRON LASER

D. Rolles [1,2*]

[1] *Max Planck Advanced Study Group, Center for Free Electron Laser Science (CFEL), Notkestaße 85, D-22603 Hamburg, Germany*

[2] *Max-Planck-Institute for Medical Research, Jahnstraße 29, D-69120 Heidelberg, Germany*

Keywords: femtosecond diffractive imaging, X-ray diffraction, Free Electron Laser

**) e-mail: daniel.rolles@mpimf-heidelberg.mpg.de*

The construction and commissioning of several VUV and X-Ray Free Electron Lasers (FELs) around the world presents exciting new opportunities to study phenomena that are far beyond the reach of current experimental capabilities. The broad scope of the proposed research at these facilities also provides excellent chances for enriching interdisciplinary collaborations between the physical, chemical, material and biological sciences. For instance, the high brightness and the ultra-short time structure of the FEL radiation allows time-resolved experiments on the femtosecond scale that follow (bio-)chemical reactions or probe the dynamics of fundamental processes in atomic, molecular and condensed matter physics.

Of particular interest is the so-called femtosecond diffractive imaging of nanometer- to micrometer-sized objects [1]. With this technique, a single diffraction pattern can be recorded from a large macromolecule, a virus or a cell before the sample explodes [2].

In this talk, I will review the basics of the femtosecond diffractive imaging technique and present results obtained using the first soft-X-ray FEL in the world, the FLASH facility at DESY in Hamburg. Using intense VUV radiation between 7 and 32 nm, diffraction images were obtained for various physical and biological targets ranging from van-der-Waals clusters to DNA molecules [3] and small living organisms. These experiments demonstrate the capability of single-shot imaging of nanoscale objects and represent an important step towards imaging uncrystalized biomolecules with sub- nanometer resolution.

Within a few years, several new FELs, which are currently under construction around the world, will allow extending the single particle imaging technique to the hard x-ray regime. An outlook on these planned experiments will be provided and the accompanying challenges will be discussed.

References

[1] H.N. Chapman *et al*., "Femtosecond diffractive imaging with a soft-X-ray free-electron laser", *Nature Phys.* **2**, (2006) 839-843.

[2] R. Neutze, R. Wouts, D. Van Der Spoel, E. Weckert, J. Hajdu, "Potential for biomolecular imaging with femtosecond X-ray pulses", *Nature* **406** (2000) 752-757.

[3] M.J. Bogan *et al*., "Single particle X-ray diffractive imaging", *Nanoletters* **8** (2008) 310-316.

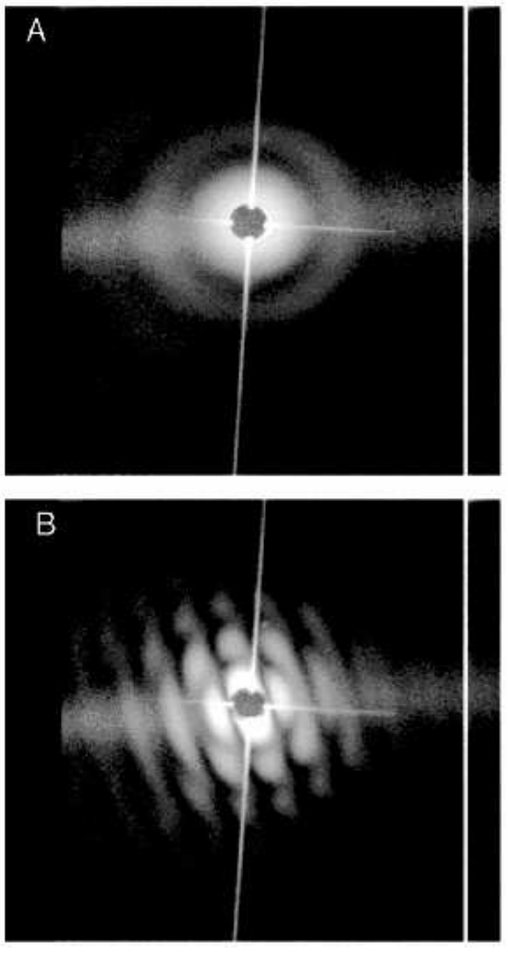

Figure 1. FLASH X-ray coherent diffraction patterns of (A) a single particle and (B) two particles [3].

L41

TEMPERATURE AND PRESSURE-INDUCED SPIN-STATE TRANSITIONS: APPLICATIONS OF HIGH-RESOLUTION X-RAY SPECTROSCOPY

G. Vankó*

MTA KFKI Research Institute for Particle and Nuclear Physics, H-1525 Budapest, P. O. Box 49, Hungary

Keywords: spin-state transition, X-ray spectroscopy, transition metals, magnetism, photoswitchable compounds

**) e-mail: vanko at rmki.kfki.hu*

The spin state of the transition metal compounds is a major parameter determining the material's chemical and physical properties. The properties may be as different for different spin states as if the metal ion were replaced by a different element. The metal ion in octahedral surroundings with electron configuration $d^4 \ldots d^7$ can exist in low spin (LS) or high spin (HS) state, depending on the energy separation of the t_{2g} and e_g levels caused by the crystal field [1, 2]. Upon external conditions, such as temperature, applied pressure, or strong magnetic field, irradiation by light, *etc*. the spin state of a compound may revert. With the spin state transition most physical and chemical properties of the system change, including bond lengths, multiplicity, density, electronic and heat transport properties. Determination of the spin state is therefore crucial in many fields, including inorganic and organometallic chemistry, solid state and geosciences. In a number of molecular systems of medium ligand field strength, the spin state can be switched back and forth between the LS and the HS states by triggering a redistribution of the 3*d* electrons on the t_{2g} and e_g levels [2]. The spin state can also change upon temperature in certain oxides with strongly correlated electrons: a prominent example being $LaCoO_3$, in which the Co^{3+} ions in octahedral environment undergo two broad magnetic transitions, the one at higher temperature being accompanied by a metal-insulator transition. These transitions in $LaCoO_3$ involve the change of the spin state; however, the nature of the transition is still debated [3,4]. Being crucial to the transport properties, knowledge of the spin state in such oxides is indispensable to the understanding the electronic structure [5]. In addition to thermal effects, external pressure often causes spin state transitions. In systems exhibiting temperature-induced transitions, this occurs at relatively low (≈10 kbar) pressures [2, 3]. Shrinking of bond length is accompanied by rapid increase in the ligand-field splitting ($10\,Dq \propto r^{-5}$), therefore even compounds exhibiting high spin state at ambient conditions undergo a spin state transition to LS state at high enough pressures [6–10].

Sample environments necessary for extreme conditions or the presence of different magnetic components in the sample might limit or hinder the use of conventional techniques to determine the spin states of the transition metal in compounds. Element selective techniques with highly penetrating hard X rays therefore find numerous applications in determining the total spin momentum of the transition metal.

Hard X-ray spectroscopies fulfil all criteria to probe the spin state in the bulk [11–14]. In order to demonstrate the above we have conducted systematic investigations on spin transition complexes of Fe^{3+}, Fe^{2+} and Co^{2+} (well below and above their transition temperatures) [15,16]. As we shall see, these molecular compounds cover almost the entire $d^4 \ldots d^7$ range, have unambiguous spin states and show diverse spin transitions. As an example, the effects of the thermally induced transitions will be shown by X-ray spectra of $[Fe(phen)_2(NCS)_2]$, a widely studied family of spin-transition complexes, with a $3d^6$ central ion. The compound exhibits a $^1A_{1g}$ ($t_{2g}^6 e_g^0$, S=0, LS) to $^5T_{2g}$ ($t_{2g}^4 e_g^2$, S=0, HS) transition at 178 K. The full K-emission spectrum of $[Fe(phen)_2(NCS)_2]$ is displayed in Figure 1 for both HS and LS states. As it is seen, all emission features undergo a relevant modification upon the change in the spin state. The Kβ intensity drops in the Kβ' satellite region when the 3d spin momentum is diminished. The variation of the Kα line shape is more complex, but the differences are substantial. The sensitivity of the Kα (Kβ) emission lines arise from the exchange interaction between the $\underline{2p}$ ($\underline{3p}$) core hole and the unpaired 3*d* electrons in the final state. The large spatial overlap of the 3*d* orbitals with the $\underline{3p}$ core hole results in a large 3*p*3*d* exchange coupling, which leads to a splitting as high as 15 eV. Beside this dominant feature, manifested in the clear separation of the Kβ' satellite, the spectrum is influenced by other interactions, too. Due to a smaller overlap, the 2p3d exchange coupling is smaller, which leads to a splitting of 1-2 eV in the Kα spectrum. This is in the range of the line width of the Kα lines, therefore, the change in the spin state appears as a mere variation of the line broadening. Thus, while the total variation of the Kα spectrum is bigger than that of the Kβ, as it is evident from the spectra in Figure 1, the interpretation of the Kβ spectra is more straightforward. An additional advantage of the Kβ is its higher energy especially in case of strongly absorbing samples or sample environments.

The highest energy features in Figure 1, Kβ" and $K\beta_{2,5}$, emerge due to valence electrons filling the 1s core hole; their final states are identical to those in photoelectron spectroscopy, thus prominent chemical sensitivity is expected in this spectral region [11]. These peaks are also modified upon the spin transition; however, the spectral variations stem from the changes in the bonding. Being weak and unrelated to the spin

momentum, these high energy lines are of little use as probes of the spin state.

In the spin transition regime the XES spectra were shown to consist of superposed HS and LS states [17, 16, 18]. This allows a precise determination of the HS fraction for two-state transitions [16], and has been exploited in several studies [3, 10, 18, 19]. Reassuringly, XES and soft X-ray absorption spectroscopy (XAS) gave similar results for the less unambiguous transitions of $LaCoO_3$, [3, 4] (see Figure 2). XES with careful line-shape analysis is becoming an established probe of the spin state [16, 7, 18].

As the rearrangement of the electrons at the spin transition affects the electronic structure and the local geometry, XAS can also be used to follow spin transitions. K-edge X-ray absorption was applied by several authors to study structural variations accompanied by the spin transition, or to follow the evolution of the transition [12, 13]. The pre-edge region, stemming from $1s \rightarrow 3d$ transitions (in case of an octahedral environment), is expected to be most sensitive to the spin state, since the variation in the $3d$ populations obviously change the density of states and the electron-electron interaction energies alike. However, due to its quadrupolar origin, this spectral region is of low intensity, not well separated from the edge tail, poorly resolved, therefore little effort has been made to explore spin states from such spectra. Better separation of the pre-edge features is achieved by combining XAS with XES. This technique, the resonant X-ray emission spectroscopy (RXES), provides details on the redistribution of electrons on the $3d$ levels associated with the spin-state transition. It reveals features at the X-ray absorption pre-edge that are hardly accessible through standard XAS measurements; this is clearly demonstrated in Fig. 3 with spectra of $[Fe(phen)_2(NCS)_2]$.

In addition to the above techniques, non-resonant inelastic X-ray scattering has proven great potential in studying *d-d* excitations [20]; therefore, it can open new opportunities in spin state studies.

Finally, we report on hard X-ray induced excited spin-state trapping (HAXIESST) in $[Fe^{II}(phen)_2(NCS)_2]$ [21]. In Figure 4, results of a rapid energy scan are displayed at 30 K, far below the transition temperature, reflecting an LS state. However, according to a second, longer scan by the intense X-ray beam an anomalous metastable HS state appears to form. Previously green light had been found to populate the metastable low-temperature HS state of this molecule; a phenomenon called light-induced excited spin-state trapping (LIESST). This switching to the HS state proceeds through several excited states; the excitation and relaxation mechanisms are determined by the strongly coupled electron, magnetic, and structural dynamics. With a certain branching ratio the molecule transforms to the HS state. The relevant vibrational modes being inactive, non-adiabatic multi-phonon relaxation is hindered below 50 K, which leads to a very small HS→LS tunnelling rate [22]. At higher temperatures, where the higher vibrational states of the HS become populated, the relaxation speeds up as a result

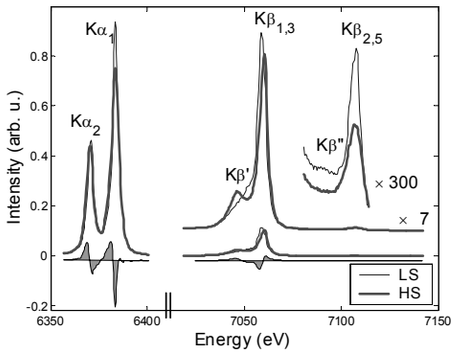

Figure 1. Full K-emission spectra of $[Fe(phen)_2(NCS)_2]$ in the HS (thick line) and LS (thin line) state. The Kβ and the valence emission regions are also shown in magnified forms. Below the spectra, the shaded area displays the HS–LS spectral difference.

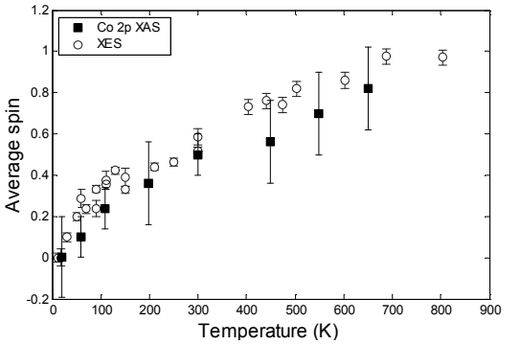

Figure 2. Temperature evolution of the average cobalt spin momentum in $LaCoO_3$. The analysis based on the XES data [3] is in fair agreement with the results obtained from $L_{2,3}$ spectroscopy [4].

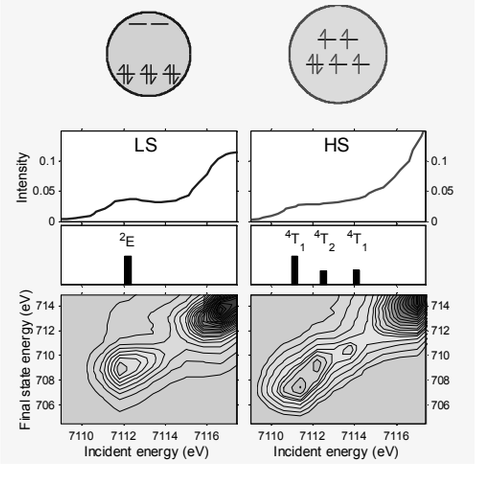

Figure 3. *Top*: The pre-edge region of the Fe K absorption edge of $[Fe(phen)_2(NCS)_2]$ [12]. *Middle*: transitions predicted by multiplet theory. *Bottom*: $1s2p_{3/2}$ RXES spectra. (*Above* the spectra the distribution of the $3d$ electrons on the t_{2g} and e_g levels is shown.)

L41

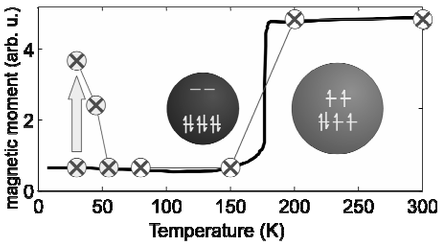

Figure 4. Magnetic moment of $[Fe^{II}(phen)_2(NCS)_2]$ determined from X-ray emission data (circles with symbol X) and from conventional magnetization measurements (solid line).

of a larger overlap of the higher lying vibrational wavefunctions of both spin states. The remarkably similar temperature dependence of the metastable HS population created by light and X-rays suggest similar relaxation mechanisms. While the low-*T* HS state and its decay conditions are the same in LIESST and HAXIESST, the excitation is obviously different: visible light can induce the necessary ligand-field excitations, unlike the hard X-rays. The spin-state trapping occur via relaxation processes that follow electronic excitations caused mostly by secondary electrons. Irradiation with hard X-rays may populate metastable states even when optical excitation is limited by sample characteristics or by its environment, as in the cases of non-transparent samples or cells for extreme conditions. This result unveils the non-innocent nature of low-temperature hard X-ray investigations, where spectroscopy or diffraction experiments might lead to excitations similar to visible light-induced excitations.

Acknowledgements: The author would like to thank the ID16 and ID26 staff of the ESRF, as well as J. Badro, F. M. F. de Groot, G. Molnár, Z. Németh, F. Renz, J.-P. Rueff, and A. Shukla for collaborations and discussions. Support by the Hungarian Scientific Research Fund (OTKA) under contract No. K 72597, and the Bolyai János Fellowship of the Hungarian Academy of Sciences are acknowledged.

References

[1] S. Alvarez, J. Cirera, "How high the spin? Allowed and forbidden spin states in transition-metal chemistry" *Angew. Chem. Int. Ed.* **45** (2006) 3012–3020.

[2] *Spin Crossover in Transition Metal Compounds I-III,* in: *Topics in Current Chemistry*, P. Gütlich, H.A. Goodwin, (Eds.), (Springer, Berlin-Heidelberg 2004) Vols. 233-235.

[3] G. Vankó, J.-P. Rueff, A. Mattila, Z. Németh, A. Shukla, "Temperature and pressure-induced spin-state transitions in $LaCoO_3$", *Phys. Rev. B* **73** (2006) 024424.

[4] M.W. Haverkort, Z. Hu, J.C. Cezar, T. Burnus, H. Hartmann, *et al.*, "Spin state transition in $LaCoO_3$ studied using soft x-ray absorption spectroscopy and magnetic circular dichroism", *Phys. Rev. Lett*. **97** (2006) 176405.

[5] A. Maignan, V. Caignaert, B. Raveau, D. Khomskii, G. Sawatzky, "Thermoelectric power of $HoBaCo_2O_{5.5}$: possible evidence of the spin blockade in cobaltites", *Phys. Rev. Lett.* **93** (2004) 026401.

[6] J.-P. Rueff, C.-C. Kao, V.V. Struzhkin, J. Badro, J. Shu, R.J. Hemley, H.K. Mao, "Pressure induced high-spin to low-spin transition in FeS evidenced by x-ray emission spectroscopy", *Phys. Rev. Lett.* **82** (1999) 3284–3287.

[7] J.-P. Rueff, A. Shukla, A. Kaprolat, M. Krisch, M. Lorenzen, F. Sette, R. Verbeni, "Magnetism of Invar alloys under pressure examined by inelastic x-ray scattering", *Phys. Rev. B* **63** (2001) 132409.

[8] J. Badro, G. Fiquet, F. Guyot, J.-P. Rueff, V.V. Struzhkin, G. Vankó, G. Monaco, "Iron partitioning in the earth's lower mantle; toward a deep lower-mantle discontinuity", *Science* **300** (2003) 789–791.

[9] J. Badro, J.P. Rueff, G. Vankó, G. Monaco, *et al.*, "Electronic transitions in perovskite: possible non-convecting layers in the lowermost mantle", *Science* **305** (2004) 383–386.

[10] J.-F. Lin, G. Vankó, S.D. Jacobsen, V. Iota, V.V. Struzhkin, V.B. Prakapenka, *et al.*, "Spin transition zone in Earth's lower mantle", *Science* **317** (2007) 1740–1743.

[11] P. Glatzel, U. Bergmann, "High resolution 1s core hole x-ray spectroscopy in 3*d* transition metal complexes - Electronic and structural information", *Coord. Chem. Rev.* **249** (2005) 65–95.

[12] V. Briois, C. Cartier dit Moulin, P. Sainctavit, C. Brouder, A.-M. Flank, "Full multiple scattering and crystal field multiplet calculations performed on the spin transition $Fe^{II}(phen)_2(NCS)_2$ complex at the iron K and $L_{2,3}$ X-ray absorption edges", *J. Am. Chem. Soc.* **117** (1995) 1019.

[13] C. Hannay, M.-J. Hubin-Franskin, F. Grandjean, V. Briois, J.-P. Itié, A. Polian, S. Trofimenko, G.J. Long, "X-ray absorption spectroscopic study of the temperature and pressure dependence of the electronic spin states in several iron(II) and cobalt(II) tris(pyrazolyl)borate complexes", *Inorg. Chem.***36** (1997) 5580–5588.

[14] K. Tsutsumi, H. Nakamori, K. Ichikawa, "X-ray Mn Kβ emission spectra of manganese oxides and manganates", *Phys. Rev. B* **13** (1976) 929–933.

[15] G. Vankó, T. Neisius, F. Renz, A. Shukla, F. de Groot *et al.*, "Molecular spin transitions studied with X-ray emission spectroscopy", *ESRF Highlights* 2002, pp. 59–60.

[16] G. Vankó, T. Neisius, G. Molnár, F. Renz, S. Kárpáti, A. Shukla, F.M.F. de Groot, "Probing the 3*d* spin momentum with x-ray emission spectroscopy: the case of molecular spin transitions", *J. Phys. Chem. B* **110** (2006) 11647.

[17] X. Wang, F.M.F. de Groot *et al.*, "Spin-polarized x-ray emission of 3d transition-metal ions : A comparison via Kα and Kβ detection" *Phys. Rev. B* **56** (1997) 4553.

[18] G. Vankó, F.M.F. de Groot, "Comment on « Spin crossover in (Mg,Fe)O: A Mössbauer effect study with an alternative interpretation of x-ray emission spectroscopy data »", *Phys. Rev. B* **75** (2007) 177101.

[19] R. Lengsdorf, J.-P. Rueff, G. Vankó, T. Lorenz, L.H. Tjeng, M.M. Abd-Elmeguid, "Spin-state-driven metal-insulator transition in $(La,Sr)CoO_3$ under high-pressure", *Phys. Rev. B* **75** (2007) 180401.

[20] M.W. Haverkort, A. Tanaka, L.H. Tjeng, G.A. Sawatzky, "Nonresonant inelastic x-ray scattering involving excitonic excitations: The examples of NiO and CoO", *Phys. Rev. Lett.* **99** (2007) 257401.

[21] G. Vankó, F. Renz, G. Molnár, T. Neisius, S. Kárpáti, "Hard X-ray induced excited spin-state trapping" *Angew. Chem. Int. Ed.* **46** (2007) 5306 –5309.

[22] A. Hauser, "Light-induced spin crossover and the high-spin → low-spin relaxation", *Top. Curr. Chem.* **234** (2004) 155, and references therein.

L42

TEMPORAL STRUCTURE OF SR – APPLICATION TO STUDY BIOMOLECULES IN UV AND VISIBLE RANGE

K. Polewski

Department of Physics, University of Life Sciences in Poznan, ul. Wojska Polskiego 38/42, PL 60-637 Poznan

Keywords: fluorescence lifetimes, biomolecules, FLIM, confocal microscope, imaging

Email: polewski@up.poznan.pl

SR is delivered to the stations as a set of bunches with temporal resolution, depending on the properties of the storage ring, ranging from tens of ps to ns. This property has been used to study kinetic and dynamic properties of biomolecules and biological processes.

Due to stability and tunability of SR the **time-resolved fluorescence spectroscopy lifetimes and anisotropy** on biological and non-biological samples were measured at different excitation and resolution.

Figure 1 shows an example of application of temporal structure and spectral properties of SR to simultaneously (in one measurement) study all the spectroscopic properties of biomolecules like fluorescence emission, lifetimes and polarization.

Both the spectral and temporal calibrations of the fluorescence analyzer are independent of the polarization of the fluorescence. The ~100 ps temporal resolution of the resistive-anode detector is well matched to the ~1 ns FWHM pulses of light produced by the synchrotron storage ring at NSLS taken at U9B with Omnilyzer.

Temporal structure of SR was also applied to such techniques as fluorescence lifetime correlation spectroscopy or time-resolved UV circular dichroism.

The development of imaging techniques has significantly extended the area of possible application of time resolved studies. Observed dynamic development of techniques is leading to **visualization of biological structures and processes in situ** where imaging and spectroscopy information is obtained simultaneously.

To obtain three-dimensional fluorescence images, **fluorescence lifetime imaging microscopy (FLIM)** was used with spectrally and spatially resolved imaging.

Confocal Fluorescence Microscopy is a powerful technique that can be used to reveal fine details of many important biological processes. Scanning microscope combines synchrotron and laser light with confocal microscopy, FLIM, and spectroscopy giving a flexible, wavelength-tunable fluorescence microscope able to produce high resolution data.

This unique combination may help to reveal the fine details of metabolism in cells. Better knowledge of such properties of cell membranes in understanding crucial processes such as transport of substances in and out of cells may be achieved with **Time-resolved Confocal Fluorescence Lifetime** microscope.

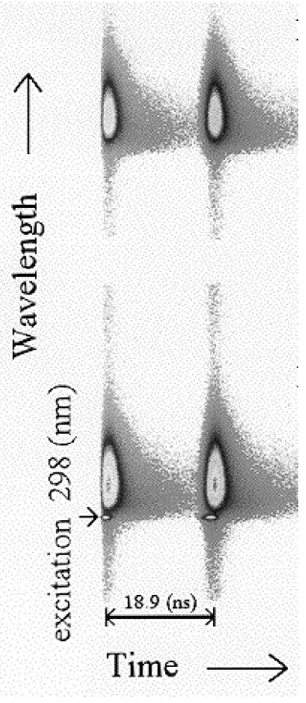

Figure 1.

[L.A. Kelly, J.G. Trunk, K. Polewski, J.C. Sutherland, Simultaneous resolution of spectral and temp-oral properites of UV and visible fluores-cence using single-photon counting with a position-sensitive detector. *Rev. Sci. Instrum.* **66** (1995) 1496-1498].

Multidimensional single-molecule visualization microscope provides the only direct way to investigate signaling events involved with a high spatial and temporal resolution and allows the visualization of the dynamic behavior of individual transmembrane molecules.

The optical system which allows collection of two fluorescence images using vertically and horizontally polarized light gives detailed information on the fluidity of samples such as cell membranes or the viscosity of the environment.

This presentation indicates that application of temporal structure of SR to study biological processes posses great potential which, hopefully, will be explored by many beamlines in the nearest future to deliver important data of biological significance.

L43

DETERMINATION OF PARTIAL STRUCTURE FACTORS USING A THIRD GENERATION SYNCHROTRON SOURCE: In-Se AMORPHOUS FILMS

Andrzej Burian

A. Chelkowski Institute of Physics, University of Silesia, ul. Uniwersytecka 4, 40-007 Katowice, Poland

Keywords: structure factor, In-Se,amorphous thin film

In the structural studies of non-crystalline materials such as glasses, amorphous films and alloys, liquids and other disordered materials there is much interest in maximizing the amount of information about such systems. The structure of non-crystalline materials is usefully expressed in terms of the pair distribution function, which is obtained from the structure factors via the sine Fourier transform. When a sample contain n atomic species there are $n(n\text{-}1)/2$ distinct partial structure factors. It should be noted that knowledge of the partial structure factors is the most complete information that can be obtained from a scattering experiment for non-crystalline materials [1-3].

The resonant changes in the complex X-ray atomic scattering factors defined as

$$f(K,E) = f_0(K) + f'(E) + if''(E)$$

can be used to vary the weights $W_{jk}(K,E)$ of the individual partial structure factors $S_{jk}(K)$ to the total structure factors $S(K,E)$

$$S(K,E) = \sum_{j=1}^{n}\sum_{k=1}^{n} W_{jk}(K,E) S_{jk}(K),$$

where $K=4\pi\sin\theta/\lambda$, λ is the wavelength, E is the energy of the incident photons,

$$W_{jk}(K,E) = c_j c_k \,\mathrm{Re}\frac{f_j(K,E) f_k(K,E)}{< f(K,E) >^2},$$

$$< f >= \left| \sum_{j=1}^{n} c_j f_j \right|^2$$

and c_j indicates the concentration of the jth atomic species.

Anomalous X-ray scattering has been used to determine the partial structure factors for vacuum evaporated In-Se films containing 50 and 66 at.% Se. The X-ray scattering data were collected at the European Synchrotron Radiation Facility (ESRF, Grenoble, France) on the ID01 beam line (anomalous X-ray scattering) using incident photon energies tuned exactly at the Se and In absorption K-edges (12653 and 27950 eV, respectively) and below the edges at 11800 and 27000 eV. The edge positions were determined experimentally for each sample from the fluorescence EXAFS scans. The values of the real and imaginary parts of the atomic scattering factors f' and f'' for the energies at the Se and In edges were calculated from previously recorded EXAFS data using the Kramers-Kronig relationship within the frame of the optical theorem [4]

$$f''(E) = \frac{mcE}{4\pi\hbar e^2}\mu(E)$$

$$f'(E) = \frac{2}{\pi} VP\int_0^{\infty} \frac{E' f''(E)}{E^2 - E'^2} dE' + \Delta f',$$

in which m and e indicate the mass and charge of an electron, c is the light velocity, $\mu(E)$ is the linear absorption coefficient and VP denotes the Cauchy principal value of the integral.

From the determined structure factors the partial pair distribution functions $4\pi r^2\rho_{jk}(r)$ were computed as follows

$$d_{jk}(r) = \frac{2}{\pi}\int_0^{K_{\max}} K[S(K)-1]\frac{\sin(\pi K/K_{\max})}{\pi K/K_{\max}}\sin(Kr)dK$$

$$4\pi r^2\rho_{jk}(r) = c_j\left[4\pi r^2\rho_0 + r d_{jk}(r)\right],$$

where ρ_0 is the macroscopic number density. The availability of the intense radiation source as the third generation synchrotron has made it possible to obtain reliable data much better conditioned when compared with previously obtained results. The obtained results show that both investigated amorphous films exhibit certain degree of chemical disorder within the model based on crystalline InSe. The present findings are compared with the results of similar studies carried out for the amorphous Cd-As amorphous films using a second generation source as well as with the isotopic substitution technique developed for neutron scattering.

References

[1] A. Bienenstock, in: *Methods in the Determination of Partial Structure Factors*, (World Scientific, Singapore, 1993), p. 123.

[2] D. Raoux, in: *Methods in the Determination of Partial Structure Factors*, (World Scientific, Singapore, 1993), p. 130.

[3] Y. Waseda, *Anomalous X-Ray Scattering for Materials Characterization: Atomic-Scale Structure Determination*, (Springer Tracts in Modern Physics, vol. 179, Berlin, 2002).

[4] R.W. James, *The Optical Principles of the Diffraction of X-Rays*, (Bell, London, 1983).

P1

EXAFS ANALYSIS OF Fe^{2+} WATER AND ACETONE BASED SOLUTION

W. Olszewski [1*], K. Szymański [1], P. Zaleski [1], and D. Zając [2]

[1] *Faculty of Physics, University of Białystok, ul. Lipowa 41, 15-424 Białystok, Poland*
[2] *Deutsches Elektronen-Synchrotron-Hasylab, Notkestr. 85, 22607 Hamburg, Germany*

Keywords: Extended X-ray Absorption Fine Structure (EXAFS), aqueous electrolytes, nonaqueous electrolytes

**) e-mail: wojtek@alpha.uwb.edu.pl*

Most of the electrodeposition processes are performed in aqueous solutions. However, in case of chemically reactive metallic layers like Rare Earths, aluminium or alkaline metals, the use of nonaqueous electrolytes is necessary.

We have found a method of electroplating shiny 3*d* metallic layers (Fe, Co, Ni, Cu and Zn) from new type of electrolyte, which consists mainly of acetone [1]. Small concentration of cations (of the order of 10^{-2} Mol/dm^3) and the same current conditions of deposition for each element make this deposition method promising for applications.

Because of very small content of water, the electrolyte cannot be classified either as aqueous or as non-aqueous. We investigate the aqueous and nonaqueous electrolytes by Extended X-ray Absorption Fine Structure (EXAFS) to see the possible differences in local structure of the cations.

The initial measurements were performed at DORIS ring at Hasylab, DESY. Typical results are shown in Fig. 1.

Experiments indicate that the shape of absorption curve of water solution weakly depends on the cation concentration. Obtained absorption curves are similar to the published measurement results for aqueous concentrated solutions of cations [2, 3]. As can be seen in Fig. 1, the shape of acetone based solutions is different. We note that the differences are present at extended as well as at near absorption edge region. Our results indicate that local structure of 3*d* cations in aqueous and acetone solutions are remarkably different.

Acknowledgements: This work was supported by the I-20060174 EC project.

References

[1] W. Olszewski, K. Szymański, M. Biernacka, R. Sobiecki, "3*d*-metallic layers electrochemically deposited from nearly nonaqueous electrolyte", *Mater. Sci.-Poland* (2007), in press.

[2] M. Benfatto, P. D'Angelo, S. Della Longa, N.V. Pavel, "Evidence of distorted fivefold coordination of the Cu^{2+} aqua ion from an x-ray-absorption spectroscopy quantitative analysis", *Phys. Rev. B* **65** (2002) 174205.

[3] P. D'Angelo, M. Benfatto, S. Della Longa, N.V. Pavel, "Combined XANES and EXAFS analysis of Co^{2+}, Ni^{2+}, and Zn^{2+} aqueous solution", *Phys. Rev. B* **66** (2002) 064209.

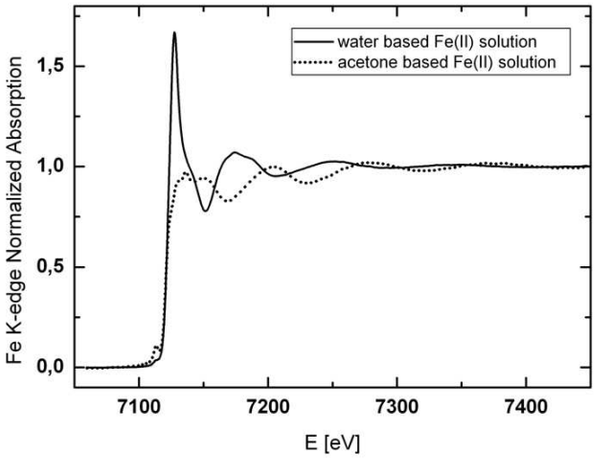

Figure 1. Fe *K*-edge normalized absorption of Fe^{2+} electrolytes based on water and on acetone solutions.

P2

X-RAY ABSORTPTION SPECTROSCOPY FOR PARTIALLY DEUTERATED AMMONIUM HEXACHLOROPALLADATE

D.A. Zając [1,2*], Z.T. Lalowicz [2], A. Birczyński [2], and A.M. Szymocha [2]

[1] *Hasylab at DESY, Notkestrasse 85, 22607 Hamburg, Germany*

[2] *H. Niewodniczański Institute of Nuclear Physics of PAN, Radzikowskiego 152, 31-342 Kraków, Poland*

Keywords: EXAFS, NMR, hexachlorometallate, deuteron, relaxation, ammonium ion

**) e-mail: dariusz.zajac@desy.de*

Ammonium hexachloropalladate belongs to the family of ammonium hexachloro-metallates $(NH_4)_2MCl_6$, where M is 3*d* metal *eg*.: Pd, Pt, Ir, Os or *p*-elements *eg*.: Se, Sn, Te, Pb. The compounds with 3*d* elements exhibit a stronger covalent M-Cl bonding and a smaller unit cell, compared to the *p*-elements [1]. First NMR observations show a decrease of the spin-lattice relaxation time (T_1) at the order-disorder phase transition, which is related to ordering of the ammonium cations [2]. Additionally, the deuteration can induce a transition from the cubic phase to the low symmetry phase [3].

In this paper, we present EXAFS data, together with NMR T_1 relaxation time data, for ammonium hexachloropalladate samples deuterated at 30%, 50% and 70%, labelled as D30, D50 and D70, respectively. XAS experiments have been done at beamline C at Hasylab at DESY, Hamburg, Germany in the fluorescence mode at the Pd K-edge. NMR experiments had been done at the Department of Magnetic Resonance Spectroscopy at Institute of Nuclear Physics PAN, Krakow, Poland.

XANES experiments clearly show that all deuterated samples have a Pd:K edge position shifted by +2.0(2) eV compared to the metallic Pd (used as a reference) edge position 24350 eV. EXAFS experiments reveal clearly that the first shell Cl peak is observed at 2.189(5) Å, 2.196(5) Å and 2.195(5) Å for 30%, 50% and 70% deuterated samples, respectively (Fig. 1). The full-width-half-maximum (FWHM) of this line was derived: 0.33(1) Å, 0.32(1) Å and 0.32(1) Å, for D30, D50 and D70, respectively. The change of position and the change of the full-width-half-maximum for the first shell Cl peak do not depend on temperature (Fig. 2). Peaks of next-neighbour shells are also visible: N at 4.3(2) Å and Cl at 5.4(3) Å and will be later analysed.

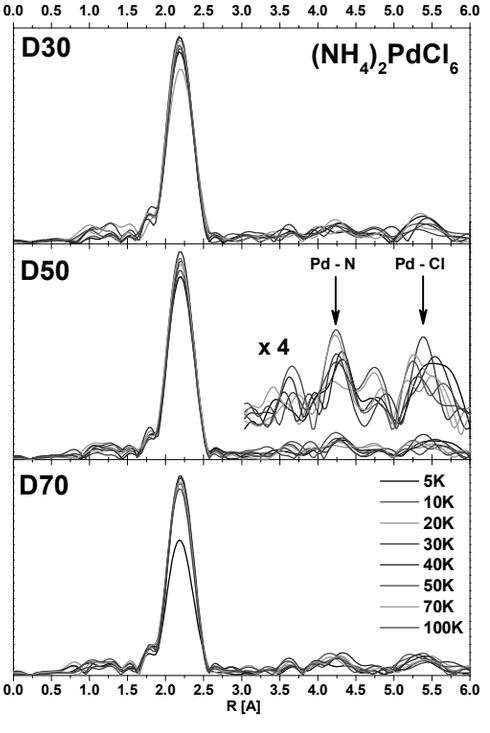

Figure 1. EXAFS spectra of 30% (D30), 50% (D50) and 70% (D70) deuterated ammonium hexachloropalladate. The enlarged region of higher *R* is presented for 50% deuteration.

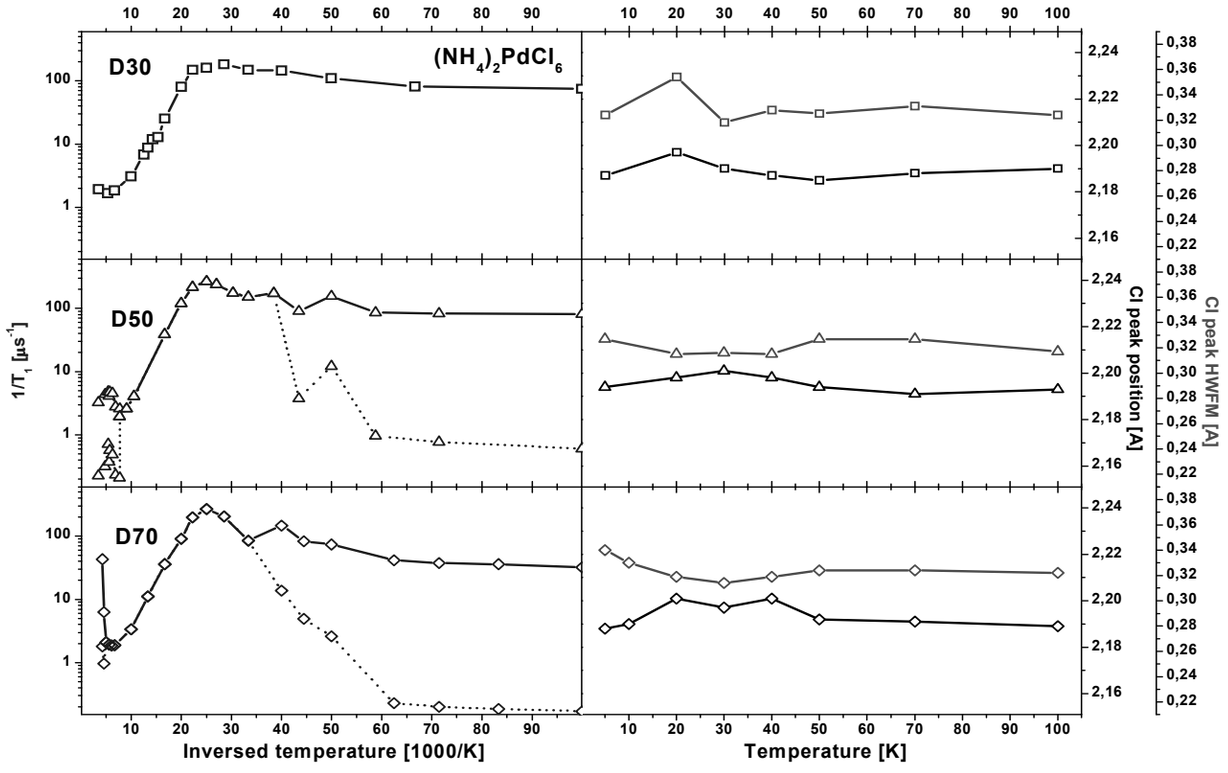

Figure 2. Deuteron relaxation rate (left, blue line), the centre of the first neighbour Cl peak (right, black line) and FWHM of this peak (right, green line) for 30% (squares), 50% (triangles) and 70% (diamonds) deuterated ammonium hexachloropalladate.

The maximum of the spin-lattice relaxation rate can be explained by rotation of the ammonium tetrahedrons about threefold symmetry axes. For 50% and 70% deuterated samples two exponential behaviour of T_1 is also observed. The unchanged position of the first Cl peak together with unchanged FWHM indicates that the ammonium ion rotation has a local character and does not affect the Pd and Cl crystallographic sublattice. Only between about 25 K and 50 K there are small shifts in both values which may be related to a correlation frequency of ammonium ions of the order of 10^8 s^{-1} in this range.

Acknowledgements: Samples were kindly donated by M. Prager, Forschungszentrum Jülich.

References

[1] A. Birczyński, Z.T. Lalowicz, Z. Łodziana, "Rotational barriers in ammonium hexachlorometallates as studied by NMR, tunnelling spectroscopy and ab initio calculations", *Chem. Phys.* **299** (2004) 113-122.

[2] M. Punkkinen, E.E. Ylinen, "Spin–lattice relaxation via limited jumps in NH_4 compounds", *Physica B* **337** (2003) 111-121.

[3] Y. Kume, H. Muraoka, O. Yamamuro, T. Matsuo, "Deuteration-induced phase transition in ammonium hexachloroplumbate", *J. Chem. Phys.* **108** (1998) 4090.

P3

WHITE BEAM SYNCHROTRON RADIATION AND CONVENTIONAL X-RAY TOPOGRAPHY OF GdCOB:Y CRYSTAL

E. Wierzbicka [1,2*], J. Gronkowski [2], M. Lefeld-Sosnowska [2], and J. Härtwig [3]

[1] *Institute of Electronic Materials Technology, 01-919 Warsaw, Poland*
[2] *Institute of Experimental Physics University of Warsaw, 00-681 Warsaw, Poland*
[3] *E.S.R.F., BP220, 38043 Grenoble, France*

Keywords: defects, X-ray topography, oxides, nonlinear optical, synchrotron topography

**) e-mail: eolsz@fuw.edu.pl*

The non-linear optical (NLO) crystals are very important for the development of all solid state lasers. Visible and UV solid state lasers are used for industrial or medical applications.

The promising crystals in this fields are from the family of rare earth calcium oxyborates $ReCa_4O(BO_3)_3$ (ReCOB), where Re = La^{3+}, Gd^{3+}, Sm^{3+}, Y^{3+}, Nd^{3+}, Er^{3+}. Their crystal structure belongs to the monoclinic system with the space group *Cm*. The excellent non-linear optical (NLO) properties of these crystals allow its application for frequency conversion. Moreover, they can be grown by the Czochralski technique [1, 2]. The crystals are non-hygroscopic, easy to polish and of high hardness. There exist many studies about its optical properties [3].

In particular, GdCOB: 22% at. Y is one of the most attractive non-linear optical crystal. Phase-matched second and third harmonic generation in Nd:YAG laser at room temperature is possible in these crystals [4].

The non-linear optical properties of those crystals depend on their crystalline quality. Crystal lattice defects cause lattice strain which change the optical properties (*e.g*. reflective indices).

Extended crystal lattice defects in non-doped GdCOB crystals have been revealed for the first time by X-ray transmission topography in [5, 6]. Conventional, monochromatic beam SR and white beam SR X-ray topography, all in back-reflection geometry, have been successfully applied to thick GdCOB crystals in [7, 8].

The aim of this paper was the investigation of extended defects in GdCOB: 22% at. Y.

The contrasts of long straight dislocations of strong edge components were observed (D1) in topographs of GdCOB:Y. A practically dislocations free circular region can be seen in the sample centre (core). Black contrasts of circular shape corresponding to inclusions were observed as well. Topographs revealed dislocation loops generated around the inclusion. The very weak diffraction contrasts of segregation fringes can be recognized.

The diffraction contrasts of dislocations (D1) depend on the absorption of X-rays in crystal (exactly on the value of μt). In topographs obtained for $MoK\alpha_1$ (μt = 3.4) we can observe black or white diffraction contrasts (Fig. 1). The synchrotron topographs (μt < 0.6) allowed receiving only a black diffraction contrast (Fig. 2). The explanation of these features of diffraction contrasts is possible according the dynamic diffraction theory for weakly deformed crystals, taking into account the absorption effects.

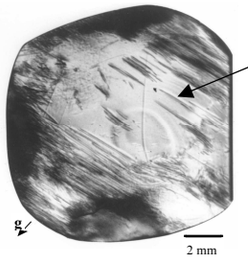

Figure 1. X-ray transmission projection topograph of sample GdCOB: 22% at. Y, $MoK\alpha_1$ radiation: 400 reflection, μt = 3.4.

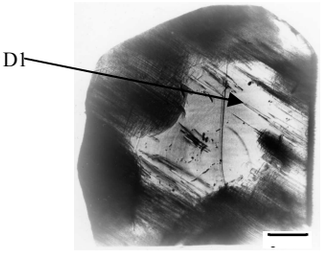

Figure 2. SR White beam transmission topograph, of sample GdCOB: 22% at.Y, λ = 0.1673 Å, 5 $\bar{1}$ 1 reflection, μt < 0.6).

Acknowledgements: The authors thank to S. Ganschow for supplying the crystal and A. Pajączkowska for discussions. This work was partly financed by Polish Ministry of Science and Higher Education, project no. N202 029 32/0780 (2007-2008).

References

[1] G. Aka, A. Kahn-Harari, D. Vivien, F. Salin, J. Godard, J. M. Benitez, *Eur. J. Solid State Inorg. Chem.* **33** (1996) 727.

[2] A. Pajączkowska, A. Kłos, B. Hilczer, N. Menguy, A. Novosselov**,** *Crys.l Growth Des.* **1** (2001) 363.

[3] T.N. Khamaganova, V.K. Trunow, B.F. Dzhurinskii, *Russ. J. Inorg. Chem.* **36** (1991) 484.

[4] H. Furuya, M. Yoshimura, T. Kobayashi, K. Murase, Y. Mori, T. Sasaki, *J. Cryst. Growth* **198/199** (1999) 560.

[5] M. Lefeld-Sosnowska, E. Olszyńska, A. Pajączkowska, A. Kłos*, J. Cryst. Growth* **262** (2004) 388.

[6] E. Wierzbicka, M. Lefeld-Sosnowska, A. Kłos, A. Pajączkowska, *phys. stat.sol. (a)* **203** (2006) 220.

[7] M. Lefeld-Sosnowska, E. Olszyńska, W. Wierzchowski, K. Wieteska, W. Graeff, A. Pajączkowska, A. Kłos, *J. Alloys Compd.* **382** (2004) 153.

[8] W. Wierzchowski, K. Wieteska, W. Graeff, E. Wierzbicka, M. Lefeld-Sosnowska, *J. Alloys Compd.* **401** (2005) 69.

P4

X-RAY TOPOGRAPHIC STUDIES OF CRYSTAL LATTICE DEFECTS IN $Ca_{0.25}Sr_{0.75}NdAlO_4$ SINGLE CRYSTAL

A. Malinowska [1, 2*], M. Lefeld-Sosnowska [3], K. Wieteska [4], W. Wierzchowski [1], W. Graeff [5], and A. Pajączkowska [1]

[1] *Institute of Electronic Materials Technology, Wólczyńska 133, 01-919 Warsaw, Poland*
[2] *Faculty of Physics Warsaw University of Technology, Koszykowa 75, 00-662 Warsaw, Poland*
[3] *Institute of Experimental Physics, University of Warsaw, Hoża 69, 00-681 Warsaw, Poland*
[4] *Institute of Atomic Energy, 05-400 Otwock-Świerk, Poland*
[5] *HASYLAB at DESY, Notkestr. 85, D-22603 Hamburg, Germany*

Keywords: X-ray topography, crystal lattice defects, solid solution

**) e-mail: malinows@if.pw.edu.pl*

Oxide materials of general composition $ABCO_4$ (where A = Ca, Sr, Ba, B = La, Nd, Pr and C = Al, Ga) with the tetragonal perovskite-related K_2NiF_4-type structure are promising substrate materials for high temperature superconducting (HTSc) thin films, elements of thermal radiation receivers and other electronic devices due to their electrochemical and thermal properties and good lattice matching [1]. Further improvement of lattice matching can be obtained using crystals of solid solution in the systems $A_xA'_{1-x}BCO_4$ or $ABC_xC'_{1-x}O_4$ when the selection of the A/A' or C/C' ratio give the possibility of obtaining the proper lattice parameter [2-4]. Crystals of high structural quality are required for the applications so the characterisation of crystal lattice defects is of great importance.

In the present paper the defect structure was studied in the single crystal of $A_xA'_{1-x}BCO_4$ type with the formula $Ca_{0.25}Sr_{0.75}NdAlO_4$ The investigations were performed by conventional projection x-ray transmission topography and synchrotron radiation white beam back reflection topography.

The main defects revealed with these topographic methods were striation fringes associated with non-homogenous crystal chemical composition, which is typical for solid solutions and doped crystals (Figs. 1, 2). They are seen as diffraction contrasts of distinct fringes in the form of concentric rings. A significantly strong effect of lattice deformation associated with striation was revealed by white beam back reflection topograph with superimposed section topograph. The local lattice misorientation (especially associated with lattice parameter change) manifests itself in the bending of the section image (Fig. 2).

Apart from striations the topographs revealed a significant concentration of individual defects, most probably a kind of inclusions (Figs. 1, 2). The nature of these defects is under investigation.

Acknowledgements: The technical assistance of J. Bondziul is much appreciated. This work was partly financed by Polish Ministry of Science and Higher Education, project no. N202 011 32/0609 (2007-2008).

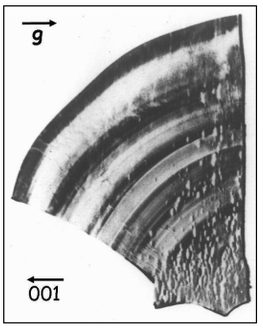

Figure 1. X-ray projection transmission topograph of the sample cut out from $Ca_{0.25}Sr_{0.75}NdAlO_4$ single crystal.

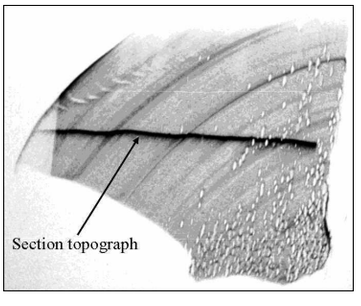

Figure 2. Synchrotron radiation white beam back reflection projection topograph with superimposed section topograph.

References

[1] A. Pajączkowska, A. Gloubokov, *Prog. Cryst. Growth Charact.* **36** (1998) 123.
[2] A. Novoselov, M. Ryumin, G. Pushkina, F. Spiridonov, G. Zimina, L. Komissarova, A. Pajączkowska, *Cryst. Res. Technol.* **40** (2005) 405.
[3] A. Novoselov, G. Zimina, A. Filaretov, O. Shlyakhtin, L. Komissarova, A. Pajączkowska, *Mater. Res. Bull.* **36** (2001) 1789.
[4] A. Novoselov, G. Zimina, L. Komissarova, A. Pajączkowska, *J. Cryst. Growth* **287** (2006) 305.

P5

ELECTRONIC STRUCTURE OF Mn DEPOSITED ZnMnO FILMS GROWN BY ALD TECHNIQUE – A RESONANT-PHOTOEMISSION-SPECTROSCOPY STUDY

I.A. Kowalik [1,2*], E. Guziewicz [1], Ł. Wachnicki [1], K. Kopalko [1], A. Wójcik [1], E. Łusakowska [1], and M. Godlewski [1]

[1] *Institute of Physics, Polish Academy of Sciences, Al. Lotników 32/46, PL-02-668 Warsaw, Poland*
[2] *MAX-lab, Lund University, Box 118, SE-22100 Lund, Sweden*

Keywords: zinc oxide, manganese, resonant photoemission, electronic structure, atomic layer deposition

**) e-mail: iwona.kowalik@maxlab.lu.se*

Zinc oxide (ZnO) structures have attracted rapidly increased attention in the last few years. This wide-band gap semiconductor (ultraviolet region E_g ~3.3 eV at room temperature) is a promising material not only as a base material for realizing transparent DMSs but also because of its electrical, optoelectronic and photochemical properties. These aspects led to many applications of this material for solar cells, transparent electrodes, gas sensors, varistors, piezoelectric transducers and optoelectronic blue/UV light emitting and light detecting devices. Mn doped ZnO is also regarded as promising material for spintronic applications since room temperature ferromagnetism was predicted for this material.

We report on resonant photoemission study of ZnMnO thin films grown at low temperature by Atomic Layer Deposition (ALD) method on Si and GaAs substrates [1]. The clean surface of ZnMnO was gradually covered with Mn in a few steps up to a thickness of 4 ML. Such a structure was then annealed in two steps – first one up to 250°C and the second one at about 450°C.

Resonant photoemission measurement, carried out for photon energies close to Mn 3*p*→3*d* transition, was applied to observe changes of Mn 3*d* states distribution in the valence band region after each stage of the experiment. The sets of photoelectron energy distribution curves (EDC) were measured for clean ZnMnO/GaAs and ZnMnO/Si surfaces and as function of Mn coverage for ZnMnO/Si structure at photon energy range 40-130 eV. Comparison of EDC taken at resonance and antiresonance for clean and Mn-enriched ZnMnO surface enabled us to reveal the Mn 3*d*-related contribution to the spectra. We observe that after annealing the Mn contribution at the Fermi edge disappeared, what indicates that whole deposited Mn built up into the ZnMnO matrix. This suggests that in case of ZnMnO grown by the ALD technique Mn easier builds up into ZnO layer than it was observed for ZnMnO monocrystal [2].

After each stage of the experiment we observed also the Mn 3*p* state at higher binding energy. At 3 ML of Mn deposition two Mn 3*p* peaks appeared (at about 41 and 48 eV of binding energy), which were getting stronger when the Mn coverage was getting thicker. This is an evidence that two different manganese states are observed in the ZnMnO interface region. After annealing one of the Mn 3*p* peaks disappeared, which means that only one manganese state is present in the obtained ZnMnO material.

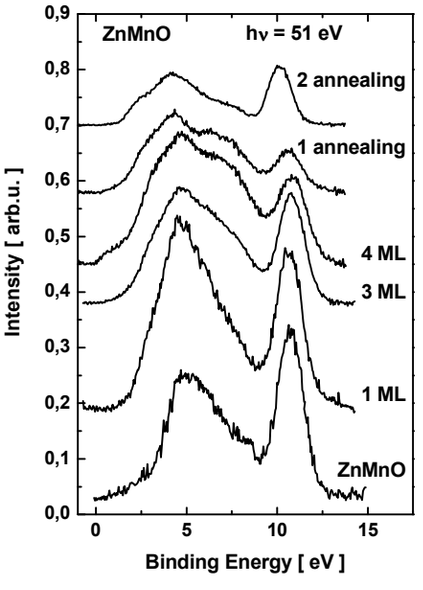

Figure 1. EDC set obtained for ZnMnO/Si sample covered stepwise covered with Mn and annealed, measured for 51 eV of photon energy (the resonance conditions).

Acknowledgements: The work was supported by polish grant of Ministry of Science and High Education 1 P03B 015 29 and by the European Community - Research Infrastructure Action under the FP6 "Structuring the European Research Area" Programme (through the Integrated Infrastructure Initiative "Integrating Activity on Synchrotron and Free Electron Laser Science").

References

[1] A. Wójcik *et al*., "Magnetic properties of ZnMnO films grown at low temperature by atomic layer deposition", *Appl. Phys. Lett.* **89** (2006) 051907.

[2] E. Guziewicz *et al*, "Zn(Mn)O surface alloy studied by synchrotron radiation photoemission", *Acta Phys. Polon.* **108** (2005) 689.

P6

CRYSTAL AND TWIN STRUCTURES OF THE ZrO_2:Sc_2O_3 CRYSTALS

T. Tataryn [1*], D. Savytskii [1], L. Vasylechko [1], D. Trots [2], and U. Bismayer [3]

[1] *Lviv Polytechnic National University, 12 Bandera Str., 79013, Lviv, Ukraine*
[2] *HASYLAB, DESY, Notkestr. 85, D-22603 Hamburg, Germany*
[3] *Mineralogisch-Petrographisches Institut, Universität Hamburg, Grindelallee 48, D-20146 Hamburg, Germany*

Keywords: crystal, powder diffraction, Laue method, phase transition, ferroelastic domain structure

**) e-mail: tarastr@yandex.ru*

An increasing interest in electrolyte materials for advanced energy applications demands investigation of their real structure and its influence on the physical properties. It is relevant to investigate the crystal and twin structures of electrolytes, for which the considered properties depend on domain walls distribution [1]. ZrO_2 doped with Sc is considered as prospective solid electrolyte for application in solid oxide fuel cells (SOFCs).

The present work is devoted to structure investigation of ZrO_2 doped by Sc_2O_3 (10 mol.%) (ZSO-10) and determination the twin structure in trigonal phase of the ZSO-10 crystal in a wide temperature range of 300-1253 K.

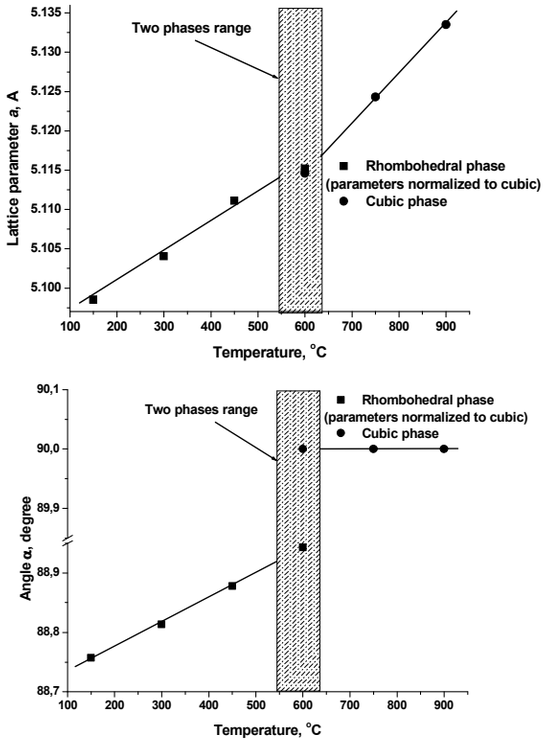

Figure 1. Temperature dependencies of the lattice parameters of ZSO-10. Parameters of the rhombohedral cell are normalized to the cubic ones.

In order to study the thermal behavior of the crystal structure of ZrO_2:Sc_2O_3 the structure investigations were carried out at a powder diffractometer at beamline B2 (HASYLAB/DESY). High-temperature diffraction data were collected in the Debye-Scherrer capillary geometry using the on-site readable image plate detector OBI and STOE furnace. Data analysis was carried out by the Rietveld method using the WinCSD program package. Determination of domains orientations was performed using the Laue method. The white beam synchrotron experiments have been carried out using the Kappa-diffractometer at HASYLAB beamline F1 equipped with MAR CCD system and a gas-stream heating device.

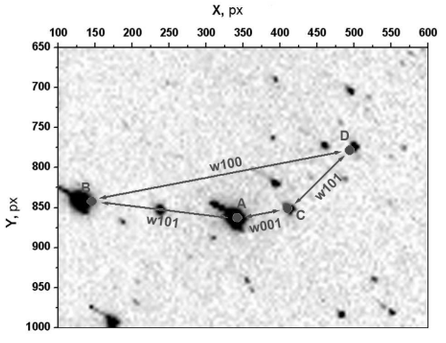

Figure 2. A section of Laue pattern collected at a CCD-sample distance of 300.4 mm and calculated spot positions for observed twin laws (with respect to reference domain *A*).

The powder diffraction examination revealed that rhombohedral structure (space group $R\bar{3}$) of ZSO-10 transforms into high-temperature cubic structure (space group $Fm\bar{3}m$) at 873 K. Temperature dependencies of the lattice parameters are presented in Fig. 1.

Analysis of Laue patterns collected at room temperature confirms that the ZSO-10 crystal was twinned relatively to intersecting (101) and (100)/(001) mirror planes in the rhombohedral phase (Fig. 2).

Acknowledgments: The work was supported by WTZ (UKR 07/009) and Ukrainian Ministry of Science (project "Segnet").

References

[1] M. Kurumada, E. Iguchi, D. Savytskii, "Correlation between high ionic conductivity and twin structure in $La_{0.95}Sr_{0.05}Ga_{0.9}Mg_{0.1}O_{3-x}$", *J. Appl. Phys.* **100** (2006) 014107.

P7

BEST - BEAMLINE FOR EDUCATION AND SCIENTIFIC TRAINING - A NEW VUV BEAMLINE AT *BESSY II*

Hendrik Vita *, **Thorsten Zandt, Lenart Dudy, Christoph Janowitz, and Recardo Manzke**

Institut für Physik, Humboldt-Universität zu Berlin, Newtonstraße 15, 12489 Berlin, Germany

**) e-mail: hendrikv@physik.hu-berlin.de*

Keywords: VUV, beamline, photoelectron spectroscopy, training

In the following description a high-resolution 5m normal–incidence–monochromator beamline behind the dipole DIP 03–1B at BESSY II is introduced.

The beamline 'BEST' is designed for high resolution photoelectron spectroscopy utilizing a Scienta SES-2002 electron analyzer, which is permanently placed as an endstation at the beamline.

The energy range of the beamline is 3-40 eV. A high precision manipulator on a closed-cycle He cryostat allows angle resolved measurements over 2π sterian below 10 K.

On this beamline students and young scientists will be introduced and continuously qualified into the fascinating possibilities of synchrotron radiation research. Optical design of the beamline and preliminary performance results will be discussed.

P8

PHASE AND STRUCTURAL BEHAVIOUR OF THE $PrAlO_3$–$LaAlO_3$ PSEUDO-BINARY SYSTEM

T.V. Basyuk [1*], T. Tataryn [1], L.O. Vasylechko [1], S. Fadyeev[1], I.I. Syvorotka [2], D. Trots [3], and R. Niewa [4]

[1] *Lviv Polytechnic National University, Semiconductor Electronics Department, 12 Bandera Str., 79013 Lviv, Ukraine*
[2] *SRC "Carat", 202 Stryjska Str., 79031 Lviv, Ukraine*
[3] *Darmstadt University of Technology, Institute for Materials Science, Petersenstraße 23, 64287 Darmstadt, Germany*
[4] *Technische Universität München, Department Chemie, Lichtenbergstraße 4, 85747 Garching b. München, Germany*

Keywords: rare-earth aluminate, perovskite, phase diagram, phase transition

At room temperature, rare earth aluminates $RAlO_3$ were found to crystallize in rhombohedral $R\bar{3}c$ (R = La, Pr, Nd), orthorhombic *Pbmn* (R = Sm–Lu, Y) and tetragonal *I*4/*mcm* ($CeAlO_3$) structures. In general, two types of phase transformations are known for $RAlO_3$ perovskites. A continuous phase transition $Pm\bar{3}m$–$R\bar{3}c$ is typical for $RAlO_3$ compounds containing "light" rare-earth metals (R = La, Ce, Pr, Nd), whereas a first-order phase transformation $R\bar{3}c$–*Pbnm* is inherent for $SmAlO_3$, $GdAlO_3$ and $EuAlO_3$. The respective praseodymium aluminate shows an exceptional behaviour among the $RAlO_3$ compounds. Besides a high-temperature (HT) phase transition from rhombohedral to cubic perovskite structure, $PrAlO_3$ undergoes a sequence of low-temperature (LT) phase transformations, which is a solely exception among all AMO_3 compounds with perovskite structures [1]. A similar complex behaviour of the phase transformations has been observed for $CeAlO_3$-based perovskites [2].

In order to study the phase and structural behaviour in the $PrAlO_3$–$RAlO_3$ (R = La) pseudo-binary systems a series of $Pr_{1-x}R_xAlO_3$ samples (x = 0.1–0.9) was prepared by a combination of solid state reaction and arc melting in Ar atmosphere. Phase analyses of the samples were performed by X-ray powder diffraction. *In situ* LT and HT structural investigations have been performed by using a high-resolution powder diffraction technique applying synchrotron at beamline B2 of the synchrotron laboratory HASYLAB at DESY.

It was established, that a continuous solid solution $Pr_{1-x}La_xAlO_3$ with rhombohedral perovskite structure exists at ambient temperature. Lattice parameters and cell volumes increase monotonically with increasing La content.

At elevated temperatures, the solid solutions $Pr_{1-x}La_xAlO_3$ undergo continuous phase transitions from rhombohedral to cubic structures. Structural transformations $R\bar{3}c$–*Imma* and *Imma*–*C*2/*m* were observed in the majority of specimens below room temperature. The temperatures of both HT and LT phase transitions decrease with decreasing Pr content in $Pr_{1-x}La_xAlO_3$, but these transformations are different in nature. The HT transition is induced by a structural deformation and its temperature decreases with increasing R-cation radius and tolerance factor. The low temperature transitions in this system are caused by electronic effects and the temperatures decrease with decreasing Pr content. Structural parameters of all five modifications of the perovskite structure found for $Pr_{1-x}La_xAlO_3$ at different compositions and temperatures are refined.

Based on the results of *in situ* synchrotron powder diffraction examinations, DTA/DSC measurements and available literature data, the phase diagram of the $PrAlO_3$–$LaAlO_3$ pseudo-binary system has been constructed (Fig. 1).

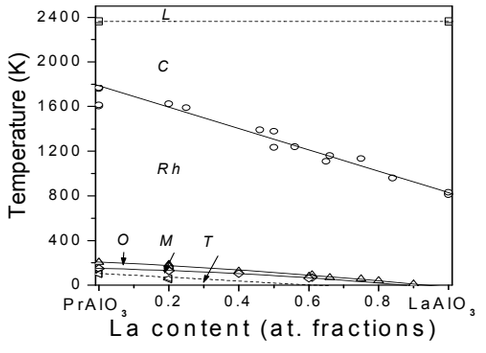

Figure 1. Phase diagram of the $PrAlO_3$–$RAlO_3$ pseudo-binary system. The symbols L, C, Rh, O, M and T indicate liquid, cubic, rhombohedral, orthorhombic, monoclinic and (pseudo)-tetragonal phase fields, respectively.

Acknowledgements: The work was supported in part by the Ukrainian Ministry of Education and Sciences (Project "Segnet") and ICDD Grant-in-Aid program. T. Basyuk gratefully acknowledges support from DAAD *(Leonhard–Euler program)*. T. Tataryn thanks the Panalytical B.V. for the financial support permitting for participation in ISSRNS'2008.

References

[1] M.A. Carpenter, C.J. Howard, B.J. Kennedy, K.S. Knight, "Strain mechanism of order-parameter coupling through successive phase transitions in $PrAlO_3$", *Phys. Rev. B* **72** (2005) 024118.

[2] L.O. Vasylechko, A. Senyshyn, D. Trots, R. Niewa, W. Schnelle, M. Knapp, "$CeAlO_3$ and $Ce_{1-x}R_xAlO_3$ (R=La, Nd) solid solution: Crystal structure, thermal expansion and phase transition", *J. Solid State Chem.* **180** (2007) 1277-1290.

P9

MICROTOMOGRAPHY OF RENAL CALCULI

G. Tatoń [1*], E. Rokita [1,2], A. Wróbel [1,2], F. Beckmann [3], P. Thor [4], and M. Worek [5]

[1] *Jagiellonian University Medical School, Department of Biophysics, Lazarza 16a, 30531 Cracow, Poland*
[2] *Jagiellonian University, Institute of Physics, Reymonta 4, 30059 Cracow, Poland*
[3] *GKSS-Research Center, Max-Planck-Straße 1, 21502 Geesthacht, Germany*
[4] *Jagiellonian University Medical School, Chair of Pathophysiology, Czysta 18, 31121 Cracow, Poland*
[5] *St. Lukas Hospital, Department of Urology, Lwowska 171a, 33100 Tarnów, Poland*

Keywords: renal calculi, nephrolitiasis, microtomography, microstructure

**) e-mail: mmtaton@cyf-kr.edu.pl*

The aim of the study was the investigation of renal calculi structure with the use of microtomography utilizing synchrotron radiation. Two problems were considred: (1) if the renal calculi developed in the first and second nephrolitiasis episodes have similar microstructure and (2) are there differences between the structure of stones which elemental composition is different from the average renal calculi population.

The renal calculi developed in the first and second nephrolitiasis episodes were collected from three patients in a standard medical procedures applied in nephrolitiasis (6 samples). A pieces of the stones with dimensions suitable for the microtomographic measurements were prepared and measured.

Additionally the samples of renal stones with unusual elemental composition were choosen and prepared for measurements. The elemental composition was previously investigated by IR spectroscopy. The cases characterised by unusuall concentrations of Mg, Ca and S were taken into consideration (5 samples). The structure as weel as the density distributions are considered so the density standard was also investigated. The standard was preparet as the pastille-sandwitch made from 5 layers of substances observed in typical renal stones (uric acid, hydroxyapatite, struvite, cysteine and calcium oxalate) (Fig. 1).

Finally, twelve samples were investigated (eleven renal stone pieces and one density standard). The beamline BW2 on HASYLAB Hamburg, Germany) equipped with microtomographic scanning system was utilized. The energy of 21 keV was applied. Achieved image resolution was about 7.6 μm. The 3D images of investigated samples were reconstructed (each of about 2 GB large) and analyzed. Achieved voxel size in reconstructed images is about 4 μm and Fig. 2. The sample of reconstructed images is presented in Fig. 2.

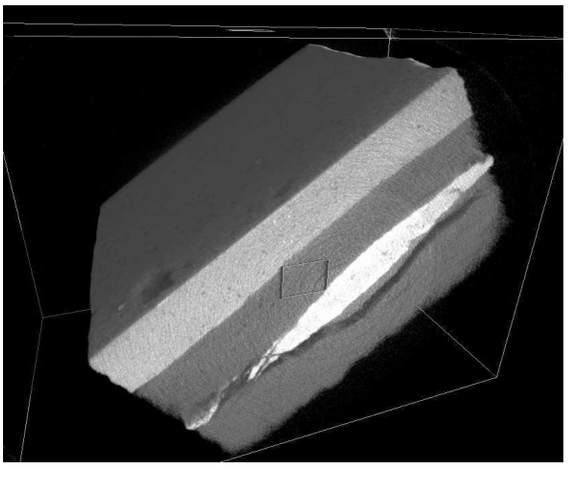

Figure 1. The reconstructed 3D image of investigated density standard. The structure of sandwitch layers is well visible.

The quantitative analysis of collected data is still in progress but first conclusions can be drown. The assumption that the renal calculi developed in the first and second stage of nephrolitiasis have different structures was not confirmed. The differences could be caused by the treatment and diet introduced for patients after first nephrolitiasis occurrence. Only in one pair of the renal calculies developed in the first and second nerphrolitiasis episodes distinct differences were observed (Fig. 3).

The microstructure of renal calculies representing unusual elemental compositions differs from the average population but the parameters describing quantitatively the microstructure have to be developed in order to draw reasonable conclusions.

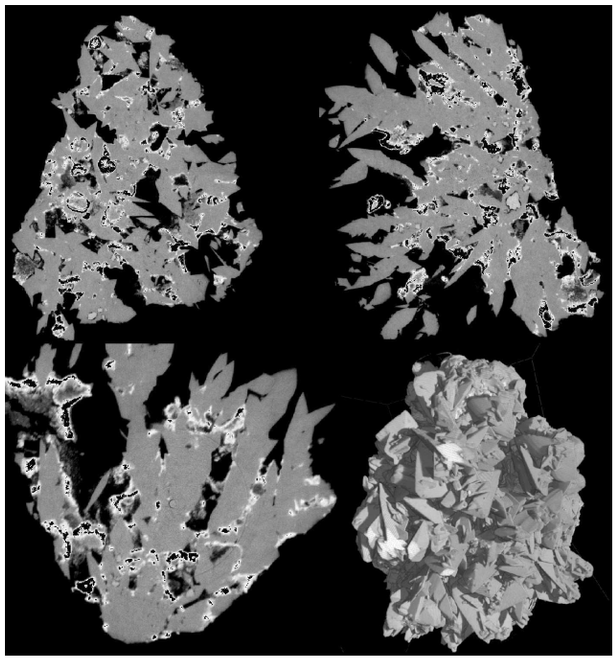

Figure 2. The reconstructed 3D image of a renal calculi sample and its cross sections in orthogonal directions.

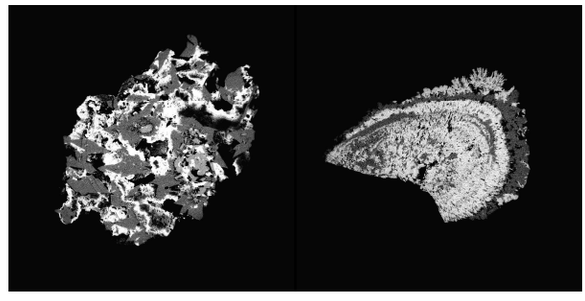

Figure 3. The cross-sections through the reconstructed 3D microtomographic images of two renal calculi samples. The sample collected during the first episode of recurrent nephrolithiasis is shown on the left while the cross-section of the second episode is presented on the right. Brighter areas represent regions characterised by higher densities.

Acknowledgement: Work supported by the European Community - Research Infrastructure Action under the FP6 "Structuring the European Research Area" Programme through the Integrated Infrastructure Initiative "Integrating Activity on Synchrotron and Free Electron Laser Science" *Contract RII3-CT-2004-506008 (IA-SFS).*

P10

EFFECT OF ANNEALING ON THE STRUCTURAL PROPERTIES OF Si:Mn

P. Romanowski [1*], J. Bak-Misiuk [1], E. Dynowska [1], A. Misiuk [2], J.Z. Domagala [1], and W. Caliebe [3]

[1] *Institute of Physics, Polish Academy of Sciences, Al. Lotnikow 32/46, PL-02668 Warsaw, Poland*
[2] *Institute of Electron Technology, Al. Lotnikow 46, PL-02668 Warsaw, Poland*
[3] *HASYLAB at DESY, Notkestr. 85, D-22603 Hamburg, Germany*

Keywords: silicon, manganese, implantation, X-ray, diffraction, synchrotron, structure

[*]) *e-mail: przemyslaw.romanowski@ifpan.edu.pl*

Ferromagnetic ordering in silicon implanted with Mn^+ ions (Si:Mn) has been reported recently. This ordering is related to the structure of Mn-enriched near-surface layer of the implanted and subsequently processed material [1, 2].

The aim of this work was to investigate an influence of Mn-implantation dose, D, substrate temperature during implantation, T_s, and post-implantation temperature of annealing, T_a, on the structure of Si:Mn exhibiting magnetic properties [2, 3], prepared from Si with various interstitial oxygen concentrations, c_o.

Single crystalline Czochralski-silicon wafers were implanted with 160 keV Mn^+ ions to doses, $D = 2\times10^{15}$, 1×10^{16} or 1.2×10^{16} cm^{-2}, T_s = 340 or 610 K. Projected range (R_p) of Mn^+ was equal to 140 ± 50 nm. The c_o value, in Cz-Si was up to 9×10^{17} cm^{-3}. Si:Mn was processed after implantation for 1 h at T_a up to 1270 K under ambient pressure (10^5 Pa).

Structural characterization of the near-surface polycrystalline layers was performed using synchrotron radiation at the W1.1 beamline at DESY-HASYLAB (Hamburg). The monochromatic X-ray beam of wavelength λ = 1.54056 Å was used. The phase analysis of the near-surface layers was performed using coplanar 2θ scans in the grazing incidence geometry.

The structure of Si:Mn samples was also investigated by X-ray diffractometry in the double and triple axis configurations using high-resolution Phillips-MRD diffractometer. Reciprocal space maps (RSMs) for the 004 reflections were registered.

For Cz-Si:Mn prepared at T_s = 340 K, with $D = 2\times10^{15}$ cm^{-2} or 1×10^{16} cm^{-2}, the implanted layer remains to be amorphous both after implantation and after annealing at T_a = 610 K (Fig. 1a). The reflections originating from polycrystalline Si were detected in the case of $D = 1\times10^{16}$ cm^{-2} and T_s = 340 K after the treatment at T_a = 1270 K. It shows on re-crystallization of nano-crystalline layer (Fig. 1b). Simultaneously the diffraction peaks of small intensity, corresponding to the Mn_4Si_7 phase, were detected.

The defect structure of Si:Mn depends first of all on T_s during implantation, on oxygen concentration, c_o, on Mn^+ dose, D, as well as on the annealing conditions.

Acknowledgements: This work was partially supported by the European Community - Research Infrastructure Action under FP6 "Structuring the European Research Area" Programme (through the Integrated Infrastructure Initiative "Integrating Activity on Synchrotron and Free Electron Laser Science", Contract RII3-CT-2004-506008).

References

[1] M. Bolduc, C. Awo-Affouda, A. Stollenwerk, M.B. Huang, F.G. Ramos, G. Agnello, V.P. LaBella, "Above room temperature ferromagnetism in Mn-ion implanted Si", *Phys. Rev. B* **71** (2005) 033302.

[2] A. Misiuk, J. Bak-Misiuk, B. Surma, W. Osinniy, M. Szot, T. Story, J. Jagielski, "Structure and magnetic properties of Si:Mn annealed under enhanced hydrostatic pressure", *J. Alloys Compds.* **423** (2006) 201-204.

[3] Shengqiang Zhou, K. Potzger, Gufei Zhang, A. Muecklich, F. Eichhorn, N. Schell, R. Groetzschel, B. Schmidt, W. Skorupa, M. Helm, J. Fassbender, D. Geiger, "Structural and magnetic properties of Mn-implanted Si", *Phys. Rev. B* **75** (2007) 085203.

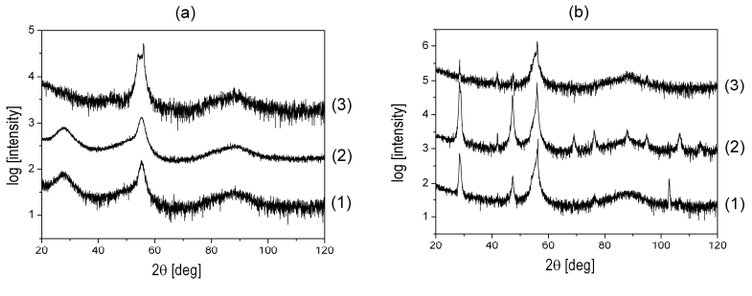

Figure 1. Coplanar 2θ scans in grazing incidence geometry for Cz-Si:Mn implanted with different conditions and annealed at T_a = 610 K (a) and T_a = 1270 K (b) for 1 h under ambient pressure: T_s = 340 K, $D = 2\times10^{15}$ cm^{-2} (1); T_s = 340 K, $D = 1\times10^{16}$ cm^{-2} (2); T_s = 610 K, $D = 1\times10^{16}$ cm^{-2} (3).

P11

ELECTRONIC STRUCTURE AND HYDRO-OXIDATION OF $LaNiO_{3-\delta}$ THIN FILMS

S. Mickevičius [1*], S. Grebinskij [1], V. Bondarenka [1], H. Tvardauskas [1], M. Senulis [1], V. Lisauskas [1], K. Sliužienė [1], and B.A. Orlowski [2]

[1] *Semiconductor Physics Institute, A. Goštauto 11, 00-00 Vilnius, Lithuania*
[2] *Institute of Physics, PAS, Al. Lotnikow 32/46, 02-668 Warsaw, Poland*

Keywords: synchrotron radiation, X-ray photoelectron spectroscopy, $LaNiO_3$

**) e-mail: orbro@ifpan.edu.pl*

$LaNiO_3$ is one of the few conductive oxides with a crystal structure suitable for integration in epitaxial heterostructures with perovskites of enormous technological potential such as colossal magnetoresistance materials, high-temperature superconductors and ferroelectrics.

It is known that electronic structure of $LaNiO_{3-\delta}$ strongly depends on the degree of stoichiometry δ and metal-dielectric transition take place at $\delta \approx 0.25$ [1]. Moreover, the considerable segregation of elements takes place in chemically synthesized $LaNiO_{3-z}$ samples i.e. the surface concentrations of various species differ from the volume one. Another factor to be considered is the tendency of rare earth and nickel oxides to absorb water vapor.

In the previous paper [2] it was shown that the interaction with ambient water lead to the formation of lanthanum and nickel hydroxide containing phase at $LaNiO_{3-\delta}$ surface. The thickness of hydroxide enriched ~ 2 nm layer was estimated by means of Tunable High-Energy X-ray photoelectron spectroscopy using synchrotron radiation

In this paper, in addition to resistivity measurements, we utilize the surface sensitivity of XPS to study the influence of preparation conditions and heat treatment in various atmospheres on the properties of $LaNiO_{3-\delta}$ film.

It was found that after annealing in vacuum at 700°C the relative concentration of hydroxide species increases and electrical conductivity becomes dielectric in nature.

The $LaNiO_{3-\delta}$ films remain metallic after high-temperature (750°C) annealing in an oxygen atmosphere, while concentration of the hydroxide species slightly decreases.

Unfortunately, the ESCA sensitivity is insufficient to determine surfaced chemical composition with an accuracy enough to distinguish are the oxygen vacancies or La/Ni hydroxide species responsible for metal-dielectric transition after high-temperature annealing in vacuum.

Acknowledgements: This work was done in part within the research projects 72/E-67/SPB/DESY/P-03/DWM 68/2004-20061 and EC program G1MA-CT-2002-4017 (Center of Excellence CEPHEUS) and P03B 053 26.

References

[1] M. Abbate, G. Zampieri, F. Prado, A. Caneiro, J.M. Gonzalez-Calbet, M. Vallet-Regi, "Electronic structure and metal-insulator transition in $LaNiO_{3-\delta}$", *Phys. Rev. B* **65** (2002) 155101-155106.

[2] S. Mickevicius*;* S. Grebinskij, V. Bondarenka, V. Lisauskas, K. Sliuziene, H. Tvardauskas, B. Vengalis, B.A. Orlowski, V. Osinniy, W. Drube, "The surface hydro-oxidation of $LaNiO_{3-x}$ thin films", *Acta Phys. Polon. A* **112** (2007) 113-120

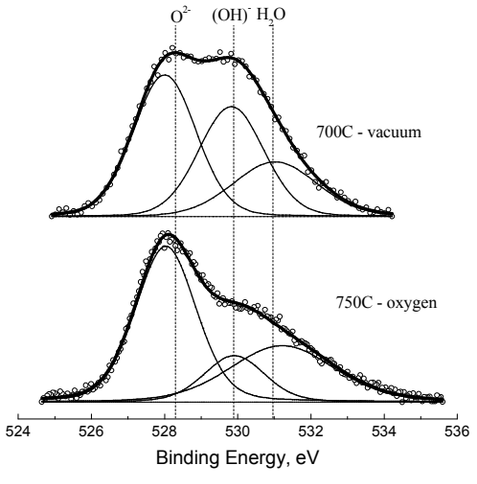

Figure 1. O 1s XPS spectra of $LaNiO_{3-\delta}$ films annealed in vacuum and in oxygen.

P12

ELECTRON MOMENTUM DENSITY OF HEXAGONAL MAGNESIUM STUDIED BY HIGH RESOLUTION COMPTON SCATTERING

M. Brancewicz [1*], A. Andrejczuk [1], Y. Sakurai [2], M. Itou [2], L. Dobrzyński [1,4], E. Żukowski [1], and S. Kaprzyk [3]

[1] Faculty of Physics, University of Bialystok, ul. Lipowa 41,15-424 Bialystok, Poland
[2] Japan Synchrotron Radiation Research Institute (JASRI), SPring-8, Mikazuki, Sayo, Hyogo 679-5198, Japan
[3] Faculty of Physics and Nuclear Techniques, Academy of Mining and Metallurgy Al. Mickiewicza 30, 30-059 Krakow, Poland
[4] The Soltan Institute for Nuclear Studies, 05-400 Otwock-Swierk, Poland

Keywords: Compton scattering, momentum density, synchrotron radiation, magnesium

**) e-mail: brancew@alpha.uwb.edu.pl*

The significant role of valence electrons in matter is undisputed. Compton scattering, which provides information on momentum density distribution of free or weakly bound electrons, allows one to study subtle effects of electron interactions in various materials at momentum near Fermi surface. Especially valuable information is obtained when a high resolution Compton experiment can be carried out [1].

The directional Compton Profiles (CPs – one directional projections of electron momentum density distribution) of hcp single crystal of magnesium have thus been measured along [100], [110] and [001] directions using high energy (115.6 keV) synchrotron radiation and high-resolution (FWHM = 0.12 a.u.) Compton Cauchois-type X-ray spectrometer at SPring-8 (beamline BL08W) [2]. Subtraction of the profiles measured along two specific crystallographic directions removes the isotropic core-electron contributions and forms so-called difference profile, which shows the anisotropy of valence electron momentum density distribution in the material under study. The difference profiles become thus a source of valuable information about the behaviour of valence electrons.

The experimental data were compared with corresponding theoretical Korringa-Kohn-Rostoker (KKR) semirelativistic calculations and previous low-resolution (0.42 a.u.) Compton measurements, performed with the use of high-energy (662 keV) gamma ^{137}Cs source operating at the Faculty of Physics, University of Bialystok [3]. Both, the experimental and theoretical directional Compton profiles, show very small anisotropy of the electron momentum density in this hexagonal metal, at most half of the anisotropy observed typically in cubic systems. Our present data (Fig. 1) confirm presence of sharp fermiology-related features predicted by KKR theory. These features were smeared out and not observed in previous low-resolution measurements. We note, however, that the amplitude of the first peak at 0.25 a.u. is lower than KKR theory predicts. This may be probably due to correlation effects, not fully accounted in the theory.

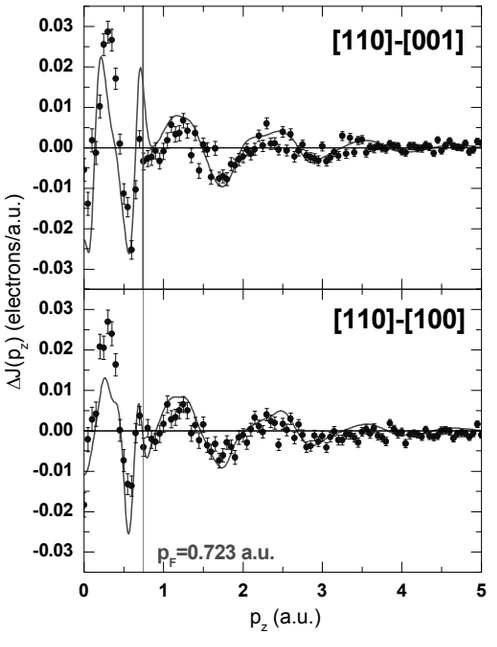

Figure 1. High resolution (FWHM = 0.12 a.u.) experimental (solid circles) and theoretical (solid lines) anisotropies of the directional Compton profiles of Mg. The vertical line shows the Fermi momentum 0.723 a.u.

References

[1] M. Brancewicz, A. Andrejczuk, L. Dobrzyński, H. Reniewicz, E. Żukowski, "A need for high-resolution Compton scattering study of hcp metals with the use of synchrotron radiation", *Nucl. Instrum. Meth. Phys. Res. B* **255** (2007) 395–398.

[2] Y. Sakurai, M. Itou, "A Cauchois-type X-ray spectrometer for momentum density studies on heavy-element materials", *J. Phys. Chem. Solids* **65** (2004) 2061-2064.

[3] M. Brancewicz, H. Reniewicz, A. Andrejczuk, L. Dobrzyński, E. Żukowski, S. Kaprzyk, "Electron momentum density of hexagonal magnesium studied by Compton scattering", *Solid State Phenom.* **112** (2006) 123-131.

P13

XANES OF Mn IN $CuIIIS_2$ (III = Al, Ga, In) CHALCOPYRITES

R. Bacewicz [1*], W. Zalewski [1], M. Wierzbicki [1], S. Schorr [2], and B. Korzun [3]

[1] *Faculty of Physics, Warsaw University of Technology, ul. Koszykowa 75, 00-662 Warsaw, Poland*

[2] *Hahn-Meitner Institut, Glienicker Straße 100, D-14109 Berlin, Germany*

[3] *Joint Institute of Physics of Solids and Semiconductors, 17 P. Brouki, Minsk 220072, Belarus*

Keywords: XANES, diluted magnetic semiconductors, chalcopyrite

**) e-mail: bacewicz@if.pw.edu.pl*

In search for suitable spintronic materials, diluted magnetic semiconductors have been studied for a long time. However, there are still difficulties in obtaining room temperature ferromagnetism, which is a prerequisite of spintronic applications, in typical elemental and binary semiconductors. In recent years room temperature ferromagnetism has been found in some of Mn-doped chalcopyrites [1]. The theoretical calculations show that the ferromagnetic ordering in such systems depends critically on the site occupation of Mn in the host lattice. According to theoretical predictions, the stable ferromagnetic ordering is obtained when Mn substitutes on the III group atom site in $CuIIIS_2$ (III = Al, Ga, In) compounds. Using the X-ray absorption fine structure for determining the Mn site preference encounters some difficulties when atomic numbers of constituent cations (Cu and III) are close to each other. In such a case, similar photoelectron scattering amplitudes and phases prevent from discrimination between two possible substitution sites Mn_{Cu} and Mn_{III} in the EXAFS analysis [3, 4]. However, we expect that some specific features of electronic structure (local density of states) reflected in the X-ray absorption near edge structure (XANES) show differences for these two sites.

In this report we present an attempt to determine the site preference of Mn atoms from the XANES study of three Mn doped compounds: $CuAlS_2$, $CuGaS_2$ and $CuInS_2$. We used polycrystalline samples with varying Mn concentration within each series. A fluorescence detector was employed to record the Mn K edge XAFS spectra at A1 station at HASYLAB.

We used two methods of modeling XANES: the real-space multiple-scattering method represented by the FEFF 8.4 program and the full-potential linear augmented plane wave (FLAPW) in the Wien2k package. Special attention has been paid to reconstruction of the pre-edge structure of the spectra which is sensitive probe of the charge state and the local electronic structure of Mn atoms. We found that the Mn_{Cu} substitution gives generally much weaker pre-edge peak than the Mn_{III} site substitution. However, the intensity of the pre-edge structure shows strong dependence on the Fermi energy, which is hard to control in the studied materials. Applicability of the XANES spectra for the Mn site determination is discussed by comparison of the results of two theoretical methods with the experimental data.

References

[1] S. Cho, S. Choi, G.B. Cha, S.C. Hong, S. Cho, Y. Kim, J.B. Ketterson, S.-Y. Jeong, G.-C. Yi, *Sol. State Commun*. **122** (2002) 165.

[2] Y-J. Zhao, A. Zunger, *Phys. Rev. B* **69** (2004) 104422.

[3] R. Bacewicz, A. Pietnoczka, W. Gehlhoff, V.G. Voevodin, *phys. stat. sol. (a)* **204** (2007) 2296.

[4] W. Zalewski, R. Bacewicz, J. Antonowicz, S. Schorr, C. Streeck, B. Korzun, *phys. stat. sol. (a)* in press.

P14

PREPARATION AND DIFFRACTION STUDIES OF POLYCRYSTALLINE Cu-Fe MATERIALS

J. Darul [*], **W. Nowicki, and P. Piszora**

Faculty of Chemistry, Adam Mickiewicz University, Grunwaldzka 6, PL-60780 Poznań, Poland

Keywords: $CuFe_2O_4$, crystal structure and symmetry, Jahn-Teller ion, XRD

*) *e-mail: jola@amu.edu.pl*

Ferrimagnetic cubic spinels are technically important materials, they have been extensively investigated in order to improve good soft magnetic compounds. Considering the various spinel ferrites, cooper ferrite, $CuFe_2O_4$, has gained a prominent interest among materials science for various applications. Since of Cu^{2+} is a Jahn-Teller ion, it gives the anomalous favorable properties and also exhibits phase transition from tetragonal to cubic, depending on the temperature. $CuFe_2O_4$ can be described as a cubic close-packed arrangement of oxygen ions, with Cu^{2+} and Fe^{3+} ions at two different crystallographic sites [1-4]. The cation distribution in this oxide can be presented by the formula: $(Cu_x^{2+}Fe_{1-x}^{3+})_A[Cu_{1-x}^{2+}Fe_{1+x}^{3+}]_BO_4$. The parameter of inversion, x, is equal to 0 for inversion spinels, and to 1, when the spinel is normal. Copper ions migrate from octahedral (B-sublattice) to tetrahedral places (A-sub-lattice). When the spinel is synthesized using classical ceramic technologies (high temperature treatment of the initial oxides of the metal cations) with strict stoichiometry, it has a tetragonal structure of hausmannite type with crystal cell parameters a = 8.20 Å and c = 8.60 Å; c/a = 1.05. The c/a ratio can be changed via decreasing the copper concentration, or alternatively by temperature treatments [1].

A citrate process as an alternative synthesis route has been successfully employed to synthesize polycrystalline cooper iron oxide with nominal composition, $CuFe_2O_4$, with improved properties for specific applications, such as magnetic powder for massive storage devices. Corresponding amounts of the copper and iron nitrates (*Merck*) were taken in a 1:2 mole ratio along with 3 moles of citric acid (*Merck*), and dissolved in deionised water, with continuous stirring. This mixture was slowly evaporated and then dried at 120°C over night. The dried powder was crushed and calcined (300°C, 600°C and 900°C) for 5 h. The compounds formation and crystallinity of the materials were identified by XRD patterns, which were recorded on a Bruker D8 Advance diffractometer, with CuKα radiation.

Investigations on the high temperature phase transitions were carried out at the synchrotron beamline B2 at HASYLAB (DESY, Hamburg). The diffractometer was equipped with capillary furnace (STOE) and the on-site readable image-plate detector OBI. Samples mounted into quartz capillaries of diameter 0.3 mm were heated and cooled at the temperature range from RT to 900°C. The wavelength was 0.49342 Å.

The aim of the work was to establish by means of powder diffraction studies the structural properties, especially the temperature phase transition from tetragonal to cubic (400°C-425°C) and the cation distribution in $CuFe_2O_4$. Determination of the transition points, the temperature ranges of the crystalline phases coexistence, and the ions distribution in the spinel lattice, were undertaken. The structure refinement of all polymorphs using Rietveld profile analysis, based on the synchrotron X-ray data, were performed**.**

Acknowledgements: The synchrotron measurements at DESY-HASYLAB were supported by the IA-SFS-Contract No. RII3-CT-2004-506008 of European Commission. We would like to thank Dr. D. Trots (Hasylab) for his assistance during experiments.

References

[1] M.U. Rana, M. Islam, T. Abbas, "Cation distribution and magnetic interactions in Zn-substituted $CuFe_2O_4$ ferrites", *Mater. Chem. Phys*. **65** (2000) 345-349.

[2] B.J. Evans, S. Hafner, "Mössbauer resonance of Fe^{57} in oxide spinels containing Cu and Fe", *J. Phys. Chem. Solids* **29** (1968) 1573-1588.

[3] J.Z. Jiang, G.F. Goya, H.R. Rechenberg, "Magnetic properties of nanostructured $CuFe_2O_4$", *J. Phys.: Condens. Matter.* **11** (1999) 4063-4078.

[4] J.A. Gomes, M.H. Sousa, G.J. da Silva, F.A. Tourinho, R. Itri, G. de M. Azevedo, J. Depeyrot, "Cation distribution in cooper ferrite nanoparticles of ferrofluids", *J. Magn. Magn. Mater.* **300** (2006) e213-e216.

P15

SHORT RANGE ORDER IN Pd AND PdO NANOPARTICLES EMBEDDED IN CARBONACEOUS MATRIX STUDIED WITH THE *XAFS* SPECTROSCOPY

R. Nietubyć [1*], E. Czerwosz [2,3], R. Diduszko [2], and M. Kozłowski [2,4]

[1] *Andrzej Soltan Institute for Nuclear Studies, PL-05400 Świerk. Poland.*

[2] *Tele and Radio Research Institute, ul. Długa 44/50, PL-00241 Warsaw, Poland .*

[3] *Jan Kochanowski University of Humanities and Sciences, Al. Świętokrzyska 15, PL-25490 Kielce, Poland*

[4] *Institute of Physics PAS, Al. Lotników 32/46 PL-02668 Warsaw, Poland*

Keywords: nanoparticle, XASF, absorption spectroscopy, palladium

**) e-mail: r.nietubyc@ipj.gov.pl*

Nanocrystalline films formed of nano-Pd grains embedded in carbon matrix show a highly developed surface. Films were obtained during the physical vapour deposition (PVD) process from two separated sources containing fullerene and palladium acetate. TEM observations revealed nano-Pd grain shapes. Significant fraction of constituent atoms was located in the grain boundary region. Those atoms occur in the environment different than that in the bulk crystal. The short-range order around Pd atoms was investigated by mean of Pd K- and L-edge X-ray absorption fine structure (XAFS) spectroscopy in order to find what kind and how far extended is a geometrical arrangement around those atoms.

XAFS measurements were performed at A1 beamline at DORIS III storage ring in Hasylab for the films prepared with various temperatures and Pd concentrations. Fourier Transform curves calculated for the measured fine structure oscillations showed that palladium atoms are involved in Pd–Pd and Pd–O bonding. For the samples containing palladium oxide, the range of order was found limited to the first and second coordination shells only. For those samples, the corresponding parameters describing contribution from Pd–O–Pd scattering path were found equal within their error ranges. The second shell, although, observed in FT, was strongly disordered. Corresponding Debye-Waller factor was found greater than 0.8. The electron wave backscattered on that shell contributes to the EXAFS in a very short *k* range only, thus precludes the reasonable FT analysis.

We performed FEFF calculations [1] of Pd K-edge EXAFS for Pd fcc and PdO tetragonal crystal structures and separated the contributions originating from particular scattering paths. The minor contribution coming form Pd–Pd'–Pd was observed as a hump disturbing the main oscillation at $k = 4$ Å^{-1}. The magnitude of this feature was evaluated and interpreted in terms of changes in the atomic order occurring in the range of second coordination shell.

The applied analysis permitted to conclude qualitatively on the highly disordered structure. We found that the creation of amorphous palladium oxide deteriorates the growth of metallic grains.

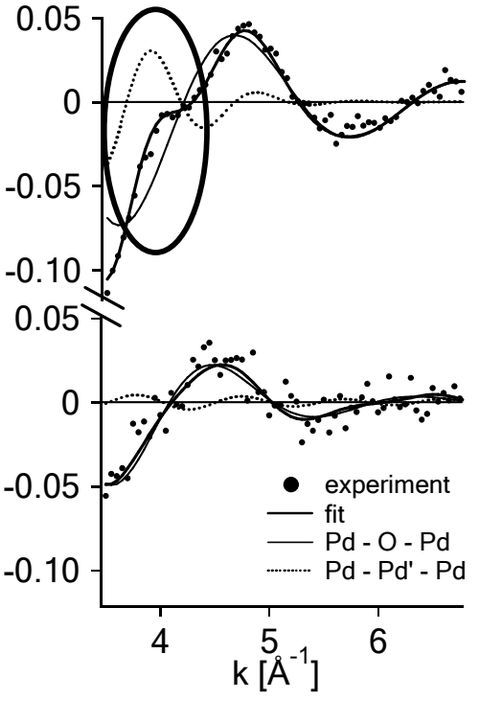

Figure 1. PdO Pd K-edge fine structure oscillations split into contributions. The second coordination shell is manifested by the feature in the oval.

References

[1] B. Ankudinov, J.J. Rehr, S.D. Conradson, "Real-space multiple-scattering calculation and interpretation of x-ray absorption near-edge structure", *Phys. Rev. B* **58** (1998) 7565-7576.

P16

XAFS STUDY OF SURFACE OXIDISED Fe PARTICLES

W. Szczerba [1*], M. Sikora [1], P. Chometowski [1], Cz. Kapusta [1], D.A. Zajac [2], C. Marquina [3], D. Serrate [3], and M.R. Ibarra [3,4]

[1] *Department of Solid State Physics, Faculty of Physics and Applied Computer Science, AGH University of Science and Technology, Al. Mickiewicza 30, 30-059 Kraków, Poland*

[2] *Institute of Nuclear Physics, Polish Academy of Sciences, ul. Radzikowskiego 152, 31-342 Kraków, Poland*

[3] *Facultad de Ciencias, Universidad de Zaragoza-CSIC, Pedro Cerbuna 12, 50009 Zaragoza, Spain*

[4] *Instituto de Nanociencia de Aragon, Universidad de Zaragoza, Pedro Cerbuna 12, 50009 Zaragoza, Spain*

Keywords: XAFS, surface oxidised Fe particles, Fe oxides

**) e-mail: wsz@agh.edu.pl*

A study of surface oxidised iron particles by means of X-ray Absorption Spectroscopy (XAS) at the Fe K, $L_{2,3}$-edges and the O K-edge is presented.

Powder samples were prepared by ball milling and subsequently thermally treated in vacuum or air. The XAS study of the samples and the reference Fe oxides in the XANES range of the Fe K-edge has been carried out at the synchrotron laboratory HASYLAB, Hamburg. Simultaneous measurements in the transmission geometry and total electron yield (TEY) have been carried out. The transmission spectra which correspond to probing of the bulk do not reveal the presence of iron oxides within 1% error margin, except for the sample annealed in air at 300°C. Its spectrum consists of the contributions of 95% metallic Fe, 4% magnetite and 1% hematite. The TEY spectrum of the sample, which corresponds to a few hundreds of nanometres probing depth, contains contributions of 45% metallic Fe, 42% magnetite and 13% hematite. Taking into account different probing depths of both methods the average thickness of the oxide layer could be determined.

The XANES spectra of the samples studied and the reference oxides at the Fe $L_{2,3}$-edges, O K-edge and the EXAFS spectra at the O K-edge have been measured at the synchrotron laboratory ELETTRA, Trieste. The TEY detection mode was used, which in the case of the iron $L_{2,3}$-edges and the oxygen K-edge has the probing depth of a few nanometres.

The O K-edge XANES spectra and their derivatives as well as the EXAFS spectra have been fitted with a linear combination of the spectra of the reference oxides. This provided the information on the content of individual oxide species in the surface layers, which is particularly valuable for the samples thermally untreated and annealed in vacuum, where the oxide layer is of nanometric thickness. A relation of the content and thickness of the oxide layer to the magnetoresistive properties of the material is discussed.

Acknowledgements: A support from the European Commission, Project Nº: 027827, IST-2004-2.4.2 and from the Polish Ministry of Science and Higher Education, Project Nº: 60/6.PR UE/2007/7 is acknowledged.

P17

STRAIN PROFILES IN 6H SiC CRYSTALS IMPLANTED WITH 160 keV H^+ IONS

W.K. Wierzchowski [1*], K. Wieteska [2], A. Turos [1,4], W. Graeff [3], R. Ratajczak [4], G. Gawlik [1], and J. Jagielski [1]

[1] *Institute of Electronic Materials Technology, Wólczyńska 133, PL 01-919 Warsaw, Poland*
[2] *Institute of Atomic Energy, 05-400 Otwock-Świerk, Poland*
[3] *HASYLAB at DESY, Notkestr. 85, D-22603 Hamburg, Germany*
[4] *Soltan Institute for Nuclear Studies, 05-400 Otwock-Świerk, Poland*

Keywords: silicon carbide, H implantation, synchrotron

**) e-mail: wierzc_w@itme.edu.pl*

Silicon carbide is a perspective material for application in technology of high temperature semiconductor devices and for GaN based blue light optical elements. It is also a semiconductor with physical and material properties differing very much from the previously dominating ones and yet not very well known. The application of SiC in electronic industry increases systematically. The implantation technique is used in many technological applications. On this reason the systematical studies of implantation effect are very important.

It was well established that the effective evaluation of implantation induced strain profile is possible when a distinct interference effects are observed in X-ray diffraction patterns. To achieve this goal the implantation was performed in highy in highly perfect {00.1} oriented 6H SiC wafers manufactured by Cree. The samples were implanted with 160 keV H^+ ions to the fluencies 2×10^{15} cm^{-2} and 5×10^{15} cm^{-2}. They were examined before and after implantation with a number of synchrotron X–ray methods and Rutherford back scattering. The X–ray methods of characterization included the investigation of rocking curves recorded with a small 50×50 μm^2 probe beam and white beam Bragg case section and projection topography.

The synchrotron topographic examination performed before the implantation confirmed a high perfection of the samples containing well resolved individual dislocations of the density smaller than 10^3 cm^{-2}. The use of numerical simulation of topographic images confirmed the dominating concentration of screw dislocations along [00.1] direction. The implanted layers provided distinct interference effects in the rocking curves and Bragg-case section topographs (strain modulation fringes) [1]. Good visibility of interference maxima enabled effective evaluation of the strain profile by fitting the theoretical rocking curves to the experimental ones. The evaluated strain profiles approximated by browsed Gaussian curve were similar to the distribution of point defects calculated with SRIM2000. The profiles were similar to the distribution of defects numerically calculated from the channeling measurements.

Acknowledgements: Support of the grant No. 10000200002 is acknowledged.

References

[1] K. Wieteska, W. Wierzchowski, W. Graeff, G. Gawlik, "X–ray synchrotron diffraction studies of $A^{III}B^{V}$ semiconductor compounds implanted with hydrogen", *phys. stat. sol. (a)* **203** (2006) 227-235.

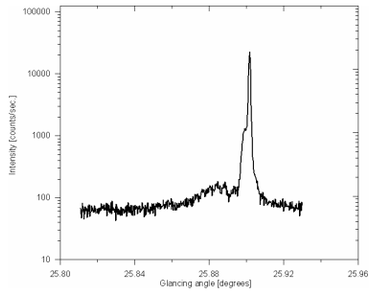

Figure 1. Experimental rocking curve of 6H SiC implanted with 160 keV H^+ ions to the dose 5×10^{15} cm^{-2} in 00.12 reflection of 0.1115 nm radiation.

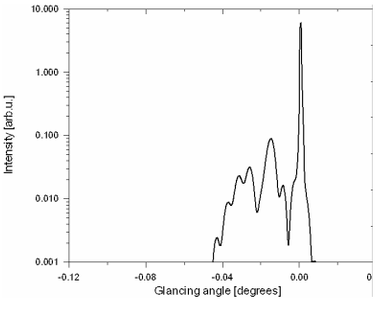

Figure 2. Theoretical rocking curve corresponding to the experimental one shown in Fig. 1.

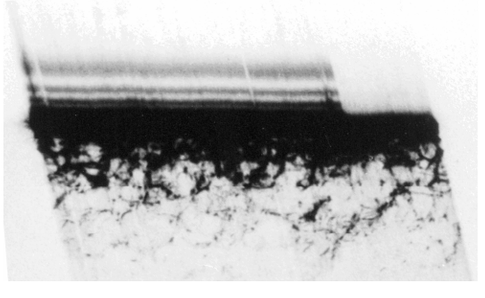

Figure 3. Strain modulation fringes revealed in Bragg-case section synchrotron topographic image of the same sample as in the case of Figure 1.

P18

XAFS STUDY OF $BaCe_{1-x}Ti_xO_3$ PROTONIC SOLID ELECTROLYTES

P. Seremak-Peczkis [1*], K. Schneider [1], W. Zajączkowski [1], Cz. Kapusta [1], D. Zając [2,3], P. Pasierb [4], E. Drożdż-Cieśla [4], and M. Rękas [4]

[1] *AGH University of Science & Technology, Faculty of Physics and Applied Computer Science, Dept. of Solid State Physics, PL-30059 Krakow, Poland*

[2] *Institute of Nuclear Physics PAS, Dept. of Magnetic Resonance Spectroscopy, PL-31342 Krakow, Poland*

[3] *Hasylab at DESY, D22607 Hamburg, Germany*

[4] *AGH University of Science & Technology, Faculty of Materials Science and Ceramics, PL-30059 Krakow, Poland*

Keywords: protonic electrolytes, fuel cells,barium cerate, barium titanate, synchrotron radiation, XAFS

**) e-mail: kameres@interia.pl*

In this work the local structures and valence properties of Ti in $BaCe_{1-x}Ti_xO_3$ materials were investigated. The materials belong to a new class solid electrolytes which can be used in intermediate temperature fuel cells. The series of four compounds with different titanium content x (0-0.3) was studied by means of X-ray absorption fine structure (XAFS) spectroscopy.

Powders of $BaCe_{1-x}Ti_xO_3$ (x = 0.0, 0.05, 0.07, 0.10, 0.15,0.20 and 0.30) were prepared by solid-state reaction method. Barium carbonate $BaCO_3$ (99.9%), cerium (IV) oxide CeO_2 (99.9%) and TiO_2 nanopowder (99.7%). The structural studies by X-ray diffraction have shown that undoped material crystallizes in orthorhombic phase, while the increasing concentration of Ti dopant up to x = 0.2 leads to the ordering of the structure to phases with higher symmetries (tetragonal and even cubic).

The XAFS measurements have been carried out at Hasylab/DESY synchrotron facility in the XANES (X-ray Absorption Near Edge Structure) region and in the EXAFS (Extended X-ray Absorption Fine Structure) region. The Ti:K edge spectra were measured at the CEMO station with the transmission mode. The XANES results obtained at the Ti:K edge are shown in Fig. 1 and the EXAFS results are presented in Fig. 2.

The XANES spectra show a complex structure with a pre-edge peak, which is especially pronounced in the x=0.3 compound. This indicates a low symmetry of the Ti environment here, in contrast to the other compounds.

The Fourier transforms of the EXAFS show the main peak corresponding to the oxygen nearest neighbours at the distance from the Ti ion closer by 0.1 Å in the x=0.3 compound than in the other. The second nearest neighbour peak, which corresponds mainly to metal ions, decreases its intensity with increasing Ti content. This is related mainly to a smaller photoelectron scattering amplitude of Ti due to its Z number smaller than that of Ce. A much smaller amplitude of the second nearest neighbour peak and its different shape in the x=0.3 compound can possibly be attributed to its different structure. The results of the XAFS study are compared to those of X-ray diffraction measurements and magnetometry.

Acknowledgements: This paper was supported by the Polish Ministry of Science and Higher Education, Projects no. PBZ/MEiN/ 01/2006/57 and R15 019 02.

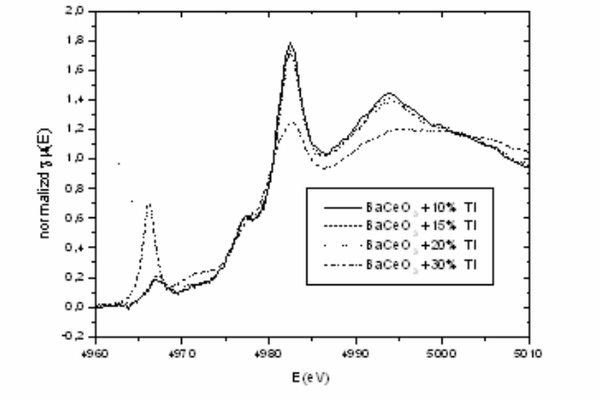

Figure 1. Normalized XANES spectra at the Ti:K edge for the $BaCe_{1-x}Ti_xO_{3-d}$ compounds.

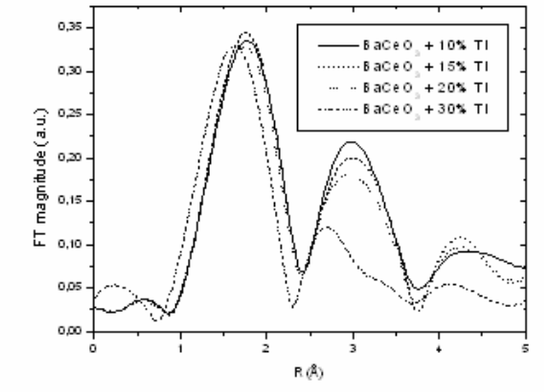

Figure 2. Fourier transforms of the Ti:K edge EXAFS function for the $BaCe_{1-x}Ti_xO_{3-d}$ compounds.

P19

XAS STUDY OF CARBON COATED Fe AND Fe_3O_4 DERIVED NANOPARTICLES

K. Schneider [1*], Cz. Kapusta [1], D.A. Zajac [2,3], C.I. Marquina [4], and M.R. Ibarra [4]

[1] *Faculty of Physics and Applied Computer Science, AGH University of Science&Technology, 30-059 Kraków, Poland*
[2] *Hasylab at DESY, D22607 Hamburg, Germany*
[3] *Institute of Nuclear Physics, Polish Academy of Sciences, 31-342 Kraków, Poland*
[4] *Instituto Nanociencias de Aragon, Universidad de Zaragoza, Spain*

Keywords: carbon coating, iron nanoparticles

**) e-mail: kryschna@agh.edu.pl*

Results of a XAS study of new magnetic nanoparticle materials derived from iron metal and iron oxide are presented. The materials have potential biomedical applications, *e.g.* as contrast agents in MRI. Several samples of carbon coated nanoparticles have been obtained by arc melting of graphite electrodes willed with metallic Fe or magnetite. Three fractions of nanoparticles from different places of the furnace: top, walls and bottom have been collected.

In order to determine the local structure and the Fe valence state in the materials, the X-ray absorption spectroscopy in the XANES and EXAFS range was used. The experiments were performed at the Fe:K edge at room temperature in Hasylab/DESY, Hamburg. Metallic Fe, hematite, maghemite and magnetite were used as references.

The edge energy and shape in the spectra of the Fe and Fe_3O_4 derived nanoparticle materials are similar to those of metallic iron (Fig. 1). This reveals a reduction of magnetite to metallic iron by carbon upon arc melting.

The contents of different iron species in the materials studied determined from the linear combination fits of their spectra with those of the reference samples using the least squares method in the Ifeffit pack software are presented in Table 1.

Table 1. Percentage contents of different iron species in the materials studied.

sample	Fe	□-Fe_2O_3	□-Fe_2O_3	Fe_3O_4
Fe_3O_4 top	99.1	0	3.9	0
Fe_3O_4 walls	95.9	0	7.7	0
Fe_3O_4 bottom	93.8	0	9.1	0
Fe top	97.1	2.9	0	0
Fe walls	95.3	4.7	0	0
Fe bottom	92.0	8.0	0	0

The Fourier transforms of the EXAFS functions obtained from the Fe:K edge spectra of the magnetite derived nanoparticle materials reveal their close similarity to that of metallic Fe and are unlike to that of magnetite (Fig. 2). Also the Fourier transforms of the EXAFS functions of the iron derived nanoparticle materials are similar to that of metallic Fe. However, the distance of the 1st neighbour peak is of 0.2 Å smaller than that in the Fe metal. This suggests a compression of the lattice, possibly due to incorporation of carbon atoms which have their radius smaller than that of iron.

Preliminary MRI experiments performed on water suspensions of the materials studied idicate their high efficiency in increasing the T2 and T2* contrasts.

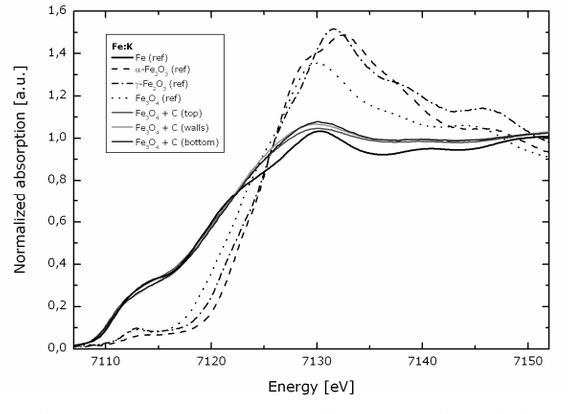

Figure 1. XANES spectra at the Fe: K edge of the carbon coated nanoparticle materials together with the spectra of the reference samples.

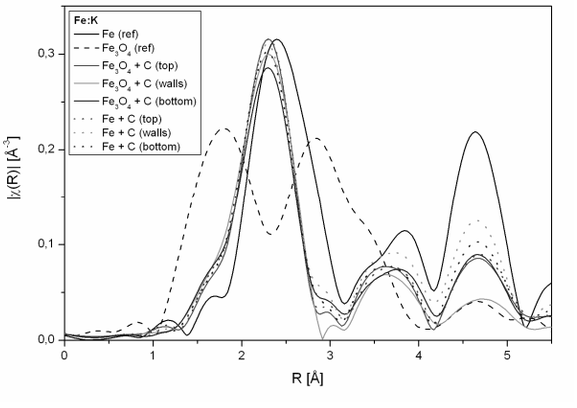

Figure 2. Fourier transforms of the Fe:K edge EXAFS functions of carbon coated Fe and Fe_3O_4 derived nanoparticle materials.

P20

XAFS STUDY OF Mo AND W DOPED TiO_2 NANOPOWDERS

K. Schneider [1*], A. Padoł [1], M. Sikora [1], Cz. Kapusta [1], K. Michalow [2,3], Th. Graule [2], A. Heel [2], M. Radecka [3], M. Rekas [3], and D. Zajac [4,5]

[1] *AGH University of Science and Technology, Faculty of Physics and Applied Computer Science, Dept. of Solid State Physics, PL-30059 Krakow, Poland*
[2] *EMPA Materials Testing and Research, Laboratory for High Performance Ceramics, CH-8600 Dübendorf, Switzerland*
[3] *AGH University of Science and Technology, Faculty of Materials Science and Ceramics, PL-30059 Krakow, Poland*
[4] *Institute of Nuclear Physics PAS, Department of Magnetic Resonance Spectroscopy, PL-31342 Krakow, Poland*
[5] *Hasylab at DESY, D22607 Hamburg, Germany*

Keywords: XAFS, titania, absorption spectroscopy, vacancy

**) e-mail: krystyna.schneider@agh.edu.pl*

The solar light-assisted generation of hydrogen from water using semiconductor electrode has attracted a growing interest in the search for new environment-friendly energy sources [1]. In recent years, the main photo-electrode candidate has been established to be TiO_2 [2]. A disadvantage of TiO_2 in the application as the photo-electrode is a poor absorption of visible light due to its wide energy gap (ca 3.2 eV) and losses in recombination processes of the photo-charge pairs. Several techniques for improving the photo-response of TiO_2 towards visible range have been proposed. Among them the most promising appears to be doping by other transition metals like W and Mo into TiO_2 crystal lattice. The aim of this work is the study of the incorporation mechanism of these elements into the TiO_2 crystal lattice and their impact on the local structure of nanocrystalline TiO_2 by means of X-ray absorption fine structure (XAFS) spectroscopy.

Nanoparticle materials of WO_x-TiO_2 have been synthesized by Flame Spray Synthesis (FSS) process by oxidation of metal-organics precursors [3]. Titanium tetraiso-propoxide (TTIP) and tungsten hexacarbonyl (THC) dissolved in tetrahydrofuran (THF) were used as a precursor sources of TiO_2 and WO_3, respectively. Concentration of W (0.1 - 1 at%) has been varied by changing experimental parameters like flow rate or concentration of precursors. Particle size, phase composition and morphology of the nanopowders were studied using BET, X-ray diffraction (XRD) and transmission electron microscopy (TEM), respectively.

XAFS experiments have been carried out in the synchrotron laboratory HASYLAB/DESY, Hamburg. The measurements at the K edge of titanium were done at the experimental station E4 at room temperature in transmission mode. The main peak located at about 1.7 Å, which corresponds to oxygen neighbours to a titanium ion reveals a decrease with increasing doping level. The effect can be attributed to the increasing amount of oxygen vacancies in the next neighbour shell to the Ti ions. The peak at about 3.4 Å which corresponds to Ti neighbours also decreases its intensity with increasing doping, which possibly indicates an increased amount of Ti vacancies. The 0.5% Mo doped sample is an exception with a similar amount of Ti vacancies as in the pristine TiO_2.

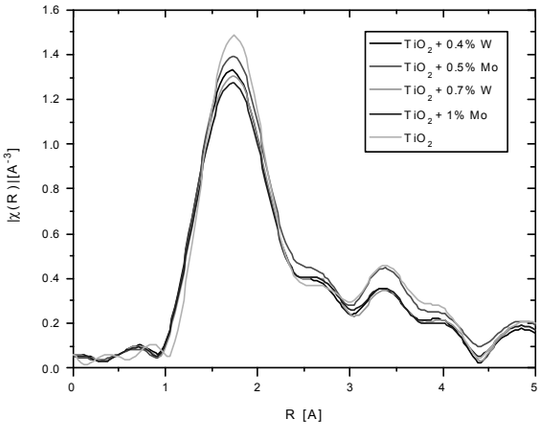

Figure 1. Fourier transforms of the Ti:K edge EXAFS functions.

The Ti:K edge XAFS study of the TiO_2-based nanomaterials indicates an increased amount of oxygen and titanium vacancies on doping with an exception for low Mo doping which creates oxygen vacancies only. The results are compared to the Mo:K edge and W:L edges XAFS and the X-ray diffraction data.

Acknowledgements: This paper was supported by the Polish Ministry of Science and Higher Education, Projects no. PBZ/MEiN/ 01/2006/57 and R15 019 02.

References

[1] A. Fujishima, K. Honda, *Nature* **238** (1972) 37.

[2] T. Bak, J. Nowotny, M. Rekas, C.C. Sorrell, *Int. J. Hydrogen Energy* **27** (2002) 991.

[3] K.K. Akurati, A. Vital , U.E. Klotz, B. Bommer, T. Graule, M. Winterer, *Powder Technolog.* **165** (2006) 73.

P21

MICROSCOPIC AND RESONANT PHOTOEMISSION STUDY OF Si\Gd

B.A. Orlowski [1*], B.J. Kowalski [1], E. Lusakowska [1], I.A. Kowalik [1], M.A. Pietrzyk [1], E. Guziewicz [1], E. Nossarzewska-Orlowska [2], and R.L. Johnson [3]

[1] *Polish Academy of Sciences, Institute of Physics, Al. Lotników 32/46, Warszawa 02-668, Poland*

[2] *Institute of Electronic Materials Technology, Silicon Department (IEMT), Wolczynska 133, Warszawa 01-919, Poland*

[3] *University of Hamburg, Institute for Experimental Physics, Luruper Chausse 149, Hamburg D-22761, Germany*

Keywords:Silicon, Gadolinium, photoemission, synchrotron

**) e-mail: orbro@ifpan.edu.pl*

The paper presents study of Gd atoms deposited on Si(111) surface with application of Atomic Force Microscope (AFM) and Fano-type resonant photoemission with application of synchrotron radiation (Flipper II, HASYLAB, Hamburg). The application of synchrotron radiation in the region of energy hv corresponding to the Gd 4*d*-4*f* transition (130 – 170 eV) gave the possibility to measure Fano-type resonant photoemission spectra [1]. The layers of thickness 2, 20, 150 and 3000Å were deposited in UHV conditions. The spectra of Si valence band with contribution of Gd 4*f* and 6*s* electrons were studied *in situ* by resonant photoemission spectroscopy for layer of Gd with 2 Å thick deposited on Si(111) clean surface. The photoemission study gave the curve of the Fano resonance shape with resonance for *hv* = 151.8 eV and antiresonance for *hv* = 146.8 eV. The Gd 4*f* localized electrons gave the contribution to the valence band density of states located at 9.8 eV below the valence band edge. The Gd layers of thickness 20, 150 and 3000 Å were deposited in UHV conditions and the AFM images were taken in the normal atmosphere conditions. The AMF study showed remarkably deep craters created deep in silicon crystal surface region under deposited 150 Å of Gd layer. Creation of the craters can be correlated to the high chemical reactivity of Gd atoms with Si. The Gd atom has configuration Gd $4f^7 5d^1 6s^2$ of the valence electrons and it is the next after Eu with

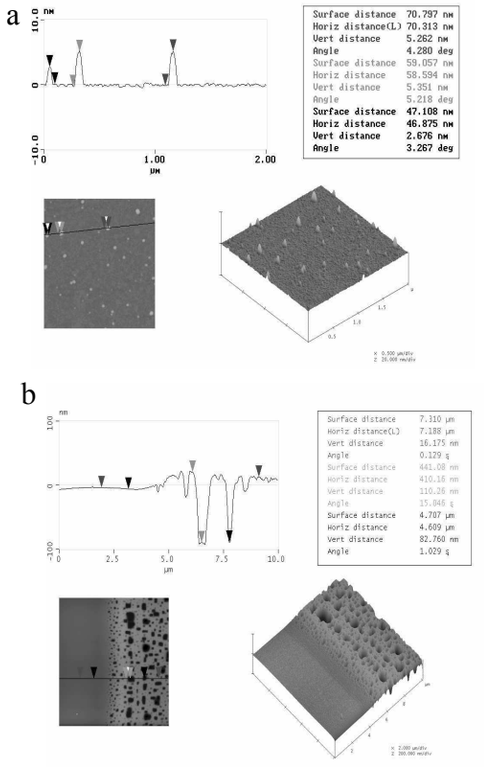

Figure 1. AFM images from Si surface deposited with 20 Å layer of Gd (a) and Si surface deposited with 150 Å layer of Gd (b). In (b) the border of Si-Si/Gd region is presented.

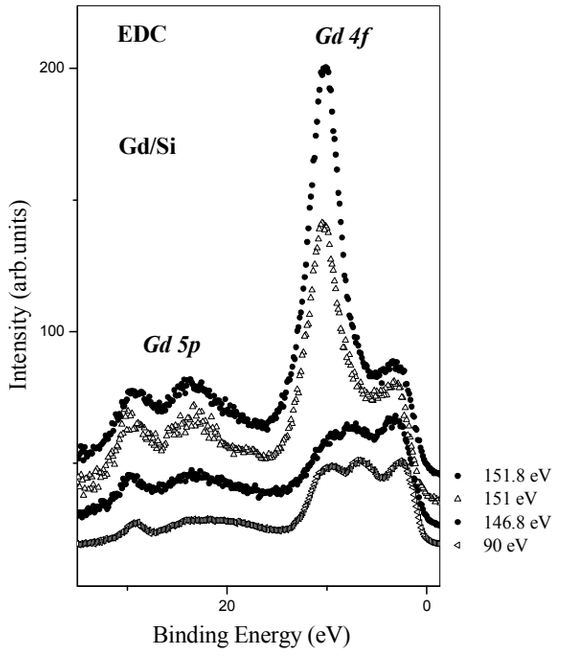

Figure 2. The set of EDCs measured for deposited 2 Å of Gd on Si(111) surface. The binding energy range covers the region of the silicon valence band and Gd 4*f* and 5*p* shells.

P21

electrons configuration Eu $4f^7 6s^2$. The high reactivity can be caused by lightly bound Gd $5d^1$ electron which frequently contributes to the conduction band of semiconductors and Gd atom is a donor impurity in most semiconductor compounds and appears as Gd^{3+} ion. The reaction of Gd and Si atoms has an explosive character and the dominant diffusion component is silicon [2-4]. It leads to the diffusion of Si into the Gd islands and it is causing the creation of craters in silicon crystal substrate.

Acknowledgements: This work was supported in part within: MSHE of Poland research projects DESY/68/2007 and grant N202 101 31/0749 32 as well as by the European Community under Contract RII3-CT-2004-506008 (IA-SFS) (via DESY/HASYLAB).

Reference

[1] B.A. Orlowski, E. Guziewicz, E. Nossarzewska-Orlowska, A. Bukowski, R.L. Johnson, *Surf. Sci.* **507-510C** (2002) 218.

[2] G.L. Molnar, G. Peto, Z. Vertesy, E. Zsoldos, *Appl. Phys. Lett.* **74** (1999) 1672.

[3] J.E.E. Baglin, F. M. d'Huerle, C.S. Petersson, *J. Appl. Phys.* **52** (1981) 2841.

[4] G.L. Molnar, I. Gerocs, G. Peto, E. Zsoldos, E Jaroli, J. Gyulai, *J. Appl. Phys.* **64** (1988) 6746.

P22

PHOTOEMISSION STUDY OF SiC (0001) SURFACE WITH DEPOSITED Mn ATOMS

B.A. Orlowski [1*], M.A. Pietrzyk [1], V. Osinniy [1], M. Szot [1], E. Lusakowska [1], K. Grasza [1,2], and R.L. Johnson [3]

[1] *Institute of Physics, Polish Academy of Sciences, Al. Lotnikow 32/46, 02-668 Warsaw, Poland*
[2] *Institute of Electronic Materials Technology, 133 Wolczynska str., Warsaw, Poland*
[3] *Hamburger Synchrotronstrahlungslabor HASYLAB am Deutschen Elektronen-Synchrotron DESY, Notkestr. 85, D-22603 Hamburg, Germany.*

Keywords: photoemission, manganese, SiC

**) e-mail: orbro@ifpan.edu.pl*

In presented paper the of SiC(0001) surface after sequential coverage by Mn atoms and annealing in Ultra High Vacuum (UHV) was studied. The resonant Photoemission Spectroscopy (RPS) and Atomic Force Microscopy methods were used. The SiC crystal was grown by the seeded physical vapor transport method in the Institute of Electronic Materials Technology at Warsaw [1-2] in quasi-equilibrium conditions with low rate (0.05-0.2 mm/h) deposition on Si (0001) surface of 6H-SiC seeds. The shape and morphology of the crystallization front, defects in crystal and wafers cut of it was presented in the paper [2].

The photoemission data were obtained with the Tunable VUV Photoelectron Spectrometer at the beam line E1 (FLIPPER II) of DORIS storage ring at HASYLAB (Hamburg, Germany). The Energy Distribution Curves (EDCs) of photoemitted electrons were measured for the valence band region and for Si 2*p* and Mn 3*p* core levels. Photoelectrons were analyzed with a double-pass cylindrical mirror analyzer with the resolution about 0.2 eV typically obtained in the experiment. Photon energy $h\nu$ = 130 eV was used to measure Si 2*p* spectra and the region of energy from 48 up to 60 eV was used to measure set of Fano resonances EDC's. In the cleaning procedure in UHV the sample was heated up to 500°C. The obtained results of SiC valence band electronic structure and Si 2*p* band are comparable to presented in papers [3] and [4] relatively. The Mn atoms were sequentially deposited (up to 3 ML) on SiC substrate in room temperature. The annealing of the sample (500°C) with deposited Mn atoms leads to the diffusion of Mn and doping of the crystal surface region.

Deposition of Mn atoms on SiC leads to the change of EDC spectra of SiC valence band. At the valence band edge appears sharp edge corresponding to the Fermi level. These sharp Fermi level edge appears due to creation of metallic islands by the part of the deposited Mn atoms. Other part of deposited Mn atoms (3ML thick) create remarkable changes as well in the spectra of the valence band. The structure appears due to creation of Mn, Si and C atoms chemical compounds in the SiC\Mn interface region. Due to annealing of the sample in temperature of 500°C the sharp edge of the Fermi level near completely disappears. These change occurs due to diffusion of Mn into the SiC crystal and possible creation of new chemical compounds. At the same time, after annealing, appears additional structure of the density of states at the valence band region.

Acknowledgements:

This work was supported in part within: MSHE of Poland grant N202 101 31/0749 32 and research project DESY/68/2007.

References

[1] K. Grasza, "A stability diagram for crystal growth from the vapor - a review", *Cryst. Res. Tachnol.* **42** (2007) 1202-1206.

[2] E. Tymicki, K. Grasza, R. Diduszko, R. Bozek, M. Gala, "Initial stages of SiC crystal growth by PVT method", *Cryst. Res. Tachnol.* **42** (2007) 1232-1236.

[3] J. Labis, J. Oh, H. Namatame, M. Taniguchi, M. Hirai, M. Kusaka, M. Iwami, "High-resolution photoemission electron spectroscopy study on the oxynitridation of 6H-SiC(0001) **-√3×√3R30°** surface", *Appl. Surf. Sc.* **237** (2004) 170-175.

[4] L.I. Johansson, P.-A. Glans, N. Hellgren, "A core level and valence band photoemission study of 6H-SiC(0001)", *Surf. Sc.* **405** (1998) 288-297.

P23

XAS STUDIES OF THE REACTION OF GOLD(III) COMPLEX IONS WITH THE SODIUM HYDROXIDE AND GLUCOSE IN ACIDIC AND ALKALINE AQUEOUS SOLUTION

K. Pacławski [1*], D.A. Zając [2,3], K. Fitzner [1], and Cz. Kapusta [4]

[1] *Department of Physicochemistry and Metallurgy of Non-Ferrous Metals, Faculty of Non-Ferrous Metals, AGH University of Science and Technology, 30 Mickiewicza Ave., 30-059 Kraków, Poland*

[2] *Hasylab at DESY, Notkestrasse 85, 22607 Hamburg, Germany*

[3] *H. Niewodniczański Institute of Nuclear Physics of PAN, 152 Radzikowskiego Street, 31-342 Kraków, Poland*

[4] *Department of Solid State Physics, Faculty of Physics and Applied Computer Science, AGH University of Science and Technology, 30 Mickiewicza Ave., 30-059 Kraków, Poland*

Keywords: XAS, EXAFS, QEXAFS, gold(III) complex ions, hydrolysis

**) e-mail: paclaw@agh.edu.pl*

The kinetics of hydrolysis reaction of gold(III) chloride complex ions has recently been studied mainly with spectrophotometry UV-Vis [1] or potentiometry [2]. However, these two techniques have some disadvantages in such an application. First, they can not be applied when the gold(III) complexes lose chromophoric groups and therefore do not absorb electromagnetic radiation in the UV-Vis region. The second one, based on the measurements of redox electrode potential, does not provide information about structures of the reactants as well as the products. Additionally, the response of such an electrode is too slow to detect the changes during relatively fast reaction.

In our study of the reaction described above we have applied the X-ray absorption spectroscopy in order to investigate changes in the structure of gold(III) complex ions during the reaction with sodium hydroxide as well as with glucose. The EXAFS and QEXAFS experiments were carried out at Hasylab/DESY in Hamburg. A special sample holder was constructed at the X1 beamline to enable the detection of the course of these reactions. All EXAFS spectra of the solutions were recorded in transmission at the Au-L_3 edge, and QEXAFS spectra were collected during the reaction every 60 second. The hydrolysis was carried out at ambient temperature (20°C) using $1x10^{-3}$ M $HAuCl_4$ solution in 0.1 M HCl and 0.1-0.5 M NaOH as reactants. A comparison of the spectra obtained before and after the hydrolysis (Fig. 1), indicate differences in the structures of gold(III) complex ions. They are attributed to the substitution of chloride ligands by the hydroxyl ions.

From all the experiments we had carried out, it was not possible to detect the changes in the structure of gold(III) complex ions during the time of reaction, because of too high rates of the process, comparing with the detection time. However, good quality spectra were obtained before and after the reactions from which the changes in the structure of these complex ions were determined (characteristic bond length for Au-Cl and Au-OH were derived). The results obtained were compared with the simulated spectra of the possible different gold(III) complex ions, present in the solution. On this basis the mechanism of the reaction was suggested.

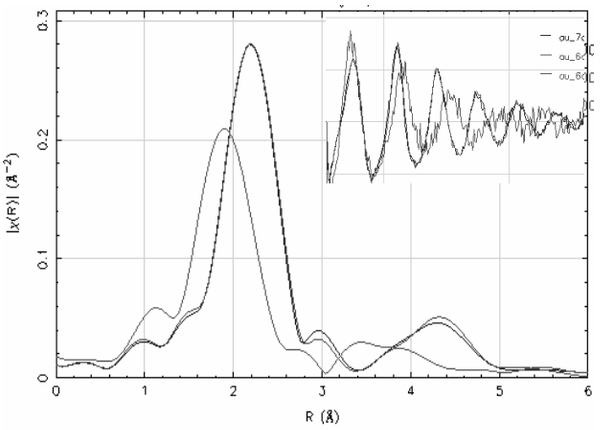

Figure 1. EXAFS functions at subsequent stages of the hydrolysis of gold(III) chloride complex ions in aqueous solution. Blue and red – pH = 1, green – pH = 8.

Acknowledgements: This work was supported by the Polish Ministry of Science and Higher Education, Grant No. 3 T08B 015 29.

References

[1] L. Gmelin, "*Gmelin Handbook of Inorganic and Organometallic Chemistry – Au*", 8th Edition (1992).

[2] N. Bjerrum, *Bull. Soc. Chim. Belg.* **57** (1948) 432-445.

P24

DETERMINATION OF LATERAL INHOMOGENEITY OF THE CHEMICAL COMPOSITION PROFILE OF AlAs/GaAs DISTRIBUTED BRAGG REFLECTORS GROWN BY MBE ON (100)-ORIENTED GaAs SUBSTRATE

J. Gaca [1], J. Gronkowski [2], A. Jasik [3], K. Pierściński [3], M. Tokarczyk [2*], and M. Wojcik [1]

[1] *Institute of Electronic Materials Technology, ul. Wólczyńska 133, 01-919 Warsaw, Poland*
[2] *Institute of Experimental Physics, University of Warsaw, ul. Hoża 69, 00-681 Warsaw, Poland*
[3] *Institute of Electron Technology, Warsaw, Al. Lotników 32/46, 02-668 Warsaw, Poland*

Keywords: X-ray diffraction, MBE, Bragg mirrors

**) darkcat35@gmail.com*

A 15-pair AlAs/GaAs distributed Bragg reflector (DBR) was grown by molecular beam epitaxy (MBE) [1]. The GaAs/AlAs heterostructure was deposited on a (001)±0.5 oriented GaAs:Si wafer with diameter of 50.8 ± 0.4 mm and thickness of about 450 μm. Optical reflectance (OR) and high resolution X-ray diffraction (HRXRD) techniques were used for characterization of the DBR structure and verification of its intended parameters.

To determine the lateral inhomogeneity of the chemical composition profile of the investigated sample, series of rocking curve measurements in the vicinity of (004) GaAs reflection were performed using a Philips high-resolution diffractometer with CuKα_1 radiation and 4-reflection Bartels monochromator Ge(220). The measurements were made along two perpendicular diameters, starting from the edge, with the interval of 1 mm. For each experimental rocking curve a simulated one was fitted with X'Pert Epitaxy 3.0b program. In this way the GaAs and AlAs layer thickness as a function of the distance from the edge of the wafer was determined (Fig. 1).

It was found that there is a region in the central part of the wafer with constant thickness of AlAs and GaAs layers. This region occupies about 25% of the surface area. It was also determined that the thickness of both layers decreases with the increasing distance from the centre of the wafer surface.

This structural feature is confirmed by optical reflectivity measurement. In Fig. 2 it is seen that the reflectivity spectra are shifted relative to each other depending on the region of the wafer where the data were collected. A blue shift of the reflectivity spectra is observed with the increase of the distance from the centre of the sample to the point where the data had been collected.

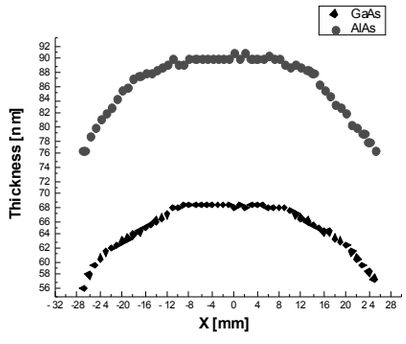

Figure 1. Thickness of the AlAs and GaAs periods for 15 pair AlAs/GaAs DBR as a function of the distance X from the centre of the sample.

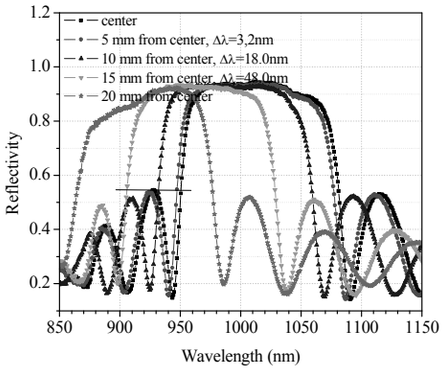

Figure 2. Reflectivity spectra for 15 pair AlAs/GaAs DBR measured as a function of the distance from the centre of the sample.

References

[1] J. Gaca, M. Wojcik, A. Jasik, K. Pierściński, M. Kosmala, A. Turos, A.M. Abdul-Kaderd, "Effects of composition grading at heterointerfaces and layer thickness variation on Bragg mirror quality", *Optoelectr. Rev.* **16** (2008) 12-17.

P25

XRADMED - BIOMEDICAL FACILITY FOR DIAGNOSTICS AND THERAPY AT POLISH SYNCHROTRON IN CRACOW: A CONCEPTUAL DESIGN

J.B. Pelka*

Institute of Physics, Polish Academy of Sciences, Al. Lotnikow 32/46, 02-668 Warsaw, Poland

Keywords: synchrotron radiation, bioimaging, phase contrast, radiography, radiotherapy

**) e-mail: pelkay@ifpan.edu.pl*

XRADMED is a biomedical facility, proposed for the Polish Synchrotron Light Source (PSLS) to be built in Cracow. The design outlines of the facility refer to solutions accepted in other biomedical beamlines. Special attention has been paid to the machines characterized by parameters similar to that planned at PSLS, like the Canadian CLS (BMIT) [1], the Australian ALS (BL-10) [2] and the Catalonian ALBA [3]. XRADMED is aimed at application of SR x-ray techniques for imaging, diagnostics and therapy in biological and medical systems, including humans and animals. Some of the proposed solution are on the top edge of currently developed accelerator and x-ray optics technology. Their feasibility and efficiency has been confirmed at the above mentioned biomedical beamlines.

XRADMED will be equipped in two different types of radiation sources, that will be constructed in two phases. First the bending magnet (BM) will be built, and afterwards the more advanced and powerful superconducting wiggler (SCW) will be added. A significant part of infrastructure will be shared by both beamlines.

The BM beamline will host a wide range of imaging techniques, exploiting absorption and phase contrast, with diffraction enhanced imaging (DEI), phase contrast imaging (PhCI) operating in computed tomography (CT) and in planar modes, absorption spectroscopy imaging and fluorescence imaging, among others. The beamline will serve as a place to test and validate new ideas, to develop new imaging and therapy technologies, and will relieve some of the imaging program from the SCW beamline after its construction. The dose rates available at the BM line will be, however, insufficient to most of time-resolved techniques, or to avoid blur due to natural body movements (like respiratory or heart action) during a single-shot irradiation of live animals or humans.

The innovative SCW beamline is designed to provide tunable monochromatic beam, of width up to 25 cm, that allows for imaging and treatment of a wide variety of subjects, from mice to large domestic animals, with spatial resolution down to 10 μm and below. The SCW beamline will host a number of imaging capabilities, including K-edge subtraction (KES), diffraction enhanced imaging (DEI), multiple image radiography (MIR), phase contrast imaging (PCI) as well as normal absorption imaging in both projection and CT modes of operation. In addition, the beamline will deliver a filtered white beam, foreseen to reach the entrance dose rates up to 3500 Gy/s, invaluable in some imaging and therapy techniques, like microbeam radiation therapy (MRT) or synchrotron stereotactic radiation therapy (SSRT). Monochromatic x-ray flux of up to 10^{14} ph/s/cm^2 will be available.

Upon completion, the XRADMED will constitute a world class facility with unique synchrotron specific imaging, diagnostics and therapy capabilities. It will be ready to cope with unsolved, the most crucial issues in biology, medicine, agriculture, ecology, biotechnology and other areas related to life sciences. The research teams at XRADMED will be able to develop strong experimental programs, competitive to that at other biomedical synchrotron facilities over the world.

Acknowledgments: This work has been partially supported by the grant of Ministry of Science and Higher Education of Poland, SPB nr. DESY/68/2007.

References

[1] Canadian Light Source Activity Report 2001–2004; Editor: M. Dalzell; CLS Document No. 0.18.1.2; Canadian Light Source Inc. 2005 (http://www.lightsource.ca/).

[2] R.A. Lewis, "Medical applications of synchrotron radiation in Australia", *Nucl. Instrum. Meth. Phys. Res. A* **548** (2005) 23–29.

[3] A. Bravin, R. Noguera, M. Sabés, J. Sobrequés, *ALBA Biomedical Beamline (ABME). A Proposal for the ALBA S.A.C.*, (Barcelona 2004).

[4] http://synchrotron.pl/.

P26

THE CRYSTALLOGRAPHIC STRUCTURE OF CATALYTICALLY GROWN ZnTe AND ZnMgTe NANOWIRES

E. Dynowska [1*], W. Szuszkiewicz [1], J.Z. Domagala [1], E. Janik [1], T. Wojtowicz [1], and W. Caliebe [2]

[1] *Institute of Physics, Polish Academy of Sciences, al. Lotników 32/46, 02-668 Warszawa, Poland*
[2] *Hasylab at DESY, Notkestr. 85, D-22603 Hamburg, Germany*

Keywords: nanowires, ZnTe, MBE technology, x-ray diffraction, synchrotron radiation

**) e-mail: dynow@ifpan.edu.pl*

One-dimensional semiconductor nanostructures in the form of free-standing nanowires (NWs) have become the focus of many research laboratories over the last years due to their use in basic physics investigations, as well as due to their potential applications in electronics and photonics devices. Using modern epitaxial growth techniques and the substrates activated by catalyst drops, NWs with radii of the order of tens of nanometers and lengths up to tens of micrometers can be obtained.

In this paper we describe the structural properties of ZnTe and ZnMgTe NWs grown by molecular beam epitaxy (MBE) using the (100), (110) and (111)-oriented GaAs substrates covered by gold/gal eutectic droplets serving as nanocatalysts. The NWs had diameters ranging from 30 to 70 nm and lengths between 1 and 2 μm [1,2]. The detailed characterization of the NWs by: field emission scanning electron microscopy (FE-SEM), high resolution transmission electron microscopy (HRTEM), energy-dispersive x-ray spectroscopy (EDXS) and x-ray diffraction (XRD) was previously reported. The FE-SEM and HRTEM studies shown that, independently on the orientation of the GaAs substrate, ZnTe NWs grow preferentially along <111>-type directions of the substrate and their growth axis is also <111>.

The main topic of this paper are the results of XRD studies. The measurements were performed using synchrotron radiation at the W1.1 beamline at DESY-Hasylab. The monochromatic x-ray beam of wavelength λ = 1.54056 Å was used. Two modes of measurement were applied: symmetrical ω-2θ scan and coplanar 2θ scan in the glancing incidence geometry. In the first mode of measurement the detector position (2θ angle) was coupled with the maximum intensity of the proper rocking curve (ω angle) resulting from the crystallographic orientation of the GaAs substrate. Such measurement allows to detect the lattice planes of NWs parallel to the crystallographic orientation of the substrate. In the second mode of measurement the rotational axis of the sample (ω axis) has been aligned exactly with the sample surface and then the sample was rotated about this axis by a very small angle α (here equal to 1º). During measurement the angular position of the sample with respect to the incident x-ray beam (α) was fixed while the detector was rotated in the wide range of 2θ angles in the plane perpendicular to the sample surface. Such technique is very sensitive to very thin layers. The examples of the diffraction patterns obtained in this two modes for ZnTe NWs grown on GaAs (001)-oriented substrate are shown in Figs. 1 and 2.

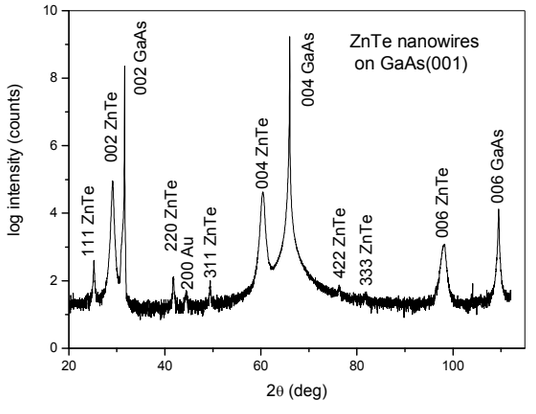

Figure 1. The x-ray ω-2θ scan obtained for ZnTe NWs grown on (001)-oriented GaAs substrate.

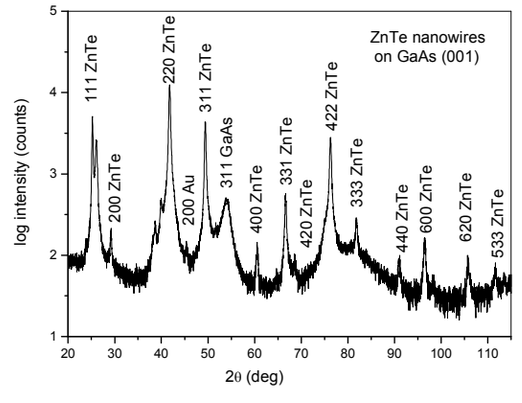

Figure 2. The x-ray 2θ scan obtained in glancing incidence geometry for ZnTe NWs grown on (001)-oriented GaAs substrate.

P26

Analysis of the ω-2θ pattern shows that the crystallographic orientation of the substrate imposes the orientation of the NWs: the strongest among observed reflections of ZnTe are indexed 002, 004 and 006, respectively, which correspond to analogous reflections of the GaAs substrate. This means that the (100) lattice planes of the NWs are parallel to the (100) lattice planes of the substrate. Additional small peaks visible in Fig. 1 (*e.g.* indexed as 111, 220, 311…), as confirmed by 2θ scan performed in the glancing incidence geometry (Fig. 2), originate mainly in the thin polycrystalline layer of ZnTe that forms directly on the GaAs substrate between the NWs.

The measurements performed for the NWs grown on (110) and (111)-oriented GaAs substrates lead to similar conclusions confirming the epitaxial relation between the substrate and the growing NWs.

The important question is the crystal structure of NWs. Detailed structural information concerning the single ZnTe NWs was obtained from HRTEM studies. Electron diffraction from a large number of the NWs reveals pattern characteristic for the zincblende (ZB) crystal structure with lattice parameter a = 0.61 nm [2]. This value, within frames of accuracy typical for electron diffraction, seems to be the same as that for bulk ZnTe (a = 0.6103 nm). However, on the base of x-ray diffraction measurements, the ZB lattice parameter of ZnTe NWs calculated from symmetrical reflections 400, 440 and 333, respectively, was slightly larger than that for bulk ZnTe and equals to a = 0.6112 nm for (100)-oriented substrate, a = 0.6107 nm for (110)-oriented substrate and a = 0.6109 nm for (111)-oriented substrate (all values are obtained with accuracy of ± 0.0002 nm).

In order to explain such results we assumed that the real unit cell of NWs has to be deformed along the [111] crystallographic direction of zincblenede unit cell. Such deformation would lead to the rhombohedral unit cell. We suppose that the source of such deformation is the special defect structure inside NWs visible in the HRTEM studies. According to these results for the majority of NWs the bottom part reveals a high number of stacking faults and/or microtwins [2]. As a result the mean interplanar spacing along [111] direction changes leading to rhombohedral distortion of the ZB unit cell. To check this supposition we have undertaken an attempt of lattice parameters calculation of such distorted unit cell.

As it is known, the rhombohedral unit cell is characterized by two lattice parameters a and α, where $a = b = c$, $\alpha = \beta = \gamma \neq 60°$. So, the knowledge of at least two different interplanar spacing is necessary for description of such crystal structure. In our calculations we used the interplanar spacing calculated from x-ray ω–2θ scans obtained for differently oriented ZnTe NWs, d_{400}, d_{440} and d_{333}, changing properly their *hkl* indexes. We assumed that the defect structure has the same character in all these NWs, so the unit cell distortion should also be the same. The *hkl* indexes transform to the defined above rhombohedral unit cell as follows: from 400 in cubic cell to 220, from 440 – to 422 and from 333 – to 333, respectively. Next, we have calculated rhombohedral lattice parameters of ZnTe NWs, solving the system of equations proper for rhombohedral crystals for d_{220} and d_{422} values. We obtained the lattice parameters a = 0.4320 ± 0.0004 nm and α = 60.06 ± 0.01°. In order to check the correctness of this result we calculated the d_{333} value for this unit cell and compared this with the experimental d_{333} value obtained for (111)-oriented ZnTe NWs – these values are the same within the accuracy of 0.0001 nm. Therefore, we believe that the procedure used for above calculations is correct. Similar calculations performed for ZnMgTe NWs grown on the (100) and (110)-oriented GaAs substrates gave the rhombohedral unit cell with parameters: a = 0.4353 ± 0.0004 nm and α = 60.04 ± 0.01°. On the basis of the above result we can state that the shape of the unit cell is the same as in the case of ZnTe NWs (the angle α is practically the same in both cases), while the a parameter is larger due to bigger size of Mg atoms built in ZnTe lattice.

Summarizing, we can say that in the light of x-ray studies the crystal structure of ZnTe NWs differs from that in the bulk material: due to the defect structure created during growth of NWs the ZB unit cell is distorted to the rhombohedral one.

Acknowledgements:

This research was partially supported by the Ministry of Science and Higher Education (Poland) through Grants N507 030 31/0735 and N515 015 32/0997, and by the Network "New materials and sensors for optoelectronics, information technology, energetic applications and medicine", as well as by the European Community - Research Infrastructure Action under the FP6 "Structuring the European Research Area" Programme (through the Integrated Infrastructure Initiative "Integrating Activity on Synchrotron and Free Electron Laser Science", Contract RII3-CT-2004-506008).

References

[1] E. Janik, J. Sadowski, P. Dluzewski, S. Kret, L.T. Baczewski, A. Petroutchik, E. Lusakowska, J. Wróbel, W. Zaleszczyk, G. Karczewski, T. Wojtowicz, A Presz, "ZnTe nanowires grown on GaAs (100) substrates by molecular beam epitaxy", *Appl. Phys. Lett.* **89** (2006) 133114.

[2] E. Janik, P. Dłuzewski, S. Kret, A. Presz, H Kirmse, W. Neumann, W. Zaleszczyk, L.T. Baczewski, A. Petroutchik, E. Dynowska, J. Sadowski, W. Caliebe, G. Karczewski, T. Wojtowicz, "Catalytic growth of ZnTe nanowires by molecular beam epitaxy: structural studies", *Nanotechnology* **18** (2007) 475606.

P27

DEFECTS IN Si-Ge ANNEALED UNDER HIGH HYDROSTATIC PRESSURE

A. Misiuk [1*], K. Wieteska [2], J. Bak-Misiuk [3], W. Wierzchowski [4], P. Romanowski [3], A. Wnuk [4], B. Surma [4], W. Graeff [5], and M. Prujszczyk [1]

[1] *Institute of Electron Technology, Z12, Al. Lotników 32/46, 02-668 Warsaw, Poland*
[2] *Institute of Atomic Energy, 05-400 Otwock-Świerk, Poland*
[3] *Institute of Physics, PAS, Al. Lotników 32/46, 02-668 Warsaw, Poland*
[4] *Institute of Electronic Materials Technology, 133 Wolczynska Str., 01-919 Warsaw, Poland*
[5] *HASYLAB at DESY, Notkestr. 85, D-22603 Hamburg, Germany*

Keywords: Si-Ge, uniformity, annealing, hydrostatic pressure, defects

**) e-mail: misiuk@ite.waw.pl*

Silicon-germanium single crystals (Si-Ge) are of growing interest, mostly because of their application in optoelectronics [1]. Even in the case of low Ge content, such wafers indicate the presence of growing bands related to non-uniform Ge distribution.

Annealing of Si-Ge (grown by the Czochralski method), especially under enhanced pressure of inert gas ambient (HP), results in transformation of its defect structure [2]. This effect is related to precipitation of interstitial oxygen (O_i) always present in such material.

The defect structure of Si-Ge samples with different Ge and O_i contents (Table 1), subjected to processing for 5 h at up to 1400 K under HP up to 1.1 GPa, has been investigated by synchrotron (at HASYLAB), high resolution X-ray, photoluminescence (PL) and infrared (IR) methods.

Synchrotron topographs of as grown and processed Si-Ge revealed the presence of dense growth bands (Fig. 1) connected with segregation of Ge, and dislocations, often forming the glide bands. The dislocation density exceeded 10^3 cm^{-3}; most of dislocations exhibited features related to their decoration with impurities.

Annealing at 1270 / 1400 K under 10^5 Pa resulted in markedly increased lattice parameter, *a*, caused, probably, by re-distribution of Ge in the Si-Ge lattice improving its homogeneity. The same processing under HP also resulted in changed *a* (Fig. 2). This change is related to partial HP-induced precipitation of O_i's, as confirmed also by PL and IR measurements. Both, oxygen precipitation and sample homogenisation, are observed after processing of Si-Ge, especially under HP.

Table 1. Investigated Si-Ge samples: content of Ge, orientation, and concentration of O_i, c_o ($\times 10^{17}$ cm^{-3}).

at. % of Ge	orientation	c_o
1.4×10^{-3}	001	6.5
1.4	111	9.0
1.8	111	10
2.6	111	8.0

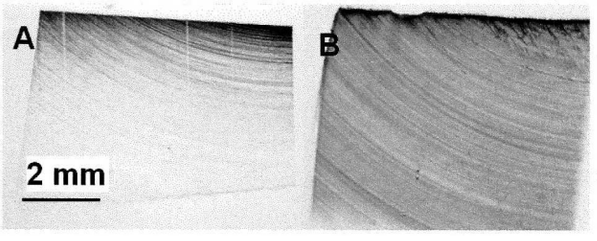

Figure 1. Bragg case synchrotron section (A) and projection (B) topographs of $Si_{0.982}Ge_{0.018}$ annealed at 1400 K under 10^5 Pa.

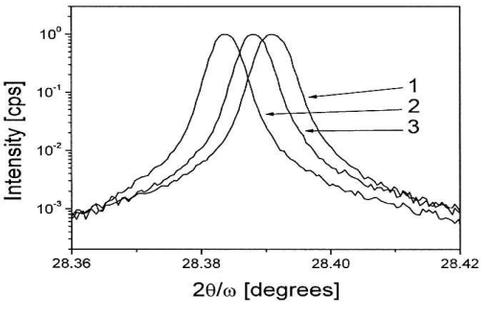

Figure 2. $2\Theta/\omega$ scan (111 reflection) for $Si_{0.986}Ge_{0.014}$: 1 – as grown; 2, 3 – processed for 5 h at 1270 K under 10^5 Pa (2) or 1.1 GPa (3).

Acknowledgements: The authors are indebted to Dr N.V. Abrosimov from the Institute of Crystal Growth, Berlin and Prof. Deren Yang from the State Key Laboratory of Silicon Materials, Hangzhou, China, for some Si-Ge samples.

References

[1] S. Pizzini, M. Acciarri, S. Binetti, A. LeDonne, S. Marchionna, M. Bollani, "Defect studies on silicon and silicon-germanium for PV and optoelectronic applications", *Mater. Sci. Semicond. Process.* **9** (2006) 66-73.

[2] A. Misiuk, C.A. Londos, J. Bak-Misiuk, Deren Yang, W. Jung, M. Prujszczyk, "Stress-dependent transformation of interstitial oxygen in processed Ge-doped Cz-Si", *Nucl. Instrum. Meth. Phys. Res. B* **253** (2006) 205-209.

P28

STRUCTURAL STUDIES OF WIDE-GAP QUANTUM DOTS BASED ON InGaN

E. Piskorska-Hommel [1,2*], A. Wolska [2], I.N. Demchenko [2,3], J.I. Flege [1], R. Hildebrand [1], T. Yamaguchi [1,4], and D. Hommel [1]

[1] *Institute of Solid State Physics, University of Bremen, Otto-Hahn-Allee 1, D-28359 Bremen, Germany*
[2] *Institute of Physics, Polish Academy of Sciences, Al. Lotników 32/46, 02-668 Warsaw, Poland*
[3] *University of Nevada - Las Vegas, USA*
[4] *Research Organization of Science & Engineering, Ritsumeikan University, Shiga, Japan*

Keywords: quantum dots, InGaN, x-ray absorption, synchrotron radiation

**) e-mail: e.piskorska@ifp.uni-bremen.de*

Processes of self-organization during epitaxial growth of semiconductor heterostructures represent methods for the fabrication of the very small nanostructures (quantum wires and dots) with electronic and optical properties very promising for their technological applications, like optical sensors, lasers or storage media [1]. The Stransky-Krastanov (S-K) growth mode is a well-known method to obtain such self-organized dots (QDs). Nevertheless, in case of InGaN the structures obtained in S-K mode are not stable during the overgrowth by GaN. A challenging task is to growth stable InGaN nanostructures. The structural properties play an important role in determining the performance of the light-emitting devices. Extended X-ray Absorption Fine Structure (EXAFS) refers to the oscillation caused by interference of the photoelectron wave of excited atoms scattered on the neighbors. Therefore from such an EXAFS analysis the local structure around a studied element can be derived, i.e. the radial distance (R) between the absorbing atom and its surrounding atoms, the number of atoms in the coordination shell and the mean-square deviation from ideal atomic position due to thermal vibrations and structural disorder (σ^2, Debye-Waller factor).

InGaN crystallizes in the wurtzite structure. Two kinds of In-N bonds can be distinguished: a longer single bond along the *c*-axis (*b*) and three shorter bonds with respect to the *c*-plane (*d*), as displayed in Fig. 1.

Due to the natural polarization of the synchrotron radiation information about anisotropy of bonds in the crystal and strain anisotropy can be extracted [2].

The InGaN quantum dots were grown by metal organic vapour phase epitaxy (MOVPE) on a sapphire (0001) substrate covered with 2 μm GaN layer deposited by MOVPE as well to ensure a superior growth start of the dots. Part of the samples were capped by a thin layer of GaN deposited at different growth temperatures. In case of high temperature capping the InGaN dots are dissolved forming a quantum well like layer [3]. The uncapped quantum dots were initially studied for the next determination of capping layer influence on the changes of the local structure (strain field) around In atoms.

The EXAFS spectra for investigation of InGaN self-assembled QDs at the K-edge of In were recorded at the beamline BM08 at the ESRF in Grenoble. Data were collected in fluorescence mode using a 13-elements high purity Ge detector. Indium L-edge XANES data were collected at the Advanced Light Source (ALS). The incident beam was monochromatized using double crystal the Si(111) monochromator. Fluorescence X-ray intensity from the sample were measured by a Hamamatsu (type S3584, 28 mm by 28 mm active area) Si photodiode. The measurements were done with taking into account polarization effect of synchrotron radiation.

The x-ray absorption spectroscopy was used to estimate the atomic ordering in QDs, the bond length between absorbing atoms and its surroundings as well as the anisotropy of the bonds. The result of the analysis will be discussed.

Acknowledgements: This work was supported in part by Polish State Committee for Scientific Research *(Grant No **N202 142 32/3888**)* and DFG Research Group "Physics of nitride-based, nanostructured light-emitting devices" in Bremen.

References

[1] J. Stangl, V. Holý, G. Bauer, *Rev. Mod. Phys.* 76 (2004) 725.

[2] K. Lawniczak-Jablonska, T. Suski, Z. Liliental-Weber, E.M. Gullikson, J.H. Underwood, R.C.C Perera, T.J. Drummond, *Appl. Phys. Lett.* **70** (1997) 2711- 2713.

[3] A. Pretorius, T. Yamaguchi, C. Kübel, R. Kröger, D. Hommel, A. Rosenauer., *phys. stat. sol.* (c) **3** (2006) 1679-1682.

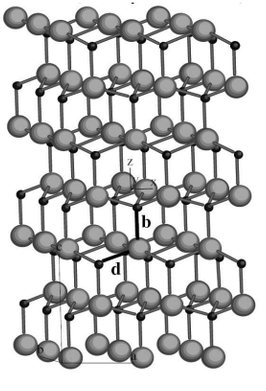

Figure 1. The wurtzite structure of GaN crystal and the bond length (*b*, *d*).

P29

XRR INVESTIGATIONS OF II-VI AND III-NITRIDR BASED DBR STRUCTURES, MULTILAYERS AND SUPERLATTICES

R. Hildebrand [1*], Th. Schmidt [1], A. Zargham [1], C. Kruse [1], K. Otte [1], D. Hommel [1], and J. Falta [1]

[1] *Institute of Solid State Physics, University of Bremen, Otto-Hahn-Allee 1, 28359 Bremen, Germany*

Keywords: x-ray reflectivity, DBR, GaN, AlN, InGaN, VCSEL, superlattice, multilayer, synchrotron radiation,

**) e-mail: hildebrand@ifp.uni-bremen.de*

Surface and interfacial roughness is a major issue for many technologically relevant multilayer systems in magnetism, optics and semiconductor physics. In optoelectronic applications, interfacial roughness affects especially the electrical and optical properties of light emitting semiconductors such as vertical cavity surface emitting lasers (VCSELs). On one hand this leads to an enhanced non-radiative recombination of the carriers, on the other hand the emitted light will be partially scattered or absorbed at the interfaces of the distributed Bragg reflectors (DBRs), which are usually applied as high quality reflectors in VCSELs and waveguides. Thus the interface quality will not only affect the efficiency, but also the lifetime of light emitting devices.

Using x-ray reflectivity (XRR) we have investigated DBRs and related built-in super-lattices for the blue to violet (AlN/InGaN) [1] and blue to green (MgS/ZnCdSe) [2] spectral regions, respectively. For the XRR experiments a double crystal monochromator setup with symmetrically cut Si(111) crystals was used at the BW1 beamline at HASYLAB (DESY, Hamburg). The scans were recorded in conventional θ–2θ geometry. All structures were grown by molecular beam epitaxy in our institute in Bremen.

As an example for the composition of DBRs with embedded superlattice a transmission electron micoroscopy (TEM) image of a II-VI mirror is shown in FiG. 1.

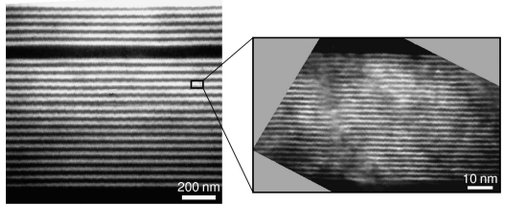

Figure 1. TEM of a similar II-VI 16 × DBR with embedded super-lattice in one of the two DBR-mirrorlayers.

The nitride samples consist a period of 30 double layers, and the zincselenide structures consist of 18 double layers. The aim of the study is to compare the established ZnSe-system with the nitrides.

The measurement shown the lowest reflec-tivity in III-V system in comparison with II-VI. The low reflectivity by the nitrides is caused due to the large lattice mismatch with respect to the sapphire (0001) substrate and due the significant surface mosaicity [3] of GaN, thus the enhanced roughness, which negatively influences the contrast in the measurements (Fig. 2). Roughness is an important parameter for the preparation and further reflectivity simulations from which we can obtain also information like electron density, and layer thickness [4].

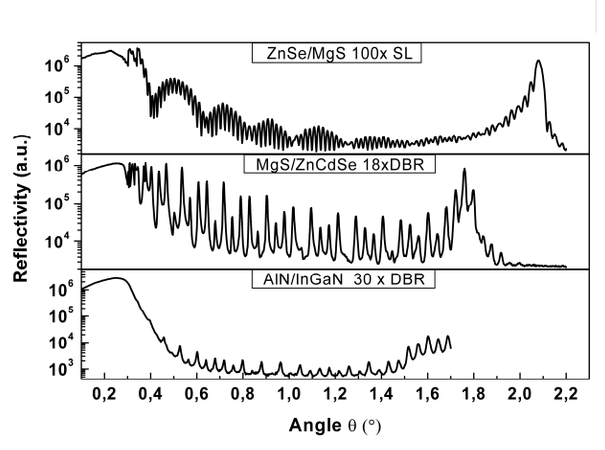

Figure 2. XRR - curves for ZnSe/MgS super-lattice, MgS/ZnCdSe 18 × DBR and AlN/InGaN 30 × DBR structures recorded up to the first order short-period superlattice Bragg peak.

Acknowledgements: This work was supported by the DFG Research Group "Physics of nitride-based, nanostructured light-emitting devices" grant No. FOR 506 in Bremen.

References

[1] H. Lohmeyer, K. Sebald, C. Kruse, R. Kröger, J. Gutowski, D. Hommel, J. Wiersing, F. Jahnke, "Crack free monolithic nitride vertical-cavity surface-emitting laser structures and pillar microcavities" *phys. stat. sol.* (a) **203** (2006) 1749.

[2] C. Kruse, S.M. Ulrich, G. Alexe, E. Roventa, R. Kröger, B. Brendemühl, P. Michler, J. Gutowski, D. Hommel, "Green monolithic II-VI vertical-cavity surface-emitting laser operating at room temperature", *phys. stat. sol.* (b) **241** (2004) 731.

[3] M. Siebert, Th. Schmidt, J. Falta, S. Figge, S. Einfeldt, D. Hommel, HASYLAB, Annual Report, vol. 1 (2003) p.559.

[4] U. Pietsch, V. Holý, T. Baumbach, "High-Resolution X-Ray Scattering", 2nd edition, (Springer, 2004).

P30

X-RAY ABSORPTION AND MAGNETIC CIRCULAR DICHROISM ON MnSb LAYERS GROWN BY *MBE*

A. Wolska [1*], K. Lawniczak-Jablonska [1], M.T. Klepka [1], J. Sadowski [1,2], E. Holub-Krappe [3], A. Persson [4], and D. Arvanitis [4]

[1] *Institute of Physics PAS, al. Lotników 32/46, 02-668, Warsaw, Poland*
[2] *Lund University, MAX-Lab, Lund SE-221 00, Sweden*
[3] *Hahn-Meitner Institute, Department of Magnetism, Glienicker Str. 100, D-14109 Berlin, Germany*
[4] *Physics Department, Uppsala University, Box 530, 75121 Uppsala, Sweden*

Keywords: MnSb, EXAFS, XMCD, spintronics

**) e-mail: wolska@ifpan.edu.pl*

Among the compounds which can be used in spintronic applications, these created by introducing ferromagnetic inclusions in a semiconductor matrix seem to be very promising. In order to obtain materials with desired magnetic properties, it is reasonable to start with inclusions with a Curie temperature (T_C), above room temperature. One of the candidate materials is MnSb. It was showed that bulk MnSb has T_C of 587 K and the $Mn_{1-x}Sb_x$ layers grown on GaAs reach a T_C of 620 K [1, 2]. This indicates that MnSb can be a good compound to form ferromagnetic nano inclusions above room temperature.

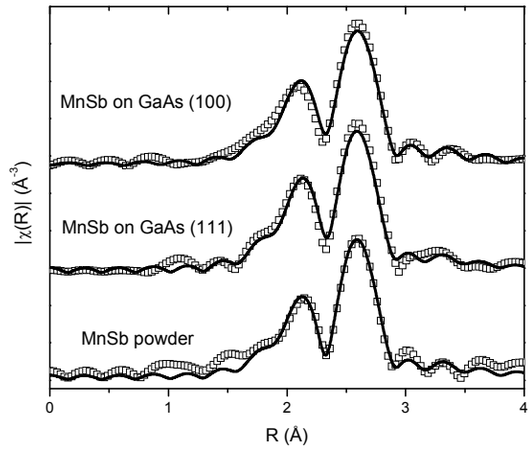

Figure 1. EXAFS spectra of the MnSb samples (squares) and the results of the fitting (full line).

Before establishing the best growth conditions for the new multiphase material, the characterization of thin layers is needed. The MnSb layers were grown on two types of substrates: GaAs(111) and GaAs(100) by MBE. The substrate temperature was about 250°C, the growth rate 20 nm/h. Prior to the MnSb growth the GaAs substrates were subjected to the typical procedure of native oxide desorption and high temperature GaAs buffer growth.

The XANES and EXAFS spectra at the Mn K-edge were measured at Hasylab (A1 station) using a single element germanium fluorescence detector. Additional spectrum of powdered MnSb standard sample was measured in transmission mode. The XMCD spectra at the Mn $L_{3,2}$-edges and Sb $M_{5,4}$-edges were measured at MAX-lab (beamline D-1011). The spectra were collected in the total electron yield mode with the samples remanently magnetized.

Table 1. Results of fitting MnSb layers on GaAs (111) and GaAs (100) together with the powder MnSb reference sample.

	powder	on GaAs (111)	on GaAs (100)
N_{Sb}	[6]	5.7 ± 0.7	5.6 ± 0.7
N_{Mn}	[2]	2.7 ± 0.6	2.2 ± 0.6
R_{Sb}	2.77 ± 0.01	2.76 ± 0.01	2.76 ± 0.01
R_{Mn}	2.84 ± 0.02	2.84 ± 0.02	2.84 ± 0.03

The Artemis and Athena programs [3], using the IFEFFIT data analysis package, were used for the analysis of the EXAFS data. The Fourier transforms of the EXAFS data show that the local surrounding of the Mn atoms up to 3 Å in thin layer samples resembles that of the MnSb powder sample (Fig. 1), although, they differ in details. Table 1 presents the results of the simultaneous fitting of all spectra, where the numbers of nearest neighbours for the powder sample were fixed according to the known crystallographic data. This helped to determine the amplitude reduction factor which was used in fitting the thin layer samples, in order to determine the number of nearest neighbors. The obtained results confirmed that the investigated layers consist of MnSb compound but can slightly differ in the number of defects or stoichiometric ratio.

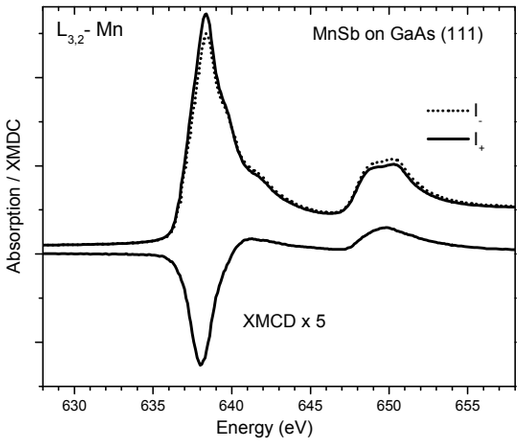

Figure 2. Dichroic XAS and XMCD spectra of the MnSb on GaAs (111) sample recorded at 100 K.

The dichroic signal obtained at 100 K was almost identical for both samples. An example of XMCD data is presented in Fig. 2. For the room temperature measurements, the XMCD signals were around two times weaker and showed slight differences between the samples. The shape of the signal agreed with those showed in Ref. 4. However, the absorption spectra show a smaller difference in the intensity between both polarizations. This can be due to the fact that the spectra presented in Ref. 4 were gathered with the samples under an applied magnetic field of 1.1 T, and not in remanence like in our case.

In conclusion, the EXAFS analysis confirmed that the local structure around Mn atoms is similar for both investigated layers and close to the one of MnSb. The XMCD signals of the samples show small differences in intensity at room temperature, an effect which disappears at 100 K. What's more, the XMCD at Sb $M_{5,4}$-edge is also visible and shows a similar temperature dependence.

Acknowledgements: This work was partially supported by national grant of Ministry of Science and High Education N202-052-32/1189 as well as by DESY/HASYLAB, MAX-lab (EC support program: Transnational Access to Research Infrastructures) and the European Community under Contract RII3-CT-2004-506008 (IA-SFS).

References

[1] A.F. Panchula, C. Kaiser, A. Kellock, S.S. Parkin, "Spin polarization and magnetotransport of Mn–Sb alloys in magnetic tunnel junctions", *Appl. Phys. Lett.* **83** (2003) 1812-1814.

[2] H. Akinaga, K. Tanaka, K. Ando, T. Katayama, "Fabrication and magneto-optical properties of epitaxial ferromagnetic $Mn_{1-x}Sb$ thin films grown on GaAs and sapphire", *J. Cryst. Growth* **150** (1995) 1144-1149.

[3] B. Ravel, M. Newville, "ATHENA, ARTEMIS, HEPHAESTUS: data analysis for X-ray absorption spectroscopy using IFEFFIT", *J. Synchrotr. Rad.* **12** (2005) 537-541.

[4] A. Kimura, S. Suga, T. Shishidou, S. Imada, T. Muro, S. Y. Park, T. Miyahara, T. Kaneko, T. Kanomata, "Magnetic circular dichroism in the soft-x-ray absorption spectra of Mn-based magnetic intermetallic compounds", *Phys Rev. B* **56** (1997) 6021-6030.

P31

A Fe-XANES STUDY OF AMORPHOUS ANALOGS OF PHOSPHO-OLIVINES Li_xFePO_4

M. Wasiucionek *, R. Bacewicz, J. Antonowicz, J.E. Garbarczyk, and P. Jóźwiak

Faculty of Physics, Warsaw University of Technology, Koszykowa 75, 00-662 Warsaw, Poland

Keywords: XANES, olivines, cathode materials, glassy conductors, Fe K-edge

** e-mail: mwas@mech.pw.edu.pl*

In recent years crystalline phospho-olivines $LiFePO_4$ have attracted much interest of many scientific and R&D groups worldwide as very promising cathode materials for Li-ion batteries [1]. Their performance in batteries is comparable to that of $LiCoO_2$ used in commercial cells, but they are safer, less toxic, more stable and much cheaper than the latter and therefore have a potential to replace them in the near future. The only major problem with olivines is their low electronic conductivity at room temperature. One of the possible solutions to this problem is nanocrystallization of the amorphous analogs of crystalline olivines [2].

A number of studies have shown that the electrical conduction phenomena in olivines depend much on their local structure and relative population of aliovalent Fe^{2+} and Fe^{3+} sites. XANES is an adequate tool to probe the local order around Fe ions and valence states of these ions. It is especially effective when used in conjunction with other methods.

A series of glassy analogs of phospho-olivines of the general formula Li_xFePO_4, where $0 \le x \le 1$, were prepared by a standard melt-quenching method [2]. The samples were characterized using a number of techniques: impedance spectroscopy, differential thermal analysis DTA, chemical analyses by ICP. The ICP analyses showed a slight deviation of the actual chemical composition from the nominal one.

Several compositions, corresponding to $x = 0$, 0.4, 0.8 and 1 were studied by XAFS spectroscopy (at K-absorption edge of iron) at the A1 station in HASYLAB in Hamburg. Samples were characterized, not only in their "as-received" form, but also after heat treatment at temperatures 510-530°C. At these temperatures, determined by DTA, the nanocrystallization of the glassy samples took place. Our studies have shown than the annealing at such conditions leads to appearance of crystalline grains, not exceeding 100 nm in size, embedded in the glassy matrix.

A XANES part of X-ray absorption spectra for as-received samples Li_xFePO_4 with intermediate lithium contents ($x = 0.4$, Fig. 1a) consists of a pre-peak with a maximum at 7112.8 eV containing a shoulder at 7111 eV, and an absorption edge with the mid-point at ca 7119 eV. After the annealing, the height of the prepeak decreases and more clearly is visible its complex structure. The peak consists of two overlapping contributions from Fe^{2+} and Fe^{3+} central ions. The absorption edge does not shift following the annealing (Fig. 1a).

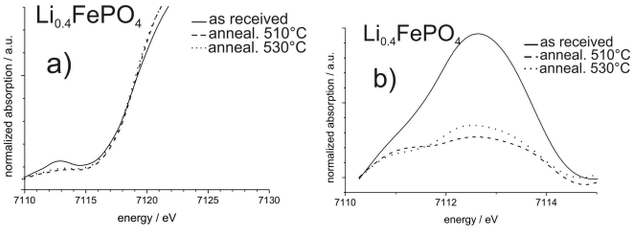

Figure 1. Fe K-edge X-ray absorption spectra of samples $Li_{0.4}FePO_4$: a) prepeak and absorption edge, b) close-up of the prepeak..

The observed change in the relative sizes of two components of the prepeak (*i.e.* centred at 7111 eV – Fe^{2+}, and at 7112.8 eV – Fe^{3+}) after the annealing, indicates that the relative populations of Fe^{2+} and Fe^{3+} sites become comparable to each other. Such a situation is advantageous for the electrical conduction via a small-polaron hopping mechanism. Since the subsequent hops of a small polaron occur between aliovalent Fe^{2+}/Fe^{3+} sites, comparable concentrations of these sites should lead to higher values of the overall electrical conductivity. Our conductivity measurements have indeed shown that the annealing leads to an increase in electrical conductivity [2].

Summarizing, the XANES spectra have confirmed that the conductivity increase of the samples annealed at 510-530°C can be explained by a change of relative populations of Fe^{2+}/Fe^{3+} sites.

Further studies on correlations between XANES spectra and results of other investigations of the amorphous analogs of olivines are in progress.

References

[1] B.L. Ellis, W.R.M. Makahnouk, Y.Makimura, K. Toghill, L.F. Nazar, "A multifunctional 3.5 V iron-based phosphate cathode for rechargeable batteries", *Nature Mater.* **6** (2007) 749-753.

[2] P. Jozwiak, J.E. Garbarczyk, M. Wasiucionek, I. Gorzkowska, F. Gendron, A. Mauger, C.M. Julien, "DTA, FTIR and impedance spectroscopy studies on lithium-iron phosphate glasses with olivine-like local structure", *Solid State Ionics* **179** (2008) 46-50.

P32

XAFS STUDY OF THE $Ge_{1-x}Eu_xTe$ and $Ge_{1-x}Mn_xTe$ THIN LAYERS

A. Wolska *, B.J. Kowalski, M. Pietrzyk, W. Knoff, and T. Story

Institute of Physics, PAS, Al. Lotnikow 32/46, 02-668 Warsaw, Poland

Keywords: EXAFS, XANES, thin layers, rare earth elements

**) e-mail: wolska@ifpan.edu.pl*

Diluted magnetic semiconductors (DMS) have been shown to be the very promising materials for spintronic purposes. Usually, II-VI and III-V materials are considered and very intensively investigated in pursuit of the compound with the Curie temperature (T_C) above room temperature. On the other hand, the IV-VI type semiconductors, like the GeTe crystals doped with transition metals and/or rare earth elements also show properties interesting from spintronics point of view. In case of GeTe doped with Mn, Curie temperature (T_C) depends on the Mn concentration and can reach 140 K for $Ge_{0.5}Mn_{0.5}Te$ [1]. Adding another dopant, like Eu, influences magnetic properties even further. T_C becomes relatively high at markedly lower Mn content and it becomes, in case of $Ge_{0.89}Mn_{0.07}Eu_{0.04}Te$, comparable to that of $Ge_{0.6}Mn_{0.4}Te$. Apparently, the interaction between *d* and *f* states of both dopants changes magnetic order in the system. Therefore, it is important to determine energy distribution and positions of Mn 3*d* and Eu 4*f* states. What's more, the knowledge about the position and local structure around magnetic ions is also necessary to broaden the understanding of the origin of ferromagnetism in the investigated system.

The best tool for examining an average local atomic structure around selected element is EXAFS (Extended X-ray Absorption Fine Structure). This technique is sensitive to the specific element and gives the information about the number and type of neighbouring atoms, as well as the structural disorder. However, some limits exist in this method too. The Mn K-edge (6539 eV) and Eu L_3-edge (6977 eV) are too close to obtain a full-range EXAFS spectrum for Mn and can influence XANES (X-ray Absorption Near Edge Structure) spectrum for Eu. Therefore, it is important to investigate also materials without co-doping and, as a first step, the results of analysis for the samples with one type of dopant are presented here.

The $Ge_{1-x}Mn_xTe$ (x = 0.08, 0.10) and $Ge_{1-x}Eu_xTe$ (x = 0.005, 0.007) thin layers were grown on BaF_2 (111) substrates by the MBE method. The substrate temperature was kept at 400-450°C. The obtained layers were of 0.25 μm thick. The XANES and EXAFS spectra were measured at the HASYLAB, A1 station. Measurements were carried out at the Ge K-edge, Mn K-edge and Eu L_3-edge using a 7-element Ge fluorescence detector. During measurements the samples were cooled to liquid nitrogen temperature in order to minimize thermal disorder. The FEFF8.4 code [2] was used to calculate theoretical XANES spectra. The Artemis and Athena programs [3], using IFEFFIT data analysis package, were applied to analysis of the EXAFS data.

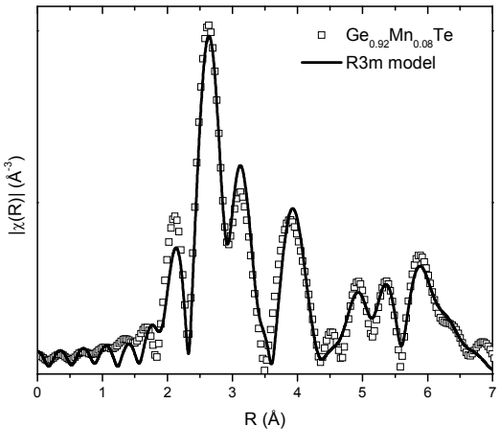

Figure 1. FT experimental EXAFS spectrum (squares) and fit of theoretical model (solid line) of the Ge K-edge in the $Ge_{0.92}Mn_{0.08}Te$ sample.

The Ge K-edge EXAFS was measured for the doped samples and for the reference GeTe layer. Since, the amount of Ge atoms was relatively high, the existence of self-absorption effect was checked using the Booth and Bridges algorithm for thin samples. The calculations excluded the need of correction. EXAFS analysis was carried out using the same model and the same set of parameters in each case. In this way the comparison between the samples was possible. For the GeTe sample, in addition to the regular Ge-Te bonds, around 12% of Ge-Ge bonds were found. This behaviour was also observed by Kolobov *et al.* in the thin GeTe layers. [4] However, in case of doped samples, adding additional Ge atoms in the first shell led to the unphysical parameters. It appears that presence of dopants eliminates the additional Ge-Ge bonds.

The EXAFS analysis of Ge K-edge shows that all samples posses the GeTe structure with *R*3*m* space group. Figure 1 presents the fitting results for *R*3*m* model in a range up to 7 Å for one of the samples doped with Mn. The analysis of Mn K-edge for the same sample,

P32

$Ge_{0.92}Mn_{0.08}Te$, is shown in Figure 2. In this case, a model with *R*-3*m* structure fits the spectrum better. There is no contradiction between both results. EXAFS gives average information about structure around investigated element in a short radial distance. It means that the dopants can modify their neighbourhood but this does not affect the whole structure (unless when their amount stays at the low level). Table 1 presents the bond lengths found from EXAFS analysis. For the central Ge atom the first shell consists of two subshells where 3 Te and 3 Te atoms are located at slightly different distances (2.83 Å and 3.14 Å). The Mn atoms are located in the substitutional Ge positions but they modify the nearest neighbourhood in such a way that the Te atoms form one shell only. The distances to the second shell consisting of two Ge subshells are very close in both cases.

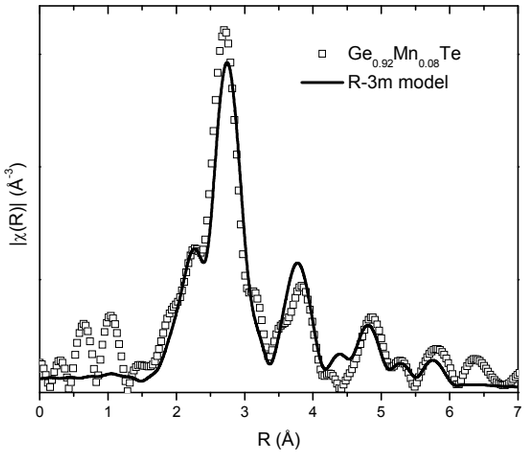

Figure 2. FT experimental EXAFS spectrum (squares) and fit of theoretical model (solid line) of the Mn K-edge in the $Ge_{0.92}Mn_{0.08}Te$ sample.

In case of the $Ge_{1-x}Eu_xTe$ samples, the amount of Eu dopant was too low to give good quality EXAFS data. Therefore, only the XANES spectra were recorded. In order to check the possible Eu surrounding, the calculations of XANES spectra were performed. There were four models considered: Eu in the Ge substitutional position ($GeEu_{Ge}Te$), EuTe, EuO and Eu. The comparison with the experimental data enabled to exclude the presence of Eu and EuO inclusions in the investigated samples.

Table 1. The distances found between the absorbing Ge or Mn atoms and the two neighbouring shells (each consisting of two subshells).

	R_{Te1} [Å]	R_{Te2} [Å]	R_{Ge1} [Å]	R_{Ge2} [Å]
Ge	2.83 ± 0.01	3.14 ± 0.01	4.15 ± 0.01	4.29 ± 0.01
Mn	2.93 ± 0.01	2.93 ± 0.01	4.10 ± 0.01	4.23 ± 0.01

We conclude that Mn dopants substitute the Ge atoms in the GeTe layers and slightly modify the first shell consisting of Te atoms. In case of Eu dopants, it seems that Te atoms are also preferred as the first neighbours in the $GeEu_{Ge}Te$ compound and/or the EuTe inclusions.

Acknowledgements: This work was partially supported by national grant of Ministry of Science and High Education N202 101 31/0749 and by DESY/HASYLAB and the European Community under Contract RII3-CT-2004-506008 (IA-SFS).

References

[1] Y.Fukuma, T. Murakami, H. Asada, T. Koyanagi, "Film growth of $Ge_{1-x}Mn_xTe$ using ionized-cluster beam technique", *Physica E* **10** (2001) 273-277.

[2] A.L. Ankudinov, B. Ravel, J.J. Rehr, S.D. Conradson, "Real-space multiple-scattering calculation and interpretation of x-ray-absorption near-edge structure", *Phys. Rev. B* **58** (1998) 7565-7576.

[3] B. Ravel, M. Newville, "ATHENA, ARTEMIS, HEPHAESTUS: data analysis for X-ray absorption spectroscopy using IFEFFIT", *J. Synchrotr. Radiat.* **12** (2005) 537-541.

[4] A.V. Kolobov, J. Tominaga, P. Fons, T. Uruga, "Local structure of crystallized GeTe films", *Appl. Phys. Lett.* **82** (2003) 382-384.

P33

INTERACTION OF INTENSE ULTRASHORT XUV PULSES WITH SILICON

R. Sobierajski [1,6*], M. Jurek [1], D. Klinger [1], J. Krzywinski [1], J.B. Pełka [1], L. Juha [2], J. Chalupský [2], J. Cihelka [2], V. Hajkova [2], U. Jastrow [3], S. Toleikis [3], H. Wabnitz [3], K. Sokolowski-Tinten [4], N. Stojanovic [3,4], S. Hau Riege [5], R. London [5], and A.R. Khorsand [6]

[1] *Institute of Physics Polish Academy of Sciences, Al. Lotników 32/46, PL 02-668 Warszawa, Poland*

[2] *Institute of Physics AS CR, Na Slovance 2, 182 21 Prague 8, Czech Republic*

[3] *HASYLAB/DESY, Notkestrasse 85, D-22603 Hamburg, Germany*

[4] *Institut für Experimentelle Physik, Universität Duisburg-Essen, 47048 Duisburg, Germany*

[5] *Lawrence Livermore National Laboratory, Livermore, CA 94550, USA*

[6] *FOM-Institute for Plasma Physics Rijnhuizen, NL-3430 BE Nieuwegein, The Netherlands*

Keywords: XUV, FEL, damage , silicon, melting, ablation

**) e-mail: ryszard.sobierajski@ifpan.edu.pl*

IV-th Generation Light Sources provide extremely intense, ultra short pulsed radiation in the XUV spectral range. One of them – FLASH (Free electron LaSer in Hamburg) - emits $10^{11\text{-}13}$ photons of the energy in the range of 30-100 eV, formed in 25 fs long bunches [1]. Its radiation can be focused down to the spot of 10 μm diameter to study the processes of the radiation damage to solids samples [2].

The irradiation of solid materials with such short wavelength femtosecond pulses offers a number of advantages. First of all, it permits a high degree of electronic excitation but with a strongly reduced influence of optical nonlinearities *i.e.*, multiphoton absorption and free carrier absorption. Moreover, for frequencies range between the plasma frequency and the frequency of the innershell absorption edge, the absorption length for solids varies over orders of magnitude. Therefore, ultrashort XUV pulses allow the preparation of rather well-defined excitation conditions for a variety of excitation depths.

We report on the results of experiments performed at FLASH on the interaction of ultrashort high intensity 10^{12}–10^{14} W/cm^2 XUV pulses with solid silicon surfaces. Silicon is a suitable material for comparisons, broadly studied with femtosecond optical lasers and picoseconds XUV lasers. Moreover it is a standard substrate material for for the optical coatings in XUV optics where radiation damage is a key issue. Samples were irradiated by single shots of FLASH radiation. The permanent structural modifications of the irradiated surfaces were characterized by means of phase contrast optical microscopy, AFM (see Fig. 1), Raman spectroscopy and X-ray micro diffraction.

Mechanisms of different, intensity dependent stages of the surface damage are described. Damage thresholds of each stage are estimated for various excitation depths. The influence of the energy diffusion/penetration on the damage thresholds is presented. The results are discussed regarding the problem of radiation damage of optical surfaces.

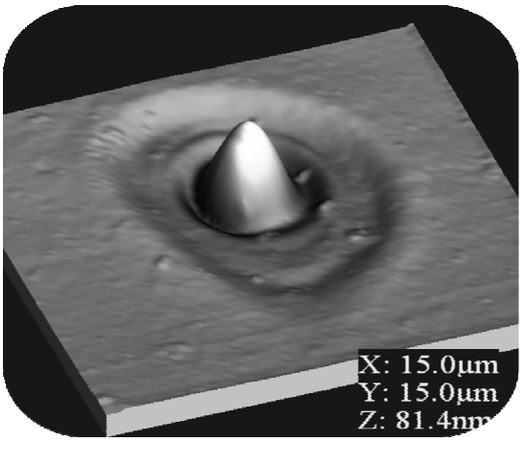

Figure 1. AFM depth map of the irradiation spot on the Si sample.

Acknowledgements: The authors are greatly indebted to the machine operators, run coordinators, scientific and technical teams at the FLASH facility for enabling an outstanding performance.

References

[1] V. Ayvazyan *et al.*, "First operation of a free-electron laser generating GW power radiation at 32 nm wavelength", *Eur. Phys. J. D* **37** (2006) 297-303.

[2] S.P.Hau-Riege, R.A. London, J. Krzywinski, R. Sobierajski, R.M. Bionta, M.A. McKernan, S.L. Baker, R. Nietubyc, J.B. Pelka, M. Jurek, L. Juha, J. Chalupsky, J. Cihelka, V. Hajkova, A. Velyhan, J. Krasa, J. Kuba, K. Tiedtke, S. Toleikis, T. Tschentscher "Damage threshold of inorganic solids under free-electron-laser irradiation at 32.5 nm wavelength", *Appl. Phys. Lett.* **90** (2007) 173128.

P34

LASER ABLATION OF AMORPHOUS SiO_2 BY ULTRA-SHORT PULSES OF XUV FREE ELECTRON LASER

D. Klinger [1], R. Sobierajski [1,8], M. Jurek [1], J. Krzywinski [1,5], J.B. Pelka [1], D. Żymierska [1*], J. Chalupský [2,3], L. Juha [2], V. Hájková [2], J. Cihelka [2], T. Burian [2,3], L. Vyšín [2,3], H. Wabnitz [4], K. Tiedtke [4], S. Toleikis [4], T. Tschentscher [4], R. London [5], S. Hau-Riege [5], K. Sokolowski-Tinten [6], N. Stojanovic [6], J. Hajdu [7], A.R. Khorsand [8], and A.J. Gleeson [9]

[1] *Institute of Physics, Polish Academy of Sciences, Al. Lotników 32/46, PL-02-668 Warsaw, Poland*
[2] *Institute of Physics, Czech Academy of Sciences, Na Slovance 2, 182 21 Prague 8, Czech Republic;*
[3] *Czech Technical University in Prague, Brehova 7, 115 19 Praha 1, Czech Republic*
[4] *Deutsches Elektronen-Synchrotron DESY, Notkestrasse 85, D-22603 Hamburg, Germany*
[5] *Lawrence Livermore National Laboratory, 7000 East Avenue, Livermore, CA 94550, USA*
[6] *University of Duisburg-Essen, D-45117 Essen, Germany*
[7] *Uppsala University, Uppsala, SE-75124 Sweden*
[8] *FOM-Institute for Plasma Physics Rijnhuizen , P.O. Box 1207, 3430 BE Nieuwegein, The Netherlands*
[9] *CCRLC Daresbury Laboratory, Warrington, Cheshire, WA4 4AD, UK*

Keywords: dielectrics, laser processing, XUV free electron laser, material modification, laser ablation, fused silica

**) e-mail: contact: zymier@ifpan.edu.pl*

The interaction of ultrashort laser pulse with dielectric materials involves the processes that can lead to surface ablation, resulting in minimal aside damage. For sufficiently high carrier densities (>10^{21} electrons/cm^3) dielectric breakdown occurs, eventually in the form of the ablation of the thin surface layer. The investigations realised in the last decade have lead to better clarity of the interaction mechanism by studying the influence of the pulse duration [1-6] and the material [7-10] on the ablation threshold. The differences in the results demonstrate that many questions referred to ablation of dielectric materials by ultrashort pulses remain open as before.

In this work we provide a research of ablation threshold value in the most widely studied dielectric material, fused silica. Structural modifications were induced with the intense XUV femtosecond pulses generated by the TESLA test facility free electron laser (TTF FEL) at DESY, Hamburg. The investigated samples were irradiated during a few following phases of the experiment with different wavelength of the radiation. The experimental data are quoted in Table 1.

Effects of the laser ablation were studied by means of the interference microscopy. Typical pictures of the modified surfaces are shown in Fig. 1 and Fig. 2. We started an analysis with the determination of the areas of the ablated regions by means of an integrating program. The threshold fluency was obtained from studies of the damage area as a function of the laser pulse energy. This investigation has been performed according to a procedure suggested by Liu [11].

For laser pulses with a Gaussian spatial beam profile, the laser fluence F_0 and the diameter D of the modified area are related by [12, 13]

$$D^2 = 2\omega_0^2 \ln(F_0 / F_{th}) \quad (1)$$

where F_{th} is the fluence threshold value (threshold value is the value of energy density for this surface structure of the ablated area is modified) and ω_0 being the $1/e^2$ beam radius.

Laser fluence can be calculated from the relation between Gaussian beam radius and the measured pulse energy

$$F_0 = 2E_{pulse}/\pi\omega_0^2 \quad (2)$$

As a result of varying of the laser pulse energy at constant pulse duration different diameters of the damage spots are obtained. For a Gaussian shaped beam the dependence can be obtained from a plot of the squared outer damage diameter D^2 versus the incident energy of the laser pulse in logarithmical scale due to Eq. 1. From the slope of a linear fit we can calculate the value of ω_0. In this moment we can calculate the laser fluency F_0 on the surface. The threshold fluency F_{th} we determined via linear extrapolation of D^2 to 0.

Table 1. Wavelengths of the laser radiation generated during Phase 1 ÷ Phase 3 of the ablation experiment with TTF FEL.

	Phase 1	Phase 2	Phase 3
wavelength [nm]	32	13.2	7

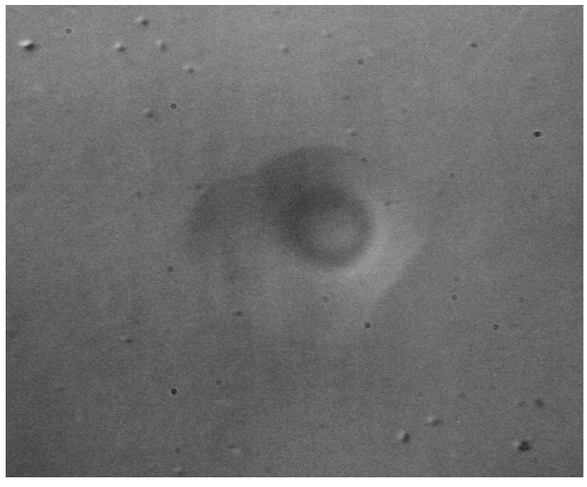

Figure 1. Typical shape of the crater created in fused silica by femtosecond ablation in single-shot regime.

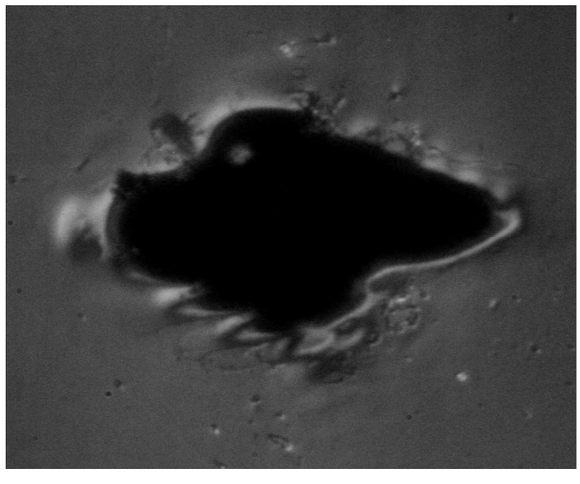

Figure 2. Typical shape of the crater created in fused silica by femtosecond ablation in multi-shot regime.

Acknowledgements: This work was supported in part by the Ministry of Science and Higher Education (Poland) under special research project No. DESY/68/2007.

References

[1] M. Lenzner, "Femtosecond laser-induced damage of dielectrics", *Int. J. Mod.Phys.B* **13** (1999) 1559-1578.

[2] An-Chun Tien, S. Backus, H. Kapteyn, M. Murnane, G. Mourou, "Short-pulse laser damage in transparent materials as a function of pulse duration", *Phys. Rev. Lett.* **82** (1999) 3883-3886.

[3] D. Du, X. Liu, G. Korn, J. Squier, G. Mourou, "Laser-induced breakdown by impact ionisation in SiO_2 with pulse widths from 7 ns to 150 fs", *Appl. Phys. Lett.* **64** (1994) 3071-3073.

[4] B.C. Stuart, M.D. Feit, A.M. Rubenchik, B.W. Shore, M.D. Perry, "Laser-induced damage in dielectrics with nanosecond to subpicosecond pulses", *Phys. Rev. Lett.* **74** (1995) 2248-2251.

[5] A. Rosenfeld, M. Lorenz, D. Ashkenasi, P. Rudolph, J. Krueger, W. Kautek, *Appl. Phys. A* **69** (1999) 759-761.

[6] T.Q. Jia, Z.Z. Xu, R.X. Li, D.H. Feng, X.X. Li, C.F. Cheng, H.Y. Sun, N.S. Xu, H.Z. Wang, "Formation of nanogratings on the surface of a ZnSe crystal irradiated by femtosecond laser pulses", *Phys. Rev. B* **72** (2005) 1254291-1254294.

[7] D. von der Linde, H. Schueler, "Breakdown threshold and plasma formation in femtosecond laser-solid interaction", *J. Opt. Soc. Am. B* **13** (1996) 216-222.

[8] K. Sokolowski-Tinten, J. Bialkowski, M. Boing, A. Cavalleri, D. von der Linde, "Thermal and nonthermal melting of gallium arsenide after femtosecond laser excitation", *Phys. Rev. B* **58** (1998) 805-807.

[9] I.H. Chowdhury, A.Q. Wu, X. Xu, A.M. Weiner, "Ultra-fast laser absorption and ablation dynamics in wide-band-gap dielectrics", *Appl. Phys. A* **81** (2005) 1627-1632.

[10] K. Sokolowski-Tinten, J. Bialkowski, A. Cavalleri, D. von der Linde, A. Oparin, J. Mejer-ter-Vehn, S.I. Anisimov, "Transient states of matter during short pulse laser ablation", *Phys. Rev. Lett.* **81** (1998) 224-227.

[11] J.M. Liu, "Simple technique for measurements of pulsed Gaussian-beam spot sizes", *Opt. Lett*. **7** (1982) 196-196.

[12] J. Jandeleit, G. Urbasch, H. Hoffmann, H.G. Treusch, E. Kreutz, "Picosecond laser ablation of thin copper films" *Appl. Phys. A* **63** (1996) 117-121.

[13] S. Baudach, J. Bonse, W. Kautek, „Ablation experiments on polyimide with femtosecond laser pulses", *Appl. Phys. A* **69** [Suppl.1] (1999) S395-S398.

P35

NATURAL MINERALS – THE MAJOR AND MINOR ELEMENTS CHEMICAL BONDING

M.T. Klepka [1*], R. Minikayev [1], K. Lawniczak-Jablonska [1], A. Wolska [1], I.N. Demchenko [1], and M. Jablonski [2]

[1] *Institute of Physics PAS, al. Lotników 32/46, 02-668 Warsaw*
[2] *Szczecin University of Technology, Institute of Chemistry and Environmental Protection Al. Piastow 42, 71–065, Szczecin, Poland*

Keywords: ilmenite, XANES, XRD, synchrotron

**) e-mail: mklepka@ifpan.edu.pl*

Natural minerals are commonly used in many industrial processes. The content of elements in an ore, and their chemical state depends strongly on the worldwide location of the place where they are collected and can differ even in the same deposit. To properly adjust the chemical reaction used in industry, the knowledge about content of elements and their chemical bonding is very important. The phase content is usually given in form of common oxides. This can significantly differ from real phase content and ionic state of elements. In the presented paper, we demonstrate the usefulness of X-ray absorption (XAS) technique for estimation of chemical states of the majority and minority elements, taking natural ilmenites as the example.

Natural minerals – ilmenites are used in production of white pigment (TiO_2), which reaches several million tons per year. Reaction of titanium raw material with sulphuric acid is the first step of industrial process [1, 2]. Ilmenites, like many natural minerals, have a complicated morphology (Fig. 1) and the standard procedures used in industrial chemical analysis do not provide sufficient information.

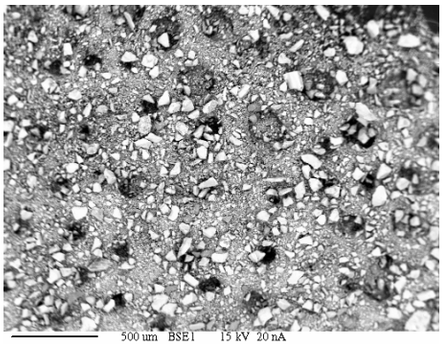

Figure 1. SEM picture of Norwegian ilmenite.

Ilmenites are originated in several places on earth. Our studies were focused on minerals from Norway, Australia, China and India.

The main phases which involve Fe and Ti are usually relatively easy to estimate but estimation of content and chemical state of minority elements is much more complicated. The X-ray powder diffraction (XRD) pattern is very complicated due to many diffraction peaks as well as similarity of phases, which are formed by substitution of minority elements into the majority phase lattice.

In the presented work phases based on major and minor elements in minerals listed above were studied using XRD and XAS. XAS analysis allowed identifying phases based on major elements like Fe, Ti [3-5] as well as minor elements like Mg, Mn [6,7] and Cr. In some of the minerals minor elements were found in more than one phase.

Chemical states of major and several minor elements were evaluated by applying the principal components analysis of X-ray absorption spectra using XANDA code. Knowing that the shape of XANES spectra is a fingerprint of chemical state of elements we consider that the XAS is a good tool for estimation of the phase content in ilmenites.

Acknowledgements: This work was partially supported by national grant of Ministry of Science and High Education N202-052-32/1189 and by DESY and BESSY and the EC under Contract RII3-CT-2004-506008 (IA-SFS).

References

[1] T. Chernet, "Applied mineralogical studies on Australian sand ilmenite concentrate with special reference to its behaviour in the sulphate process", *Miner. Eng.* **12** (1999) 485.

[2] R.G. Teller, M.R. Antonio, "The chemistry of the thermal decomposition of pseudobrookite ferrous titanium oxides", *J. Solid State Chem.* **88** (1990) 351-367.

[3] M. Klepka, K. Lawniczak-Jablonska, M. Jablonski, A. Wolska, R. Minikayev, W. Paszkowicz, A. Przepiera, Z. Spolnik, R. Van Grieken, "Combined XRD, EPMA and X-33399333ray absorption study of mineral ilmenite used in pigments production", *J. Alloys Compds.* **401** (2005) 281-288.

[4] M. Klepka, K. Lawniczak-Jablonska, M. Jablonski, M. Walczak, H. Rossner, "The oxidation state and phase content of Fe in Norwegian ilmenite estimated using XANES spectra", *BESSY Annual Report 2005.*

[5] M. Klepka, K. Lawniczak-Jablonska, M.S. Walczak, M. Jabłoński, "Estimation of Fe – phases content in Norwegian ilmenite using XANES spectra", *Hasylab Annual Report 2005.*

[6] M.T. Klepka, I.N. Demchenko, K. Lawniczak-Jablonska, M. Jablonski, "XANES study of Mg based phases in ilmenites", *Bessy Annual Report 2007.*

[7] M.T. Klepka, A. Wolska, K. Lawniczak-Jablonska, M. Jabłoński, "XANES study of Mn based phases in ilmenites", *Hasylab Annual Report 2007.*

P36

CREATION OF MnAs NANOCLUSTERS AT PROCESSING OF GaMnAs

J. Bak-Misiuk [1*], J.Z. Domagala [1], E. Dynowska [1], P. Romanowski [1], J. Sadowski [1,2], A. Misiuk [3], and W. Caliebe [4]

[1] *Institute of Physics, PAS, Al. Lotnikow 32/46, PL-02668 Warsaw, Poland*
[2] *Lund University, MAX-Lab, Lund SE-221 00, Sweden*
[3] *Institute of Electron Technology, Al. Lotnikow 46, PL-02668 Warsaw, Poland*
[4] *HASYLAB at DESY, Notkestr. 85, D-22603 Hamburg, Germany*

Keywords: GaMnAs, GaAs, MnAs, MBE, nanocluster, X-ray diffraction, synchrotron measurement

**) e-mail: bakmi@ifpan.edu.pl*

Annealing of GaMnAs layers at 700-1000 K can result in the compressive strain changing to the tensile one. This effect is related to a creation of MnAs nanoclusters embedded in the GaAs matrix and indicating the preferred crystallographic orientation [1-3]. Depending on the MnAs cluster size, the granular GaAs:MnAs material exhibits a ferromagnetic/ superparamagnetic behavior at room temperature [1].

The goal of present work was determination of the effect of annealing at various conditions on the defect structure of the GaMnAs heteroepitaxial layers grown on the GaAs substrates.

Three GaMnAs samples differs by Mn concentration were studied (A66 - 2%, A831 - 6%, A832 - 7%.). GaMnAs layers were deposited on 001 oriented GaAs by the MBE method. After layer deposition, the A66 sample was annealed in Ar atmosphere for 1 h at 670 K under ambient pressure (10^5 Pa) or under enhanced hydrostatic pressure (p = 1.1 GPa). The other A66 sample processed for 1 h at T = 670 K under 10^5 Pa was subsequently treated at 920 K for 1 h, also under p = 1.1 GPa. The A831 and A832 samples were annealed for 1 h at 770 K or at 870 K under 10^5 Pa.

Structural characterization of the layers, before and after processing, was performed using synchrotron radiation at the W1.1 beamline at DESY-Hasylab. Following measurements were performed:

i) 2θ scans in the glancing incidence geometry,

ii) ω scans across the 002 and 004 GaAs reflections,

iii) 2θ-ω scans across the 224 GaAs reflection.

The phase analysis of the near surface layers was performed using diffraction synchrotron radiation in the glancing incidence geometry. In this method a sample is placed in the fixed position while the angle between the sample surface and X-ray beam is small (1° in our case). The intensity of diffracted beam was detected by the counter rotating in the plane perpendicular to the sample surface within the large 2θ angles. The described geometry of measurements has been applied for investigation of the phase composition of the thin near surface polycrystalline layers.

By an analysis of the 2θ scans, the diffraction peaks, originating from the polycrystalline orthorhombic MnAs phase, were detected for the A831 and A832 samples after their annealing at 670 K and 870 K. Also the polycrystalline hexagonal MnAs inclusions as well as the cubic Mn ones were detected in the case of A832 sample. In the case of sample A66, the hexagonal inclusions were detected only in the case of sample treated at 920 K under p = 1.1 GPa. Using the ω scan around the 002 and 004 GaAs reflections and the 2θ-ω scan around the 224 GaAs reflections, the lattice parameters of hexagonal MnAs crystallites, with a well-defined orientation relationship in respect to the GaAs matrix, were determined from the positions of the 11.0 and 03.0 reflections of hexagonal MnAs [2-4]. For the A831 and A832 samples annealed at 870 K, the lattice parameters were: a = 3.710 Å and c = 5.785 Å. In the case of A66 sample, annealed at 870 K, the a and values were 3.765 Å and 5.648 Å, respectively. The reflections originating from the hexagonal MnAs clusters with preferred orientation were not detected for samples annealed at 670 K/770 K under ambient pressure or at 670 K under enhanced pressures. An influence of defects on the structural changes in the temperature-pressure treated samples will be discussed.

Acknowledgments: This work was partially supported by the European Community - Research Infrastructure Action under the FP6 "Structuring the European Research Area" Programme (through the Integrated Infrastructure Initiative "Integrating Activity on Synchrotron and Free Electron Laser Science", Contract RII3-CT-2004-506008) and by the Ministry of Science and Higher Education (Poland) through Grant No. N20205232/1189.

References

[1] M. Moreno, A. Trampert, B. Jenichen, L. Daweritz, K. Ploog, *J. Appl. Phys.* **92** *(*2002) 4672-4676.

[2] M. Moreno, V. Kaganer, B. Jenichen, L.A. Trampert, L. Daweritz, K. Ploog, *Phys. Rev. B* **72** (2005) 115206-1- 8.

[3] M. Moreno, B. Jenichen, L. Daweritz, K. Ploog, *Appl. Phys. Lett*. **86** (2005) 161903–1-3.

P37

STRUCTURAL PROPERTIES OF MnSb LAYERS GROWN ON GaAs SUBSTRATE

J. Bak-Misiuk [1*], E. Dynowska [1], P. Romanowski [1], J.Z. Domagala [1], J. Sadowski [1,2], R. Jakiela [1], and W. Caliebe [3]

[1] *Institute of Physics, Polish Academy of Sciences, Al. Lotnikow 32/46, PL-02668 Warsaw, Poland*

[2] *Lund University, MAX-Lab, Lund, SE-221 00, Sweden*

[3] *HASYLAB at DESY, Notkestr. 85, D-22603 Hamburg, Germany*

Keywords: spintronics, X-ray, diffraction, synchrotron measurements, structure

[*]) *e-mail: bakmii@ifpan.edu.pl*

Ferromagnetic semiconductors have recently received much interest, since they hold out prospects for using electron spins in electronic devices. Although large effort has been done all over the world to prepare room temperature ferromagnetic III-V semiconductors [1], no fully satisfying material has been fabricated as so far. On the other hand, it has been demonstrated that, in effect of annealing of magnetic GaMnAs semiconductors at high temperature, of about 700 K, specific ferromagnetic MnAs precipitates are fairly easily produced, yielding multi-phase materials [2]. It has been shown that bulk MnSb has T_C of 587 K [3]. Therefore it can be considered as a good candidate to form nanoinclusions, ferromagnetic at above room temperature.

MnSb layers were grown by MBE method on the GaAs (100) substrate with the MnAs buffer layer or directly on the GaAs(111) substrate. Depth profiles of Ga, As, Mn and Sb atoms in the samples were determined by SIMS method. Structural characterization of the layers was performed using synchrotron radiation at the W1.1 beamline at DESY-Hasylab. Monochromatic X-ray beam of λ = 1.54056 Å wavelength was used.

As follows from SIMS results, the near surface layers of both samples were enriched in Ga.

To determine the crystallographic orientation of the layers, the 2θ-ω scans were made. In the case of layer grown on GaAs(100), the 2θ-ω pattern shown an existence of two hexagonal MnSb domains with the (101) and (110) orientations, respectively. The phase analysis of the near surface layers was performed using diffraction in the glancing incidence geometry (2θ scan). Polycrys-talline phases of zinc-blende GaSb and of hexagonal MnSb were detected for this sample.

For layer grown on GaAs(111), the observed diffraction peaks have been indexed as 001 MnSb and 111 GaSb (Fig. 1). No diffraction peaks originating from polycrystalline inclusions were found for this sample in the 2θ patterns. The small fraction of (102)-oriented MnSb was detected for both sample kinds (Fig. 1).

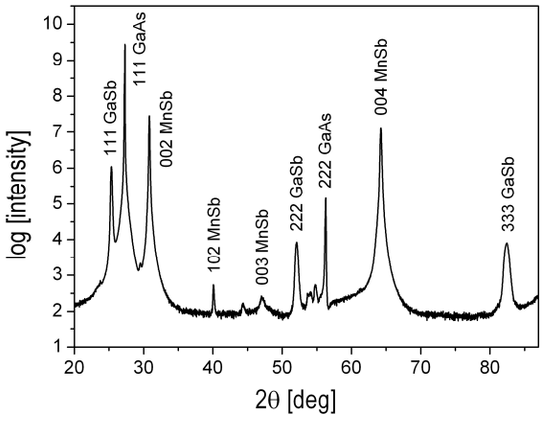

Figure 1. 2θ-ω scan for MnSb grown on GaAs (111) substrate.

Acknowledgements: This work was partially supported by the European Community - Research Infrastructure Action under FP6 "Structuring the European Research Area" Programme (through the Integrated Infrastructure Initiative "Integrating Activity on Synchrotron and Free Electron Laser Science", Contract RII3-CT-2004-506008) and by national grant of Ministry of Science and High Education N202-052-32/1189.

References

[1] T. Dietl, H. Ohno, F. Matsukura, J. Cibert, D. Ferrand, "Zener model description of ferromagnetism in zinc-blende magnetic semiconductors", *Science* **287** (2000) 1019-1022.

[2] M. Moreno, V.M. Kaganer, B. Jenichen, A. Trampert, L. Daweritz, K.H. Ploog, "Micromechanics of MnAs nanocrystals embedded in GaAs", *Phys. Rev. B* **72** (2005) 115206-1 - 115206-8.

[3] K. Ohno, M. Shuzo, M. Oshima "Ga segregation in MnSb epitaxial growth on GaAs (100) and (111) *B* substrates", *Phys. Rev. B* **64** (2001) 085328-1–08538-8.

P38

ANGLE-RESOLVED PHOTOEMISSION STUDY OF GeTe AND $Ge_{1-x}Mn_xTe$

B.J. Kowalski [1], M.A. Pietrzyk [1], W. Knoff [1], J. Sadowski [1,2], J. Adell [3], and T. Story [1]

[1] *Institute of Physics, Polish Academy of Sciences, Al. Lotników 32/46, 02-668 Warsaw, Poland*
[2] *MAX-lab, Lund University, Box 118, SE-22100 Lund, Sweden*
[3] *Department of Physics, Chalmers University of Technology and Goteborg University, S-412 96 Goteborg, Sweden*

Keywords: photoemission, GeTe< GeMnTe,

**) e-mail: kowab@ifpan.edu.pl*

GeTe is a narrow-gap semiconductor which occurs in two crystalline structures: cubic (the rock salt structure) and rhombohedral (distorted NaCl structure). Its electronic structure was thoroughly studied for both structures by means of various calculation methods. In particular, the bonding character and its changes were considered. However, the set of related experimental data remains quite small.

Interest in GeTe has revived recently due to phenomena discovered in GeTe-based diluted magnetic semiconductors (DMS) (in view of emerging spintronic applications). $Ge_{1-x}Mn_xTe$ exhibits ferromagnetism with the Curie temperature which strongly depends on Mn concentration and can be as high as 140 K [1]. Such properties of this material inspired extensive investigations of GeTe-based DMSs but the set of experimental data concerning the electronic band structure of these materials still has to be markedly increased.

In this paper, we report an angle-resolved photoemission study of rhombohedral GeTe and $Ge_{1-x}Mn_xTe$ surface alloy prepared by *in situ* Mn deposition on the sample at elevated temperature. The GeTe epilayers were grown by MBE on BaF_2 substrates. The clean and ordered sample surface was prepared for photoemission experiments by cycles of Ar^+ ion sputtering and annealing under UHV conditions. In the experiments performed with use of the photoelectron spectrometer at BL41 in MAXlab synchrotron radiation laboratory of Lund University (Sweden) we acquired, for the first time, to our knowledge, the data revealing the valence band structure of GeTe along the Γ-T and T-W directions in the Brillouin zone. The bands along the Γ-T direction were mapped in the normal-emission mode with photon energy in the range of 20-35 eV, while for the T-W direction – in the off-normal mode (for the photon energy of 20 eV for θ = 0° and increased for higher angles in order to compensate changes in the normal component of the $\boldsymbol{k}$ vector). The dispersion of the main features in the spectra corresponded well to the band structure calculated by an empirical pseudopotential method [2].

For $Ge_{1-x}Mn_xTe$ surface alloy, the band structure was mapped along the T-W direction. By comparison of the data collected for GeTe and $Ge_{1-x}Mn_xTe$, we were able to reveal the contribution of Mn 3*d* states to the valence band of the system. It appeared in the deeper part of the valence band (1.5-6 eV with respect to the valence band edge) with a maximum intensity at about 3.5 eV. Such a result confirms the Mn 3*d* states distribution in $Ge_{1-x}Mn_xTe$, recently calculated with use of the density-functional theory [3].

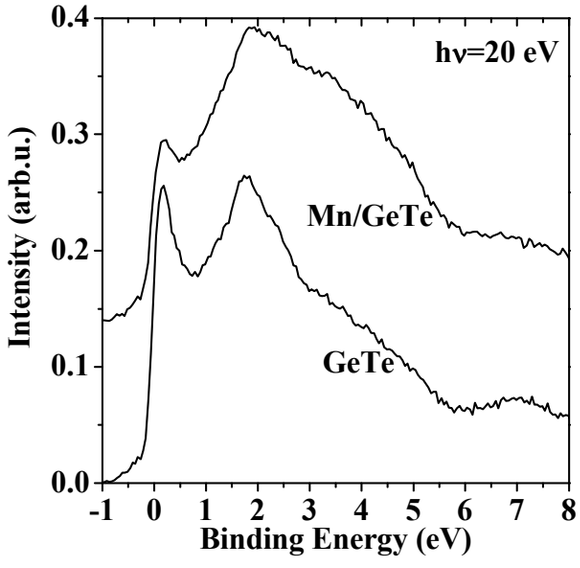

Figure 1. A comparison of the spectra taken from GeTe and Mn/GeMnTe for the T point in the Brillouin zone).

Acknowledgements: The authors acknowledge support by MSHE (Poland) grant N202 101 31/0749 and by the European Community - Research Infrastructure Action under the FP6 "Structuring the European Research Area" Programme (through the Integrated Infrastructure Initiative "Integrating Activity on Synchrotron and Free Electron Laser Science").

References

[1] Y. Fukuma, T. Murakami, H. Asada, T. Koyanagi, *Physica E* **10** (2001) 273.

[2] H.M. Polatoglou, G. Theodorou, N.A. Economou, *Physics of Narrow Gap Semiconductors. Lecture Notes in Physics,* vol. 152 (Springer Verlag, Berlin 1982) p. 221.

[3] A. Ciucivara, B.R. Sahu, L. Kleinman, *Phys. Rev. B* **75** (2007) 241201(R).

P39

Ga INTERSTITIAL SITE OCCUPATION BY Mn ATOMS IN GaAs: EXAFS AND XANES EVIDENCE

K. Lawniczak-Jablonska [1*], A. Wolska [1], J. Libera [1], M.T. Klepka [1], J. Sadowski [1,2], E. Holub-Krappe [3], A. Persson [4], and D. Arvanitis [4]

[1] *Institute of Physics PAS, al. Lotników 32/46, 02-668, Warsaw, Poland*
[2] *Lund University, MAX-Lab, Lund SE-221 00, Sweden*
[3] *Hahn-Meitner Institute, Department of Magnetism, Glienicker Str. 100, D-14109 Berlin, Germany*
[4] *Physics Department, Uppsala University, Box 530, 75121 Uppsala, Sweden*

Keywords: spintronics, x-ray absorption, interstitial, semiconductors, (Ga,Mn)As

**) e-mail: jablo@ifpan.edu.pl*

A significant amount of scientific activity is devoted to studies of Mn containing semiconductors. In particular, $Ga_{1-x}Mn_xAs$ is considered as a promising material for microelectronic applications utilizing the electron spin. The location of the Mn atoms in the layers, here grown by means of MBE, is correlated with all relevant physical properties of the final material, and is therefore the subject of many studies. To avoid MnAs segregation, the MBE growth of (Ga,Mn)As must be performed at temperatures which are much lower than those normally applied (550 - 650ºC) for GaAs, *i.e.* at 180 - 300ºC, depending on Mn content [1]. Mn^{2+} ions with spin 5/2, substituting for Ga in this material, are ferromagnetically coupled due to exchange interactions with valence band holes, giving rise to the ferromagnetic behavior of $Ga_{1-x}Mn_xAs$. Substitutional Mn ions (Mn_{Ga}) act as acceptors, generating holes that mediate the ferromagnetic exchange [2]. However, a low (MBE) growth temperature leads to a high density of point defects [3]. The most important of them are known as As anti-sites (As_{Ga}) [4] and Mn interstitials (Mn_i) [5] which are double donors significantly compensating a fraction of free holes. A powerful tool for the determination of the Mn location in layer is X-ray Absorption Spectroscopy (XAS), as it probes the local atomic order and the electronic structure [6, 7]. Here we present a study of the Extended X-ray Absorption Fine Structure (EXAFS) and the X-ray Absorption Near Edge Structure (XANES) of MBE grown $Ga_{1-x}Mn_xAs$ layers.

XAS measurements were performed at liquid nitrogen temperature, at the A1 experimental station in HASYLAB (Hamburg, Germany) using a double crystal Si (111) monochromator. The Mn K-edge spectra were registered using a seven-element fluorescence Si detector. The Mn L-edges spectra were measured at MAX-lab (Lund, Sweden) at beamline D1011 applying total electron yield detection.

To analyse the EXAFS and XANES spectra different Mn positions within the GaAs matrix were considered: (i) substitutional Mn_{Ga}, (ii) interstitial (As) – with As atoms as the first neighbours, (iii) interstitial (Ga) – with Ga atoms as the first neighbours. Due to the fact that electron scattering on Ga and As atoms is very similar, the differences between different Mn position in the EXAFS spectra were not noticed within the first coordination sphere but only considering also the further neighbourhood. The analysis of up to the third sphere with only the substitutional Mn position resulted in the fit of the model to the experimental spectrum presented in Fig. 1.

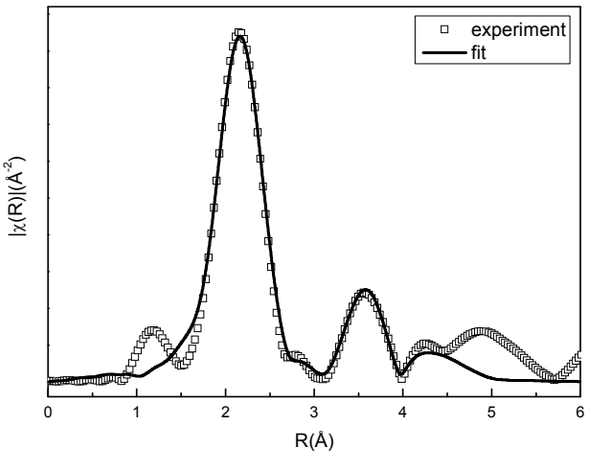

Figure 1. Modulus of the Fourier-transformed $k\chi(k)$ functions (squares) and fit (solid line) for the substitutional Mn position.

Making this assumption, it has been impossible to fit the experimental spectra around 5 Å. Considering the possibility of Mn location in the interstitial (Ga) – with Ga atoms as the nearest neighbours, allowed to simulate experimental data successfully (Fig. 2). The number of Mn atoms in this position was comparable with the one in the substitutional position.

This finding was additionally verified by ab initio calculations of the influence of the Mn atom location on the shape of the XANES spectra [8]. The calculations were performed using the FEFF 8.4 code. The theoretical predictions were compared with the experimental K and L edge XANES of Mn. The results of the performed simulation and the comparison with the XANES Mn spectra for the K as well as for the L edges confirmed that a substantial part of Mn atoms should be located in the Ga interstitial position.

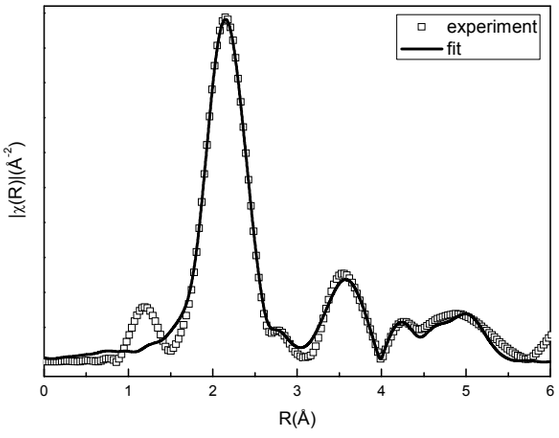

Figure 2. Modulus of the Fourier-transformed $k\chi(k)$ functions (squares) and fit (solid line) for the substitutional and the interstitial (Ga) Mn position.

Acknowledgements: This work is partially supported by the Polish National Grant of the Ministry of Science and High Education N202-052-32/1189 as well as by DESY/HASYLAB, MAX-lab (EC support program: Transnational Access to Research Infrastructures) and directly by the European Community under Contract RII3-CT-2004-506008 (IA-SFS).

References

[1] H. Ohno, Making the nonmagnetic semiconductors ferromagnetic", *Science* **281** (1998) 951.

[2] T. Dietl, H. Ohno, F. Matsukura, J. Cibert, D. Ferrand, "Zener model description of ferromagnetism in zinc-blande magnetic semiconductors", *Science* **287** (2000) 1019.

[3] A.H. Macdonald, P. Schiffer, N. Samarth, "Ferromagnetic semiconductors: moving beyond (Ga,Mn)As", *Nature Materials* **4** (2005) 195.

[4] S. Sanvito, N.A. Hill, "Influence of the local As antisite distribution on ferromagnetism in (Ga,Mn)As", *Appl. Phys. Lett.* **78** (2001) 3493.

[5] K.M. Yu, W. Walukiewicz, T. Wojtowicz, W.L. Lim, X. Liu, U. Bindley, M. Dobrowolska, J.K. Furdyna, "Curie temperature limit in ferromagnetic GaMnAs", *Phys. Rev. B* **68** (2003) 041308(R).

[6] R. Bacewicz, A. Twarog, A. Malinowska, T. Wojtowicz, X. Liu, J.K. Furdyna, "Local structurev of Mn In (Ga,Mn)As probed by x-ray absorption spectroscopy", *J. Phys. Chem. Sol.* **66** (2005) 2004.

[7] I.N. Demchenko, K. Lawniczak-Jablonska, T. Story, V. Osinniy, R. Jakiela, J.Z. Domagala, J. Sadowski, M. Klepka, A. Wolska, M. Chernyshova, "Modification of the local atomic structure around Mn atoms in (Ga,Mn)As layers by high temperature annealing", *J. Phys.: Condens. Matt.* **19** (2007) 496205.

[8] A. Wolska, K. Lawniczak-Jablonska, M.T. Klepka, R. Jakiela, J. Sadowski, I.N. Demchenko, E. Holub-Krappe, A. Persson, D. Arvanitis, "XANES studies of Mn K and $L_{3,2}$ edges in the (Ga,Mn)As layers modified by high temperature annealing", *Acta Phys. Polon.* (2007), accepted.

P40

SILVER BEHENATE UNDER PRESSURE: A PRELIMINARY STUDY

W. Paszkowicz [1], P. Piszora [2], Y. Cerenius [3], S. Carlson [3], and R. Minikayev[1]

[1] Institute of Physics PAS, Al. Lotników 32/46, PL-02668 Warsaw, Poland
[2] Department of Materials Chemistry, Faculty of Chemistry, Adam Mickiewicz University, Grunwaldzka 6, PL-60780 Poznan, Poland
[3] Lund University, MAX-lab, Lund SE-221 00, Sweden

Silver behenate, $CH_3(CH_2)_{20}COOAg$, a white plate-like powder, belongs to the family of fatty acid silver salts with the general formula $CH_3(CH_2)_nCOOAg$ adopting even n values. It is used in thermographic and photothermographic imaging processes [1], as described in many patents (see *e.g.* [2]). 15 years ago it was proposed for use as low-angle diffraction standard [3] as well as for wavelength calibration in SANS experiments [4]. Its powder pattern displays twelve strong regularly-spaced diffraction lines in the low angle region (1.5-18.2°) for CuKα. The crystal structure of silver behenate is unknown, but its large lattice spacing was determined with high accuracy to be 57.380(3) Å [3]. Despite the lack of structural information, silver behenate is frequently used in recent years as above mentioned calibration standard. Combining this standard with another (more classical, *e.g.* LaB_6 [5]) one is known to lead to improved calibration owing to full coverage of the broad angular range.

Silver behenate is known to undergo several phase transitions above the room temperature [6]. Up to now the behaviour of this material under pressure remained unknown. We have performed diffraction experiments up to 11.15 GPa, using a miniature diamond anvil cell (D'Anvils) and a membrane driven diamond anvil cell (DIACELL). The silicone oil was used as pressure transmitting medium (PTM) in the first experiment, and a 4:1 methanol-ethanol mixture in the second one. The data were collected at I711 beamline using the wavelength 0.8773 Å.

In the first experiment, there is no substantial change in the 00*l* diffraction lines (see Fig. 1). These lines become weaker and broadened with increasing pressure and those at the highest angles tend to disappear gradually in the 5-11 GPa region. At the end of this range the lines with $l > 9$ disappear completely. After release of pressure from the maximum 11.15 GPa value i) these lines return to almost the same (marginally lower) angles in respect to the starting positions; ii) the lines with $l > 9$ are not restored. The behaviour in the second experiment is qualitatively similar.

High-angle lines remain unchanged in the low pressure range up to 1.3 GPa (first experiment). At about 2 GPa they tend to broaden and overlap. This behaviour is thought to be dependent on the selection of PTM material. The broadening is weaker in the second experiment.

The interplanar spacing shortening in the studied pressure range along [001] direction is 2.8%.

There is no clear indication of phase transitions in the studied pressure range. However, the observed non-smooth variations in the $d(p)$ slope and appearance of several new (weak) reflections may indicate some marginal structural changes.

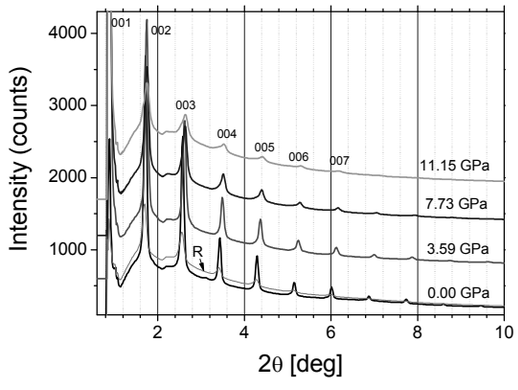

Figure 1. Selected powder diffraction patterns of silver behenate, collected at high-pressure conditions. The curve denoted by "R" refers to diffraction data collected after the release of pressure.

References

[1] T.N. Blanton, T.C. Huang, H. Toraya, C.R. Hubbard, S.B. Robie, D. Louër, H.E. Göbel, G. Will, R. Gilles, T. Raftery, *Powder Diffr.* **10** (1995) 91-95.

[2] R Owen, "Heat-sensitive copying-paper", US Patent 2,910,377, 1959.

[3] T.C. Huang, H Toraya, T.N. Blanton, Y. Wu, "X-ray powder diffraction analysis of silver behenate, a possible low-angle diffraction standard", *J. Appl. Crystallogr.* **26** (1993) 180-184

[4] U. Keiderling, R. Gilles, A. Wiedenmann, "Application of silver behenate powder for wavelength calibration of a SANS instrument - a comprehensive study of experimental setup variations and data processing techniques", *J. Appl. Crystallogr.* **32** (1999) 456-463.

[5] S. Prilliman, S. Clark, A. MacDowell, R. Celestre, J. Wickham, A.P. Alivisatos, H. Padmore, "high pressure wide and small angle scattering of nanocrystals", http://www-als.lbl.gov/als/compendium/AbstractManager/uploads/00091.pdf.

[6] T.N. Blanton, Z. Zdzieszynski, M. Nicholas, S. Misture, "In situ high-temperature X-ray diffraction study of phase transformations in silver behenate", *Powder Diffr.* **20** (2005) 94-96.

P41

Structure modification of Pr - doped ZrO_2-Y_2O_3 after heat treatment at 1200°C

E. Werner-Malento [1*], W. Paszkowicz [1], J. Fidelus [2], M. Godlewski [1] and S. Yatsunenko [1]

[1] *Institute of Physics, Polish Academy of Sciences, al .Lotników 32/46, 02-668 Warsaw*

[2] *Institute of High Pressure Physics, Polish Academy of Sciences, ul. Sokołowska 29/37, 01-142 Warsaw*

Keywords: zirconia, yttria-stabilized zirconia, Pr-doped YSZ

**) e-mail: ewerner@ifpan.edu.pl*

Yttria-stabilized zirconia (YSZ) is one of the most studied metal oxides [1, 2]. It is a relatively hard and chemically inert material. YSZ is characterized by wear resistance, high-temperature stability and corrosion resistance, superionic conductivity at high temperature. The material is mostly used in jet engines to determine oxygen content in exhaust gases, to measure pH in high-temperature water, as membranes for high temperature solid oxide fuel cell, as a component of waveguides, laser mirrors and optical filters, as well as for electrolytes or insulators in microelectronic devices.

Several zirconia polymorphs are known (monoclinic, tetragonal, cubic and rhombohedral ones). Among them, those of the highest symmetry are of most interest due to their attractive properties. To achieve this goal, thermal treatment and/or doping with yttrium or other dopants are typically used.

Nanocrystalline zirconium dioxide powder samples were characterized by X-ray diffraction using a Philips X'pert MRD diffractometer. The changes in ZrO_2 structure due to annealing, praseodymium trioxide doping (~ 0.4 mol %) and yttria doping (0 mol % Y_2O_3, 3.56 mol % Y_2O_3, and 4.79 mol % Y_2O_3) are studied. Rietveld analysis is performed using the FullProf program, based on the structure of the component phases [3]. The calculations permitted for for quantitative phase analysis and structure refinement.

The phase composition and structure of $(Zr,Y)O_2$ nanocrystals prepared by treatment at 70°C and 1200°C are studied and compared with pure ZrO_2 samples. Changes in the structure and phase composition due to addition of yttria, Pr doping and annealing are observed. The unannealed undoped sample contains the tetragonal (78%) and monoclinic (22%) phases. The addition of yttria results in disappearing of the minority monoclinic component, in agreement with literature data. The axial ratio of the tetragonal phase shows a clear decreasing tendency. Some of the observed trends are similar to those observed in Ref. 4. The effect of the Pr doping on the phase content and lattice parameters is marginal.

.

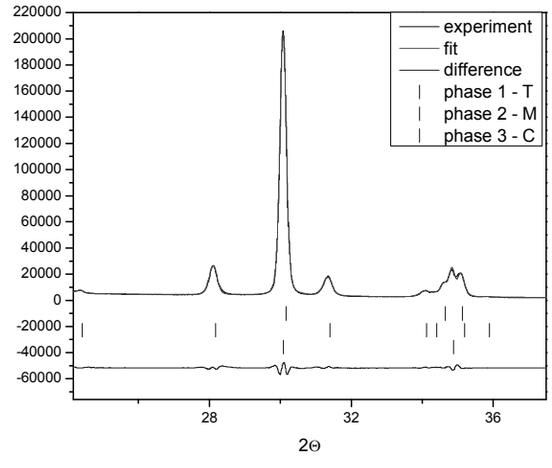

Figure 1. Experimental X-ray diffraction patterns of Pr-doped YSZ (4.79 mol % of yttria). The vertical bars show the peak positions for the tetragonal phase (upper), monoclinic phase (center) and cubic phase (lower).

Acknowledgements: "This work was supported by grant no. N N508 0851 33 of MNiSW granted for the years 2007-2009."

References

[1] R.C. Garvie, R.H.J. Hannink, R.T. Pascoe, "Ceramic Steel?", *Nature* **258** (1975) 703.

[2] M. Yashima, K Ohtake, H. Arashi, M. Kakihana and M. Yoshimura, "Determination of cubic-tetragonal phase boundary in $Zr_{1-x}Y_xO_{2-x/2}$ solid solutions by Raman spectroscopy", *J. Appl. Phys*. **74** (1993), 7603-7605.

[3] ICSD database (Karlsruhe 2008)

[4] X. Bokhimi, A.Morales, A.Garcia-Ruiz, T.D.Xiao, H.Chen and P.R.Strutt, "Transformation of yttrium-doped hydrated zirconium into tetragonal and cubic nanocrystalline zirconia", *J. Solid State Chem*. **142** (1999), 409-418.

P42

EFFECT OF γ-RAYS ON THE STRUCTURE AND ELECTRICAL PROPERTIES OF ZnO/TiO_2 CERAMICS

Suzan Abd El All [*1] **and Gamil Ali El-Shobaky** [2]

[1] *Radiation Physics Department, National Center for Radiation Research and Technology(NCRRT), NasrCity, 002 Cairo, Egypt*

[2] *Department of Physical Chemistry, National Research Center, Dokki, 002 Cairo*

Keywords:Ceramics,Irradiation,ZnO,TiO_2

**) e-mail: t suzy_a_m@yahoo.com*

A number of recent studies concern the phase diagram and characterization of the ZnO-TiO_2 system. This system attracts the attention of researchers because of its importance in practical applications [1-5].

ZnO/TiO_2 powders were synthesized by sol-gel method using zinc chloride and titanium chloride in molar ratio of 1:1as reactants. Ammonium hydroxide was used to precipitate Zn^{2+} and Ti^{2+} cations as hydroxides simultaneously. **T**he hydroxide precursor powder was calcined at various temperatures ranging from 500-1000°C for constant time of 6 h. The as-prepared material was irradiated using γ-rays ^{60}Co at different doses. The phase content and lattice parameters and effect of radiation were studied by the powder X-ray diffraction. The particle size and morphology were studied by SEM.

The characteristics of the ZnO/TiO_2 samples were found to depend on the calcination temperature and irradiation dose. Heating at 500°C led to a mixture of Ti_3O_5 (monoclinic), $ZnTiO_3$ (rhombohedral) with addition of a few extra lines of other oxides as secondary phases. With increasing the temperature to 1000°C we observe the changes of the phase composition during the process manifested by changes in X-ray diffraction pattern from the mixture.

The γ-irradiation is found to significantly influence the structure of the irradiated solid. The system shows a decrease in the crystallite size from 130 nm to 63 nm for sample irradiated. Moreover, this treatment resulted in a significant increase in the electrical conductivity (10^2-10^3-fold) of the material.

Acknowledgements: The authors wish to thank Prof. Wojciech Paszkowicz for discussion of the diffraction results.

References

[1] O. Yamaguchi, M. Morimi, H. Kawabata, K. Shimizu, "Formation and transformation of $ZnTiO_3$", *J. Am. Ceram. Soc*. **70** (1987) C97.

[2] S.F. Wang, F. Gu, M.K Lü, C.F. Song, S.W. Liu, D.. Xu, D.R. Yuan, "Preparation and characterization of sol–gel derived $ZnTiO_3$ nanocrystals", *Mater. Res. Bull.* **38** (2003) 1283-1288.

[3] Y.-S. Chang, Y.-H. Chang, I.-G. Chen, G.-J. Chen, Y.-L. Chai, S. Wu, T.-H. Fang, The structure and properties of zinc titanate doped with strontium. *J. Alloys Compds.* **354** (2003) 303-309.

[4] S-L Yang,, J.M. Wu, "Cooling rate effects on the electrical properties of TiO_2-based varistors", *J. Am. Ceram. Soc.* **76** (1995) 2203-2208.

[5- Y.-S. Chang, Y.-H. Chang, I.-G. Chen, G.-J. Chen, "Synthesis and characterization of zinc titanate doped with magnesium", *Solid State Commun.* **128** (2003) 203-208.

P43

SAXS STUDIES OF d(TTAGGG)$_4$ OLIGOMER IN SOLUTION

Maciej Kozak [1*], Agnieszka Wlodarczyk [2], and Andrzej Dobek [2]

[1] *Department of Macromolecular Physics, Faculty of Physics, A. Mickiewicz University, Umultowska 85, 61-614 Poznań, Poland;*

[2] *Department of Molecular Biophysics, A. Mickiewicz University, Umultowska 85, 61-614 Poznań, Poland.*

Keywords: small angle X-ray scattering, low resolution structure, DNA

**) e-mail: mkozak@amu.edu.pl*

Telomeres are specialized DNA structures located at the end of eukaryotic chromosomes. They consist of small, repeated DNA sequences (*e.g.*, TTGGGG in Tetrahymene, TTAGGG in human). Telomeres play an essential role in maintenance of eukaryotic chromosome within a cell by specifically binding to structural proteins. These proteins cap the ends of linear chromosomes, preventing nucleolytic degradation, end - to - end fusion, irregular recombination, and other events that are normally lethal to a cell. Chromosomal ends progressively shorten with each replication cycle, a process that seems to be linked to the limited proliferative ability of normal somatic cells. The loss of the telomeric tandem eventually leads to the cell death [1–3].

The aim of our studies was the characterisation of low resolution structure and conformational changes of a synthetic d(TTAGGG)$_4$ oligomer in solution with the presence of different monovalent cations.

The small angle X-ray scattering measurements were performed on the X33 camera of the EMBL on the DORIS storage ring at DESY, Hamburg using linear gas proportional detector with delay line readout. The d(TTAGGG)4 oligomer (2, 4, 6, 8 and 10 mg/ml) was measured in 10 mM Tris/HCl pH 7.3 solution with and without K^+ cations (0.1 – 100 mM KCl). The sample-to-detector distance was 1.7 m. The data were normalized to the incident beam intensity, corrected for detector response and the scattering of the buffer was subtracted using the computer program PRIMUS.

The radius of gyration RG, calculated for d(TTAGGG)$_4$ oligomer (10 mg/ml in 10 mM Tris/HCl) was 1.42 nm. The pair distance distribution function, P(r), yielded a maximum dimension of 4.4 nm. On the basis of SAXS data, the low-resolution structure in solution has been reconstructed using *ab inito* methods and program DAMMIN [4].

Acknowledgements: The data collection was supported by European Community - EMBL Hamburg Outstation, contract number: RII3-CT-2004-506008.

References

[1] D. Rhodes, P. Koenig, „Recognition of telomeric DNA“, *Trends Biochem. Sci.* **22** (1997) 43-47.

[2] D. Rhodes, R. Giraldo, “Telomere structure and function”, *Current Opin. Struct. Biol.* **5** (1995) 311-322.

[3] R. J. Wellinger, K. Ethier, P. Labrecque, V.A. Zakian, “Evidence for a new step in telomere maintenance”, *Cell* **85** (1996) 423-433.

[4] D.I. Svergun, “Restoring low resolution structure of biological macromolecules from solution scattering using simulated annealing”, *Biophys. J.* **76** (1999) 2879-2886.

P44

SAXS-WAXS STUDIES OF THE LOW RESOLUTION STRUCTURE IN SOLUTION OF GLUCOSE ISOMERASE FROM *STREPTOMYCES RUBIGINOSUS*

Maciej Kozak*, Michał Taube

Department of Macromolecular Physics, Faculty of Physics, A. Mickiewicz University, Umultowska 85, 61-614 Poznań, Poland

Keywords: small angle X-ray scattering, glucose isomerase, low resolution structure

**) e-mail: mkozak@amu.edu.pl*

Glucose isomerase (D-xylose ketol-isomerase; EC. 5.3.1.5) is an enzyme catalysing the reaction of isomerisation of D-glucose to D-fructose. The protein molecule (MW = 172 kDa) is a homotetramer built of four identical subunits [1,2]. Each monomer consists of two domains of which the larger contains the (α/β)8 motif of the TIM barrel type. The crystal structure of glucose isomerase has been determined by X-ray diffraction techniques to a high resolution (0.099 nm) [PDB code: 1MNZ].

The structure and conformation of isomerase molecule in solution (at pH 6 and 7.6; with and without of substrate) has been studied by small and wide angle scattering of synchrotron radiation (SAXS-WAXS). Solution scattering measurements were performed on the EMBL X33 at DESY, Hamburg (Germany). A linear gas proportional detector with delay line readout has been used. Camera length, *i.e.*, sample-to-detector distance, was 2.2 m, corresponding to the scattering vector range: $0.12 < s < 9.8$ nm^{-1} ($s = 4\pi\sin\theta/\lambda$ with 2θ the scattering angle and the X-ray wavelength, 0.15 nm).

On the basis of SAXS-WAXS data, the low-resolution structure in solution has been reconstructed using *ab inito* methods and programs DAMMIN [3] and GASBOR [4]. A comparison of the models of glucose isomerase shows only insignificant differences between the model in solution and the crystal structure.

Acknowledgements: The research was supported in part by a research grant (2P03B 06525) from the Polish Committee of Scientific Research. The data collection was supported by European Community - EMBL Hamburg Outstation, contract number: RII3-CT-2004-506008.

References

[1] H.L. Carrell, B.H. Rubin, T.J. Hurley, J.P. Glusker, "X-ray crystal structure of D-xylose isomerase at 4-A resolution", *J. Biol. Chem.* **259** (1984) 3230-3236.

[2] H.L. Carrell, J.P. Glusker, V. Burger, F. Manfre, D. Tritsch, J.F. Biellmann, "X-ray analysis of D-xylose isomerase at 1.9 A: Native enzyme in complex with substrate and with a mechanism-designed inactivator", *Proc. Natl. Acad. Sci. USA* **86** (1989) 4440-4444..

[3] D.I. Svergun, "Restoring low resolution structure of biological macromolecules from solution scattering using simulated annealing", *Biophys. J.* **76** (1999) 2879-2886.

[4] D.I. Svergun, M.V. Petoukhov, M.H.J. Koch, "Determination of domain structure of proteins from X-ray solution scattering", *Biophys. J.* **80** (2001) 2946–2953.

P45

THE FTIR AND SAXS STUDIES OF INFLUENCE OF A MORPHOLINE DERIVATIVES ON THE DMPC-BASED BIOLOGICAL MEMBRANE SYSTEMS

Maciej Kozak [1*], Kamil Szpotkowski [1], Anna Kozak [2], Ryszard Zieliński [3], Daria Wieczorek [3], Michał J. Gajda [4], Ludwik Domka [5]

[1]*Department of Macromolecular Physics, Faculty of Physics, A. Mickiewicz University, Umultowska 85, 61-614 Poznań, Poland*

[2]*Department of Water Protection, Faculty of Biology, A. Mickiewicz University, Umultowska 89, 61-614 Poznań, Poland*

[3]*Department of Technology and Environmental Protection, Faculty of Commodity Science, Poznań University of Economics, Niepodległości street 10, 60 - 967, Poznań, Poland*

[4]*European Molecular Biology Laboratory, Hamburg Outstation, c/o DESY, Notkestraße 85, 22603 Hamburg, Germany*

[5]*Department of Metalorganic Chemistry, Faculty of Chemistry, A. Mickiewicz University, Grunwaldzka 85, 60-780 Poznań, Poland*

Keywords: infrared spectroscopy, small angle X-ray scattering, phospholipids, DMPC, cationic surfactants

**) e-mail: mkozak@amu.edu.pl*

Biological membranes are selectively permeable lipid bilayers found in all cells. Besides making the cell walls, the inner system of membranes divides the cell into a number of compartments, which permits simultaneous occurrence of many metabolic reactions requiring different conditions. The main structural elements of the cell membranes are phospholipids, including phosphocholine derivatives [1-3]. The study was undertaken to establish the effect of a cationic surfactant (alkyl derivative of morpholine) on the stability of the model system of biological membrane based on DMPC (1,2-dimyristoyl-sn-glycero-3-phosphocholine).

The method applied was the Fourier transform infrared spectroscopy (FTIR) and small angle X-ray scattering. Measurements were performed on an FTIR-Raman IFS-66 (Bruker) spectrometer equipped with a cell with KRS-5 windows for investigation of solutions in temperatures 10-70ºC and in the range 4500 cm^{-1} – 600 cm^{-1}. The frequencies characterising the symmetric and antisymmetric stretching vibrations of the CH_2 groups in the carbon chains of fatty acid residues were analysed. Depending on surfactant concentration, the temperature range of the main phase transition in DMPC was shifted towards lower temperatures.

The series of SAXS measurements were performed at DESY (Hamburg, Germany; Beam Line X33). Measurements were performed in temperatures 4 - 60 °C for the scattering vectors: $0.05 < s < 5.0$ nm^{-1} ($s = 4\pi\sin\theta/\lambda$). The SAXS results confirmed the changes of DMPC main phase transition observed by FTIR. Also the effect of the surfactant on the growth of the model aquatic organism *Scenedesmus communis* was analysed.

Acknowledgements: The project have been financially supported by the Rectors of the A. Mickiewicz University and University of Economics, Poznan, within the interdisciplinary grant AE-UAM Nr 512 00 068. The data collection was supported by European Community - EMBL Hamburg Outstation, contract number: RII3-CT-2004-506008.

References

[1] *Lipid bilayers – structure and interactions,* N.J. Katsaras, T. Gutberlet (Eds.) (Springer-Verlag, Berlin-Heidelberg 2001).

[2] R.A. Schwendener, "Liposomes in biology and medicine", *Adv. Experim. Med. Biol.* **620** (2007) 117-128.

[3] R. Koynova, M. Caffrey, "Phases and phase transitions of the phosphatidylcholines", *Bba-Rev Biomembranes* **1376** (1998) 91-145.

P46

THE EFFECT OF SELECTED CATIONIC SURFACTANT ON THE STRUCTURE OF HYDRATED DMPC STUDIED BY SMALL ANGLE X-RAY SCATTERING (SAXS)

Maciej Kozak [1*], Kamil Szpotkowski [1], Anna Kozak [2], Ryszard Zieliński [3], Daria Wieczorek [3], Michał J. Gajda [4], Ludwik Domka [5]

[1] Department of Macromolecular Physics, Faculty of Physics, A. Mickiewicz University, Umultowska 85, 61-614 Poznań, Poland

[2] Department of Water Protection, Faculty of Biology, A. Mickiewicz University, Umultowska 89, 61-614 Poznań, Poland

[3] Department of Technology and Environmental Protection, Faculty of Commodity Science, Poznań University of Economics, Niepodległości str. 10, 60-967 Poznań, Poland

[4] European Molecular Biology Laboratory, Hamburg Outstation, c/o DESY, Notkestraße 85, 22603 Hamburg, Germany

[5] Department of Metalorganic Chemistry, Faculty of Chemistry, A. Mickiewicz University, Grunwaldzka 85, 60-780 Poznań, Poland

Keywords: small angle X-ray scattering, phospholipids, DMPC, cationic surfactants

**) e-mail: mkozak@amu.edu.pl*

In water environment phospholipids are capable of forming different structural phases. Depending on their concentration, pH of the environment and the length of hydrophobic chains, they can form a series of lamellar or micellar phases. In the mixtures with some surfactants or other phospholipids (mixtures of phospholipids of long and short chains) bicellar systems are formed [1-3]. The study has been performed on the model systems of biological membranes obtained on the basis of 1,2-dimyristoyl-sn-glycero-3-phosphocholine (DMPC). The influence of a cationic surfactant from the group of morpholine derivatives on the structure of the model system of biological membranes has been determined by the small angle X-ray scattering method (SAXS).

A series of the SAXS measurements was performed at DESY (EMBL BL X33, Hamburg, Germany) using the synchrotron radiation (λ=0.15 nm) and the Pilatus photon counting detector. Measurements were performed at temperatures ranging from 4 to 60°C and for the scattering vector $0.05 < s < 5.0$ nm^{-1} ($s = 4\pi\sin\theta/\lambda$). The measurements were supplemented with tests of the environmental toxicity of the surfactant used. The SAXS results implied a gradual disappearance of the lamellar phase typical of DMPC and a probable formation of the bicellar phase.

Acknowledgements: The project have been financially supported by the Rectors of the A. Mickiewicz University and University of Economics, Poznan, within the interdisciplinary grant AE-UAM Nr 512 00 068. The data collection was supported by European Community - EMBL Hamburg Outstation, contract number: RII3-CT-2004-506008.

References

[1] N.E. Gabriel, M.F. Roberts, "Spontaneous formation of stable unilamellar vesicles", *Biochemistry* **23** (1984)., 4011-4015.

[2] J. Katsaras, T.A. Harroun, J. Pencer, M.P. Nieh, "Bicellar Lipid Mixtures as used in Biochemical and Biophysical Studies", *Naturwissenschaften* **92** (2005) 355-366.

[3] G. Raffard, S. Steinbruckner, A. Arnold, J.H. Davis, E.J. Dufourc, "Temperature-composition diagram of dimyristoylphosphatidylcholine - dicaproylphosphatidylcholine 'bicelles' self-orienting in the magnetic field. A solid state H-2 and P-31 NMR study", *Langmuir* **16** (2000) 7655-7662.

II Krajowa Konferencja
Polski Synchrotron - Linie Eksperymentalne
Ameliówka, 20 - 21 czerwca 2008 roku

II[nd] National Conference: Polish Synchrotron - Beamlines
Ameliówka, 20-21 June 2008

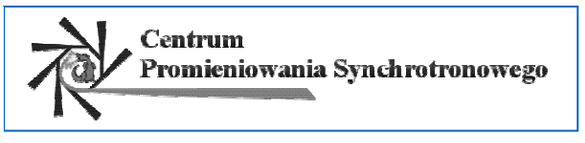

INSTYTUT FIZYKI
Polskiej Akademii Nauk

Program Committee: Edward A. Görlich (UJ), Mirosław Handke (AGH), Mariusz Jaskólski (UAM), Maciej Kozak (UAM), Wojciech M. Kwiatek (IFJ PAN), Krzysztof Lewiński (UJ), Krystyna Ławniczak-Jabłońska (IF PAN), Wojciech Paszkowicz (IF PAN), Krzysztof Polewski (AR Poznan), Jacek Szade (UŚ)

Organizing Committee: Edward A. Görlich (UJ)[Chairman], Bogdan Kowalski (IF PAN), Wojciech Paszkowicz (IF PAN), Paweł Starowicz (UJ), Krzysztof Tomala (UJ)

The Conference follows immediately the 9th International School and Symposium on Synchrotron Radiation in Natural Science (ISSRNS'2008, June 15-20, 2008) and takes place in the Ameliówka Hotel (Mąchocice Kapitulne near Kielce) on 20 – 21 June, 2008.
This is the latest in a series of meetings dedicated to the planned beamlines at the Polish Synchrotron and in particular will be concerned with:

- **Suggested scientific program for the beamlines - presentations of original research works carried out at similar beamlines of the existing synchrotrons, emphasizing particularly the technical aspects.** *)
- Information about the progress in the technical specification for individual beamlines.
- Requirements concerning the layout and possible special equipment of the hutches for a given beamline and the suggested station(s), together with assumptions for the architectural design.
- Organization-matters concerning the working groups responsible for the individual beamlines, the procedures for coordination between the teams and the Accelerator Project Group.
- Appraisal of progress in preparation of the Conceptual Design Report.
- Exchange of experiences & coordination between working teams.
- The financial conditions of the beamline working groups.

*) **Presentations** (15 minutes) of original research works on the similar, respective beamlines at the existing synchrotrons, particularly **emphasizing the technical aspects - are invited !**
Please submit **the abstract in English** of approx. half a page length **by 16-th May 2008**. We ask you to indicate to which planned beamline of Polish Synchrotron the paper refers to (synchrotron.pl > Project Specification > Beamlines) **The Conference language is English.**

Program arrangement:

Friday 20th June 2008	**$14^{\underline{00}}$ - $16^{\underline{00}}$**	**Session I**
	$16^{\underline{00}}$ - $16^{\underline{30}}$	Coffee break
	$16^{\underline{30}}$ - $18^{\underline{30}}$	**Session II**
	$19^{\underline{30}}$	Conference Dinner
Saturday 21th June 2008	**$9^{\underline{00}}$ - $10^{\underline{45}}$**	**Session III**
	$10^{\underline{45}}$ - $11^{\underline{15}}$	Coffee break
	$11^{\underline{15}}$ - $13^{\underline{30}}$	**Session IV**
	$13^{\underline{30}}$	Debate ending

LIST OF CONTRIBUTIONS

IInd National Conference: Polish Synchrotron-Beamlines, Ameliowka June 20-21, 2008

Author(s)	Paper title
M. Zubek, B. Mielewska, M. Dampc, M.R.F. Siggel-King, G.C. King	Threshold photoelectron spectra of tetrahydrofuran and α-tetrahydrofurfuryl alcohol over the energy range 9eV to 30 eV
M. Pajek, J. Szlachetko, D. Banaś, W. Cao, J.-Cl. Dousse, J. Hoszowska, Y. Kayser, A. Kubala-Kukuś, M. Szlachetko, M. Salome, J. Susini	Resonant raman scattering in synchrotron radiation based X-ray fluorescence analysis
Stanisław Rabiej	Investigations of the internal structure and thermal properties of the homogeneous ethylene-1-octene copolymers
Andrzej J. Wojtowicz	UV and VUV spectroscopy of rare earth activated wide bandgap materials
Andrzej Pawlak	Investigations of cavitation during deformation of polymers by saxs studies
Andrzej Kuczumow	Some remarks on W2 line construction derived from the experiments on biomaterials in Lure and Hasylab
Wojciech Paszkowicz	On Polish contribution to the use of synchrotron sources in natural sciences
M. Sikora, K. Knizek, Cz. Kapusta, Z. Jirak, V. Prochazka, D. Rybicki, P. Glatzel	Spin state evolution of transition metals in the co doped manganese perovskites
Wojciech Rypniewski	Specifications for the macromolecular crystallographic beam line PLU4A
Henryk Fiedorowicz	Microprocessing polymers using synchrotron and laser plasma EUV sources
G. Vankó, F.M.F. de Groot	Resonant X-ray emission spectroscopy unveils fine details of cobalt 1s pre-edges
J. Bąk-Misiuk, J. Domagała, J. Gronkowski, M. Leszczyński, G. Kowalski, A. Shalimov, W. Wierzchowski, K. Wieteska	Line PLM5A:"X-ray diffraction topography and high resolution diffraction of monocrystaline materials"
J.T. Bonarski, L. Tarkowski	Proposal of synchrotron beamline PLM6 "X-DAS"
E. Czerwosz, M. Kozłowski	Measuring position for investigation of work function from defferent materials
K. Ławniczak-Jabłońska	The short overview of the applications of X-ray absorption spectroscopy for material characterization at Institute of Physics in Warsaw
Maciej Kozak	The applications of small angle scattering of synchrotron radiation in structural biology
Jerzy Pełka	Biomedical Facility at Polish Synchrotron in Cracow
Robert Nietubyć	Project of an undulator beamline for ultraviolet and soft x radiation

C1

THRESHOLD PHOTOELECTRON SPECTRA OF TETRAHYDROFURAN AND A-TETRAHYDROFURFURYL ALCOHOL OVER THE ENERGY RANGE 9 eV TO 30 eV

M. Zubek [1*], B. Mielewska [1], M. Dampc [1], M.R.F. Siggel-King [2], and G.C. King [3]

[1] *Department of Physics of Electronic Phenomena, Gdańsk University of Technology, ul. Narutowicza 11/12, 80-952 Gdańsk, Poland*

[2] *Daresbury Laboratory, Daresbury, Warrington, WA4 4AD, UK*

[3] *School of Physics and Astronomy, Manchester University, Manchester M13 9PL, UK*

Keywords: threshold photoionization, tetrahydrofuran

**) e-mail: mazub@mif.pg.gda.pl*

Tetrahydrofuran (THF), C_4H_8O and α-tetrahydrofurfuryl alcohol (THFA), $C_5H_{10}O_2$ molecules are considered to be the simplest model analogues of deoxyribose, the subunit of the DNA sugar backbone, for investigations of its interactions with ionizing radiation. Although, there have been recently a number of electron impact studies of these molecules (*e.g.* [1-3]), relatively little is known about their interactions with ultraviolet radiation [4, 5]. In this communication we present results of threshold photoionization measurements of THF and THFA with the use of monochromatic synchrotron radiation. The operation of the threshold photoelectron spectrometer used for these experiments is based on the penetrating field technique [6]. In the measurements it was tuned to detect photoelectrons with energies of less than 5 meV. The spectra for single photoionization were recorded in the photon energy range 9-30 eV, with an energy resolution of 10 meV which allowed the vibrational structures in THF to be resolved for the first time.

Fig. 1 shows the threshold photoelectron spectra of THF and THFA obtained in the energy regions above the first ionization thresholds. From a comparison of both spectra the effect of substitution of the α-H atom by the CH_2OH group is clearly seen. Well resolved oscillatory structure superimposed on the 9.7 eV band in THF is not present in the THFA spectrum. This could be a result of damping of the ring vibrations by attachment of the alcohol group. Also, the second band of THFA (10.5 eV) is absent in the THF spectrum. It thus can be assigned to ionization from the hydroxyl oxygen.

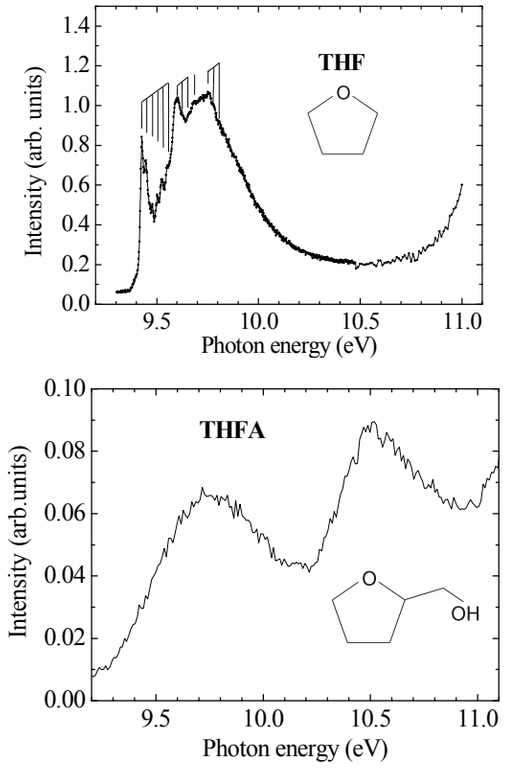

Figure 1. Threshold photoelectron spectra of THF and THFA

References

[1] M. Dampc, A.R. Milosavljevic, I. Linert, B.P. Marinkovic, M. Zubek, "Differential cross sections for low-energy elastic electron scattering from tetrahydrofuran in the angular range 20^o-180^o", *Phys. Rev. A* **75** (2007) 042710.

[2] M. Allan, "Absolute angle-differential elastic and vibrational excitation cross sections for electron collisions with tetrahydrofuran", *J. Phys. B: At. Mol. Opt. Phys.* **40** (2007) 3531.

[3] P. Sulzer, S. Ptasinska, F. Zappa, B. Mielewska, A.R. Milosavljevic, P. Scheier, T.D. Märk, I. Bald, S. Gohlke, M.A. Huels, E. Illenberger, "Dissociative electron attachment to furan, tetrahydrofuran, and fructose", *J. Chem. Phys*. **125** (2006) 044304.

[4] *Handbook of HeI Photoelectron Spectra,* K. Kimura (Eds.) (Halsted Press, New York, 1981).

[5] B.C. Ibanescu, O. May, A. Monney, M. Allan, "Electron-induced chemistry of alcohols", *Phys. Chem. Chem. Phys.* **9** (2007) 3163.

[6] R.I. Hall, A. McConkey, K. Ellis, G. Dawber, L. Avaldi, M.A. MacDonald, G.C. King, "A penetrating field electron-ion coincidence spectrometer for use in photoionization studies", *Meas. Sci. Technol.* **3** (1992) 316.

C2

RESONANT RAMAN SCATTERING IN SYNCHROTRON RADIATION BASED X-RAY FLUORESCENCE ANALYSIS

J. Szlachetko [1,3], D. Banaś [1], W. Cao [2], J.-Cl. Dousse [2], J. Hoszowska [2], Y. Kayser [2], A. Kubala-Kukuś [1], M. Pajek [1*], M. Szlachetko [2], M. Salomé [3], and J. Susini [3]

[1] *Institute of Physics, Jan Kochanowski University, 25-406 Kielce, Poland*

[2] *Department of Physics, University of Fribourg, CH-1700 Fribourg, Switzerland*

[3] *European Synchrotron Radiation Facility (ESRF), F-38043 Grenoble, France*

Keywords: resonant Raman scattering, synchrotron radiation, x-ray fluorescence, detection limits

**) e-mail: pajek@pu.kielce.pl*

Application of x-ray fluorescence (XRF) analysis for detection of low-level impurities in materials can be limited by the x-ray resonant Raman scattering (RRS) process. This effect is particularly important for detection of ultra-low concentrations of low-Z impurities in high-Z materials. In this case, the low-energy tail of strong fluorescence line of bulk material forms a "background" for detection of low-energy x-rays from the impurities. By tuning the primary x-ray beam energy below the absorption the strong x-ray fluorescence of bulk material can be eliminated, but instead, the x-ray Resonant Raman Scattering (RRS) structure appears limiting thus a sensitivity of the x-ray fluorescence technique for detection of low-Z impurities in the studied sample.

Well known example of this effect is a problem of detection of ultra-low concentrations of Al on the surface of Si-wafers, which have to be controlled below 10^{10} atoms/cm^2 level for future silicon-based microelectronic technology. It was demonstrated that in this particular case the resonant Raman scattering process limits a sensitivity of the total-reflection x-ray fluorescence (TXRF) technique [1] for detection of aluminum contamination on Si–wafer. In fact, in the TXRF method which uses semiconductor detectors, having energy resolution well above 100 eV, the Al-Kα fluorescence line is overlapping with RRS structure appearing for photon beam energies tuned below the Si-K-shell absorption edge to avoid an intense Si-Kα fluorescence. Consequently, the TXRF limits for detection of Al on Si surface are about 10^{12} atoms/cm^2 for optimized synchrotron radiation excitation conditions. Due to this limitation the TXRF method is usually combined with the vapor phase decomposition (VPD) technique enhancing by 2-3 orders of magnitude a sensitivity for detection of Al on Si-wafers.

In order to investigate new alternatives for detection of Al in silicon we have measured [2] with high-resolution the RRS spectra for Si and SiO_2 below the Si K-shell edge at the ESRF at beamline ID21. The high-resolution measurements were performed using a von Hamos Bragg-type curved crystal spectrometer [3]. In these measurements, which were performed at different photon beam energies tuned below the Si-K absorption edge, the x-ray RRS spectra were measured for the first time and the total x-ray cross sections for the at the $1s2p$ RRS process in Si and SiO_2 were obtained. In general, the experimental RRS cross sections are well described by the theoretical calculations based on the Kramers-Heisenberg approach. We have also demonstrated that from the measured RRS x-ray spectra the density of unoccupied states in silicon can be derived, giving thus similar information as one obtained by using the x-ray absorption techniques.

Guided by the results obtained for the RRS in silicon we have proposed to measure the ultra low level Al impurities on Si by using the high-resolution grazing emission x-ray fluorescence (GEXRF) technique, which is an "inverse" TXRF method. The results demonstrate that the high-resolution GEXRF method can be successfully applied for detection of low-level Al impurities in silicon. However, the further aspects of application of a high-resolution synchrotron radiation based GEXRF technique in material science will be discussed separately.

References

[1] R. Klockenkämper, "Total Reflection X-ray Fluorescence Analysis" (Wiley, New York, 1997).

[2] J. Szlachetko, J-Cl. Dousse, J. Hoszowska, M. Pajek, R. Barrett, M. Berset, K. Fennane, A. Kubala-Kukuś, M. Szlachetko, "High-resolution study of x-ray resonant Raman scattering at the K edge of silicon", *Phys. Rev. Lett.* **97** (2006) 073001.

[3] J. Hoszowska, J.-Cl. Dousse, J. Kern, Ch. Rhême, "High-resolution von Hamos crystal spectrometer", *Nucl. Instr. Meth. Phys. Res. A* **376** (1996) 129.

C3

INVESTIGATIONS OF THE INTERNAL STRUCTURE AND THERMAL PROPERTIES OF THE HOMOGENEOUS ETHYLENE-1-OCTENE COPOLYMERS

Stanisław Rabiej

University of Bielsko-Biała, ul. Willowa 2, 43-300 Bielsko-Biała, Poland

Keywords: copolymers, melting, crystallization, SAXS, WAXS

e-mail: stanisław.rabiej@ath.bielsko.pl

Performed investigations were part of a broader program dedicated to the studies on relationships between the molecular structure of homogeneous copolymers, their crystallization, solid state morphology and melting behavior. Two problems were investigated:

1) The influence of short 1-alkene side branches existing in the macromolecules of copolymers on the structure of their crystalline and amorphous phases,
2) A dual melting phenomenon occurring in isothermally crystallized ethylene-1-alkene copolymers.

Wide angle- (WAXS) and small angle- (SAXS) x-ray scattering methods were main sources of information. Simultaneous, real time WAXS and SAXS investigations were performed during crystallization and melting of the copolymers with high time- and temperature- resolution. The measurements took place in the EMBL laboratory of DESY in Hamburg. In the case of the second problem, two additional methods: differential scanning calorimetry (DSC) and small angle light scattering (SALS) were also used apart from x-ray scattering. A combination of these four methods resulted in a comprehensive, dynamic picture of the structural transformations taking place in the copolymers during melting and crystallization at different levels of molecular organization: from unit cell up to spherolitic structure. Performed investigations have given interesting data on the mechanisms of the deformation of crystalline structure caused by the presence of side branches in investigated copolymers as well as on the influence of temperature and the length of those branches on the type of deformation. It was shown, that as a result of segregation of the fragments of macromolecular chains, taking place in the initial stage of crystallization, two populations of crystalline lamellae of different thermal stability and consequently different melting temperature are formed.

C4

UV AND VUV SPECTROSCOPY OF RARE EARTH ACTIVATED WIDE BANDGAP MATERIALS

Andrzej J. Wojtowicz

Instytut Fizyki, Uniwersytet M. Kopernika, ul. Grudziądzka 5, 87-100 Toruń, Poland

Keywords: rare-earth activated fluorides, luminescence, UV–VUV spectroscopy

email: andywojt@fizyka.umk.pl

The growing interest in UV and VUV spectroscopy of rare earth activated solid state materials is generated by new and demanding applications such as uv and vuv solid state lasers, fast and efficient scintillator materials and "quantum-cutting" phoshors driven by mercury free discharge radiation.

In this Communication we will survey UV and VUV spectroscopy experiments performed at the Superlumi station of Hasylab, DESY, Hamburg, on samples of BaF_2 and $(Ba,La)F_2$ crystals activated with Ce and Er. The experiments include luminescence and luminescence excitation spectra as well as time profiles obtained under selective VUV and UV pulsed synchrotron excitation. We will demonstrate that these experiments reveal some interesting features of these systems that depend both on the peculiar complex characteristics of rare-earth ions as well as the influence of the host material.

In particular we will analyze and compare the excitation spectra of the $5d \rightarrow 4f$ emission in Ce and $4f^{10}5d \rightarrow 4f^{11}$ emissions in Er activated BaF_2 and $(Ba,La)F_2$. The unusual fast and efficient emission from the low spin $4f^{10}5d$ state in $(Ba,La)F_2$ points to significance of the highly lying Er^{3+} $4f^{11}$ levels on the nonradiative and radiative transitions between low and high spin states of the Er^{3+} $4f^{10}5d$ configuration.

We will also analyze the information revealed by the excitation spectra of the Ce^{3+} $5d \rightarrow 4f$ as well as Er^{3+} $4f^{n-1}5d \rightarrow 4f^n$ and $4f^n \rightarrow 4f^n$ emissions on the energy transfer mechanisms from the fluoride host to the rare earth ions. We will demonstrate that the fast energy transfer channels involve free and bound excitons while the generation of the free electrons and holes leads to slow processes dependant on hole and electron trapping.

Eventually we will use the information supplied by UV and VUV synchrotron studies to discuss possible applications of fluorides activated by Ce and Er.

C5

INVESTIGATION OF CAVITATION DURING DEFORMATION OF POLYMERS BY SAXS STUDIES

Andrzej Pawlak

Center of Molecular and Macromolecular Studies, Polish Academy of Sciences, ul. Sienkiewicza 112, 90-363 Lodz, Poland

Keywords: polymers, plastic deformation, SAXS, WAXS

e-mail: apawlak@bilbo.cbmm.lodz.pl

The plastic deformation of polymers is a subject of intensive studies, because the knowledge of deformation mechanisms has both scientific and technological importance.

Recently, we have shown that the significant role in deformation process may play cavities formed during stretching of the polymer specimen. The cavitation is observed in semi-crystalline polymers if the strength of amorphous phase is lower than the strength of crystalline elements. It is possible, by modifying solid-state morphology or deformation condition, to control the behaviours of polymer (*e.g.* polyethylene, polypropylene) and observe cavitational or not cavitational plastic deformation in the same type of material. The typical size of voids in polymers is 2-10000 nm. Nanometer size cavities are usually detected by the SAXS technique. Application of the synchrotron radiation gives a chance to observe a formation of cavities *in situ* during deformation.

The radiation from synchrotron in Hamburg was used for simultaneous SAXS and WAXS observations of changes in the structure of polypropylene and polyethylene samples. Technical reasons limited our experiments to measurements of specimens after the mechanical test. It was shown that the increase of testing temperature leads to not cavitational behaviour. If the annealing process was applied to not cavitating sample the cavitation was observed again during tensile test.

The synchrotron studies were supported by laboratory SAXS, WAXS, differential scanning calorimetry, and scanning electron microscopy experiments.

C6

SOME REMARKS ON W2 LINE CONSTRUCTION DERIVED FROM THE EXPERIMENTS ON BIOMATERIALS IN *LURE* AND *HASYLAB*

Andrzej Kuczumow

Department of Chemistry, John Paul II Catholic University of Lublin, 20-718 Lublin, Poland

Keywords: biomaterial, beamline, EXAFS, XANES

e-mail: kuczon@kul.lublin.pl

W2 line (X-Ray Microscopy / Microtomography) in National Light Source should be precisely designed. It results from our experience with lines D15 at LURE, L and MAXIM at HASYLAB, 1B2 White/Microprobe Beamline of Pohang Light Source that such line, planned for the microanalysis of composite materials demands combining the following facilities in one device: X-ray fluorescence in reflection mode; X-ray diffraction in transmission mode; micro-EXAFS and XANES + small angle scattering. The coupling with the real time and place observation by the optical microscope with image processing program is obligatory. The coupling with the tabletop Raman system would be of utmost significance. Such line would allow making the near total analytical and structural studies on the samples. The examples of analyses, where the parallel determination of the elemental composition, organic components and crystallographic structure was essential were cited. Also, other examples where the micromechanical (hardness, friction) or surface (roughness) features were added to the above mentioned characteristics.

C7

ON POLISH CONTRIBUTION TO THE USE OF SYNCHROTRON SOURCES IN NATURAL SCIENCES

W. Paszkowicz

Institute of Physics, Polish Academy of Sciences, 02-668 Warsaw, Poland

Keywords: database, synchrotron, light source, publication

**) e-mail: paszk@ifpan.edu.pl*

At the early stage of efforts aiming for building sources of intense radiation in Poland it seems interesting to summarise the scientific output of Polish scientists to the field of synchrotron design, construction, and application of intense sources in materials science (materials physics, chemistry, crystallography, structural biology *etc.*). Recapitulating the design and construction of synchrotron rings and beamlines is worth a dedicated study, we will only mention the important role of Prof. Bronislaw Buras in designing the synchrotron rings at Hasylab and ESRF (mentioned in [1]) during his employment (from 1970's to 1990's) in Denmark, some contribution of Institute of Nuclear Research (later Institute for Nuclear Studies) in Swierk in construction of several rings in Europe, and a joint contribution of a number of scientific institutions in Poland to the design of free electron lasers at DESY. The activity of commercial enterprises in this field such as KUMA/Oxford Diffraction (advanced diffractometers at beamlines at ESRF and at Pohang Light Source) or Prevac is worth mentioning.

In the present study we will focus on the scientific papers produced with participation of Polish (or foreigners affiliated in Poland) authors/co-authors. The first literature search plus the data provided by many Polish authors permitted to construct a list of about 1100 papers that was published at the PSRS webpages in 2006. In the collected data the publications connected with high-energy physics and with astrophysics are not included. Further efforts permitted to extend the list to more than 1630 scientific publications, covering the period 1977 - beginning of 2008.

The pioneering experimental studies have been performed by A. Kisiel starting from mid 1970s. These investigations were followed by other, mostly young, scientists at non-dedicated and (later) at dedicated synchrotron sources in Europe and in United States (also in Canada and Japan) (see, *e.g.* [2-3]). The studies including the (mostly experimental) results connected with intense sources resulted, also, in tens of MSc, PhD and DSc theses at many universities in Poland.

About 50% of the scientific papers were published in 35 journals that can be termed as 'popular' (*i.e.* at least 10 papers in each of them). The most popular are *Journal of Alloys and Compounds* (166 papers), *Acta Physica Polonica A* (147), *Physical Review B-Condensed Matte*r (90), *Surface Science* (38) and *Journal of Physics: Condensed Matter* (35). The number of papers in high-impact-factor journals is about 70 (*Physical Review Letters* 24, *Chemical Physics Letters* 17, *Applied Physics Letters* 14, *Nature* (various mutations) 6, *Europhysics Letters* 4, *Science* 2). The total number of publication in biological periodicals and crystallographic journals are also high. Such papers start also to appear in journals devoted to medicine. In recent years, the number of papers exceeds 150 per year and tends to systematically grow (see Fig. 1). Building a database of Polish publications in the field of intense radiations sources and their applications is anticipated. The already found data will be available at the PSRS webpages and linked to the CPS webpage. Extensions, supplements and corrections are welcome.

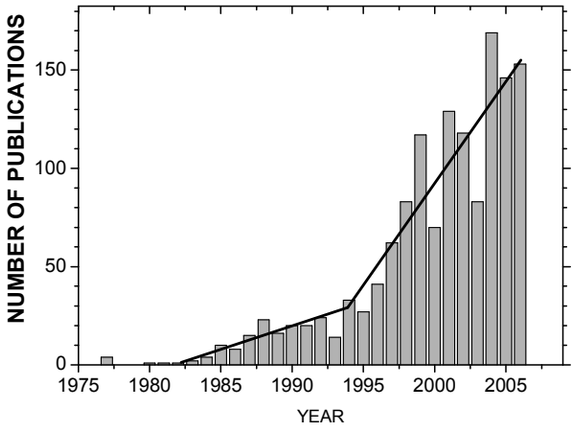

Figure 1. Polish publications in journals and books connected with intense radiation sources and their applications.

Acknowledgements: The author acknowledges provision of the data on publications provided by many colleagues from various scientific institutions.

References

[1] L. Gerward, this issue.

[2] W. Wierzchowski, this issue.

[3] G. Kowalski, this issue.

[4] A. Kisiel, this issue.

C8

SPIN STATE EVOLUTION OF TRANSITION METALS IN THE CO DOPED MANGANESE PEROVSKITES

M. Sikora [1,2], K. Knizek [3], Cz. Kapusta [2], Z. Jirak [3], V. Prochazka [4], D. Rybicki [2], P. Glatzel [1]

[1] *European Synchrotron Radiation Facility (ESRF), BP220, F-38043 Grenoble Cedex, France*

[2] *Solid State Physics Department, Faculty of Physics and Applied Computer Science, AGH University of Science and Technology, Av. Mickiewicza 30, 30-059 Cracow, Poland*

[3] *Institute of Physics, Cukrovarnická 10, 162 53 Prague 6, Czech Republic*

[4] *Faculty of Mathematics and Physics, Charles University, V Holešovičkách 2, 180 00 Prague 8, Czech Republic*

Keywords: perovskite, spin state, X-ray absorption, $LaMnO_3$, charge transfer

**) e-mail: sikora@esrf.fr*

The solid solution system $LaMn_{1-x}Co_xO_3$ reveals ferromagnetic interactions that are dominating for intermediate values of *x*, which is in contrast to the behavior of the end members that are either antiferromagnetic, $LaMnO_3$, or diamagnetic, $LaCoO_3$. The net magnetic moment possibly arises from a complex set of oxygen mediated Mn-Co interactions. Among them the ferromagnetic Mn^{3+}-O-Mn^{4+}, Mn^{3+}-O-Mn^{3+}, Co^{2+}-O-Mn^{4+} and antiferromagnetic Mn^{4+}-O-Mn^{4+}, Co^{2+}-O-Co^{2+}, Mn^{3+}-O-Co^{2+} superexchange interactions are most likely.

In order to determine, which of the mentioned interactions dominates the properties of the series the study of effective charge and spin state of manganese and cobalt have been performed by means of high resolution X-ray K_β emission and fluorescence detected K-edge absorption spectroscopy (XANES).

The absorption spectra recorded at the Mn K-edge reveal a gradual shift to higher energy with simultanous decrease of the first moment of the K_β emission line with increasing Co content. The evolution is more pronounced for compounds with higher manganese content.

Also the Co K-edge absorption spectra shift to higher energies with increasing Co content, while the emission spectra of Co reveal a distinct K_β' (low-energy satellite) feature, characteristic for high spin configurations. This is especially pronounced at low Co content.

The observed effects are unambiguously attributed to a charge transfer from Mn to Co sites accompanied by a change of the spin state of the cobalt ions. The relation between bulk magnetic properties and effective spin moments of Mn and Co, derived from combined analysis of the absorption and emission data, is discussed.

C9

MICROPROCESSING POLYMERS USING SYNCHROTRON AND LASER PLASMA EUV SOURCES

H. Fiedorowicz

Institute of Optoelectronics, Military University Technolog, 2, Kaliskiego St, 00-908 Warsaw, Poland

Keywords:organic polymers, laser plasma EUV sources

e-mail: hfiedorowicz@wat.edu.pl

Organic polymers (PMMA, PTFE, PET, and PI) are considered as important materials in micro- and nanoengineering, especially for biological and medical applications. Various techniques are used to produce mechanical or electromechanical parts in micro- or nanoscale from these materials, however, some polymers (*i.e.* PTFE) require special techniques for making microparts with a high aspect ratio and sub-micron structural accuracy. It was demonstrated that direct photo-etching using synchrotron radiation can be applied in high aspect ratio micromachining of PTFE. In the experiments it was found that the photons with lower energy (below 350 eV) dominate the processing. In direct photo-etching of polymers with radiation in this wavelength range a single photon carries enough energy to break any chemical bond and create in this way small fragments of a polymer chain. Because of very low penetration-depth of low-energy photons the material is removed only from the surface and a very thin near-surface layer. Radiation in this wavelength range (extreme ultraviolet – EUV) can be also produced in laboratory plasma sources, including discharge and laser plasmas. In this paper we present the results of the experiments on direct photo-etching of organic polymers with EUV radiation from laser plasma sources. The sources are based on a laser-irradiated gas puff target approach. The use of the gas puff target eliminates the target debris problem. The laser plasma EUV source producing radiation in the wavelength range from 5 to 20 nm in result of irradiation of a gas puff target with 0.8 J/3 ns laser pulses from a Nd:YAG laser in 10 Hz operation rate was used for microprocessing polymers. The source could be equipped with various EUV optical systems. Strong enhancement of the processing was observed for the samples heated up to 200ºC. The results of investigations using laser plasma EUV sources are presented and compared with experiments with synchrotrons.

C10

RESONANT X-RAY EMISSION SPECTROSCOPY UNVEILS FINE DETAILS OF COBALT 1s PRE-EDGES

G. Vankó [1*] and F.M.F. de Groot [2]

[1] *MTA KFKI Research Institute for Particle and Nuclear Physics H-1525 Budapest, P. O. Box 49, Hungary*

[2] *Inorganic Chemistry and Catalysis, Department of Chemistry, Utrecht University, Sorbonnelaan 16, 3584 CA Utrecht, Netherlands*

Keywords: transition metals, electronic structure, X-ray absorption, resonant X-ray emission, nonlocal transitions

**) e-mail: vanko@rmki.kfki.hu*

X-ray absorption spectroscopy (XAS) at the 3*d* metal K edges can be separated into a pre-edge region and an edge region. The pre-edge is rich in information, as it reflects valence and spin state, coordination number and local symmetry simultaneously. However, there are several obstacles to address the fine details of the pre-edge, including its low intensity, the poor separation from the tail of the main edge, and the smearing due to the large lifetime broadening of the 1s core hole in the XAS final state. Combination of absorption and emission spectroscopy, the resonant X-ray emission spectroscopy (RXES) can overcome these problems and can unveil the details of the underlying transitions [1]. This will be demonstrated by applying RXES 1) to resolve resonances of different sites that happen to appear at the same incident energy in Co_3O_4, 2) to disprove an assignment based on deceptive XAS spectral shapes in $LaCoO_3$, and 3) to study nonlocal 1*s*3*d* transitions to 3*d* orbitals of the neighbouring metal atoms. The latter will constitute the main part of the talk, and thus it is described in more details in what follows.

Over the last five decades, the pre-edge is ascribed to 1*s*3*d* quadrupole transitions to the empty 3*d* (or mixed 3*d*-4*p*) states and the edge region to the onset of 1*s*4*p* transitions to the (4)*p* conduction band. Accumulating theoretical and experimental evidence indicate that this description is incomplete, and non-local (off-site) transitions to neighbouring metal 3*d* orbitals may also take place [2,3]. We performed a detailed investigation of pre-edges on compounds containing (almost centrosymmetric) CoO_6 clusters with high-resolution 1*s*2*p* RXES [4]. Our strategy to search for non-local excitations was to vary the Co(4*p*)–O(2*p*)–Co'(3*d*) mixing by varying the Co–O bond length and the Co–O–Co angle: optimal mixing is expected at short bond lengths and linear Co–O–Co arrangement. We found that non-local effects are visible for all low-spin Co(III) oxides, where the intensity of the non-local peak is larger for the corner-sharing oxides $LaCoO_3$ and $EuCoO_3$ versus the edge-sharing oxides $LiCoO_2$ and $AgCoO_2$. In addition, angular dependent experiments reveal the different origin of the pre-edge features: while the local transition is quadrupolar, the non-local one shows a dipolar character, as expected. The absence of the non-local peak for $Co(acac)_3$, a low-spin Co(III) system with isolated Co-ions, further supports its non-local nature (see Figure 1). The non-local peaks are neither visible for CoO, a high-spin Co(II) system with significantly longer Co–O bond distances. The absence of non-local effects and the rich multiplet structure makes CoO the ideal system to show the improvement in the resolving power of our RXES experiment with 0.3 eV (FWHM) energy resolution as well as to demonstrate the coherent second-order nature of the underlying scattering process. These results have important consequences on the interpretation of the pre-edges (and thus the lowest-lying excitations) of highly correlated transition metal compounds with a short metal-ligand distance. In these, typically high-valent systems, the usual interpretation of quadrupole pre-edge plus dipole edge fails and the dominant pre-edge structure can be the non-local dipole feature.

The offered interpretation of the pre-edges has far reaching implications within physics, but also in many applied fields. Our results suggest that application of resonant techniques are in many cases indispensable to the understanding of the pre-edge region, whose intuition-based analysis can otherwise fail.

References

[1] F.M.F. de Groot, A. Kotani, *Core Level Spectroscopy of Solids*, (Taylor & Francis, New York, 2008).

[2] D. Cabaret, Y. Joly, H. Renevier, C.R. Natoli, "Pre-edge structure analysis of Ti K-edge polarized X-ray absorption spectra in TiO_2 by full-potential XANES calculations", *J. Synchrotron Rad.* **6** (1999) 258.

[3] A. Shukla, M. Calandra, M. Taguchi, A. Kotani, G. Vankó, S.-W. Cheong, "Polarized resonant inelastic X-ray scattering as an ultra-fine probe of excited states in La_2CuO_4", *Phys. Rev. Lett.* **96** (2006) 077006.

[4] G. Vankó, F.M.F. de Groot, S. Huotari, R.J. Cava, T. Lorentz, M. Reuther, "Intersite 4*p*-3*d* hybridization in cobalt oxides: A resonant x-ray emission spectroscopy study", *arXiv:0802.2744v1 [cond-mat.str-el]*.

C11

LINE PLM5A: "X-RAY DIFFRACTION TOPOGRAPHY AND HIGH RESOLUTION DIFFRACTION OF MONOCRYSTALINE MATERIALS"

J. Bąk-Misiuk[1], J. Domagała[1], J. Gronkowski[2], M. Leszczyński[3]. G. Kowalski[2], A. Shalimov[1], W. Wierzchowski[4*], K. Wieteska[5]

[1] *Institute of Physics PAS Al. Lotników 32/47, 01-142 Warsaw Poland*
[2] *Department of Physics Warsaw University, ul. Hoża 69, 00-681, Warsaw Poland*
[3] *Institute of High Pressures PAS -UNIPRESS/Topgan, ul. Sokołowska 29/37, 01-142 Warsaw Poland*
[4] *Institute of Electronic Materials Technology, ul. Wólczyńska 133*
[5] *Institute of Atomic Energy, 05-400 Otwock-Świerk, Poland*

Keywords: diffraction topography, high resolution diffraction

**) e-mail: wierzc_w@itme.edu.pl*

The beamline will be used for investigation with synchrotron X-ray diffraction topography and high resolution X-ray diffraction.

The proposed beamline will contain two experimental stations. The first one, located 30-35 m from the source of radiation will serve for high resolution diffraction of monocrystalline materials. The second station will be dedicated mainly to diffraction topographic experiments employing both white and monochromatic beams. This station will be located at further distance from the synchrotron. The reason for that is to provide enhanced resolution in topographic experiments at the level of 0.5 μm. The distance from the source will be dependent on the focusing of the electron beam – the distance of 65 m corresponds to the maximal dimensions of apparent source on the level 0.2×0.4 mm^2. It is also expected that the topographic station will enable to obtain some images with phase contrast and eventually X-ray tomographic studies.

The important assumption of the present concept is the location of the beamline at a permanent magnet wiggler, as the which can provide enhanced intensity, important both for diffractometric and the topographic station located at the further distance from the source. The second reason is the shift of the wavelength spectrum towards shorter wavelength.

The proposed solution should provide a beamline competitive with most others in Europe and US [1,2]. The possibilities of topographic station will be significantly lower in case of building the normal short line on bending magnet. The lower intensity of the beam will also reduce a number of application in case of High Resolution Diffractometry

Technical data

1 Source: permanent magnet wiggler
2 Energy of wavelength: Between 3 - 60 keV
3 Energy resolution ΔE/E: between 10^{-4} – 10^{-5}
4 Flux at first optical element: -Diffractometric station: 2×10^{11} ph/(sec·0.1% bandwidth) (1mm×1mm) (with monochromator), -Topographic station Flux at the sample 10^{10}-10^{11} ph/(sec·0.1% bandwidth) (5mm×10mm) (without monochromator)
5. Beamline optics and apparatus
- Optics: flat, diffractive at both stations,
- Apparatus: precise heavy load multi circle goniometers at both stations, with the possibility of using channel-cut analysers at diffractometric station.
- Piezo-electically controlled double crystal monochromator enabling easy wavelength tuning at diffractometric station.
- Piezo-electically controlled double crystal monochromator with the possibility of passing directly the white beam at the topographic station.
- Fast shutter, choppers for decreasing the beam intensity and laser systems for adjustment at topographic station.
6. Sample environment: For some experiments heating furnaces or cryogenic devices, should be available.It can be also possible to use epitaxial MBE reactors provided by users.
7. Beam size at sample: - diffractometric station: typically 1mm × 1 mm or lower; - topographic station: typically 1 cm × 0.5 cm in special cases up to 10 cm × 5 cm

8 Detectors
- Diffractometric station: high resolution PSD, scintillation and proportional counter
- Topographic station: photographic films, high resolution image plate, CCD camera with scintillation screen, scintillation or proportional counters for controlling of the setting of monochromatic beam topographs

9 Polarization: linear

10 Length:
- Diffractometric station: distance from the source to the sample 25 m and from the sample to the detector 20- 60 cm (with the possibility of using the channel cut analyzers in front of the detector).

- Topographic station: distance from the source to the sample 65- 90 m (essential for obtaining the sufficient resolution and coherence of the beam) and from the sample to the detector (photographic plate) – 10-60 cm

Application possibilities:

The diffractometric station:

1. The diffractometric station will provide the possibilities of precise recording of rocking curves and investigation of the reciprocal space maps of crystalline materials such as single crystal and layered (epitaxial, implanted etc.) structures as well as low dimensional structures.
2. High brilliance of the synchrotron beam 2-8 orders higher than in the case of conventional arrangements will enable the detection of a very low intensities of the diffuse scattered radiation and interference maxima, which are lower and located far from the diffraction maximum.
3. The synchrotron beam can be spatially restricted to several tenth of micrometers eliminating the influence of sample bandings and enabling studying the local differences of diffraction properties.
4. The diffractometric station will provide very highly collimated beam and analyzers with high resolution. In some cases fast measurements exploring high resolution PSD can be realized.
5. The station will enable relatively easy tuning of the wavelength and the change of the penetration depth, providing the possibility of the scanning of the strains along the depth of the low dimensional system together with controlling the chemical composition and the structure
6. The concentration and dimension of point defects and their clusters can be determined.
7. Non coplanar glide geometry can be realized enabling the evaluation of lattice parameter parallel to the surface, and providing the possibilities of studying of ultra thin layers.
8. The correlation effects connected with low dimensional systems and defect structure can be evaluated.
9. Easy tuning of the energy will also enable the optimization of radiation wavelength for different materials and problems.
10. The additional equipment such as cryostats, high temperature chambers and MBE reactors can be mounted for *in situ* investigations.

The topographic station:

1. X ray topographic investigation with high spatial resolution – better than 1 μm and with wider possibilities of choosing the reflection and wavelength.
2. High brilliance of the synchrotron source enables shortening the exposure times as well as very efficient realization of methods requiring strong restriction of wave front (section and pin-hole topography)
3. The methods requiring high angular collimation of the beam can be easily realized.
4. The interference effects occurring in the synchrotron topographs can be studied in aspect of diffraction physics and used for more precise evaluation of lattice strain and identification of crystallographic defects.
5. High coherence of the synchrotron beam enables an improvement of the resolution and obtaining of the phase contrast and related effects at high film to crystal distances [3-5].
6. The synchrotron topographic methods should provide visualization of lattice deformation and strain in single crystals, semiconductor wafers, layered and low dimensional structures. Analysis of extended crystal defects, particularly number, distribution and origin of dislocations, precipitates can be possible.
7. Some X-ray tomographic experiments can be possible.

References

[1] A.N. Danilewsky, R. Simon, A. Fauler, M. Fiederle, K.W. Benz: "White beam X-ray topography at the synchrotron light source ANKA, Research Centre Karlsruhe": *Nucl. Instrum. Meth. Phys. Res. B* **199** (2003) 71-74.

[2] B.M. Murphy, S.P. Collins, M. Golshan, M. Moore, J. Reid, G. Kowalski: „SRS station 16.3: high-resolution applications" *Nucl. Instrum. Meth. Phys. Res A* 467-468 (2001) 1014-1018.

[3] G. Kowalski, M. Moore, S. Nailer: "Application of x-ray phase-contrast imaging to polycrystalline CVD diamond" J. Phys. D: Appl. Phys. **32** (1999) A166-A171. [4] A.W. Stevenson, T.E. Gureyev, D. Paganin, S.W. Wilkins, T. Weitkamp, A. Snigirev, C. Rau, I. Snigireva, H.S. Youn, I.P. Dolbnya, W. Yun, B. Lai, R.F. Garrett, D.J. Cookson, K. Hyodo, M. Ando: "Phase-contrast X-Ray imaging with synchrotron radiation for materials science applications" *Nucl. Instrum. Meth. Phys. Res. B* **199** (2003) 427-435.

[5] Diamond Beamline Proposal 048 "A Coherent X-ray Diffraction and XPCS Beamline for the Diamond Light Source".

.

C12

PROPOSAL OF SYNCHROTRON BEAMLINE PLM6 "X-DAS"

J.T. Bonarski and L. Tarkowski *

Institute of Metalurgy and Materials Science, Polish Academy of Sciences
ul. Reymonta 25, 30-059 Kraków, Poland

Keywords: crystallographic texture, residual stresses, X-ray diffraction, thin layers, gradient materials, texture tomography, texture topography

**) e-mail: nmtarkow@imim-pan.krakow.pl*

The X-DAS beamline should enable research experiments on very thin (also biological specimens) as well as "optically thick" (high *Z*) samples which are subject to investigation both in solid state physics and materials engineering. Intention of the proposal is an experimental line adapted to a wide- and a small-angle X-ray scattering techniques denoted as WASX and SAXS, respectively. Simultaneous registration of diffraction effects by the both techniques is practicable by means of suitable goniometers and detectors. This way the X-DAS beamline will provide an unique experimental setup for *in-situ* research of phase transition and precipitation effects.

Destination of the X-DAS beamline is mezo- and micro- scale characteristics of functionally graded and layered structures especially by means of advanced methods developed also at the home Institute, like the X-ray texture tomography (see Fig. 1), planar- and depth-configuration of residual stresses, phase composition and volume fraction in texturized materials, line profile analysis, and non-standard experiments using polarized synchrotron beam.

In the case of possible higher-energy photon beam (> 20 keV), the intended beamline will enable to realize the above mentioned characteristics for bulk materials and in real construction components.

Application field of the research problems undertaken (solved) by means of the X-DAS beamline covers such problems like:

- characterization of structure of advanced materials,
- diagnosing of structure degradation in exploitation conditions,
- improvement of efficiency of the solar cells developed and manufactured at the IMMS in Cracow,
- a new material research in the field of structure inheritance and interactions of metal/ceramic/polymers with human body tissue applied *e.g.* in construction of the Polish artificial heart.

Besides the above mentioned fields of investigation, the X-DAS beamline will be capable to serve as an experimental set-up for a widely-applied X-ray diffraction techniques demanding intensive and parallel photon beam.

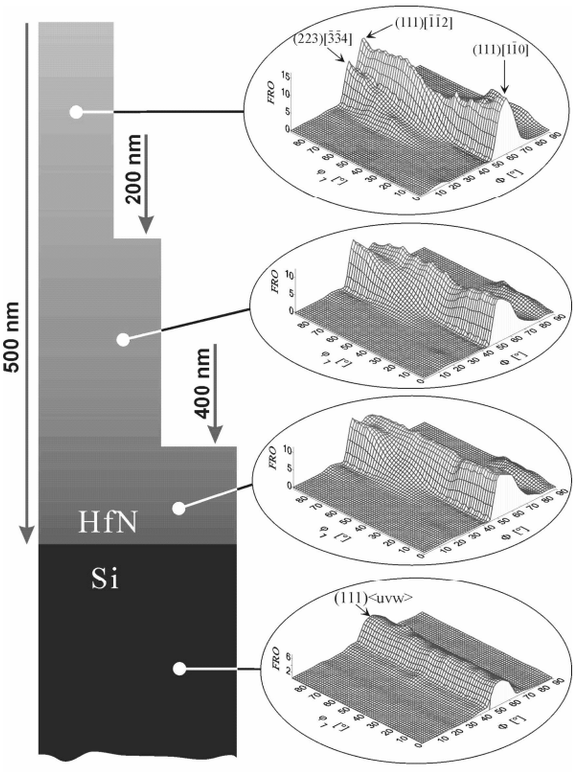

Figure 1. X-ray Texture Tomography reveals the depth-profile of the space arrangement of grains/crystals in HFN layer, about 500 nm thick, deposited on Si (111) crystal, presented in the form of ODF (Orientation Distribution Function) sections in the Euler angle space for $\varphi_2 = 45°$. The identified texture components for chosen tomographic layers of the thickness: 200 nm, 400 nm and 500 nm are indicated in the figure. Better space resolution of the tomography is possible using synchrotron beam only.

INVESTIGATION OF WORK FUNCTION OF DIFFERENT MATERIALS USING A SYNCHROTRON BEAMLINE

E. Czerwosz * **and M. Kozłowski**

Tele & Radio Research Institute, ul. Ratuszowa 11, 04-350 Warsaw, Poland

Keywords: synchrotron beam, work function

**) e-mail: czerwosz@pie.edu.pl*

Photoelectron spectroscopy in VUV range and soft X-ray radiation may be used in investigating electron structure of different materials [1,2]. In addition one can infer about material structure and about the electron work function [3].

During the meeting we want to discuss the possibility of building an experimental station including a vacuum monochromator and a suitable system for electron detection. Discussing a mounting system of various samples and data acquisition possibilities is of great importance. Our group is interested in participating in building of the station and its usage.

References:

[1] R. Mitsumoto *et al*., "Electronic structure and chemical bonding of fluorinated fullerenes studied by nexafs, ups and vacuum-uv absorption spectroscopies", *J. Phys. Chem. A* **102** (1998) 552-560.

[2] J. Ghijsen, R.L. Johnson, A. Elschner, N. Koch, "VUV photoemission using synchrotron light: A tool for characterizing surfaces and interfaces occurring in OLEDs", *J. Alloys Compods*. **382** (2004) 179-186.

[3] E. Czerwosz, P. Dłużewski, M. Kozłowski, R. Nowakowski, T. Stacewicz, "Photoelectric work function determination for the nanostructural carbonaceous films", *Vacuum* **70** (2003) 237-241.

C14

THE SHORT OVERVIEW OF THE APPLICATIONS OF X-RAY ABSORPTION SPECTROSCOPY FOR MATERIAL CHARACTERIZATION AT INSTITUTE OF PHYSICS IN WARSAW

K. Lawniczak-Jablonska

Institute of Physics, Polish Academy of Sciences, Al. Lotnikow 32/46, PL–02668 Warsaw, Poland

Keywords: X-ray absorption, semiconductors, biomaterials

e-mail: jablo@ifpan.edu.pl

The most important feature of the X-ray absorption spectroscopy is the elemental sensitivity that allows to separate structural information concerning a particular element in a multi-element compound even if the content of this element is very low and the system is disordered. The shape of the XANES spectra depends on the density of the unoccupied states in a given compound, and thus it can be considered as fingerprint of chemical bonds. The absorption edge energy can be correlated with charge transfer in the investigated element. In the case when a mixture of the several compounds containing the same element is present in the investigated sample, the analyzed spectrum is a weighted sum of the single-phase spectra of these compounds. This can be used for quantitative estimation of the concentration of particular phases in a sample. The EXAFS oscillations are created in X-ray absorption process due to the scattering of internal photoelectrons on the neighbouring atoms, therefore, the analysis of these oscillations is a source of information on a short-range order in the samples. This is of particular value in the case of investigation of buried low dimensional structures, dopants in the semiconductors or biomaterials used in pharmacology or medical diagnosis and therapy. The examples of studies performed at several absorption stations at different synchrotrons will be presented.

C15

BIOMEDICAL FACILITY AT POLISH SYNCHROTRON IN CRACOW

J.B. Pelka

Institute of Physics, Polish Academy of Sciences, Al. Lotnikow 32/46, 02-668 Warsaw, Poland

e-mail: pelkay@ifpan.edu.pl

A project of biomedical facility at the Polish Synchrotron Light Source (PSLS) [1] to be built near Cracow will be presented. The design outlines of the facility take into consideration construction principles and experience at other dedicated biomedical beamlines [2, 3]. A special attention was paid to solutions accepted in design of beamlines for biology and medicine at storage rings with parameters similar to that planned at PSLS. That are the Canadian CLS (BMIT) [4], the Australian ALS (BL-10) [5] and the Catalonian ALBA [6].

The proposed facility is aimed at application of SR x-ray techniques for imaging, diagnostics and therapy in biological and medical systems, including humans and animals. Some of considered solutions are on the top edge of currently developed accelerator and x-ray optics technology, with feasibility and efficiency confirmed at the above mentioned biomedical beamlines.

The facility will take advantage of two different types of radiation sources: the bending magnet (BM) and the more advanced and powerful superconducting wiggler (SCW). The sources with the accompanying infrastructure will be constructed subsequently in two phases with BM first, and afterwards the SCW will be added. A significant part of infrastructure will be shared by both beamlines.

The BM beamline will host a wide range of imaging techniques exploiting absorption and phase contrast with diffraction enhanced imaging (DEI), phase contrast imaging (PhCI) operating in computed tomography (CT) and in planar modes, and fluorescence imaging, among others. The beamline will also serve as a place to test and validate new techniques, to develop new ideas in imaging and therapy technologies, and will relieve some of the imaging program from the SCW beamline after its construction. The dose rates available at the BM line will be, however, insufficient to most of time-resolved techniques.

The innovative SCW beamline is designed to provide tunable monochromatic beam, of width up to 25 cm, suitable for imaging and treatment of a wide variety of subjects, from mice to large domestic animals, with spatial resolution down to 10 μm and below. The SCW beamline will host a number of imaging capabilities, including K-edge subtraction, diffraction enhanced imaging, multiple image radiography, phase contrast imaging, as well as normal absorption imaging. The SCW beamline will deliver also a filtered white beam, foreseen to reach the entrance dose rates on the order of 3500 Gy/s or higher, invaluable in some imaging and therapy techniques, like microbeam radiation therapy or synchrotron stereotactic radiation therapy. Monochromatic X-ray flux of up to 10^{14} ph/s/cm^2 will be available.

The design of the monochromators and the front ends of the beamlines will cover specific demands of biomedical applications, with high stability under radiation load, precise and fast beam locking/shutting, radiation protection and fast air volume exchange. Design of all of the components, windows, slits, filters and shutters, monochromators and slits will be focused on the heavy duty stability, performance and radiation security.

Due to specificity of objects being studied at the biomedical facility, including live animals and humans, a significant additional area of 70-100 m^2 for preparation rooms, labs, rest rooms, is foreseen.

The life sciences and medical program at the facility will be extended to other beamlines of the PSLS. Especially important are here the microbeam line and protein structure line, as well as IR. Due to its exceptional intensity, high energy SCW source at the biomedical facility, part of beamtime will be allocated to studies extending beyond the strict biomedical program. One of the fields is here material science exploiting higher photon energies (defectoscopy, strain studies, high Z materials absorption and phase contrast imaging, etc.)

Upon completion, the biomedical facility with its unique synchrotron specific imaging, diagnostics and therapy capabilities will be ready to cope with unsolved, the most crucial issues in biology, medicine, agriculture, ecology, biotechnology and other areas related to life sciences. The research teams at the facility will be able to develop strong, worldwide, competitive scientific and medical programs.

References

[1] http://synchrotron.pl/.

[2] R. Meuli, Y. Hwu, J.-H. Je., G. Margaritondo, "Synchrotron radiation in radiology: radiology techniques based on synchrotron sources", *Eur. Radiol.* **14** (2004) 1550–1560.

[3] J.B. Pełka, "Promieniowanie synchrotronowe w biologii i medycynie", *Synchr. Rad. Nat. Sci*. **6** No. 1-2 (2007) 99-107, English version in preparation.

[4] *Canadian Light Source Activity Report 2001* – 2004; Editor: M. Dalzell; CLS Document No. 0.18.1.2; Canadian Light Source Inc. 2005 (http://www.lightsource.ca/).

[5] R.A. Lewis, "Medical applications of synchrotron radiation in Australia", *Nucl. Instrum. Meth. in Phys. Res. A* **548** (2005) 23–29.

[6] A. Bravin, R. Noguera, M. Sabés, J. Sobrequés, *ALBA Biomedical Beamline (ABME). A Proposal for the ALBA S.A.C.*, Barcelona 2004.

C16

THE APPLICATIONS OF SMALL ANGLE SCATTERING OF SYNCHROTRON RADIATION IN STRUCTURAL BIOLOGY

Maciej Kozak

Dep[artment of Macromolecular Physics, Faculty of Physics, A. Mickiewicz Univesrsity
Umultowska 85, 61-614 Poznań, Poland

Keywords: SAXS, synchrotron radiation, structure in solution

e-mail: mkozak@amu.edu.pl

Profound progress in molecular biology observed over the last two decades produced a demand for effective tools for structural analysis of proteins. An excellent tool supplementing crystallography and NMR for this purpose is the small angle X-ray scattering (SAXS) [1]. The SAXS method can be applied to biological systems ranging from small proteins or lipids to large multimeric proteins and even such huge systems like ribosomes or viruses [2]. It allows determination of the structural parameters of the molecules studied such as the radius of gyration, the maximum size of particle, and provides information on the conformational changes taking place in solution [3]. The use of small angle X-ray scattering in structural analysis enables a verification of the crystal structure of biomolecules with the data collected in solution. The SAXS data and the *ab initio* calculations provide also the information on the shape of the protein molecules in solution [4]. The measurements with the use of synchrotron radiation allow collection of the scattering data for protein solutions in the wide angle range (WAXS). The WAXS data provide valuable information on the low-resolution structure of proteins [5]. The above-mentioned possibilities of SAXS application in investigation of biological systems should be taken into regard in designing the SAXS measuring line within the project on the polish national source of synchrotron radiation.

The presentation gives analysis of performance of selected and the most popular applications of the SAXS method in investigation of biological systems. The possibilities of the SAXS method with the use of synchrotron radiation are illustrated on the four examples: small protein xylanase XYNII from *Trichoderma longibrachiatum* [6,7], human ketohexokinase, human protein HC [8] and glucose isomerase from *Streptomyces rubiginosus.*

Acknowledgements: The work was supported by the Polish Ministry of Science and Higher Education (grant No. 2P03B 06525). The data collection was supported by European Community - EMBL Hamburg Outstation, contract number: RII3-CT-2004-506008.

References

[1] S.K. Burley, "An overview of structural genomics", *Nature Structural Biology* **7** – Structural Genomics Suppl., (2000) 932 – 934.

[2] D.I. Svergun, M.H.J. Koch, "Advances in structure analysis using small-angle scattering in solution", *Curr. Opin. Struct. Biol.* **12** (2002) 654–660.

[3] D.I. Svergun, C. Barberato, M.H.J. Koch, L. Fetler, P. Vachette, "Large differences are observed between the crystal and solution quaternary structures of allosteric aspartate transcarbamylase in R state", *Proteins: Struct. Funct. Genet.* **27** (1997) 110-117.

[4] D.I. Svergun, "Restoring low resolution structure of biological macromolecules from solution scattering using simulated annealing", *Biophys. J.* **76** (1999) 2879-2886.

[5] D.I. Svergun, M.V. Petoukhov, M.H.J. Koch, "Determination of domain structure of proteins from X-ray solution scattering", *Biophys. J.* **80** (2001) 2946–2953.

[6] M. Kozak, "Solution scattering studies of conformation stability of xylanase XYNII from *Trichoderma longibrachiatum*", *Biopolymers* **83** (2006) 95-102.

[7] M. Kozak, "Synchrotron radiation small angle scattering studies of thermal stability of xylanase XYNII from *Trichoderma longibrachiatum*". *Biopolymers* **83** (2006) 668-674.

[8] M. Kozak, A. Grubb, "SAXS studies of human protein HC (α_1-microglobulin)", *Prot. Pept. Lett.* **14** (2007), 425-429.

Index of authors

Index of keywords

Index of laboratories and beamlines

Synchrotron laboratories in the Table:

Adone – Frascati, Italy
ANKA – Karlsruhe, Germany
BESSY – Berlin, Germany
CLS – Canadian Light Source, Saskatoon, Canada
HASYLAB – Hamburg, Germany
ELETTRA – Basovizza/Trieste, Italy
ESRF – European Synchrotron Radiation Facility, Grenoble, Framce
LURE – Orsay, france
MAXlab – Lund, Sweden
NSLS – Uppton, USA
PLS – Pohang Light Source
SRS – Synchrotron Radiation Source, Daresbury, UK
SLA – Swiss Light Source, Villingen, Switzerland
SPring–8 – Super Photon ring with 8 GeV, Hyogo, Japan

USEFUL ADDRESSES

SOCIETIES and ORGANISATIONS:

Czech scientific societies http: //www.xray.cz/xray/societies.htm
Czech Synchrotron Radiation Society, a branch of the Unity of Czech Mathematicians and Physicists: http://www.xray.cz/xray/csca/synchrot.htm
Crystallographic societies: http://www.iucr.org/cww-top/geo.index.html
DGK Deutsche Gesellschaft für Kristallographie http://www.dgkristall2.de/***International Union of Crystallography:*** http://www.iucr.org
Europe: National coordinating structures of synchrotron radiation users, http: //www.esf.org/publication/71/synchrosurvey.pdf
European Crystallographic Association: http://www.ecanews.org/meetings.htm
European Synchrotron Radiation Society: http://fy.chalmers.se/esrs/
European Strategy Forum on Research Infrastructures, ESFRI
http://europa.eu/rapid/pressReleasesAction.do?reference=MEMO/06/384&format=HTML&aged=1&language=EN&guiLanguage=en.
Italian Society for Synchrotron Radiation (SILS): http://www.chem.uniroma1.it/~dicastro/sils.html, http://www.fis.uniroma3.it/sils/apertura.htm
The Japanese Society for Synchrotron Radiation Research (JSSRR): http://www.iijnet.or.jp/JSSRR/ http://www.jssrr.jp/
Komitee *Forschung mit Synchrotronstrahlung:* *http://hydrogen.physik.uni-wuppertal.de/kfsyn/start.html*
Latvian Synchrotron Radiation Society (LSRS): http://www.dragon.lv/lsrs
Polish Synchrotron Radiation Society (PSRS): http://info.ifpan.edu.pl/PTPS/index.html
Scientific societies: http://www.uksaf.org/sites.html
Scientific societies for microscopy and microanalysis: http://www.2spi.com/scisoc.html
Society of MAXlab users (FASM): http://usx218.fysik.uu.se/fasm/
World Scientific Societies: http://en.wikipedia.org/wiki/Category:Scientific_societies

LINKS TO LIGHT SOURCES:

http://www.lightsources.org/
http://srs.dl.ac.uk:1080/srworld
http://www.esrf.fr/navigate/synchrotrons.html
http://www1.psi.ch/www_sls_hn/sls_other_laboratories.htmlx
http://www-als.lbl.gov/als/synchrotron_sources.html

JOURNALS:

Journal of Synchrotron Radiation:
http://journals.iucr.org/s/journalhomepage.html
Advances in X-ray Analysis:
http://www.icdd.com/resources/axasearch/AXA_login.php (free access)

CONFERENCES AND COURSES

http://www.lightsources.org/
http://www.iucr.org/cww-top/mtg.subject.html
http://www.kongresy.waw.pl/
http://www.rsc.org/ConferencesAndEvents/
http://bazy.opi.org.pl/
http://www.allconferences.com/
http://www.semiconductors.co.uk/conferences/2005.htm
http://www.materialstoday.com/conferences_2005.htm
http://www.mnii.gov.pl/mnii/index.jsp?place=Menu06&news_cat_id=88&layout=2
http://www.desy.de/conferences/
http://www.nature.com/nature-events/home_vm.do
http://www.aps.anl.gov/Education/Courses_on_Synchrotron_Radiation/

Conference proceedings of meetings organised/co-organised by Polish Synchrotron Radiation Society, 1992-2005

1) **1st ISSRNS**, Jaszowiec 13-21.05.**1992**, eds.: K. Ławniczak-Jabłońska, G. Kowalski, ***Acta Physica Polonica A***, Vol. 82, No 1 & No 2, 1992.
2) **2nd KSUPS**, Mogilany, 1993, ed. J. Konior, ***Universitatis Iagellonicae Folia Physica*** Fasc. XXXVI, 1994.
3) **2nd ISSRNS**, Jaszowiec 18-26.05..1994, eds.: K. Ławniczak-Jabłońska, R. Iwanowski, ***Acta Phys. Polonica A***, Vol. 86, No 4 & No 5, **1994**.
4) **3rd KSUPS**, Warszawa, 6-7.06.1995, ***Zastosowanie promieniowania synchrotronowego***, ed.: E. Sobczak (Fundacja im. Wojciecha Świętosławskiego, Gliwice, **1995**).
5) **3rd ISSRNS**, Jaszowiec 31.05.– 8.06.1996, ed. J. Konior, ***Acta Phys. Polonica A***, Vol. 91, No 4 & No 5, **1997**.
6) **4th KSUPS**, Kraków-Przegorzaly, 18-19.06.1997, ***Application of Synchrotron Radiation to the Study of Inorganic and Biological Materials***, ed.: J. Grochowski, *Universitatis Iagellonicae Folia Physica* Fasc. XXXIX, **1998**.
7) **4th ISSRNS**, Ustroń-Jaszowiec, 15-20.06.1998, eds: W. Paszkowicz, E. Sobczak, ***Journal of Alloys and Compounds*****,** Vol. 286, No 1-2, **1999**.
8) **5th KSUPS**, Warszawa, 31.05.–1.06.1999, ***Synchrotron Radiation Studies of Materials***, eds.: M. Lefeld-Sosnowska, J. Gronkowski, (Institute of Experimental Physics, Warsaw University, Warsaw **1999**).
9) **5th ISSRNS**, Ustroń-Jaszowiec, 12-17.06.2000, eds: Cz. Kapusta, W.M. Kwiatek, J. Konior, M. Stankiewicz, ***Journal of Alloys and Compounds***, Vol. 328, No 1-2, **2001**.
10) **SYNCRYS 2001**, Krynica-Czarny Potok, 31.08-4.09.2001, ***Synchrotron Crystallography – from Source to Applications***, ed.: J. Grochowski in collab. with W. Paszkowicz, ***Acta Physica Polonica A***, Vol. 101, No 5, **2002**.
11) **6th ISSRNS**, Ustroń-Jaszowiec, 17-22.06.2002, ed.: W. Paszkowicz, A. Burian, J. Gronkowski, B.J. Kowalski, ***Journal of Alloys and Compounds*****,** Vol. 362, No 1-2 (**2004**).
12) **European Materials Research Society Fall Meeting, Symposium B**, 15–19.09.2003, Warsaw, Ed.: W. Paszkowicz, J. Pełka, ***Journal of Alloys and Compounds***, Vol. 382, No 1-2 (**2004**).
13) **7th ISSRNS**, Zakopane 8-13.06.2004, ed.: W. Paszkowicz, B.J. Kowalski, E.A. Görlich, Z. Kaszkur, ***Journal of Alloys and Compounds***, Vol. 401, No 1-2 (**2005**).
14) "Experimental and Computing Methods in High Resolution Diffraction Applied for Structure Characterization of Modern Materials" **(HREDAMM),** Zakopane, 13–17.06.2004, ed.: K. Lawniczak-Jablonska, ***Journal of Alloys and Compounds***, Vol. 401, No 1-2 (**2005**).
15) **7th KSUPS**, Poznąń, Sept. 2007, eds.: M. Kozak, W. Paszkowicz, ***Acta Physica Polonica (2008), in pronts***,.